SIMULTANEOUS SULFUR DIOXIDE ABSORPTION AND HYDROGEN SULFIDE GENERATION IN AN AQUEOUS SOLUTION OF SODIUM SULFIDE

by

Charles Q. Jia

A Thesis

Submitted to the School of Graduate Studies

in Partial Fulfillment of the Requirements

for the Degree

Doctor of Philosophy

McMaster University

1993

SULFUR DIOXIDE ABSORPTION

Dedicated to my wife, Hong

and

The memory of my mother, Xilun

DOCTOR OF PHILOSOPHY (1993) **McMaster University**
(Engineering) Hamilton, Ontario

TITLE: Simultaneous Sulfur Dioxide Absorption and Hydrogen Sulfide Generation in An Aqueous Solution of Sodium Sulfide

AUTHOR: Charles Qiang Jia, B.Eng. (Chongqing University)
M.Eng. (Chongqing University)
SUPERVISOR: Professor W-K. Lu

NUMBER OF PAGES: xxi, 229

ABSTRACT

In recovering flue gas desulfurization (FGD) processes, sulfur dioxide is removed from the flue gas and converted into useful products, typically, sulfuric acid, liquid sulfur dioxide or elemental sulfur. For sulfur dioxide producers located far from their customers of sulfur-containing products, elemental sulfur is desirable since it is easy to ship and to store, and is the raw material of many sulfur consuming processes. The existing technologies for elemental sulfur production from sulfur dioxide in flue gas are mainly limited by high capital and operating costs due to the complexity of process. To overcome this limitation, a new process based on aqueous Na_2S solution has been proposed by Lu and co-workers at McMaster University, in which SO_2 absorbed by Na_2S solution lowers the pH of solution and hydrogen sulfide is generated from the acidified solution. For the purpose of converting SO_2 in the flue gas to H_2S, and then to elemental sulfur, thermodynamics and kinetics of $Na_2S_{(aq)}$-SO_2-H_2S reacting system have been studied, both experimentally and theoretically. Based on experimental and computed results obtained in the present work, it is concluded that aqueous solution of sodium sulfide may be used to absorb sulfur dioxide and to generate hydrogen sulfide simultaneously by acid-base reactions. Recommendation has been made towards further development of this new technology for its commercialization.

ACKNOWLEDGMENTS

The author is indebted to his supervisor, Dr.W-K.Lu, for suggesting the subject studied here, and for his continuing guidance and encouragement throughout the course of the work. The author also wishes to express his gratitude to other members of his supervisory committee, Dr.M.H.I.Baird and Dr.M.B.Ives for their guidance in the application of chemical engineering principles and aqueous chemistry.

The advice and assistance from the staff and graduate students of the Department of Materials Science and Engineering at McMaster University are gratefully acknowledged. Special thanks go to Dr.R.Orr, Dr.E.Krause and Dr.B.R.Conard of INCO Limited for their valuable advice on the design of experiments and assessment of the data, and to Dr.E.Hileman of Department of Chemistry at McMaster University for his guidance on analytical chemistry of sulfur.

Financial support in the form of scholarships and assistantships from McMaster University and Ontario Provincial Government is gratefully acknowledged.

TABLE OF CONTENTS

ABSTRACT iii

ACKNOWLEDGEMENTS iv

TABLE OF CONTENTS v

LIST OF SYMBOLS xi

LIST OF FIGURES xiv

LIST OF TABLES xix

CHAPTER ONE: INTRODUCTION 1

CHAPTER TWO: LITERATURE REVIEW 8

2.1 Acid Rain and Man-Made SO_2 Emission 8

2.2 Flue Gas Desulfurization (FGD) 10

2.3 Hydrogen Sulfide 13

2.3.1 General Characteristics 13

2.3.2 Hydrogen Sulfide Generation 14

2.4 Aqueous Chemistry of Sulfur Species 16

2.4.1 Soluble Sulfides and Polysulfides 16

2.4.2 Elemental Sulfur 17

2.4.3 Thiosulfate 19

2.4.4 Sulfite and Bisulfite 20

2.4.5 Dithionite, Dithionate and Polythionates 22

2.5 Mass Transfer at Interface between Phases 24

2.5.1 The Two-Film Theory 24

2.5.2 Validity of The Two Film Theory 26

2.5.3 Effect of Chemical Reaction on Mass Transfer Between Phases 27

2.5.4 Simultaneous Diffusion and Chemical Reaction near An Interface 29

2.6 Bubble and Bubble Reactors 31

2.6.1 Bubble Mechanics 32
2.6.2 Mass Transfer to or from Single Bubbles 34
2.6.3 Bubble Reactors 36
CHAPTER THREE: EXPERIMENTAL TECHNIQUES 46
3.1 Semi-flow Batch Reactor (SFBR) Study 46
3.1.1 Apparatus 46
3.1.2 Procedures 48
3.2 Continuous Flow Tank Reactor (CFTR) Study 48
3.2.1 Apparatus 49
3.2.2 Procedures 49
3.3 Reagents Used and the Preparation of Solutions 50
3.3.1 Aqueous Na_2S Solution 50
3.3.2 Gases 51
3.3.3 Standard Solutions for Chemical Analysis 51
3.4 Determination of Gas Composition 52
3.5 Determination of Solution Composition 54
3.5.1 Fresh Na_2S Solution 54
3.5.2 Spent Solution 55
3.6 Measurement of pH Value of Solution 56
3.7 X-ray Identification of Pale Yellow Solids 57
CHAPTER FOUR: EXPERIMENTAL RESULTS OBTAINED USING A SEMIFLOW BATCH REACTOR 61
4.1 Qualitative Measurements 61
4.1.1 The Typical Result: The Three Stage Pattern 61
4.1.2 Formation of Elemental Sulfur in The Solution 62
4.1.3 The Colour of The Solution 63
4.1.4 The Heat of Reactions 65
4.1.5 Chemical Composition of Spent Solutions 65

4.2 Quantitative Measurements

4.2.1 Temperature Dependence of Reactions 66

4.2.2 The Effect of SO_2 Content in The Feeding Gas on Na_2S Conversion to H_2S 68

4.2.3 The Effect of Initial Sodium Sulfide Content in Solution on Na_2S Conversion to H_2S 70

4.2.4 The Effect of Flow Rate of Feeding Gas on Na_2S Conversion to H_2S 72

4.3 Determination of Favourable Conditions for H_2S Generation and Elemental Sulfur Formation 73

4.3.1 H_2S Generation at High Temperature (90°C) with Concentrated Na_2S Solution (1.9M) 73

4.3.2 Elemental Sulfur Formation at Low Temperature (1 °C) with Diluted Na_2S Solution 74

4.4 Effects of Bubble Size and Depth of Liquid Column on Na_2S Conversion to H_2S 75

4.4.1 Effects of Bubble Size on Na_2S Conversion to H_2S 76

4.4.2 Effects of Liquid Column Depth on Na_2S Conversion to H_2S 77

4.5 Estimations of G/L Interfacial Area and Bubble Residence Time in Solution Based on Measured Gas Hold-Up and Calculated Bubble Diameter 79

4.5.1 Determination of Bubble Diameter 79

4.5.2 Measurements of Gas Hold-Up and Estimations of G/L Interfacial Area and Bubble Residence Time in Solution 82

4.6 Experiments under Conditions Relevant to INCO's Operation in Thompson Manitoba 85

4.6.1 Effects of Oxygen in Feeding Gas on Na_2S Conversion to H_2S 85
4.6.2 Effects of Carbon Dioxide in Feeding Gas on Na_2S Conversion to H_2S 85
4.6.3 Effects of Minor Impurities (Fe, Cu, Ni, and Co) in Solution on Na_2S Conversion to H_2S 89
4.7 Estimation of Error Involved in The Determination of Conversion Ratio of Na_2S to H_2S 91
4.7.1 Conversion Ratio Obtained Using Semiflow Batch Reactor (SFBR) 91
4.7.2 Relative Errors of Measured Parameters 92
4.8 Summary 92
CHAPTER FIVE: EXPERIMENTAL RESULTS OBTAINED USING A CONTINUOUS FLOW TANK REACTOR 123
5.1 The Establishment of A Steady State for Hydrogen Sulfide Generation 123
5.2 Cases Without Oxygen in The Feed Gas and Impurities in The Solution 124
5.3 Cases With 1.88% O_2 in The Feeding Gas 126
5.4 Cases With Oxygen in The Feeding Gas and Impurities in The System 127
5.5 Effect of Liquid Residence Time in The Reactor on Na_2S Conversion to H_2S 128
5.6 Estimation of Error Involved in The Determination of Conversion Ratio of Na_2S to H_2S 129
5.6.1 Conversion Ratio Obtained Using Continuous Flow Tank Reactor (SFBR) 130
5.6.2 Relative Errors of Measured Parameters 130

5.7 Summary 131

CHAPTER SIX: THERMODYNAMICS OF CHEMICAL REACTIONS 138

6.1 Thermodynamic Properties of Ions in Aqueous Solution 138

6.2 Absorption of Sulfur Dioxide and Desorption of Hydrogen Sulfide 141

6.3 Dissociation of Sulfurous Acid 143

6.4 Formation of Aqueous Hydrogen Sulfide 144

6.5 Oxidation of Sulfide (Formation of Elemental Sulfur) 145

6.6 Dissolution of Elemental Sulfur 147

6.7 The Overall Reaction without Oxidation of Sulfide 151

6.8 The Overall Reaction with Oxidation of Sulfide 153

6.9 Summary 154

CHAPTER SEVEN: MATHEMATICAL MODELS 155

7.1 The Continuous Flow Tank Reactor Model 155

7.1.1 Assumptions and Their Validity 155

7.1.2 Variables and Constraints 159

7.1.3 Equilibrium Constants of Chemical Reactions 161

7.1.4 Conservation of Chemical Species 162

7.1.5 Electric Neutrality of Aqueous Solution 166

7.1.6 Computation Method and Computation Strategy 167

7.1.7 Results of Computation 167

7.1.8 Comparison between The Observed P_{H2S} and The Computed P_{H2S} 171

7.2 The Semi-Flow Batch Reactor Model 173

7.2.1 Assumptions and Their Validity 173

7.2.2 Variables and Constraints 174

7.2.3 Computation Method and Computation Strategy 176

7.2.4 Results of Computation 177
7.3 Summary 179
CHAPTER EIGHT: DISCUSSIONS AND THE UP-DATED MCMASTER-INCO PROCESS 203
8.1 The Absorption of Sulfur Dioxide 203
8.2 The Desorption of Hydrogen Sulfide 205
8.3 Conversion Ratio of Sodium Sulfide to Hydrogen Sulfide 207
8.3.1 Temperature Dependence 208
8.3.2 Effects of Feeding Stream Conditions 208
8.5 The Current Flow Sheet of The Proposed McMaster-Inco Process 214
CHAPTER NINE: CONCLUSIONS AND FUTURE WORK 216
REFERENCES
APPENDIX A: A SAMPLE OF PROGRAMS USED FOR SOLVING MATHEMATICAL MODELS 226

LIST OF SYMBOLS

a: specific gas-liquid interfacial area in reactor (cm^2/cm^3);

A: dimensionless constant defined by Eq.(4-2);

A_b: interfacial area of bubbles per unit volume of solution (cm^2/cm^3);

a_{Pi}: activity of solute i in phase P;

c: concentration of solution in liquid (g-mole/cm^3);

c_i: interfacial concentration of solution in liquid (g-mole/cm^3);

Cp: heat capacity (J/(K)(g-mole));

D: diffusion coefficient defined by Eq.(2-38);

D_b: bubble diameter (cm);

d_b: bubble diameter (cm);

d_o: orifice diameter (cm);

E_i: relative error in measurement of i (%);

F, F_g: volumetric rate of gas (cm^3/s);

FLL: flow rate of feed liquid (cm^3/s);

FLG: flow rate of feed gas (g-mole/s);

g: standard gravity (cm/s^2);

G^o: standard Gibbs free energy (J/g-mole);

H: Henry's-law constant, Y/c;

H^o: standard enthalpy (J/g-mole);

K_a: overall mass-transfer coefficient defined by Eq.(2-32);

k_C: mass transfer coefficient;

k_p: mass-transfer coefficient defined by Eq.(2-31);

k_1: first-order-reaction-rate constant (1/s);

k_Q: mass-transfer coefficient defined by Eq.(2-31);

M_i: amount of chemical species i (g-mole);

M_i: mass flux of chemical species i (g-mole/s);

N_A: molar flux of solute A (g-mole/(s)(cm^2));

N_b: number of bubbles in liquid column;

N: frequency of bubble production (1/s);

Pe: Peclet Number;

P_i: partial pressure of component i (atm);

Q_l: flow rate of liquid (cm^3/s);

Q_g: flow rate of gas (g-mole/s);

r_s: reciprocal of relative rate of solution defined by Eq.(2-37);

R: conversion ratio of Na_2S to H_2S;

R_s: rate of solution defined by Eq.(2-36);

r: radius of curvature for a spherical cap bubble (cm)

Re: Reynolds number;

Ri(c): specific consumption rate of solute i by chemical reaction (g-mole/(s)(cm^3));

s_i: surface element mean lifetime (s);

S^o: standard entropy (J/(K)(g-mole));

t: time (s);

T: temperature (K);

t_i: interphase exposure time (s);

Tr: reference temperature (K);

u: bubble rising velocity (cm/s);

V_b: volume of a bubble (cm^3);

V_g: gas hold-up volume (cm^3);

V_L: volume of solution in reactor (cm^3);

V_o: gas velocity through orifice (cm/s);

VOL: volume of solution in reactor (cm^3);

Y: mole fraction;

z: ionic charge.

Subscript:

l: liquid;

g: gas;

b: bubble;

$\oplus$: positive charge;

$\ominus$: negative charge;

Superscript:

i: in-coming stream;

o: out-going stream;

sol: solution.

Greek:

ϵ: gas hold-up;

θ: nominal liquid-holding time in reactor (s);

θ_L: diffraction angle

λ: wavelength of x-ray (nm)

μ_g: dynamic viscosity (N.s/cm^2);

μ_i: ionic strength (M);

ρ: density (g/cm^3);

ρ_g: density of gas (g/cm^3);

ρ_l: density of liquid (g/cm^3);

σ: surface tension (Mn/cm);

ϕ: reaction factor defined by Eq.(2-35);

LIST OF FIGURES

Fig.1.1: A flow sheet of the proposed process by Engineered Systems International (ESI) to convert SO_2 to elemental sulfur (after Orr and Burnett 1990)

Fig.1.2: A flow sheet of the proposed process to convert Na_2S to H_2S with SO_2 for the purpose of elemental sulfur production (after Lu 1989)

Fig.2.1: A schematic representation of pathways for atmospheric formation of sulfuric and nitric acids and their salts (after Schwartz 1986)

Fig.2.2: A pH contour of North America (after Elliott and Schwieger, 1984)

Fig.2.3: Observed change in pH between 1980 and 1990 for 103 lakes in the Sudbury area in comparison with (A) distance from smelters and (B) lake surface area (after Matuszek, Wales and Gunn 1992)

Fig.2.4: Amount of SO_2 emissions from Sudbury smelters during the period 1970 to 1990 (after Matuszek, Wales and Gunn 1992)

Fig.2.5: A categorization of sulfur dioxide removal processes (after Kohl and Riesenfeld 1985)

Fig.2.6: Activity gradients near a phase boundary (after Sherwood, Pigford and Wilke 1975)

Fig.2.7: Comparison of three theories of interfacial mass transfer accompanied by first-order irreversible chemical reaction (after Sherwood, Pigford and Wilke 1975)

Fig.2.8: Gas holdup correlation for methanol-air, water-air, and glycol-air (after Akita and Yoshida 1973)

Fig.3.1: The schematic drawing of the reactor

Fig.3.2: A schematic drawing of the experimental set-Up for the semi flow batch reactor (SFBR) study

Fig.3.3: A schematic drawing of the experimental set-Up for the continuous flow tank reactor (CFTR) study

Fig.4.1: The typical result: a three-stage pattern

Fig.4.2: An example of the pH profile and reaction temperature recorded by a chart recorder

Fig.4.3: A comparison between the diffraction peaks of sample to be identified and elemental sulfur

Fig.4.4: The content of sulfide in solution and pH value vs reaction time

Fig.4.5: Temperature dependence of H_2S content in exit gases

Fig.4.6: Temperature dependence of SO_2 content in exit gases

Fig.4.7: Temperature dependence of pH value of solution

Fig.4.8: The dependence of SO_2 content in exit gases on SO_2 content in feed gases

Fig.4.9: The dependence of H_2S content in exit gases on SO_2 content in feed gases

Fig.4.10: The dependence of pH value of solution on SO_2 content in feed gases

Fig.4.11: The dependence of H_2S content in exit gases on initial content of Na_2S in solution

Fig.4.12: The dependence of SO_2 content in exit gases on initial content of Na_2S in solution

Fig.4.13: The dependence of pH value of solution on initial content of Na_2S in solution

Fig.4.14: Effect of feed gas flow rate on H_2S content in exit gases

Fig.4.15: H_2S content in exit gases at 90 ℃ with 1.9 M Na_2S solution

Fig.4.16: H_2S content in exit gases at 1 ℃ with 0.017 M Na_2S solution

Fig.4.17: Effect of bubble size on pH value of solution

Fig.4.18: Effect of bubble size on H_2S content in exit gases

Fig.4.19: Effect of depth of liquid column on H_2S content in exit gases of second stage at 40 ℃

Fig.4.20: Effect of depth of liquid column on H_2S content in exit gases of second stage at 59 ℃

Fig.4.21: Effect of depth of liquid column on H_2S content in exit gases of second

stage at 79 °C

Fig.4.22: The bubble-diameter correlation for air at near-atmospheric pressure sparged into relatively inviscid liquids ($\mu \leq 100$ mPa.s) (after Kumar et.al 1976)

Fig.4.23: Dependence of bubble diameters on volumetric rate of gas

Fig.4.24: Effect of 2% oxygen in feed gas on H_2S content in exit gases and pH value fo solution

Fig.4.25: Composition of exit gases vs reaction time (1.2% carbon dioxide in feed gas, single-orifice bubble distributor used)

Fig.4.26: Composition of exit gases vs reaction time (1.2% carbon dioxide in feed gas, coarse bubble distributor used)

Fig.4.27: Composition of exit gases vs reaction time (10% carbon dioxide in feed gas, single-orifice bubble distributor used)

Fig.4.28: pH value of solution vs reaction time (1.2% carbon dioxide in feed gas, coarse bubble distributor used)

Fig.4.29: Effect of minor impurities (Fe, Cu, Ni and Co) on H_2S content in exit gases

Fig.5.1: An example of the system's approaching to a steady state

Fig.5.2: H_2S content in exit gases and pH value of solution under the steady state conditions

Fig.5.3: H_2S content in exit gases and pH value of solution under the steady state conditions

Fig.5.4: H_2S content in exit gases and pH value of solution under the steady state conditions

Fig.5.5: H_2S content in exit gases and pH value of solution under the steady state conditions

Fig.5.6: H_2S content in exit gases and pH value of solution under the steady state conditions

Fig.7.1: Dependence of equilibrium partial pressure of H_2S in exit gases and pH

value of exit solution on sulfide concentration in feed solution

Fig.7.2: Dependence of sulfide and bisulfide contents in exit solution on sulfide concentration in feed solution

Fig.7.3: Dependence of sulfite, bisulfite and sulfurous acid contents in exit solution on sulfide concentration in feed solution

Fig.7.4: Dependence of equilibrium partial pressure of H_2S in exit gases and pH value of exit solution on volumetric flow rate of feed solution

Fig.7.5: Dependence of sulfide and bisulfide contents in exit solution on volumetric flow rate of feed solution

Fig.7.6: Dependence of sulfite, bisulfite and sulfurous acid contents in exit solution on volumetric flow rate of feed solution

Fig.7.7: Dependence of equilibrium partial pressure of H_2S in exit gases on SO_2 partial pressure in feed gases at three different temperatures

Fig.7.8: Dependence of pH value of exit solution on SO_2 partial pressure in feed gases at three different temperatures

Fig.7.9: Dependence of sulfide content in exit solution on SO_2 partial pressure in feed gases at three different temperatures

Fig.7.10: Dependence of bisulfide content in exit solution on SO_2 partial pressure in feed gases at three different temperatures

Fig.7.11: Dependence of sulfite content in exit solution on SO_2 partial pressure in feed gases at three different temperatures

Fig.7.12: Dependence of bisulfite content in exit solution on SO_2 partial pressure in feed gases at three different temperatures

Fig.7.13: Dependence of sulfurous acid content in exit solution on SO_2 partial pressure in feed gases at three different temperatures

Fig.7.14: A comparison between computed P_{H2S} and observed P_{H2S} in exit gases, computed pH value of solution and observed pH value of solution

Fig.7.15: Computed changes in sulfide and bisulfide contents in solution with reaction

time

Fig.7.16: Computed changes in sulfite, bisulfite and sulfurous acid contents in solution with reaction time

Fig.7.17: Temperature dependence of computed equilibrium partial pressure of H_2S

Fig.7.18: Temperature dependence of computed pH value of solution

Fig.7.19: Effect of volume of solution in reactor on computed equilibrium partial pressure of H_2S in exit gases

Fig.7.20: Effect of volume of solution in reactor on computed pH value of solution

Fig.7.21: Effect of initial Na_2S content in solution on computed equilibrium partial pressure of H_2S in exit gases

Fig.7.22: Effect of initial Na_2S content in solution on computed pH value of solution

Fig.8.1 The current flow sheet of the proposed McMaster-INCO process (AGU: absorption/generation unit)

Fig.8.2 A flow sheet of the proposed two-tower AGU system in McMaster-INCO process

Fig.8.3 A flow sheet of proposed three-tower AGU system in McMaster INCO process

LIST OF TABLES

Table 4.1 Temperature dependence of the conversion ratio of sodium sulfide to hydrogen sulfide

Table 4.2 Effect of sulfur dioxide content in feeding gases on the conversion ratio of sodium sulfide to hydrogen sulfide at 79°C

Table 4.3 Effect of initial sodium sulfide content in solution on the conversion ratio of sodium sulfide to hydrogen sulfide at 79°C

Table 4.4 Effect of feed gas flow rate on the conversion ratio of sodium sulfide to hydrogen sulfide at 79°C

Table 4.5 The conversion ratio of sodium sulfide to hydrogen sulfide at high temperature and with high concentrated Na_2S solution

Table 4.6 The conversion ratio of sodium sulfide to hydrogen sulfide at 1°C and with 0.017 M Na_2S solution

Table 4.7 Conversion ratios of sodium sulfide to hydrogen sulfide for different depths of liquid column at different temperature

Table 4.8 Reynolds number and bubble diameters for different volumetric rates of gas

Table 4.9 Dependence of gas hold-up on volumetric rate of gas

Table 4.10 Dependence of interfacial area (A_b) and residence time of bubble in solution (t_b) on volumetric rate of gas

Table 4.11 Experimental conditions for the study on the effect of CO_2 in feed gas on Na_2S conversion to H_2S

Table 4.12 Amounts of carbon dioxide and sulfur dioxide absorbed in the first stage

Table 4.13 The peak values of H_2S content in exit gas and the conversion ratio of sodium sulfide to hydrogen sulfide at 85°C

Table 4.14 Effect of Impurities (Fe, Ni, Cu and Co) in solution on Na_2S conversion to H_2S

Table 5.1 A summary of chemical analysis of exit gas
Table 5.2 Molar fluxes of reactants and product and their ratios
Table 5.3 A summary of chemical analysis of exit gas
Table 5.4 Molar fluxes of reactants and product and their ratios
Table 5.5 A summary of chemical analysis of exit gas
Table 5.6 Molar fluxes of reactants and product and their ratios
Table 5.7 A summary of chemical analysis of exit gas
Table 5.8 Molar fluxes of reactants and product and their ratios
Table 6.1 Thermodynamic properties of Reaction 6-8
Table 6.2 Thermodynamic properties of Reaction 6-9
Table 6.3 Thermodynamic properties of Reaction 6-10
Table 6.4 Thermodynamic properties of Reaction 6-11
Table 6.5 Thermodynamic properties of Reaction 6-12
Table 6.6 Thermodynamic properties of Reaction 6-13
Table 6.7 Thermodynamic properties of the wet Claus reaction
Table 6.8 Thermodynamic properties of Reaction 6-15
Table 6.9 Thermodynamic properties of Reaction 6-16
Table 6.10 Thermodynamic properties of Reaction 6-17
Table 6.11 Thermodynamic properties of Reaction 6-18
Table 6.12 Thermodynamic properties of Reaction 6-19
Table 6.13 Thermodynamic properties of Reaction 6-20
Table 6.14 Thermodynamic properties of Reaction 6-21
Table 6.15 Thermodynamic properties of Reaction 6-22
Table 6.16 Thermodynamic properties of Reaction 6-23
Table 6.17 Thermodynamic properties of Reaction 6-24
Table 7.1 A summary of the variables in the CFTR model
Table 7.2 Comparison between observed and computed pH values of solution
Table 7.3 Comparison between observed and computed partial pressure of H_2S

Table 7.4 Comparison between observed and computed molar flux ratios

Table 7.5 A summary of the variables in the SFBR model

Table 8.1 Overall rates of mass transfer of SO_2 from 11% SO_2-N_2 gaseous mixture to aqueous Na_2S solution of 1.5 M and distilled water at 70 and 90 °C

CHAPTER ONE

INTRODUCTION

Of the several air pollutants that contribute to acid rain, sulfur dioxide has received special attention due to its large and increasing atmospheric content. On a global scale, two sources of sulfur dioxide predominate, man-made and natural; both sources generate comparable quantities, but the former is of more local effect.

The removal of sulfur dioxide from industrial flue gases (such as that produced by non-ferrous sulfide smelters and fossil fuel-burning power plants) has become a common commercial practice. Unfortunately, effective removal of sulfur dioxide from flue gases, and its conversion into environmentally safe products has become an expensive operation. Reducing the cost of sulfur dioxide removal from flue gas will benefit industry, consumers and the environment.

Although there are several approaches to the abatement of atmospheric sulfur dioxide, such as the use of lower sulfur-containing fuel and more fuel efficient operations, the flue gas desulfurization (FGD) process has received the most attention and intensive study. FGD processes may be classified as "throwaway" and "recovering", based on the usefulness of the sulfur-containing product from the fixed sulfur dioxide. In throwaway FGD processes, sulfur dioxide is removed from flue gas and the sulfur-

containing matter is discarded as waste solid, as in the lime/limestone process in which sulfur dioxide is converted to calcium sulfite and/or sulfate. In recovering FGD processes, sulfur dioxide is removed from the flue gas and converted into a useful product.

The typical products of recovering FGD processes are sulfuric acid, liquid sulfur dioxide and elemental sulfur. The strength of the sulfur dioxide source usually determines the type of ultimate end product. Sulfuric acid is the most economic product in terms of its production. Unfortunately, the limited storage capability and costs arising from long-distance shipping are the main disadvantages in making sulfuric acid. Liquid sulfur dioxide as a by-product is also limited by low market demand. However, since elemental sulfur is easy to ship and store, and is the raw material for many sulfur consuming processes, it is a desirable product especially for sulfur dioxide producers located far from their customers.

The existing technologies for elemental sulfur production from sulfur dioxide in flue gas share four main limitations:

[1]. the high capital cost due to the complexity of the process, such as Engineering System International (ESI) process (US Patent #4,241,041);

[2]. the high cost of operation due to the need of expensive reductants;

[3]. the poor quality of elemental sulfur when coal is used as the reductant; and

[4]. the use of organic solvents which may be a potential source of other pollutants.

ESI has developed a carbonate based process to produce hydrogen sulfide. This process consists of several steps, as shown in Fig.1.1, absorption of SO_2 by aqueous sulfite solution forming bisulfite; bisulfite neutralization by carbonate to produce sulfite and carbon dioxide gas; reduction of sulfite to sulfide by carbon; and finally generation of hydrogen sulfide gas with aqueous sulfide solution and carbon dioxide gas. Hydrogen sulfide produced from the ESI process may be readily converted to elemental sulfur via the Claus reaction. Although the chemicals are regenerable in this process, the process requires a large number of processing units and hence significant capital investment and operating cost.

Lu and co-workers (1989) have studied thermodynamics of $Na_2S_{(aq)}$-SO_2-H_2S system. In 1990, Ng studied kinetics and mechanisms of carbonation conversion of aqueous sodium sulfide to hydrogen sulfide (Ng 1990), which led to a suggestion that since sulfur dioxide is more acidic and more soluble in water than carbon dioxide, the kinetics of hydrogen sulfide generation might be improved by replacing carbon dioxide by sulfur dioxide. Based on this work, a new process of removing sulfur dioxide from flue gases was proposed by Lu and co-workers. As shown in Fig.1.2, the proposed process consists of an absorption/gen··ation unit (AGU), an evaporation unit (EU), a reduction unit (RU), a dissolution unit (DU) and a gas composition adjustment unit (GCAU). The AUG is a new reactor and the key unit, in which sulfur dioxide in the flue gas is removed and hydrogen sulfide is produced. The overall reaction anticipated is considered to be:

$$Na_2S_{(aq)} + SO_{2\,(g)} + H_2O = Na_2SO_{3\,(aq)} + H_2S_{(g)} \qquad (1\text{-}1)$$

The liquor leaving the AGU may be then fed into the EU where all or a portion of the water is evaporated. The heat required by the EU may be supplied by the hot gases generated in the RU based on coal, oil or other hydrocarbons. The product from the EU is fed into the RU, in which sodium sulfite is reduced to sodium sulfide as molten salt. In the dissolution unit (DU), solid sodium sulfide is dissolved in water. The impurities, such as coal ash, are filtered out. The sodium sulfide solution is fed back into the AGU, forming a loop. The composition of gases from the AGU is adjusted in the GCAU to meet the requirement for elemental sulfur production, for example, as prescribed by the Claus process.

The potential applications of the proposed process has been recognized by Inco Limited, which has been supporting experimental investigation of this process at McMaster University since 1990. Consequently, this process was then named the McMaster-Inco process.

The main incentive for the development of McMaster-Inco process is its simplicity and associated low capital cost for commercial application. The novel part of this process is the absorption/generation unit (AGU) in which sulfur dioxide is scrubbed by a solution of sodium sulfide and hydrogen sulfide is produced simultaneously from the solution. Although the results of calculations (Lu 1989) indicate that the generation of hydrogen sulfide from aqueous sodium sulfide solution in contact with sulfur dioxide is

thermodynamically favoured, little is known regarding the reaction mechanisms and kinetics of this system. Since aqueous sodium sulfide solution is basic and reductive in nature, both acid-base reactions and redox reactions may occur when it meets with sulfur dioxide which is both acidic and oxidic. Due to the possible redox reactions, the chemistry of this system could become very complex. Consequently, in order to commercialize the McMaster-Inco process, some key control parameters must first be identified and defined.

The aim of this investigation has been to experimentally study basic chemistry, reaction mechanisms and kinetics in this $Na_2S_{(aq)}$-SO_2-H_2S system, and to identify and define the key control parameters in the AGU. Towards these ends, mathematical models have been developed based on mass and charge balances and thermodynamic relations. It is expected that the present work will contribute to the eventual commercialization of this process.

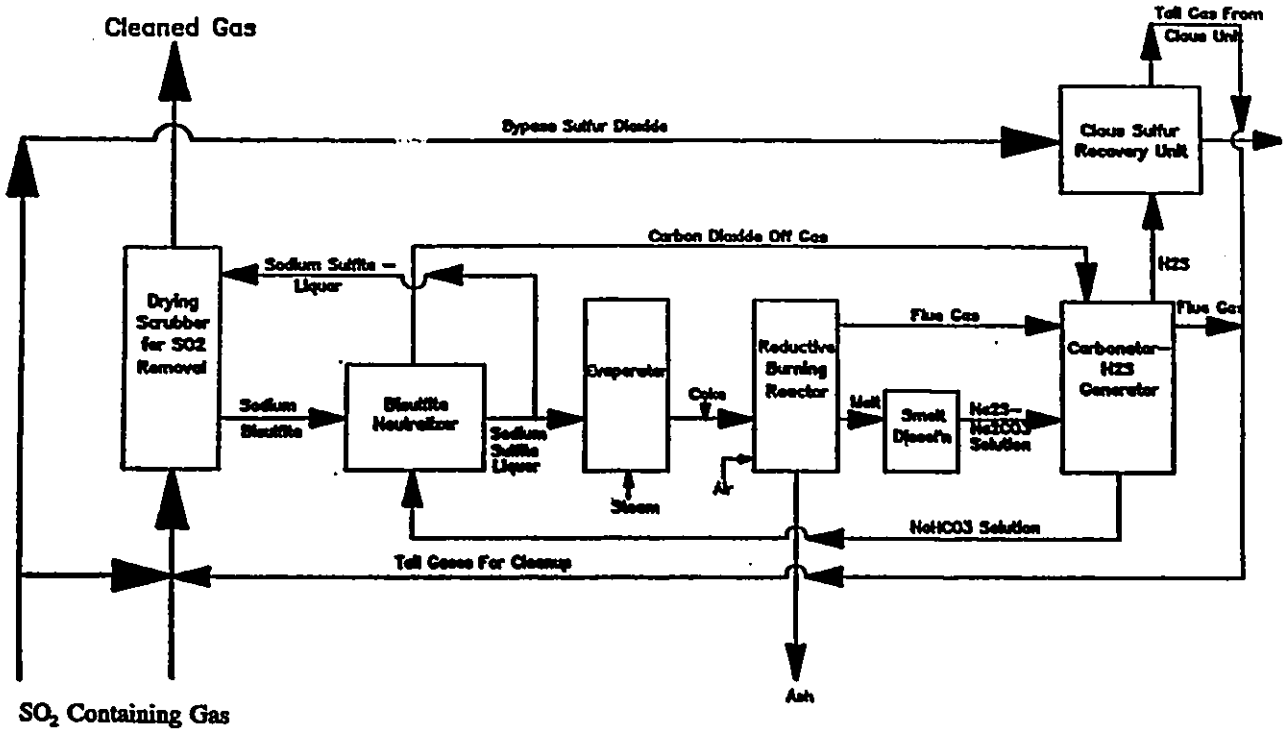

Fig.1.1: A flow sheet of the proposed process by Engineering System International (ESI) to convert SO_2 to elemental sulfur (after Orr and Burnett 1990)

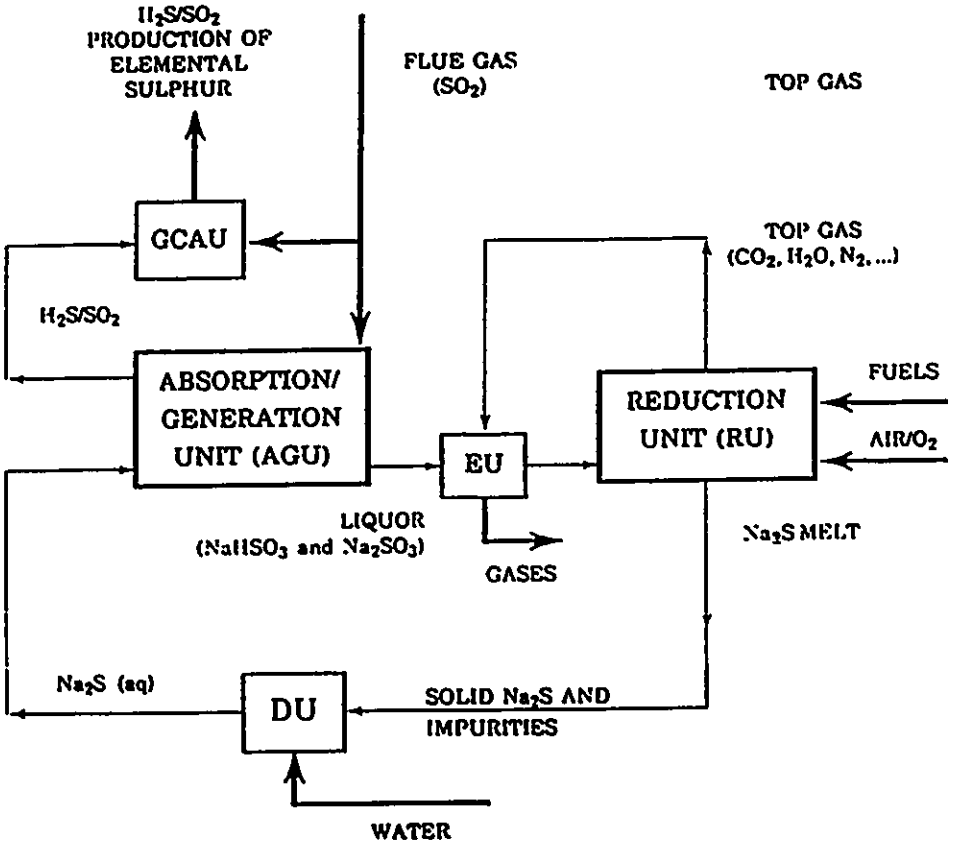

Fig.1.2: A flow sheet of the proposed process to convert Na_2S to H_2S with SO_2 for the purpose of elemental sulfur production (after Lu 1989)

CHAPTER TWO

LITERATURE REVIEW

2.1 Acid Rain and Man-Made Sulfur Dioxide Emission

Acid rain was first studied in the 1950's and 1960's by such noted scientists as E.Gorham and A.G.Gordon, who provided examples and warnings of things to come in their studies carried out at locations near large sulfur dioxide sources in English Pennines and in Canada (Gorham 1957; Gorham & Gordon 1960 and 1963). The work of Svante Oden (1967) successfully alerted the Swedish public and the scientific communities to the problem of long-range atmospheric transport and deposition of acidic substances, a phenomenon now recognized by the industrialised world as the "acid rain". Over the past 30 years, much progress has been made regarding the understanding of the formation of acid rain. It has been found that oxidation by OH radicals is the dominant gas-phase reaction in the conversion of SO_2 to H_2SO_4 (Calvert and Stockwell 1983). The process by which clouds incorporate sulfuric acids is separated into two categories depending upon whether oxidation takes place in the gaseous phase or in the aqueous phase (Schwartz 1986), as illustrated schematically in Fig.2.1.

There are two sources of global SO_2 emission which contribute to acid rain, man-made and natural (Slack and Hollinden 1975). Roughly 94% of SO_2 emissions in North America can be attributed to man-made sources. Of these man-made emissions, 70% are emitted by fossil-fuel fired power plants (Molburg 1993). In eastern Canada and the

adjacent American states, man-made emissions are believed to be responsible for the observed concentration of hydrogen ions, sulfate and nitrite found in the rain water of these regions (Elliott and Schwieger 1984). Fig.2.2 shows the pH contour map of North America for rainfall from 1979 through the end of 1981. The pH of precipitation is regularly in the 3.5-4.5 range, indicating acid concentrations which are 10 to 100 times greater than those found in normal rainfall.

In Europe, SO_2 emission from one country crosses borders to kill fish and trees and corrode buildings and monuments in neighboring countries (Levy 1992). According to the UN Economic Commission for Europe (ECE) statistics, an average reduction of SO_2 emission across Europe of 63% from 1990 level is required (Pearce 1993). In Asia, the total SO_2 emission from 25 countries east of Afghanistan and Pakistan increased by a factor of 1.6 from 18.3 Tg (1 Tg = 10^6 tonnes) in 1975 to 29.1 Tg in 1987 (Kato and Akimoto 1992). The trend of increase in SO_2 emission in Asia is expected to be maintained owing to the booming economy in China. In the United States, it was reported recently that the acidification of lakes and streams in Massachusetts has reached its highest level since 1983 when monitoring began (Godfrey 1993). A similar phenomenon has occurred in Virginia streams (ES&T, June 1993 p.998).

In Canada, increased scientific research, implication of new technologies and the dissemination of public information have led to significant improvement in the control of SO_2 emissions. In 1984, Canada committed itself to a 50% reduction in SO_2 emissions from eastern Canadian provinces by the end of 1994 (Brydges 1991). INCO Limited will retain 90% of the sulfur contained in its ore by 1994 and plans to spend

approximately $500 million dollars (cdn.) for new facilities which are close to completion. INCO's SO_2 abatement program will lower sulfur dioxide emissions at Sudbury from 685,000 tonnes per year of 1990 to 265,000 tonnes per year by 1994 (Bell,Blanco, Davies and Garritsen 1990; Landolt, Dutton, Edwards and McDonald 1992). As a result of these reductions, 25 lakes near Sudbury, Ontario, Canada have returned to an acceptable pH range in which lake trout can survive (Hauhs & Wright 1989; Gunn & Keller 1990). As well, the region is showing encouraging signs of forest regeneration despite its severely damaged soils (Winterhalder, 1988). A recent study by Matuszek, Wales and Gunn (1992) indicated that the water quality of a subset of Sudbury lakes has improved as a result of SO_2 emission reductions from Sudbury smelters. Fig.2.3 shows the observed change in pH between 1980 and 1990 for 103 lake trout lakes in the Sudbury area in comparison with distance from smelters and lake surface area, while Fig.2.4 gives the amount of SO_2 emission from Sudbury smelters during the period 1970 to 1990.

2.2. Flue Gas Desufurization (FGD)

Increasingly strict standards for sulfur dioxide emission control have prompted the development of a number of options and techniques for reducing emissions of sulfur dioxide. Among these options are the following: [1] change to low-sulfur fuel; [2] change to high grade concentration of sulfide ore (e.g. a higher Cu/S ratio); [3] construct tall stacks; [4] practise flue gas desulfurization (FGD).

For the nonferrous smelting and refining industry, in which the sulfur is originally

from sulfide ore, to lower the amount of gangue sulfide minerals by mineral dressing and to implement flue gas desulfurization (FGD) perhaps are the most practical option available today. In terms of FGD processes, many systems have been used, and a great deal of research is under way to make these processes more efficient. A detailed categorization of FGD processes by the end-product was given by Kole and Riesenfeld (1985) and is shown in Fig.2.5.

FGD processes may be further classified as throwaway or recovering depending on whether SO_2 containing end products are discarded as a solid waste or sold for reuse. Sulfur-containing by-products of FGD processes include sulfuric acid, liquid sulfur dioxide and elemental sulfur, to name a few. Industrial SO_2 emitters have been relying on the conversion of SO_2 to sulfuric acid to remove sulfur dioxide from stack gas since the 1940's (Vesilind 1988). This process has three limitations: [1] the stack gas must be cleaned of particulate matter before entering the acid plant; [2] acid formation is energetically favourable only for a fairly concentrated ($SO_2\% > 50\%$) gas stream; and [3] the storage and the long-distance shipping are costly. The concentrated sulfur dioxide may be compressed into liquid form. Unfortunately, the market for liquid sulfur dioxide is quite limited (Elliott et. al. 1984). On the other hand, elemental sulfur is easy to ship and store. It is the raw material for the principle sulfur derivative, sulfuric acid and would be the most desirable by-product for smelters located in a remote area, such as, Thompson plant of Inco Ltd (Orr and Burnett 1991).

There are two kinds of processes to reduce SO_2 to elemental sulfur, namely, dry and wet. In a dry process, the SO_2 may be reduced with either coal, hydrocarbons,

hydrogen or hydrogen sulfide at a temperature between 150°C to 1000°C (Donohue 1974). Conversely, hydrogen sulfide is the only reductant which may be utilized in a wet process (Averbukh 1969). One of the well-understood wet processes is the citrate process. In this process, a citrate solution is used to absorb SO_2 in flue gas. Then, the SO_2-loaded solution reacts with H_2S to produce elemental sulfur. The citrate process was first developed in 1970 by the Bureau of Mines at the Salt lake City Metallurgy Research Center (George, Crocker and Rosenbaum 1970). This work led to the construction of a 400 cfm pilot unit which began treating reverberatory furnace gas at a copper smelter in Arizona in November, 1970. While a series of mechanical difficulties prevented the continuous operation of the demonstration unit and resulted in the generation of limited economic and engineering data, the soundness of the process chemistry was established (Resenbaum, George and Crocker 1971). The Bureau continued to pursue the needed chemical and cost data on the process. They assembled a second-generation laboratory unit, incorporating modifications dictated by the results of the earlier work. This unit served as a prototype for a larger installation designed to treat 1,000 cfm of 0.5% SO_2 gas at the Bunker Hill lead smelter in Kellogg, Idaho (Rosenbaum, McKinney, Beard, Crocker and Nissen 1973). Hydrogen sulfide has become the preferred reductant for both dry and wet processes (Averbuhk et.al. 1969). The technology for sulfur recovery from both concentrated and dilute hydrogen sulfide is well established (Slack 1975; Kohl et. al. 1985). The inherent suitability of hydrogen sulfide to the production of elemental sulfur is attractive at the present time when attempts are made to reduce sulfur dioxide levels.

2.3 Hydrogen Sulfide

2.3.1 General Characteristics

Historically, hydrogen sulfide (H_2S) appeared first in the writing of the alchemists, but it was not until 1796 that Berthelot identified the gas which is evolved by the action of acid on metal sulfide, as reported earlier by Scheele in 1777 (Kolthoff and Elving 1961). Hydrogen sulfide is an extremely poisonous, corrosive, colourless gas having a characteristic offensive odour. Hydrogen sulfide is used in the manufacture of a variety of chemicals, and for the removal of metal impurities from process liquors. Waste hydrogen sulfide is processed to recover the sulfur, which goes primarily into sulfuric acid manufacture (Vigide and Hermida 1960). Hydrogen sulfide has been used extensively as an analytical reagent and has served generations of analysts as a qualitative and quantitative tool. In fact, an entire system for the qualitative evaluation of metal ions is based on their reactions with hydrogen sulfide (Treadwell and Hall 1956).

The decomposition of hydrogen sulfide to produce both hydrogen and sulfur has recently received a great deal of attention from several research groups. Berk, Heidemann, Svrcek and Behie (1991) investigated the decomposition of hydrogen sulfide by a two-step closed loop thermochemical process. In the first step, hydrogen sulfide decomposes by reacting with iron sulfide to produce hydrogen and a solid solution consisting of FeS and S_2. In the second step, the solid solution is decomposed at high temperatures to recover sulfur and the iron sulfide which is reused in the first step. The rate of decomposition can be increased by the use of various catalysts such as transition metal sulfides (Chivers, Hyne and Lau 1980). Chivers and Lau (1987a, 1987b) have

demonstrated experimentally that the decomposition of hydrogen sulfide can be successfully carried out over the surface of vanadium and molybdenum sulfides. Huntley (1990a, 1990b) studied the decomposition of hydrogen sulfide on the 110 plane of Ni.

2.3.2 Hydrogen Sulfide Generation

Hydrogen sulfide is found to exist naturally and in industrial products. In nature it occurs in combination with other sulfur compounds in most petroleum and natural gas deposits. In the laboratory, it is created by the action of dilute sulfuric acid or hydrochloric acid on ferrous sulfide (Treadwell and Hall 1956) in a Kipp generator. Heath (1954) describes a hand-operated high-pressure hydrogen sulfide generator. The production of hydrogen sulfide for analytical purposes from mixtures of sulfur and hydrocarbons was also reported by Vigide and Hermida (1959).

The most economical methods of generating H_2S for use as a reductant for SO_2 depends on the nature of each process and hence varies. In a process developed by Home Oil Co.Ltd (Elliott et.al. 1984), hydrogen sulfide generation is based on the reaction of methane, sulfur and steam in a fixed-bed catalytic reactor. The conversion efficiency of this process was reported to be greater than 95%. The main drawback was found to be the high cost of raw materials due to the use of methane and elemental sulfur. In a process developed by Allied Chemical Co., sulfur dioxide is reduced partially into H_2S by methane, which yields a product gas with an H_2S/SO_2 ratio of roughly 2:1 and which satisfies the requirements for the second-stage Claus reaction. This process was first successfully implemented as a method for SO_2 emission control

in the early 1970's at a sulfide ore roasting facility in Falconbridge, Canada (Elliott et.al. 1984). It appears to be a suitable choice for smelters where the inexpensive natural gas is available.

In a closed-loop aqueous carbonate process (ACP), developed by the US Environmental Protection Agency (EPA), by-products of an FGD process (mainly Na_2SO_3) are reduced into the mixture containing approximately 62% Na_2S by coal. The reduced mixture is dissolved in the aqueous medium which is then filtered to remove unreacted carbon and ash. The clear liquor reacts with CO_2 to produce a gas mixture of H_2S and CO_2 and sodium carbonate (Kohl and Riesenfeld 1985). The use of coal as a reductant is the main advantage of ACP and makes the process well-suited for use by those coal burning power plants which use sodium carbonate as the prime absorbent of SO_2 emission.

Jia and Lu (1992) studied the kinetics of hydrogen sulfide generation from calcium sulfide with carbon dioxide. Calcium sulfide may be produced by reducing $CaSO_3$ and $CaSO_4$, which are the by-products of the lime/limestone process for the removal of sulfur dioxide from flue gases. The lime/limestone process is currently the predominant process used for power plant flue gas scrubbing. Ng, Jia and Lu (1993) investigated the kinetics of hydrogen sulfide generation from sodium sulfide with carbon dioxide, the key step in the ACP process as introduced by the EPA (Kohl et.al. 1984) and another similar process proposed by Engineered Systems International (ESI) (US Patent No.4,241,041). Carbonation conversion of aqueous sodium sulfide to gaseous hydrogen sulfide has been found to be kinetically feasible.

2.4 Aqueous Chemistry of Sulfur Species

2.4.1 Soluble Sulfides and Polysulfides

Sulfides are significant constituents of alkaline wastes produced by petroleum refining and pulp-paper industries. Minor sources of sulfide waste include tanneries, gas-manufacturing plants and textile mills (Karchmer 1970).

Aqueous hydrogen sulfide behaves as an extremely weak acid in solution. Soluble sulfides readily dissolve sulfur to form polysulfides in basic solution. Upon acidification, polysulfides decompose, forming hydrogen sulfide and free sulfur. These polysulfides can act both as reducing and oxidizing agents (Chen and Morris 1972).

In aqueous solution the polysulfides, $S^{=}_2$ and $S^{=}_3$ are unstable and subject to rapid disproportionation. Only mono-, tetra- and pentasulfides are stable in solution (Schwarzenbach and Fisher 1960). The following three equations show the disproportionation and their equilibrium relationships:

$$3S_2^{2-} + 2H_2O \rightleftharpoons 2HS^- + 2OH^- + S_4^{2-} \qquad (2\text{-}1)$$

$$3S_3^{2-} + H_2O \rightleftharpoons HS^- + OH^- + 2S_4^{2-} \qquad (2\text{-}2)$$

$$4S_4^{2-} + H_2O \rightleftharpoons HS^- + OH^- + 3S_5^{2-} \qquad (2\text{-}3)$$

The acidity constants of each species are as follows, all at 20 °C and $\mu_i = 0.1$, where μ_i is the ionic strength of the solution (Schwarzenbach et.al. 1960; Widmer and Schwarzenbach 1964):

$$H_2S \rightleftarrows H^+ + HS^-; \quad pK = 6.83 \tag{2-4}$$

$$HS^- \rightleftarrows H^+ + S^-; \quad pK = 14.15 \tag{2-5}$$

$$H_2S_4 \rightleftarrows H^+ + HS_4^-; \quad pK = 3.8 \tag{2-6}$$

$$HS_4^- \rightleftarrows H^+ + S_4^-; \quad pK = 6.3 \tag{2-7}$$

$$H_2S_5^- \rightleftarrows H^+ + HS_5^-; \quad pK = 3.5 \tag{2-8}$$

$$HS_5^- \rightleftarrows H^+ + S_5^-; \quad pK = 5.7 \tag{2-9}$$

where pK = $-\log_{10}$K. Thus, H_2S_4 and H_2S_5 are much stronger acids than H_2S and are closer to complete ionization in neutral pH range. The predominant sulfide species present in natural waters between pH 6.5 to 8.5 are H_2S, HS^-, $S_4^=$ and $S_5^=$.

2.4.2 Elemental Sulfur

Sulfur is one of the few solid elements which is found in free state. Despite its abundance in the earth's crust and its environmental significance, many sulfur reaction mechanisms have yet to be explored. The readiness of the formation of the S-S bond and consequently long chains, coupled with multiple valencies, give rise to a large number

of sulfur oxyanions, whose relationships are not yet fully clarified (Chen 1970). It is known that the 8-member ring is thermodynamically stable with respect to all other forms of sulfur at room temperature (Bartlett, Lohaus and Weis 1958; Bartlett, Cox and Davis 1961).

When sulfur disproportionates in basic aqueous solution to sulfide and sulfur-oxyanion, the type of oxyanion formed depends on the base used and the reaction temperature. At temperatures near 100°C in aqueous solutions of sodium or ammonium hydroxide, the disproportionation of sulfur proceeds according to the following equation to give bisulfide and thiosulfate (Tartar and Draves 1924; Farr and Ruhoff 1956; Rasmussen, Hansford and Sachanen 1946; Rice and Sparrow 1953; Schulek and Koros 1952 and 1953):

$$1/2S_8 + 4OH^- \rightleftarrows S_2O_3^{2-} + 2HS^- + H_2O \qquad (2\text{-}10)$$

Conversely, it has been reported that magnesium hydroxide reacts to form sulfate and bisulfide at 225 °C (Datta 1952), while calcium hydroxide yields to sulfite (Bertozzi, Davisand and Fettes 1956). Between 250 to 350 °C, both sodium and ammonium hydroxide (Toland 1955) produce sulfate as the sulfur-oxyanion, although if certain conditions are met, sulfite can also form (Bertozzi 1957). A study by Pryor (1960) has shown that sodium thiosulfate decomposes to form sulfide and sulfate at high temperatures, in contrast with the room temperature, acid-catalyzed decomposition of sodium thiosulfate to sulfur and sulfite (Davis 1958).

Since bisulfide can convert sulfur to polysulfide in a wide range of reaction

temperature (Arntson, Dickson and Tunell 1958; Bartlett, Lohaus and Weis 1958), the reactions written for the disproportionation of S_8 may actually involve polysulfide, such as the following:

$$HS_5^- + 4OH^- \rightleftharpoons S_2O_3^{2-} + HS^- + H_2O \qquad (2\text{-}11)$$

2.4.3 Thiosulfate

Sulfite reacts with sulfur in alkaline solution to form thiosulfate according to the following reaction:

$$HSO_3^- + \frac{1}{8}S_8 \rightleftharpoons S_2O_3^{2-} + H^+ \qquad (2\text{-}12)$$

The reverse reaction can be brought about by weak acid. Sodium thiosulfate solution becomes turbid if exposed to the carbonic acid or air. The sulfur precipitated is amorphous and often initially colloidal (Chen 1970).

Thiosulfate may also be formed through the decomposition of higher polythionates in the presence of sulfite and sulfide (Pryor 1960) according to the following reactions:

$$S_6O_6^{2-} + SO_3^{2-} \rightarrow S_5O_6^{2-} + S_2O_3^{2-} \qquad (2\text{-}13)$$

$$S_5O_6^{2-} + SO_3^{2-} \rightarrow S_4O_6^{2-} + S_2O_3^{2-} \qquad (2\text{-}14)$$

$$S_4O_6^{2-} + SO_3^{2-} \rightarrow S_3O_6^{2-} + S_2O_3^{2-} \quad (2\text{-}15)$$

$$S_4O_6^{2-} + S^{2-} \rightarrow 1/8S_8 + 2S_2O_3^{2-} \quad (2\text{-}16)$$

In addition to the disproportionation of sulfur in alkaline solution, disproportionation of dithionite (Rinker, Lynn, Mason and Corcoran 1965) also gives thiosulfate:

$$2S_2O_4^{2-} + H_2O \rightarrow 2HSO_3^- + S_2O_3^{2-} \quad (2\text{-}17)$$

This disproportionation is rapid in acid solution, and, since thiosulfate then decomposes to S and $SO_3^{=}$, its final products are elemental sulfur and sulfite.

2.4.4 Sulfite and Bisulfite

Sulfur dioxide dissolves readily in water to form solutions of H_2SO_3. When the partial pressure of the gas phase is one atmosphere, the concentration is 1.34 M at 25 °C. This sulfurous acid is a dibasic weak acid, with the following two ionization constants (Latimer 1964):

$$H_2SO_3 \rightleftarrows H^+ + HSO_3^- \quad (2\text{-}18)$$

$$HSO_3^- \rightleftarrows H^+ + SO_3^{2-} \quad (2\text{-}19)$$

In acidic and neutral solutions, bisulfite is the predominant species. When the concentration of bisulfite is high, appreciable fractions of disulfite (metabisulfite or pyrosulfite) ions occur in equilibrium with bisulfite according to the following reaction:

$$2HSO_3^- \rightleftharpoons S_2O_5^{2-} + H_2O \qquad (2\text{-}20)$$

Upon heating, the disulfites evolve SO_2 gas and become sulfites (Karchmer 1970b):

$$S_2O_5^{2-} \rightarrow SO_3^{2-} + SO_{2(g)} \qquad (2\text{-}21)$$

In basic solution, sulfite is not stable in the presence of other sulfur-containing species and is subject to rapid oxidation in the presence of dissolved oxygen. The oxidation of sulfite ions by oxygen has been shown to proceed by way of a free radical mechanism (Backstrom 1927 and 1929; Alyea and Backstrom 1929) which is very sensitive to catalyst and inhibition. Moreover, compounds that are capable of breaking the reaction chain serve as effective inhibitors of the oxidation process while substances capable of initiating the reaction chain act as catalysts.

Oxidation of sulfite with manganese dioxide gives dithionate (Price and Oal 1962):

$$2SO_3^{2-} + MnO_2 + 4H^+ \rightarrow Mn^{2+} + S_2O_6^{2-} + 2H_2O \qquad (2\text{-}22)$$

On the other hand, oxidation by strong oxidants such as Fe^{3+}, HOCl and H_2O_2 result in the formation of sulfate:

$$HSO_3^- + H_2O_2 \rightarrow SO_4^{2-} + H_2O + H^+ \qquad (2\text{-}23)$$

Sulfide may destroy sulfites by reducing them to sulfur when the solution is acidified (Karchmer 1970b):

$$2S^{2-}+SO_3^{2-}+\ H^+\ \rightarrow\ \frac{3}{8}S_8+3H_2O \qquad (2\text{-}24)$$

2.4.5 Dithionite, Dithionate and Polythionates

Aqueous solutions of dithionites, if acidified with dilute mineral acid, turn red, become yellow on standing, and then precipitate sulfur and evolve sulfur dioxide (Thorne and Roberts 1949). Dithionites are prepared by reducing sulfites (Brasted 1961). The reduction of sulfite in aqueous solution containing excess zinc dust gives the dithionite ion, $S_2O_4^{=}$. This ion is not stable in aqueous solution and hence slow disproportionation takes places (Cotton and Wilkinson 1967) as follows:

$$2S_2O_4^{2-}+H_2O \rightleftarrows S_2O_3^{2-}+2HSO_3^- \qquad (2\text{-}25)$$

On the other hand, the dithionate ion ($S_2O_6^{=}$) is one of the most stable sulfur-oxyanions in aqueous solution. It is usually obtained by the oxidation of sulfite with manganese dioxide (Cotton and Wilkinson 1967) through the following reaction:

$$MnO_2+2SO_3^{2-}+4H^+ \rightleftarrows Mn^{2+}+S_2O_6^{2-}+2H_2O \qquad (2\text{-}26)$$

According to Brasted (1961), when hydrogen sulfide is passed into a solution of sulfurous acid slowly and intermittently over a period of several days, some of the sulfur is precipitated as elemental sulfur. At the same time, the reactions between the nascent sulfur and the sulfurous acid yield highly variable mixtures of polythionic acids, consisting mostly of tetra- and pentathionic acids, i.e. the so-called Wackenroder liquid

(Nickless 1968). The solution is strongly acidic, odourless and unstable. The higher acids gradually degrade to tri-thionic acid and finally decompose into sulfuric acid, sulfur dioxide, and free sulfur. These polythionic acids are easily oxidized to sulfuric acid, and they revert to thiosulfate if boiled with alkalies (Remy 1956).

Polythionates have the general form (SO_3-S_x-SO_3). Tri, tetra, penta and hexa-thionates have been identified on different occasions. Polythionates having more than six sulfur atoms per molecule are not stable in alkaline solution (Weitz and Spohn 1956). Some of the known reactions are the following:

[1] Degradation of higher thionates to trithionate and thiosulfate in the presence of sulfite in neutral or alkaline solution (Stamm 1941):

$$S_{x+3}O_6^{2-} + xSO_3^{2-} \rightleftarrows S_3O_6^{2-} + xS_2O_3^{2-} \qquad (2\text{-}27)$$

[2] Reduction of polythionate with sulfide in alkaline or neutral solution (Hansen 1933):

$$S_nO_6^{2-} + S^{2-} \rightleftarrows (n-3)S + 2S_2O_3^{2-} \qquad (2\text{-}28)$$

[3] Decomposition of hexa-, penta- and tetra-thionates in alkaline solution. Although $S_3O_6^{-2}$ is stable in mildly alkaline solution, it decomposes further in concentrated alkali (Geohring, Appel and Helbving 1947)as follows:

$$2S_3O_6^{2-} + 6OH^- \rightleftarrows S_2O_3^{2-} + 4SO_3^{2-} + 3H_2O \qquad (2\text{-}29)$$

$$S_6O_6^{2-} \rightleftarrows S_5O_6^{2-} + 1/8S_8 \qquad (2\text{-}30)$$

Since colloidal sulfur tends to develop in polythionate solutions, SO_3^{-2} is often not detectable, for it reacts readily with the sulfur to form thiosulfate. Conversely, thiosulfate is not stable in acidic solution and has a tendency to form polythionate in the presence of other sulfur-containing species (Pollard and Jones 1959).

2.5 Mass Transfer at Interface between Phases

Many industrial processes involve transport of solutes from one phase to another. This is the case in gas-absorption, gas-desorption, liquid-extraction and other separation processes. The solute is transported from the bulk of one phase to phase boundary, or interface, and then from the interface to the bulk of the second phase.

2.5.1 The Two-Film Theory

Whitman and Lewis (1924) first proposed the additivity of the transport resistances on the two sides of an interface. The additivity concept assumes that there is no resistance to transport at the actual interface, i.e., within distances corresponding to molecular mean free paths in the two phases on either side of the phase boundary. This is equivalent to assuming that the phases are in equilibrium at the actual points of contact at the interface. For practical purposes of process design, it is convenient, if not essential, to express transport rates in terms of bulk phase concentrations. It is helpful, therefore, to define an overall mass transfer coefficient, which is the reciprocal of the

sum of the resistances in series. Figure 2.6 illustrates the situation at a point in a mass-transfer device where a solute is being transferred at constant rate from phase G to phase L, the bulk of each being well mixed. The activity of solute in phase P is a_{PB} and in Q it is a_{QB}. Assuming equilibrium at the interface, the activities a_{Pi} and a_{Qi} are equal at the plane of contact. An overall coefficient (K_a) is defined by the following steady-state flux equations:

$$N_A = k_P(a_{PB}-a_{Pi}) = k_Q(a_{Qi}-a_{QB}) = K_a(a_{PB}-a_{QB}) \qquad (2\text{-}31)$$

Then, since $a_{Pi} = a_{Qi}$,

$$\frac{1}{K_a} = \frac{1}{k_P}+\frac{1}{k_Q} \qquad (2\text{-}32)$$

This states that the overall resistance is the sum of the two individual resistances.

For gas absorption, it is often convenient to employ solute mole fraction in the gas and solute volume concentration in the liquid. Henley and Prausnitz (1962) concluded that thermodynamic activity is not necessarily an improvement over the use of concentration as the driving force for mass transfer. If concentrations at equilibrium can be represented by Henry's law, $Y_i = Hc_i$, Eqs.2.31 and 2.32 become

$$N_A = k_Y(Y_{PB}-Y_{Pi}) = k_c(c_{Qi}-c_{QB}) = K_Y(Y_{PB}-Hc_{QB}) = K_c(\frac{Y_{PB}}{H}-c_{QB}) \qquad (2\text{-}33)$$

whence

$$\frac{1}{K_Y} = \frac{1}{k_Y} + \frac{H}{k_c} = \frac{H}{K_c} \qquad (2\text{-}34)$$

If the gas is highly soluble in the liquid, H will be small and $K_Y = k_Y$. In this case the liquid-side resistance is negligible and the flux is $k_Y(Y_{PB}-Y^*_{QB})$, where Y^*_{QB} is the gas mole fraction corresponding to equilibrium with the bulk liquid. Conversely, if the gas is insoluble (H large), the gas-side resistance $1/k_Y$ becomes negligible in comparison with the liquid-side resistance H/k_c. The relative magnitudes of the individual resistances evidently depend on gas solubility, as represented by the Henry's-law constant. According to Freier (1976), the Henry's-law constants of H_2S and SO_2 are 4.8 and 0.48 l/mol under one atmosphere, respectively.

2.5.2 Validity of The Two-Film Theory

The two-film theory employs the assumption that the phases are in equilibrium at the interface, i.e., that there is no diffusional resistance at the phase boundary (Eqs. 2.32 and 2.34). Significant interfacial resistances are encountered in some systems, however, as in the case of liquids containing surfactants which tend to concentrate at the surface. Furthermore, the diffusion of solute sometime causes an interfacial turbulence which is not related to the turbulence in the bulk of the flowing fluid. This tends to increase the rate of transfer and is equivalent to a negative interfacial resistance (Sherwood, Pigford and Wilke 1973).

Lu and Hamielec (1973) studied the role of interfacial tension in a slag/metal

reaction with mass transfer in the slag as the controlling step. They concluded that the Marangoni effect (interfacial convection due to a gradient of interfacial tension resulting from a gradient of concentration of surfactant) would lead to the observable results of fast reaction rates. Lewis (1953) and Lewis and Pratt (1953) noted ripples, erratic pulsations, and surface motion of drops in the course of measurements of interfacial tension by the pendant-drop method. Lewis observed abnormally high mass-transfer rates where marked "interfacial turbulence" was seen. According to Orell and Westwater (1962), it is clear that the turbulence noted is not that induced by motion of the bulk fluid. Olander (1964) found that interfacial turbulence caused a fourfold increase in the rate of mass transfer of nitric acid from isobutanol to water in a stirred vessel.

2.5.3 Effect of Chemical Reaction on Mass Transfer between Phases

To study the effect of chemical reaction on mass transfer, Sherwood et. al. (1973) introduced a "reaction factor" ϕ for an irreversible, first-order reaction in the liquid. The reaction factor is defined as follows:

$$\phi = \frac{k_L}{k_L^o} = \phi(k_f) \qquad (2\text{-}35)$$

where k_L and k_L° are mass transfer coefficients with and without chemical reaction; k_f is rate constant of first-order reaction (1/s).

Consider a pure gas A passing through a stirred-tank reactor containing V cubic centimeters of liquid. The gas is dispersed into the liquid by an agitator, forming a

steady stream of bubbles which present a large surface to the liquid. The liquid flows through continuously at the volumetric rate Q ml/s. Based on a steady-state material balance, the total rate of solution of solute A (R_s) is found to be:

$$R_s = k_L a V(C_i - C) = \frac{k_L^o a\theta\phi(1+k_I\theta)}{1+k_I\theta+k_L^o a\theta\phi} C_i Q \qquad (2\text{-}36)$$

where θ=V/Q is nominal liquid-holding time in the reactor; a is G/L interfacial area (cm^2/cm^3); C is concentration of A in the liquid (g-mole/cm^3) while C_i is the value at the interface. The factor C_iQ on the right of Eq.2.36 represents the rate of solution if the liquid leaves the tank physically saturated with A.

A convenient form of Eq.2.36 is obtained by solving for the reciprocal of the relative rate of solution, $r_s=R_s/C_iQ$, obtaining:

$$r_s^{-1} = \frac{1}{k_L^o a\theta\phi} + \frac{1}{1+k_I\theta} \qquad (2\text{-}37)$$

The two terms on the right may be thought of as representing the resistances to interfacial mass transfer and to chemical reaction, respectively. $k_L^oa\theta$ corresponds to the number of transfer units for a purely physical process. When $k_L^oa\theta$ is large, r may be determined by $k_I\theta$; for a large $k_L^oa\theta$ and a negligible reaction rate, r approaches unity; for large value of rate coefficient k_I, the rate of solution will be dominated by the first term. Eq.2.37 brings out the fact that, as Astarita (1966) pointed out, there are two different time scales which affect the performance of all gas absorbers in which chemical

reactions occur: the time scale of the reaction itself, determined by its rate constant, and the diffusion time scale, determined by D/k_L^{o2}. In addition, there is also a third time scale set by the size of the reactor, here the nominal liquid-holding time V/Q.

2.5.4 Simultaneous Diffusion and Chemical Reaction near An Interface

To account for the influence of a chemical reaction on the concentration of a diffusing species in the important region near an interface between phases, a reaction-rate expression has to be included in the unsteady-state diffusion equation, obtaining

$$D\frac{\partial^2 C_i}{\partial y^2} = \frac{\partial C_i}{\partial t} + R_i(C) \qquad (2\text{-}38)$$

where the term $R_i(C)$ represents the rate of loss of component i owing to chemical reaction per unit volume of the fluid (if component i is generated, $R_i(C)$ is negative). Development of the theory of diffusion-affected reactions can take on as many forms as there are different expressions for the R_i and different fluid-flow situations.

Several assumptions are usually made about the surface geometry and the fluid motion, namely, the film model (Lewis and Whitman 1924), the penetration model (Higbie 1935), and the surface replacement model (Danckwerts 1951). In the film model, the film thickness, y_0 is unknown. In the penetration model and the surface replacement model, the unknowns are the interphase exposure time (t_i) and the surface element mean lifetime (s_i). Estimation of each of these quantities required use of an experiment value of the mass transfer coefficient without chemical reaction, k_L°. Thus,

$$y_0 = \frac{D}{k_L^o} \tag{2-39}$$

$$t_i = \left(\frac{4D}{\pi k_L^{o2}}\right)^{1/2} \tag{2-40}$$

$$s_i = \left(\frac{k_L^{o2}}{D}\right)^{1/2} \tag{2-41}$$

When a reaction effect is studied, the theory has to be chosen and the corresponding parameter has to be estimated. This is for the reason that either y_0, t_i or s_i will appear in the models in combination with the reaction rate constants, indicating that when there are separate and independent time scales both for diffusion and for reaction.

Hatta (1928, 1932) studied a first-order irreversible reaction based on the film model, which led to the following equation:

$$k_L = (Dk_1)^{1/2} \tag{2-42}$$

According to surface-replacement model (Danckwerts 1951), Sherwood and his co-worker (1975) found the following equation for first-order reactions:

They also summarized the results for first-order reaction based on the penetration model as follows:

$$\phi = (1+\frac{Dk_I}{k_L^{o2}})^{1/2} \qquad (2\text{-}43)$$

$$\lim_{k_I \to 0} k_L = k_L^o \qquad (2\text{-}44)$$

$$\lim_{k_I \to \infty, K \neq \infty} k_L = (1+K)k_L^o; \quad \lim_{k_I \to \infty, K \to \infty} k_L = \sqrt{Dk_I} \qquad (2\text{-}45)$$

where K is equilibrium constant for first-order reaction. Fig.2.7 shows a comparison of three models of interfacial mass transfer accompanied by first-order irreversible chemical reaction. The differences among them are not significant.

2.6 Bubbles And Bubble Reactors

Schaftlein and Russell (1968) were the first to introduce the "ideal reactor" concepts in analyzing two-phase flow reactors. They classified these reactors into the following categories: [1] Continuous Flow Tank Reactor (CFTR), in which both the gas and liquid flowed through continuously; [2] Semi-flow Batch Reactors (SFBR), in which only the gas flowed through continuously while the liquid remained in it during the entire reaction period; and [3] Batch Reactor (BR), in which a certain amount of gas and liquid were kept and allowed to react in batch-wise manner. A bubble reactor has been used for this study in both modes of the SFBR and the CFTR. Consequently, in the following section bubble mechanics as well as the characteristics and mass transfer processes which occur in a bubble reactor will be briefly reviewed.

2.6.1 Bubble Mechanics

In order to analyze the results obtained in a bubble reactor, knowledge of the basic behaviour of gas bubbles is required. The review of bubble mechanics will focus on the formation and the motion of bubbles in liquids. Investigations on bubble mechanics are typically conducted in a system without chemical reaction.

According to Brimacombe (1991), when gas is injected into a liquid the gas disperses in the liquid phase in three different forms, namely bubble, bubbly plume and jet, corresponding to a low, moderate and high gas flow rates. The definition of low, moderate and high gas flow rates depends on the physical and chemical conditions of system. At very low gas flow rates, single bubbles are released when the buoyant force just overcomes the surface tension, at which time the bubble diameter is proportional to $d_o^{1/3}$ (d_o is orifice diameter); the size of bubble is independent of gas flow rate (the constant volume regime). As the gas flow rate increases, a force balance between the buoyancy and the force required to accelerate the liquid away from the expanding gas-liquid interface controls the bubble size. The constant volume regime of bubble is replaced by a constant frequency regime where the volume of bubble is almost proportional to gas flow rate (Datta, Napier and Newitt 1950; van Krevelen and Hoftijzer 1950; Irons and Guthrie 1978). When the gas flow rate increases further to a critical value, the growth of the interface instability is so slow compared to the interface movement that any perturbation would be swept away before it breaks the interface. As a result, a gas jet forms (Zhao and Irons 1990).

When a single gas bubble rises in a liquid, its size, shape and motion are mainly

dependent on the physical properties of the liquid and the gas flow rate (Haberman and Morton 1954; Bowman 1960; Leibson, Holcomb, Cacoso and Jacmic 1956; Jackson 1964). Grace (1973) proposed a generalized graphical correlation to allow bubble shape and velocities to be predicted for any Newtonian fluid of practical importance. Very small bubbles ($d_b < 0.1$ cm air in water) behave as rigid sphere (Sherwood et.al. 1973). Bubbles of intermediate sizes ($0.2 < d_b < 1.5$ cm air in water) become flattened and distorted, with ellipsoidal shapes. Large bubbles ($d_b > 1.5$ cm) form spherical caps and rise steadily. In the case of a non-spherical bubble, d_b represents the diameter of a sphere of the same volume.

The first theoretical work based on potential flow theory to predict the rise velocity of a spherical-cap bubble in liquids is due to Davies and Taylor (1950), which led to the well-known Davies-Taylor equation for a bubble rising in a 3-D system:

$$u = \frac{2}{3}(gr)^{1/2} \qquad (2\text{-}46)$$

where r is radius of curvature for a spherical cap bubble. The deviation of the predicted u based on Eq.2-46 to that of experimental values for bubbles rising in low-viscosity liquid are within 5%. Nickens and Yannitell (1987) studied rise velocity of a large gas bubble in a closed, vertical liquid-filled tube. They found that for negligible surface tension and negligible liquid viscosity, the bubble slip velocity is given by $u = 0.434(gr)^{1/2}$. For air/water in a 2.54 cm dia tube, the inclusion of surface tension gives $u = 0.412(gr)^{1/2}$, which was reported to be consistent with experimental observation.

2.6.2 Mass Transfer to or from Single Bubbles

Mass transfer to or from single bubbles in free rise in a liquid has been studied by a great number of investigators. Extensive reviews on this subject can be found in the books by Clift, Grace and Weber (1978) and by Azbel (1981). According to Sherwood et. al. (1975), mass transfer coefficient (k_c) may be obtained from the equation given by Levich (1962) if d_b is less than about 0.1cm.

$$\frac{k_c d_b}{D} = 1.0\left(\frac{d_b u}{D}\right)^{1/3} = 1.0Pe^{1/3} \qquad (2\text{-}47)$$

where k_c is mass transfer coefficient; u is terminal velocity of bubble; Pe is Peclet number. Various authors have found that the following equation fits the data fairly well for bubbles $d_b > 0.5$ cm (Calderbank 1967).

$$\frac{k_c d_b}{D} = 1.13\sqrt{\frac{d_b u}{D}} = 1.13Pe^{1/2} \qquad (2\text{-}48)$$

This equation was originally obtained by Bousinesq from potential flow theory for drops. With u essentially constant, this means that k_c is proportional to $d_b^{-1/2}$, and $k_c a$ is proportional to $d_b^{3/2}$.

Experimental studies on the mass transfer characteristics of a single bubble rising in a column of liquid was carried out by Coppock and Meiklejohn (1951). Diendoerfer and Humphrey (1961) studied the rate of change in volume and surface area of a single bubble rising up a long column of water. They found that the instantaneous mass transfer coefficient was a function of the column height. Similar observations were made

by Leonard and Houghton (1963). Lochiel and Calderbank (1964) developed theoretical equations to describe the mass transfer for solid spheres and rapidly circulating bubbles. Their models were then compared with experimentally observed physical mass transfer data (Calderbank and Lochiel 1964). Johnson and Akehata (1965), and Johnson, Hamielec and Houghton (1967) investigated the enhancement of mass transfer from gas bubbles due to chemical reaction and obtained numerical solutions of steady-state forced-convection mass transfer around single circulating sphere, which compared favourably with the earlier work of Lochiel and Calderbank. The theoretical models for the gas-liquid mass transfer rate at the roof of a single spherical-cap have been developed by Baird and Davidson (1962), Lochiel and Calderbank (1964) and Coppus and Rietema (1980). The basic assumption is that the concentration boundary layer is relatively thin compared to the momentum boundary layer due to the large value of the Schmidt number. The mass transfer rate at the base of a single spherical-cap bubble has been studied by Calderbank et.al. (1970), Brignell (1974), Weber (1975) and Coppus and Rietema (1980).

The difficulty in obtaining a good correlation of k_c for bubbles is enormous, since there are so many variables (Sherwood et. al. 1975). In view of this, it is interesting that for non-reacting gases in pure water with D in the vicinity of $1x10^{-5}$ to $2x10^{-5}$ cm^2/s, much of the data show k_c to fall in the relatively narrow range of 0.0015 to 0.010 cm/s, for d_b 0.2 to 5.0 cm.

2.6.3 Bubble Reactors

Bubble reactors are widely used as air-agitated fermenters, sometimes several feet in diameter and more than 50 ft tall (Sherwood et.al. 1975). They cannot handle the high gas flow rates attainable in packed columns due to the high gas pressure drop, but they are attractive for use as chemical reactors. They may be operated batchwise with respect to the liquid, or with either cocurrent or counterflow of gas and liquid. They are relatively inexpensive and easily cleaned. More importantly, the bubble swarms provide enormous surface per unit volume for gas-liquid contacting: 3-mm spherical bubbles with a gas holdup of 25% provide 46 m^2/m^3 (more than most tower packings).

Many investigators have also studied the mass transfer characteristics of bubble reactors. Li, West, Vance and Moulton (1965) investigated the liquid phase mass transfer coefficients of a bubble chain. Their results compared favourably with those predicted by the penetration model for cases with and without chemical reactions. Similar results were found by Yau (1966), Yau, Hamielec and Johnson (1969) in the study of oxidation of acetaldehyde in a single orifice bubble reactor. The relationships between the mass transfer coefficients and bubble size, bubble frequency and seal height were investigated by Bowman (1960). A review on the mass transfer in gas-liquid contacting systems was given by Sideman, Hortacsu and Fulton (1966). Unfortunately, they found that in many studies, the suggested correlations were limited to the specific equipment and range of operating conditions used by the researchers. Mathematical models (Galor and Hoelscher 1966; Johnson, Hamielec and Houghton 1967) have been built to account for bubble interaction and particle distribution in bubble swarms.

In a bubble reactor, the gas-side resistance is usually negligible in comparison with that in the liquid (Mehta and Sharma 1966). k_L in a bubble column varies little with operating conditions; k_La depends primarily on a, which various widely (Sherwood et.al. 1973). Mixing in liquid phase in a bubble column is provided solely by motion of the gas bubbles. Liquid back-mixing is rapid, the liquid maintaining a nearly uniform concentration top to bottom, even with columns having a height-to-diameter ratio of 12 or more (Yoshida and Akita 1965).

The total area of gas-liquid interface depends on the gas holdup. Gas holdup ε, defined as the volume-fraction gas in the dispersion, increases with agitation and gas flow but reaches a maximum of about 0.3 to 0.4. In the quiescent regime and steady state, gas holdup can be measured and calculated based on bubble mechanics. In the turbulent regime, it can be estimated from empirical correlations between gas holdup and superficial gas velocity (Braulick, Fair and Lerner 1965; Fair 1967b; Yoshida and Akita 1965; Akita and Yoshida 1973). Akita and Yoshida (1973) have reported extensive studies of gas absorption in bubble column 6" to 20" in diameter with aerated liquid heights up to 10 ft, using a single 0.5-cm orifice sparger. Fig.2.8 illustrates the nature of their data: A function of gas holdup, $\varepsilon/(1-\varepsilon)^4$, is proportional to the superficial gas velocity.

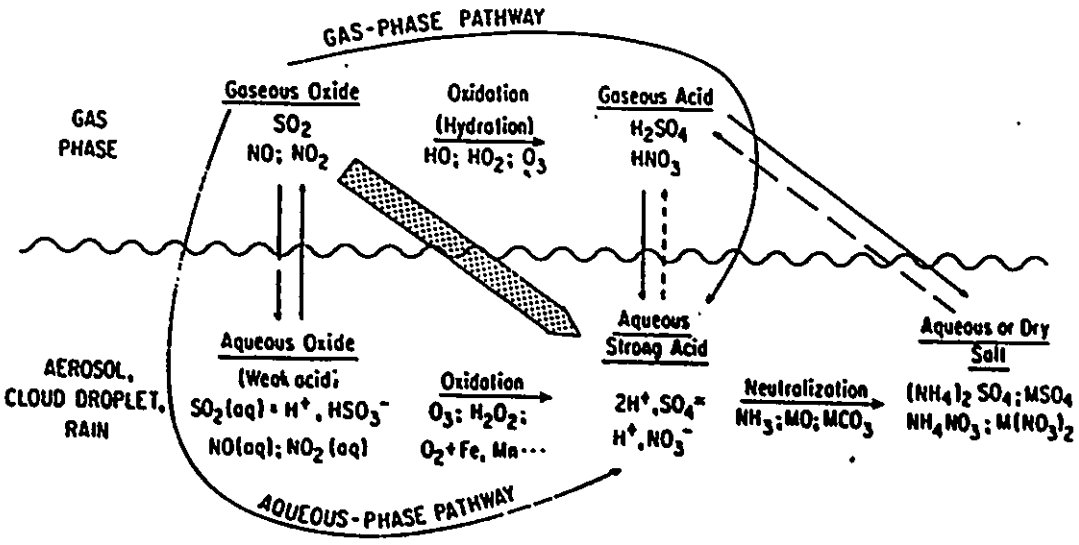

Fig.2.1: A schematic representation of pathways for atmospheric formation of sulfuric and nitric acids and their salts (after Schwartz 1986)

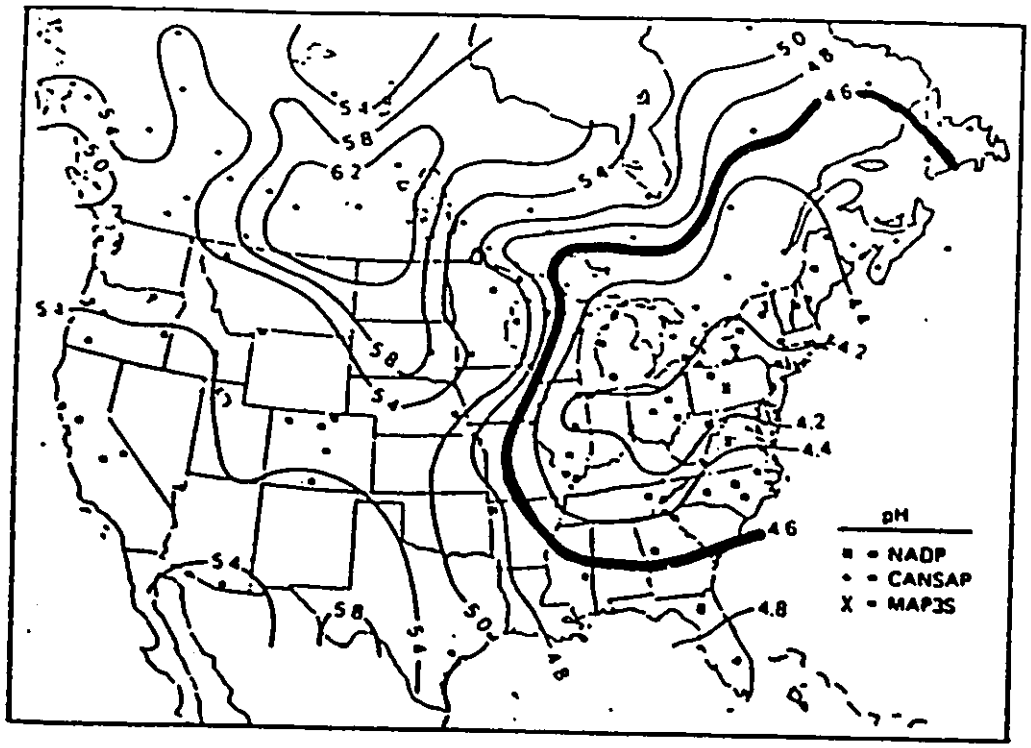

Fig.2.2: A pH contour of North America (after Elliott and Schwieger, 1984)

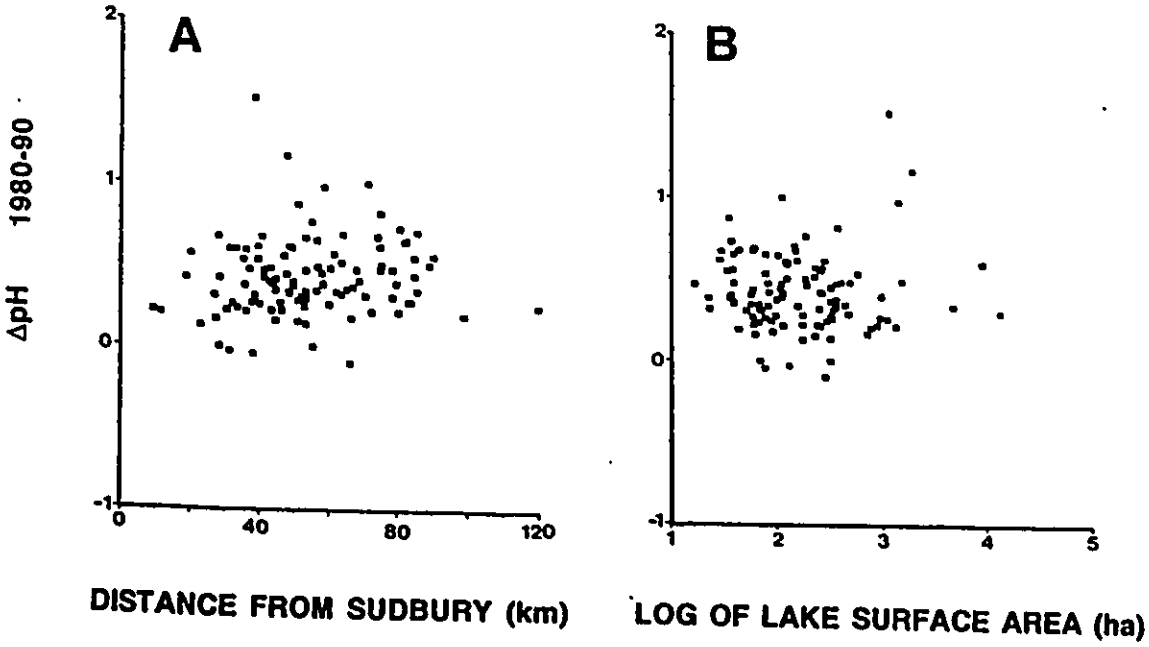

Fig.2.3: Observed change in pH between 1980 and 1990 for 103 lakes in the Sudbury area in comparison with (A) distance from smelters and (B) lake surface area (after Matuszek, Wales and Gunn 1992)

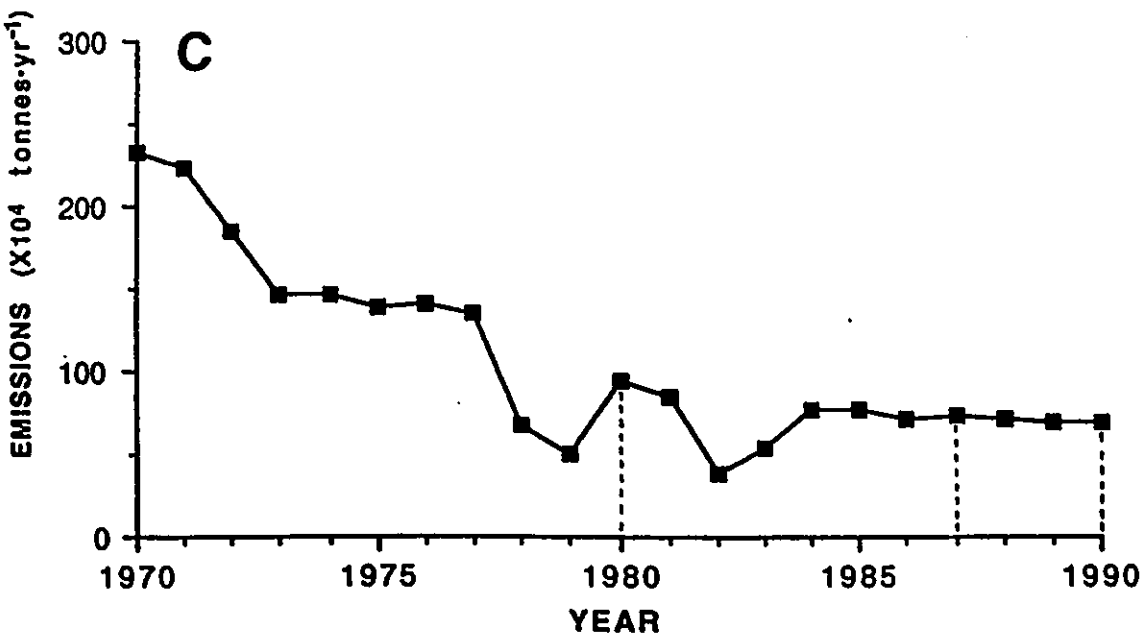

Fig.2.4: Amount of SO_2 emissions from Sudbury smelters during the period 1970 to 1990 (after Matuszek, Wales and Gunn 1992)

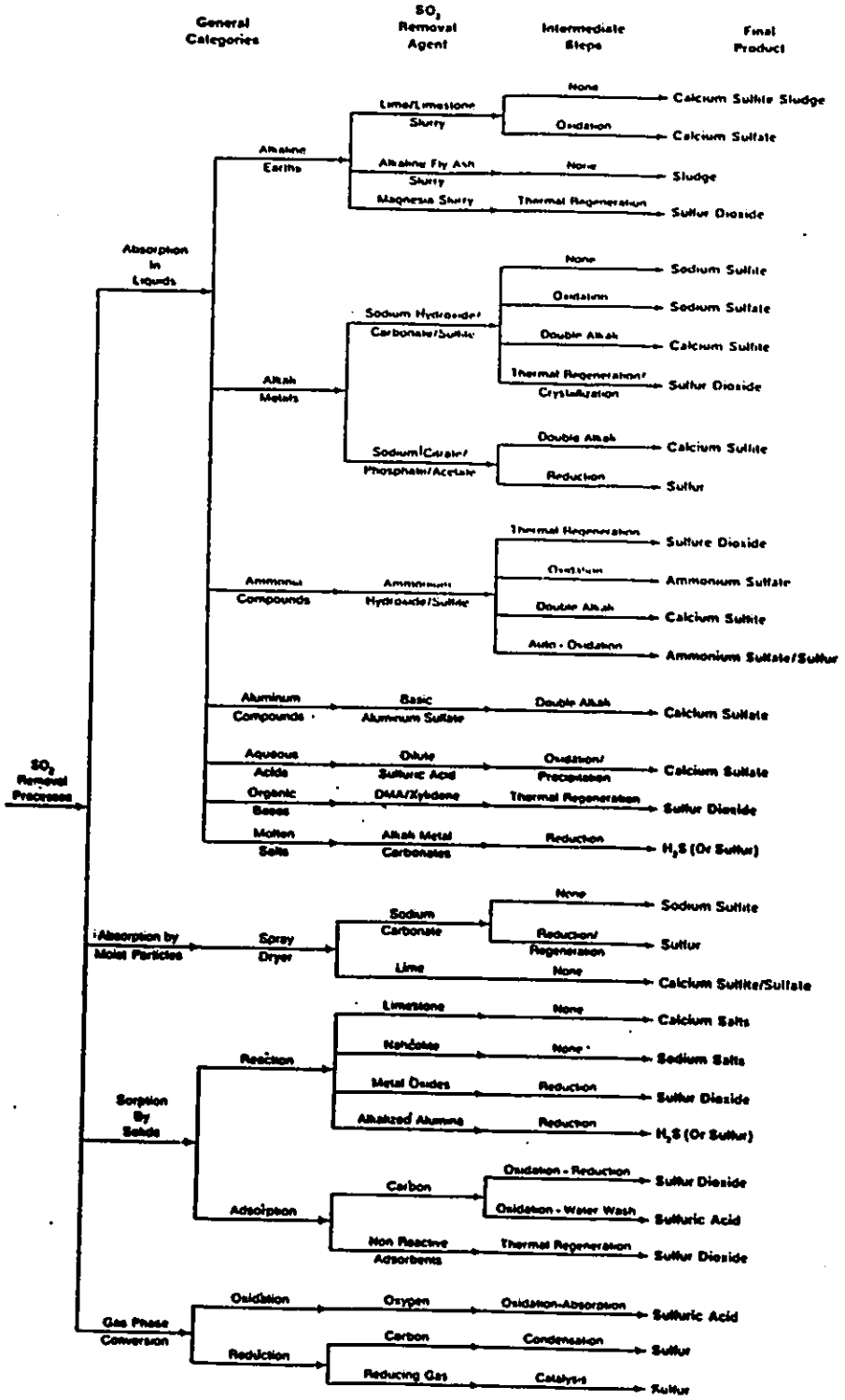

Fig.2.5: A categorization of sulfur dioxide removal processes (after Kohl and Riesenfeld 1985)

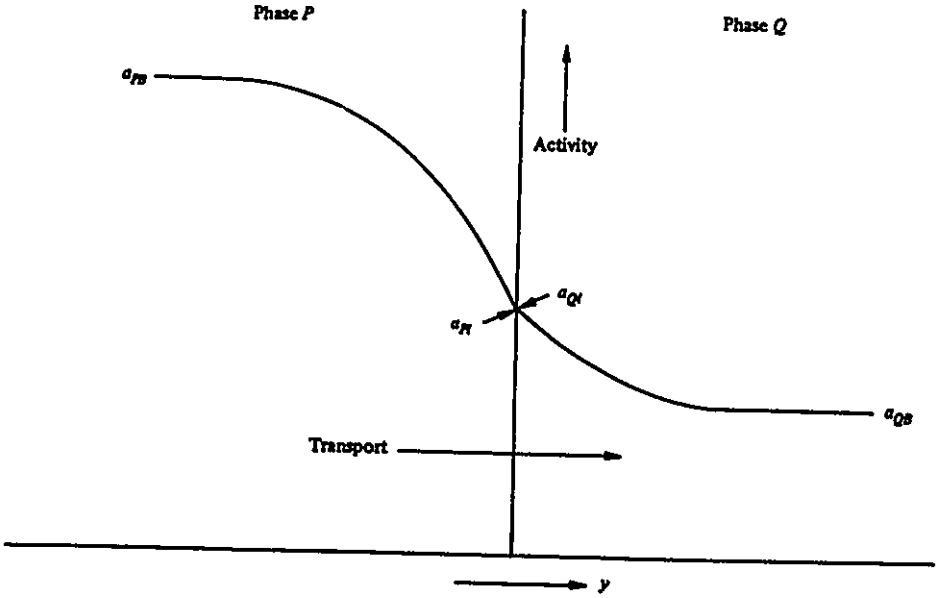

Fig.2.6: Activity gradients near a phase boundary (after Sherwood, Pigford and Wilke 1975)

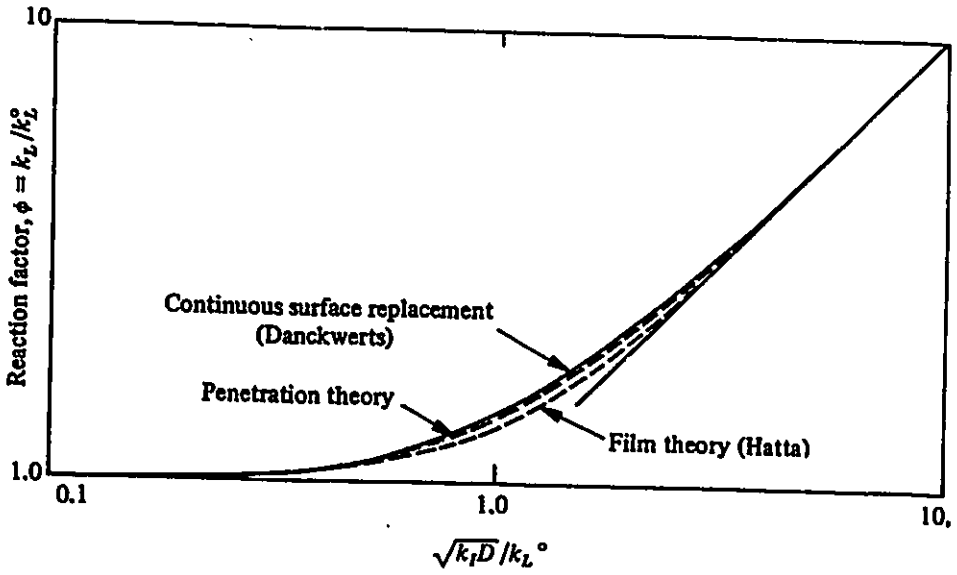

Fig.2.7: Comparison of three theories of interfacial mass transfer accompanied by first-order irreversible chemical reaction (after Sherwood, Pigford and Wilke 1975)

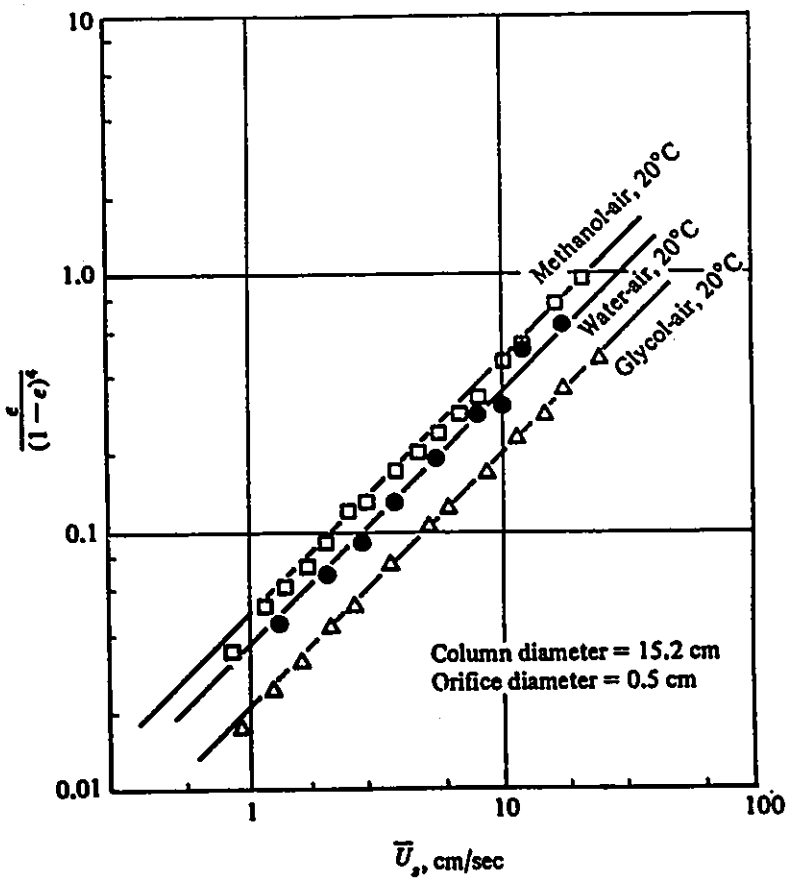

Fig.2.8: Gas holdup correlation for methanol-air, water-air, and glycol-air (after Akita and Yoshida 1973)

CHAPTER THREE

EXPERIMENTAL TECHNIQUES

In terms of experimental set-up, two types of experiments were conducted with the use of the semi-flow batch reactor (SFBR) and the continuous flow tank reactor (CFTR). In this chapter, the experimental apparatus, procedures and reagents used are described. In the sections on analytical techniques, the reliability of measurements taken is discussed.

3.1 Semi-flow Batch Reactor (SFBR) Study

In the semi-flow batch reactor, a gaseous mixture of SO_2-N_2 was continuously introduced to a column containing aqueous Na_2S solution. After the commencement of the experiment, there was no flow of liquid in or out of the system. Since the compositions of the exit gas and the solution changed significantly with time when experiments were conducted in the SFBR, the kinetics was studied by observing the relationship between the compositions of gaseous phases and that of liquid phase over wide ranges.

3.1.1 Apparatus

The reactor used in this study is shown schematically in Fig.3.1. One of the three outlets was used to insert a pH electrode. The other two were designed for

sampling when the device was used as an SFBR. The two outlets on the top of the reactor were used to feed and withdraw gases and to mount a thermocouple. Usually, gas was introduced through a fritted cylinder which was connected to a 5 mm (I.D.) glass tube. Two kinds of fritted cylinders were used (porosity: 40 to 60 microns and 80 to 100 microns). Both were 12 mm in diameter and 20 mm long. For experiments in which the effect of interfacial area was to be studied, the fritted cylinder was removed and replaced by a glass tube with a 5mm (I.D.) outlet.

All experiments were carried out isothermally. As shown in Fig.3.2, the reactor was immersed in a water bath whose temperature was controlled to within ± 1.0 °C by a Brinkmann circulator (model IC-2). Sulfur dioxide and nitrogen were delivered separately from gas cylinders, then mixed to have a pre-determined composition before its introduction into the reactor. Two rotameters, calibrated using the soap bubble method, were used to control the flow rates of sulfur dioxide and nitrogen. Between the rotameter and the reactor, there was a U-tube manometer which monitored the back pressure of the reactor. On the other side of the reactor, the exit gas passed through a condenser to remove moisture. The condenser consisted of a glass tube with three openings which was placed in a box filled with ice. Two of the openings were designed for the input and output of gas while the other was used for the withdrawal of water. After passing through the condenser, the exit gas was guided into a sampling tube. To prevent the leakage of hydrogen sulfide into the atmosphere, the exit gas from the condenser was carried to gas-washing bottles which contained an aqueous solution of sodium hydroxide (for the removal of hydrogen sulfide) before it was released to the

fume hood exhaust. For safety reasons, the experimental apparatus was contained in a confined area and vented with a fume hood.

3.1.2 Procedures

The reactor was first immersed in the water bath and was equipped with a pH electrode and a thermocouple. For each experiment a known volume (350 to 400 ml) of freshly made Na_2S solution was transferred into the reactor. After the solution and the reactor reached thermal equilibrium with the water bath, the SO_2-N_2 gaseous mixture was introduced into the solution to begin the experiment. Usually, gas samples were taken every 5 minutes when the change in gas composition was small. With the start of H_2S generation, gas samples were taken more frequently, with sampling intervals as small as 30 seconds.

Due to the generation of hydrogen sulfide, the sulfide content in the solution decreased with the increase of reaction time. With less sulfide left in the solution, the solubility of SO_2 appeared to be lower. Consequently, the continued bubbling of SO_2 led to SO_2 saturation in the solution. When a significant amount of SO_2 was detected in the exit gas, the experiment was terminated by turning off the incoming gas flow. The pH value and the temperature of solution were monitored and recorded continuously by a data logger through out the experiment.

3.2 Continuous Flow Tank Reactor (CFTR) Study

On an industrial scale, a continuous operation carried out in a packed tower or

a spray chamber is more appropriate. By using a continuous flow tank reactor (CFTR), an attempt was made to study the kinetics under a set of chosen conditions of relevance to potential commercial operation.

3.2.1 Apparatus

As shown in Fig.3.3, the experimental set-up for the CFTR was very much similar to one used for the SFBR. In the CFTR study, a peristaltic metering pump (DUNGEY INC.PS series) was set up to feed fresh liquid into the reactor and withdraw spent solution from it through two of the three outlets on its side. This pump was capable of providing a flow which ranged from 0.01 to 2000 ml/min by varying the tube size as well as the motor speed. The tubing used was made of PVC with inner and outer diameters of 3.2 and 6.4 mm, respectively. For any given tubing, the liquid flow rate depended on the speed of the motor (v) which is controlled to within $\pm 1\%$ in terms of the relative variation of speed ($\Delta v/v$). The actual flow rate was calibrated by measuring the total volume of liquid fed into the reactor by the pump for a given period of time.

3.2.2 Procedures

From the results obtained in SFBR study, it was already known that there were two sharp drops in the pH value of solution during the bubbling of SO_2-N_2 gaseous mixture into aqueous solution of sodium sulfide, when the CFTR experiments were proposed. The two drops corresponded to the start and the end of the H_2S generation. Prior to the continuous feeding and withdrawal of liquid, the procedures were the same

as one in SFBR study. The feeding of fresh liquid started when the second stage was close to the end. (i.e. just after the second drop of pH value). The spent solution was withdrawn at the same rate so that the volume of solution in the reactor remained unchanged.

After changing to the CFTR mode of operation, steady state prevailed after a period of time (up to about 30 minutes depending on experimental conditions, particularly feed rate of solution) in terms of the pH value of the solution and the H_2S content in the exit gas. Steady state conditions were maintained for another 25 to 30 minutes for a series of sampling of exit gas for chemical analysis.

3.3 Reagents Used and the Preparation of Solutions

3.3.1 Aqueous Na_2S Solution

Reagent grade Na_2S*9H_2O crystals supplied by Fisher Scientific were used to prepare aqueous Na_2S solution. Due to the hygroscopic nature of Na_2S*9H_2O crystals and about 2% sulfite and thiosulphate impurities in the Fisher reagent used, the preparation of a specific concentration of Na_2S solution could not be carried out by simply weighing solid Na_2S. Instead, the stock solution was prepared at room temperature by saturating distilled water with Na_2S*9H_2O. The actual concentration of the solution used was determined by iodometric titration with excess potassium iodate and back titration with sodium thiosulfate. To minimize the oxidation of sulfide by air, the prepared solution was stored in an air tight container.

3.3.2 Gases

Three gases were used, namely, sulfur dioxide, hydrogen sulfide and nitrogen. Sulfur dioxide and hydrogen sulfide were supplied by Canadian Liquid Air Ltd. in the form of liquid in cylinders. Purity of the anhydrous sulfur dioxide used was not less than 99.98%. The content of impurity in the electronic grade hydrogen sulfide was less than 0.001%. The nitrogen from the same company was graded at U.H.P with a minimum purity of 99.999%. Standard gas mixtures of SO_2-N_2 and H_2S-N_2 are supplied by Canadian Liquid Air for the purpose of calibration of gas chromatograph.

3.3.3 Standard Solutions for Chemical Analysis

Potassium iodate was available in high purity (KIO_3 > 99.97%) and was used for the direct preparation of standard solutions. 10.7 grams of reagent grade KIO_3 supplied by Caledon Laboratories Ltd was weighed accurately to the nearest 0.1 mg and dissolved in about 900 ml of distilled water. The reagent was then transferred to a one litre volumetric flask and diluted to obtain a 0.05 M solution.

Thiosulfate solutions are less stable than KIO_3 solution and thus cannot be used as the primary standard. It is not possible to prepare sodium thiosulfate solutions by weighing out the pure salt as purchased, since sodium thiosulfate pentahydrate effloresces very easily. To prepare the thiosulfate solution, 25 g of $Na_2S_2O_3$*$5H_2O$ and 0.1 g of sodium carbonate were dissolved in one litre of freshly boiled and cooled water. Sodium thiosulfate solutions may change in titer slowly with the lapse of time. Therefore, the solution was standardized by iodometric titration using potassium iodate as the primary

standard.

A starch solution was used as an indicator which gave an intense blue color when trace amounts of tri-iodide ions exist. A paste of 2 grams of soluble starch and 10 mg of mercuric iodide (acting as preservative) in about 30 ml of water was poured into one liter of boiling distilled water and heated until the solution was clear. It was then transferred to an air-tight bottle for storage when cooled.

3.4 Determination of Gas Composition

A gas chromatography (GC) (SHIMADZU GC-9A) device equipped with a thermal conductivity detector (TCD) was used to determine gas compositions. The GC was controlled by a microcomputer (Chrimatopac CR601) which also served as a data processor. A built-in thermal sensitive printer was capable of plotting the chromatogram and printing the processed data on the same recording paper. The differential detector yielded the familiar chromatograms of peaks rather than steps.

The column used was HayeSep Q (8'x1/8", 80/100 mesh) supplied by SUPELCO Separation Technologies, and was capable of separating N_2, SO_2, H_2S and H_2O. The temperature was computer controlled within ± 0.1 °C. Helium was selected as the carrier gas.

The sensitivity of the detector represented an important limitation upon the smallest quantity of gas that can be determined by GC. The detector was extremely sensitive (0.2 μVs). In order to reduce the noise, a minimum peak area (20 μVsec) was set. For a gas sample containing H_2S, a peak of 1733 μVs represented 1 vol% of H_2S

in a 250 μl sample. The 20 μVs represents a magnitude of 0.01 vol% (100 ppm). The actual sensitivity of the detector should have been even better than this. The sensitivities of the detector for nitrogen and sulfur dioxide were of the same order of magnitude. In addition, the ideal detector response would be linear with respect to the quantity measured. The linearity of the TCD detector used was $\pm$0.1% or better.

Integration errors were not significant. In the GC used, the peaks were processed in the mode of peak area. The maximum peak area presented is 999,999,999 μVsec (9 digits) with an integration sensitivity of 0.1 μVsec (0.1 digit). In terms of the concentration of gas, it represented about 0.5 ppm in a 250 μl gas sample.

Resolution must be considered when chromatograms contain overlapping peaks. In present study, two pairs of peaks, namely, nitrogen-carbon dioxide and hydrogen sulfide-water vapor, had small degree of overlap. The data processor used the vertical division process to separate the overlapped peaks. Since the peak of carbon dioxide was very small, with a peak area below 400 μVsec, and the overlapped area between carbon dioxide and nitrogen was less than one fifth of the total peak area of carbon dioxide (below 80 μVsec), the error due to overlap was calculated to be less than 0.04 vol% (400 ppm) in a 250 μl sample. The overlap between hydrogen sulfide and water vapor can be well controlled by removing moisture from gas samples.

In order to calibrate the GC, the standard gas mixtures of SO_2-N_2 and H_2S-N_2 were used. One-point and two-point calibration curve methods were used for sulfur dioxide and hydrogen sulfide, respectively. Using calibration curves, the systematic errors were accounted for.

To determine the precision of measurements, a series of 10 measures were taken for each of the standard gaseous mixtures. The volume of each gas sample was 250 μl. For the SO_2-N_2 mixture with 10%SO_2, the sample standard deviation (S_x) was determined to be 0.036%. For the gas mixtures with 5% and 10% H_2S, the sample standard deviations were determined to be 0.028% and 0.027%, respectively.

3.5 Determination of Solution Composition

3.5.1 Fresh Na_2S Solution

The iodometric method was used to determine sulfide concentration in an aqueous solution of Na_2S. The fresh Na_2S solution contained sodium sulfide only. Methods used in the analysis of soluble sulfide are well established (Karchmer 1970) and can generally be applied without modifications. There are many methods available to determine the Na_2S in aqueous solution containing only sulfide, such as gravimetric methods and volumetric methods. However, the iodometric determination is preferred for its good reliability. Since the standard procedure is available in textbooks (Kolthoff, Sandell, Meehan and Bruckenstein, 1969), the details of the method are not repeated here. To minimize the possible loss of sulfide due to the formation and gasification of H_2S upon addition of HCI, the burette used was equipped with an air-tight, inner joint at its tip to match the joint of the titration flask.

Typically, each sample was analyzed three times and mean values were calculated. In order to determine the precision of the method, a series of 6 measurements were conducted for a single solution. The average concentration was 1.67 M. The six

results agreed to within ± 0.04 M with a standard deviation of 0.035 M or a relative standard deviation of 2.2%.

3.5.2 Spent Solution

The spent solution was analyzed with the method recommended by Kurtenacker and Wollack (Karchmer, 1970) for mixtures of sulfide, sulfite and thiosulfate. Sulfide was removed from the sample solution by shaking with zinc carbonate and filtering. One aliquot of the filtrate was titrated with iodine solution to determine the sum of the sulfite and thiosulfate. A second aliquot was treated with an excess of formaldehyde to form the inert hydroxysulfonate and only the thiosulfate was titrated. Since significant amounts of thiosulfate had been found in some of the spent solutions, oxidation could not be ruled out entirely.

It should be pointed out that if the extent of redox reactions is significant, compositions of spent solutions are expected to be very complex. Due to the possible co-existence of aqueous hydrogen sulfide and sulfur dioxide, there is a possibility of the formation of Wackenroder solution (Nickless 1968) which consists mainly of polythionates. Individual polythionates are very similar in their chemical and physical properties, hence, they are very difficult to analyze. If the formation of Wackenroder solution was negligible, the composition of spent solutions would have been much simpler. However, due to air oxidation and possible wet Claus reaction, the spent solution may have contained sulfite (bisulfite), sulfate, sulfide (bisulfide), polysulfide and thiosulfate.

3.6 Measurement of pH Value of Solution

Since acidity of the solution plays an important role in the generation of hydrogen sulfide as well as the absorption of sulfur dioxide, the pH value of the solution was monitored continuously. A pH meter (Omega RD-2010) equipped with sensitivity and temperature compensation controls was used. The relative accuracy was claimed to be $\pm 0.1\%$ of full scale ($0 \leq pH \leq 14$) on the chart recorder by the producer (Omega Engineering). The readability was 0.05 pH unit for the meter with standard scale.

In order to detect amplifier drift that causes errors in long-term measurements, a drift test was conducted by keeping the meter running at 50 Mv for ten hours. A drift of 1.5 Mv was observed. Prior to the measurement, the pH meter was calibrated with two standard solutions (pH4 and pH10). The accuracy of the standard buffer solution used was ± 0.02 pH unit.

An accurate meter with standard solutions alone was not enough to ensure the accuracy of measurement. The proper selection and use of electrode were also very important. A combined glass electrode with a gel-filled, double junction was used for the measurement of the pH value of the solution. The combined electrode provides simplicity and capability of measuring small-volume samples. The electrode was made of a special glass to minimize sodium ion error at high pH. In the present work, both sodium and sulfide content were usually very high. With the gel filled double junction, no silver ions (from reference electrode) were present in the outer gel solution, hence, silver sulfide could not form. This resulted in a faster responding probe and a greater service life.

In order to determine the repeatability of measurements, a series of 10 measurements were conducted in a pH 10 buffer using a distilled water rinse and a tissue blot between measurements. The readings agreed within ± 0.02 pH unit.

3.7 X-ray Identification of Pale Yellow Solid

In general, a monochromatic X-ray beam interacts with a polycrystalline specimen and gives a diffraction pattern. The diffraction pattern reflects the crystal structure (the lattice spacing d_L),which is determined by Bragg's law $\lambda = 2d_L \sin\theta_L$.

A x-ray diffraction instrument (PHILIPS PW 1720) was used for the identification of the pale yellow solid formed during some of the experiments in the early stage of the present work. The powder method was used. The diffraction pattern of the solid was compared with the diffraction pattern of elemental sulfur.

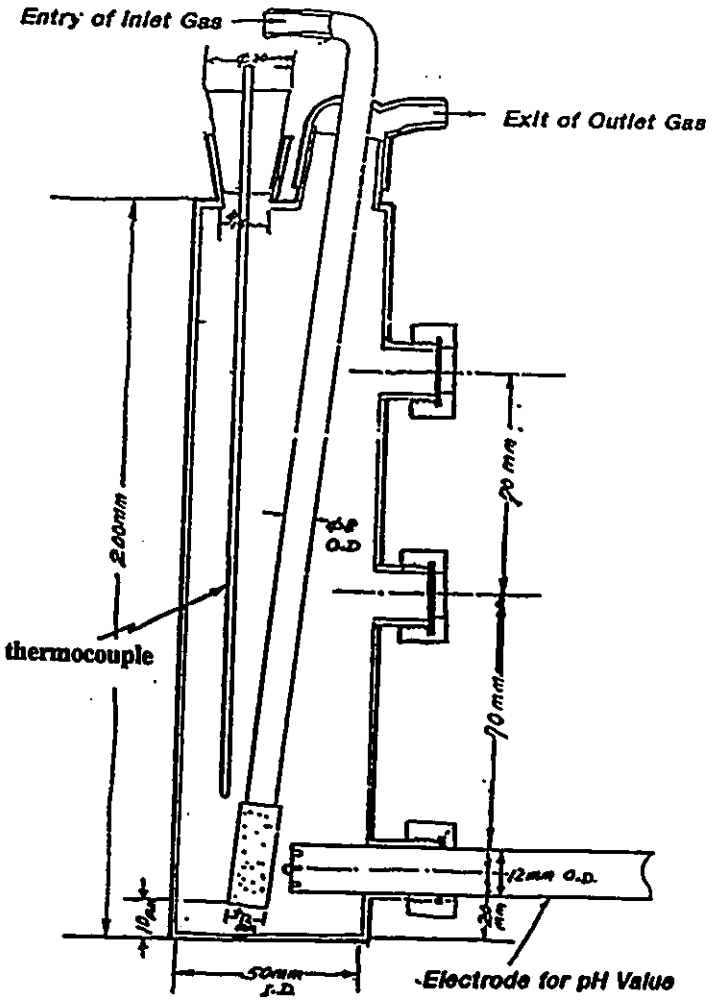

Fig.3.1: The Schematic Drawing of The Reactor

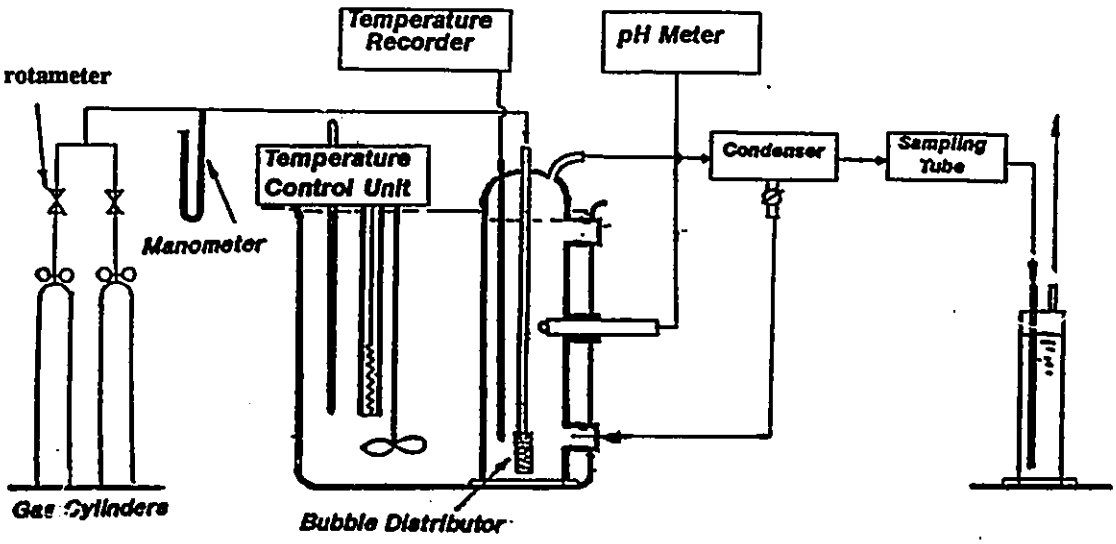

Fig.3.2: A Schematic Drawing of The Experimental Set-Up for The Semiflow Batch Reactor (SFBR) Study

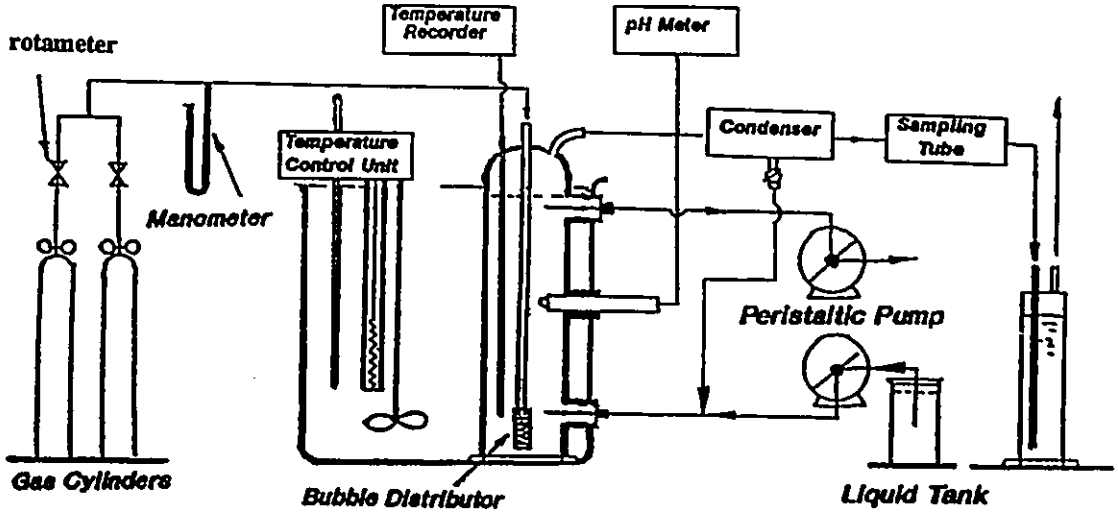

Fig.3.3: A Schematic Drawing of The Experimental Set-Up for The Continuous Flow Tank Reactor (CFTR) Study.

CHAPTER FOUR

EXPERIMENTAL RESULTS OBTAINED USING A SEMIFLOW BATCH REACTOR

In the present work, two types of experiments were conducted using the semiflow batch reactor (SFBR) and the continuous flow tank reactor (CFTR). The results presented in this chapter are based on the experiments carried out using the SFBR. Data obtained with the use of the CFTR will be presented in the next chapter.

4.1 Qualitative Measurements

4.1.1 The Typical Result: The Three-Stage Pattern

In the semiflow batch reactor (SFBR), chemical reactions were found to be a function of reaction time and to occur in three distinct stages in all experiments conducted. As an example, the experiment conducted at 35°C is outlined. The reactor was charged with 400 ml sodium sulfide solution at 0.1 M initially. The flow rate of the feeding gas, which contained 9.29 $\%SO_2$, 2.14 $\%O_2$ and a balance of N_2, was 100 ml/min.

The bubbling of sulfur dioxide-containing gas caused the changes in chemical reactions as a function of reaction time which occurred in three stages, as shown in Fig.4.1. In the first stage, sulfur dioxide was completely removed from the feeding gas by the solution. The contents of both sulfur dioxide and hydrogen sulfide in exit gas

were below the detecting limit (100 ppm). The first stage ended with the beginning of hydrogen sulfide generation. In the second stage, hydrogen sulfide formed steadily while the process of complete removal of sulfur dioxide from the feeding gas continued. The second stage ended when the generation of hydrogen sulfide terminated. In the third stage, the concentration of sulfur dioxide in the exit gas increased with time. Eventually, the content of SO_2 in the exit gas equalled the SO_2 content in the feeding gas. When this occurred, all sulfur dioxide in the feeding gas passed through the solution without reaction.

Two sharp drops in the pH value of the solution were observed, which corresponded to the beginning of the second and third reaction stages, respectively. Within each of these three stages, changes in the pH value were relatively small. Fig.4.2 shows an example of the pH profile and reaction temperature recorded by the chart recorder used in the present work.

In summary, it appeared to be feasible to remove sulfur dioxide from the flue gas under conditions corresponding to either the first or second stages and to generate hydrogen sulfide under conditions corresponding to the second stage by using an aqueous solution of sodium sulfide.

4.1.2 Formation of Elemental Sulfur in The Solution

It was observed in most of the experiments that in the first and second stages, the solution remained transparent at all times. However, in experiments conducted at low temperatures (below 49°C), low initial Na_2S contents in the solution (below 0.017M) and

high SO_2 content in feeding gas (over 54%), the formation of pale yellow precipitates was observed in the third stage. In order to determine the composition of the precipitates, they were filtered out and dried at 40°C, then identified using an X-ray diffraction method. The diffraction peaks of the sample identified match those of elemental sulfur very well, as shown in Fig.4.3. It is concluded that the precipitates formed in the third stage are elemental sulfur. It should be pointed out that the shift between the observed diffraction and the one of elemental sulfur was made intentionally for a clear separation of peaks.

To study formation mechanism of elemental sulfur precipitates, a gas mixture containing 10% SO_2 was introduced to contact a flat and quiescent surface of aqueous solution of sodium sulfide (1.5 M) at 25°C. At the moment when the gas met the solution, pale yellow solids (most likely elemental sulfur) began to precipitate on the surface of the solution. At the same time, the precipitated elemental sulfur entered the bulk solution and dissolved to form clear, yellow liquid. In the exit gas, hydrogen sulfide was detected (approximately 0.5%). This may indicate that the formation of elemental sulfur is an interfacial reaction which is likely to be wet Claus reaction between aqueous hydrogen sulfide in the solution and sulfur dioxide which entered the reaction zone from the gaseous phase.

4.1.3 The Color of The Solution

The fresh aqueous solution of sodium sulfide was transparent and colorless. The coloring of solution was observed only when the temperature and the initial sodium

sulfide content in the solution were low and the content of sulfur dioxide in the feeding gas was high, i.e. under the conditions that the formation of elemental sulfur was extensive. With the bubbling of sulfur dioxide at room temperature, the color of the solution gradually became yellow in the first stage, and then reverted back to a colorless or pale yellow solution in the second stage. In the later part of the second stage, the solution gradually became milky and the liquid phase remained colorless or pale yellow.

The color of the solution in the third stage appeared to depend on the concentration of sulfur dioxide in the feeding gas. When the gas mixture containing 10% sulfur dioxide was used, the solution in the third stage (the spent solution) was colorless. However, when a gaseous mixture containing a small amount of SO_2 was replaced by high-purity sulfur dioxide (>99 vol%), the color of the spent solution was yellow. It is known that the color of the Wackenroder's solution, which contains mainly polythionates, ranges from yellow to orange, depending on its concentration (Remy 1956).

Other experiments were performed to examine the color of aqueous solutions of sodium polysulfide, thiosulfate, sulfite and sulfate. The color of aqueous sodium polysulfide solution changed from light yellow to orange with an increase of its concentration. Conversely, the aqueous solutions of sodium thiosulfate, sulfite and sulfate solutions were colorless. The yellow color of the solution in the first and second stages is thought to be caused by the presence of polysulfide, while the yellow color of the spent solution in the third stage is likely to be caused by polythionates, i.e. the Wackenroder's solution.

4.1.4 The Heat of Reactions

The overall reaction was proven experimentally to be exothermic. A non-isothermal experiment was conducted at room temperature initially without the use of a water bath. When the gas mixture containing 10% sulfur dioxide was fed at a flow rate of 350 ml/min into the reactor containing 400 ml 0.17 M sodium sulfide solution, the temperature of solution increased with time; the temperature of the solution rose from 25 to 40 °C in thirty minutes.

4.1.5 Chemical Composition of Spent Solutions

Although much effort has been made to analyze the composition of spent solutions, acceptable and reliable results have been limited to that of sulfide solutions which contain bisulfide. The sulfide in solution is exceptional because it is the only sulfur species which exists in a reduced state. Fortunately, the progress of important reactions in this system may be adequately described by the data generated using the gas chromatography.

To study the composition change of sulfide-containing solutions with the bubbling of sulfur dioxide, high-purity sulfur dioxide was fed into the SFBR charged with 420 ml 0.25 M sodium sulfide solution at 36 °C. The flow rate of feeding gas was 220 ml/min. Liquid samples were taken and analyzed using the method described in Chapter 3. Sulfide, sulfite and thiosulfate were detected in the spent solution.

The content of sulfide in the solution as well as the pH value of solution were plotted against reaction time and are shown in Fig. 4.4. The analytical results indicate

that the concentration of sulfide declined with the bubbling of sulfur dioxide. In addition, the consumption rate of sulfide appeared to decrease with time. After the second drop in pH, i.e. at the end of second stage, the content of sulfide in solution was below its detectable limit (100ppm).

Since there was no detectable hydrogen sulfide released to the gaseous phase in the first stage, it is thought that the redox reactions were responsible for the decrease of sulfide content in solution. The SO_2 would have been the oxidizer in the absence of oxygen. Considering the generation of hydrogen sulfide in the second stage, the consumption rate of sulfide in this period of time was expected to be higher than that in the first stage. However, the opposite was observed. A logical explanation could be that the rate of redox reactions in the first stage, in terms of consumption of sulfide, was higher than the sum of the rate of redox reactions and the rate of H_2S generation in the second stage.

4.2 Quantitative Measurements

In this section, the effects of temperature in an isothermal system, the sulfur dioxide content in feeding gases, the flow rate of feeding gas and the initial sodium sulfide content in solution on the generation of hydrogen sulfide, which were studied experimentally in the SFBR, are presented and discussed.

4.2.1 Temperature Dependence of Reactions

To investigate the temperature dependence of this system, three experiments were

conducted at different temperatures, i.e. controlled at 40, 59 and 79°C with the use of a water bath. In this series of experiments, the feeding gas had 8.91% SO_2 and a flow rate of 190 ml/min. The solution in the reactor had a volume of 400 ml and an initial Na_2S concentration of 0.017 M. In the second stage, the H_2S content in exit gases increased as reaction temperature increased (Fig.4.5). During the first and second stages, sulfur dioxide was not detected in the exit gas, i.e. the SO_2 concentration remained below 100 ppm (Fig.4.6). In the third stage, sulfur dioxide was found in the exit gases. At this stage, its content increased faster with reaction time at higher temperatures, i.e. as temperature was increased in the third stage, the solution lost its ability to absorb sulfur dioxide at a high rate.

The general pattern of change of pH values remained the same. Although the initial pH value of the solution (before the bubbling of sulfur dioxide) in the first stage decreased with an increase in temperature, the temperature effect on pH value in the second stage appears to be weaker than that in first stage (Fig.4.7).

By assuming that N_2 is an inert gas, the total amount of hydrogen sulfide ($M(H_2S)$) generated in the second stage may be determined by integration, if the content of H_2S in the exit gases is known. The experimental results are listed in Table 4.1 with the total amounts of Na_2S added to the system initially ($M(Na_2S)$) and sulfur dioxide bubbled into the system during the first and second stages ($M(SO_2)$). As indicated by data in Table 4.1, the extent of Na_2S conversion to H_2S, which is represented by the molar ratio of hydrogen sulfide over sodium sulfide, was found to increase from 35% to 52% when temperature was increased from 40 to 79 °C. The corresponding molar

ratio of hydrogen sulfide over sulfur dioxide also increased from 0.14 to 0.26.

Table 4.1 Temperature Dependence of The Conversion Ratio of Sodium Sulfide to Hydrogen Sulfide

Temperature (°C)	$M(Na_2S)$ (mole)	$M(SO_2)$ (mole)	$M(H_2S)$ (mole)	$\frac{M(H_2S)}{M(SO_2)}$	$\frac{M(H_2S)}{M(Na_2S)}$
40	0.0066	0.016	0.0023	0.14	0.35
59	0.0066	0.014	0.0027	0.20	0.41
79	0.0066	0.013	0.0034	0.26	0.52

$M(Na_2S)$:Total amount of Na_2S added initially;
$M(SO_2)$: Total amount of SO_2 bubbled in the 1st and 2nd stages;
$M(H_2S)$: Total amount of H_2S generated in the 2nd stage.

It was observed that the amount of elemental sulfur formed in the third stage decreased with an increase in temperature. Furthermore, when the reaction temperature was 79 °C, no sulfur precipitation was observed in the third stage, i.e. the solution remained transparent. Since more hydrogen sulfide was generated at higher temperatures, the amount of sulfide oxidized in the solution decreased under these conditions. As indicated by data in Table 4.1, the amount of hydrogen sulfide generated with a unit amount of sulfur dioxide increased with an increase in reaction temperatures. The reason may be that less SO_2 was consumed by redox reactions at higher reaction temperatures.

4.2.2 The Effect of SO_2 Content in The Feeding Gas on Na_2S Conversion to H_2S

In this series of experiments, the content of sulfur dioxide in the feeding gas was

chosen to be 10%, 21% and 54%. The solution in the reactor had an initial Na_2S concentration of 0.016 M and an initial volume of 400 ml. All experiments were conducted at 79°C.

During the first and second stages, SO_2 was not detected in the exit gas, even through the concentration of SO_2 in the feeding gas was as high as 54 % (Fig.4.8). In the third stage, with a higher SO_2 concentration in feeding gas the sulfur dioxide content in the exit gas increased more rapidly with time.

Regarding hydrogen sulfide generation, experimental results indicate that the conversion ratio of sodium sulfide to hydrogen sulfide decreased with the increase of SO_2 concentration in the feeding gas as shown in Fig.4.9. In Table 4.2, the molar ratios of products to reactants for different SO_2 contents are listed.

Table 4.2 Effect of Sulfur Dioxide Content in Feeding Gases on The Conversion Ratio of Sodium Sulfide to Hydrogen Sulfide at 79°C

Content of SO_2 (%)	$M(Na_2S)$ (mole)	$M(SO_2)$ (mole)	$M(H_2S)$ (mole)	$\frac{M(H_2S)}{M(SO_2)}$	$\frac{M(H_2S)}{M(Na_2S)}$
10	0.0066	0.013	0.0034	0.26	0.52
21	0.0066	0.018	0.0023	0.13	0.35
54	0.0066	0.023	0.0008	0.03	0.12

$M(Na_2S)$:Total amount of Na_2S added initially;
$M(SO_2)$: Total amount of SO_2 bubbled in the 1st and 2nd stages;
$M(H_2S)$: Total amount of H_2S generated in the 2nd stage.

Figure 4.10 shows the change of pH value in each of the three stages. It was found that the duration of both stages I and II became shorter when SO_2 concentration

in the feeding gases was higher, so that the system entered the second and the third stages earlier. As well, with the increase of SO_2 content in the feeding gas, the pH value of the spent solution in the third stage dropped. Despite the large increase in the sulfur dioxide content in the feeding gas, the basic pattern of pH value in the three stages remained the same even when high-purity sulfur dioxide was used as indicated in Fig.4.4.

As mentioned in the last section, by using a gaseous mixture containing 10% sulfur dioxide at 79 °C the formation of elemental sulfur in the third stage was prevented. However, when the concentration of sulfur dioxide was increased to 21%, the formation of elemental sulfur was observed in the third stage at the same temperature. Further increases of sulfur dioxide concentration resulted in more elemental sulfur being formed.

4.2.3 The Effect of Initial Sodium Sulfide Content in Solution on Na_2S Conversion to H_2S

For comparison with earlier experiments, the initial sodium sulfide concentration in solution was increased from 0.017 to 0.166 M while the reaction temperature was kept at 79°C. The volume of the solution was 400 ml. The gas mixture containing 10% SO_2 was fed into the solution at a flow rate of 190 ml/min.

With the increase of initial sodium sulfide concentration, the amount of hydrogen sulfide in exit gases increased as shown in Fig.4.11. The SO_2 contents in the exit gases were plotted against reaction time and are shown in Fig. 4.12. The SO_2 content in the exit gas was below the detecting limit (100 ppm) in the first and second stages, and was

independent of the initial Na_2S concentration. Once the system entered the third stage, the content of sulfur dioxide released from the concentrated spent solution appeared to be higher than that from the diluted spent solution, i.e. the concentrated spent solution seemed to have less capacity to absorb sulfur dioxide than the diluted spent solution after all sulfide in the solution was consumed.

The general pattern of change in pH values remained the same despite the large increase of sodium sulfide concentration (Fig.4.13). The pH value of the solution in the first and third stages was higher for the concentrated solution. However, in the second stage, the pH value of both solutions appeared to fall into the same range (pH6 to pH8).

Table 4.3 Effect of Initial Sodium Sulfide Content in Solution on The Conversion Ratio of Sodium Sulfide to Hydrogen Sulfide at 79 °C

Content of Na_2S (M)	$M(Na_2S)$ (mole)	$M(SO_2)$ (mole)	$M(H_2S)$ (mole)	$\frac{M(H_2S)}{M(SO_2)}$	$\frac{M(H_2S)}{M(Na_2S)}$
0.017	0.0066	0.013	0.0034	0.26	0.52
0.166	0.0664	0.071	0.037	0.51	0.56

$M(Na_2S)$:Total amount of Na_2S added initially;
$M(SO_2)$: Total amount of SO_2 bubbled in the 1st and 2nd stages;
$M(H_2S)$: Total amount of H_2S generated in the 2nd stage.

The molar ratios of product to reactant were determined and are listed in Table 4.3. The conversion ratio of sodium sulfide to hydrogen sulfide increased from 0.52 to 0.56 when the sodium sulfide content increased from 0.017 to 0.166 M. The molar ratio of hydrogen sulfide to sulfur dioxide nearly doubled (from 0.26 to 0.51). No formation of elemental sulfur in the third stage was observed under conditions studied in this series of experiments.

4.2.4 The Effect of Flow Rate of Feeding Gas on Na_2S Conversion to H_2S

Three experiments were conducted at 80 °C to investigate the effect of the feeding gas flow rate. The flow rates of the gas, containing 10% SO_2, were maintained at 190, 250 and 320 ml/min. The solution in the reactor had a volume of 400 ml and an initial Na_2S concentration of 0.017 M.

The three-stage pattern of change as a function of reaction time was observed in all three experiments. In the first and second stages, the removal of sulfur dioxide from the feeding gases by the solution was complete and independent of the feeding gas flow rate in the range studied. No sign of the formation of elemental sulfur was observed in the third stage for all three experiments. The flow rate of feeding gas appeared to have a small, positive effect on the peak value of hydrogen sulfide content in exit gas, as shown in Fig.4.14.

Table 4.4 Effect of Feed Gas Flow Rate on The Conversion Ratio of Sodium Sulfide to Hydrogen Sulfide at 80 °C

Flow Rate of Feeding Gas (ml/min)	$M(Na_2S)$ (mole)	$M(SO_2)$ (mole)	$M(H_2S)$ (mole)	$\frac{M(H_2S)}{M(SO_2)}$	$\frac{M(H_2S)}{M(Na_2S)}$
190	0.0066	0.013	0.0034	0.26	0.52
250	0.0066	0.014	0.0035	0.25	0.53
320	0.0066	0.014	0.0036	0.26	0.54

$M(Na_2S)$:Total amount of Na_2S added initially;
$M(SO_2)$: Total amount of SO_2 bubbled in the 1st and 2nd stages;
$M(H_2S)$: Total amount of H_2S generated in the 2nd stage.

The calculated conversion ratios of sodium sulfide to hydrogen sulfide are given in Table 4.4. Although the increase in the conversion ratio was not large enough to confirm a positive effect, it was clear that the increase of gas flow rate did not show any

adverse effects. There was no noticeable change in the molar ratio of hydrogen sulfide to sulfur dioxide.

4.3 Determination of Favourable Conditions for H_2S Generation and Elemental Sulfur Formation

In Section 4.2, it was found that the generation of hydrogen sulfide in the SFBR could be enhanced by increasing reaction temperature and the initial sodium sulfide concentration in solution. Conversely, the formation of elemental sulfur is favored under lower temperatures and in more diluted Na_2S solutions. In this section, the experimental results under extended conditions are described.

4.3.1 H_2S Generation at High Temperature (90°C) with Concentrated Na_2S Solution (1.9M)

To enhance the generation of hydrogen sulfide, an experiment was conducted at 90°C with 350 ml of 1.92 M Na_2S solution. The feeding gas, containing 10% of SO_2, was fed into the solution at 340 ml/min.

Table 4.5 The Conversion Ratio of Sodium Sulfide to Hydrogen Sulfide at High Temperature and with High Na_2S Concentration Solution

Temperature (°C)	$M(Na_2S)$ (mole)	$M(SO_2)$ (mole)	$M(H_2S)$ (mole)	$\frac{M(H_2S)}{M(SO_2)}$	$\frac{M(H_2S)}{M(Na_2S)}$
90	0.67	1.1	0.54	0.49	0.81

$M(Na_2S)$:Total amount of Na_2S added initially;
$M(SO_2)$: Total amount of SO_2 bubbled in the 1st and 2nd stages;
$M(H_2S)$: Total amount of H_2S generated in the 2nd stage.

As shown in Fig.4.15, in the second stage the concentration of H_2S in exit gas reached a very high level (over 15%), which was even higher than the concentration of SO_2 in feeding gases (10%). The calculated results of mass flux are listed in Table 4.5. It is encouraging to see that over 80% of the Na_2S had been converted into H_2S. Until the end of the second stage, SO_2 in the feeding gas was removed completely by the solution. The molar ratio of total H_2S generated to total SO_2 absorbed in first two stages reached 0.49, which implied that more of the dissolved SO_2 was participating in the formation of H_2S. There was no sign of the formation of elemental sulfur in the third stage.

4.3.2 Elemental Sulfur Formation at Low Temperature (1°C) with Diluted Na_2S Solution (0.017M)

The purpose of the experiment was to study the feasibility of formation of elemental sulfur without the release of hydrogen sulfide. Elemental sulfur is a desirable final product and can be obtained by treating sulfur dioxide in flue gases. The present study is based on a proposed McMaster-INCO process, in which hydrogen sulfide is generated from reactions between aqueous Na_2S solution and SO_2-containing gaseous mixture; the H_2S generated is to be used to produce elemental sulfur in an additional step via a Claus reaction. If elemental sulfur can be generated directly from aqueous Na_2S solution and SO_2 without the generation of H_2S, the process of converting SO_2 in flue gas to elemental sulfur could be further simplified.

The experiment was conducted at 1 °C using an ice-water bath. The concentration

of sodium sulfide in the 400 ml solution charged into the reactor was 0.017 M. A feeding gas containing 9.99% SO_2 was introduced into the reactor at a rate of 190 ml/min.

Table 4.6 The Conversion Ratio of Sodium Sulfide to Hydrogen Sulfide at 1°C and with 0.017M Na_2S Solution

Temperature (°C)	$M(Na_2S)$ (mole)	$M(SO_2)$ (mole)	$M(H_2S)$ (mole)	$\frac{M(H_2S)}{M(SO_2)}$	$\frac{M(H_2S)}{M(Na_2S)}$
1	0.0066	0.017	0.0015	0.09	0.23

$M(Na_2S)$:Total amount of Na_2S added initially;
$M(SO_2)$: Total amount of SO_2 bubbled in the 1st and 2nd stages;
$M(H_2S)$: Total amount of H_2S generated in the 2nd stage.

As expected, extensive formation of elemental sulfur was observed in the third stage. However, despite the use of a diluted solution at low temperature, significant amounts of hydrogen sulfide were detected in the second stage (Fig.4.16). As shown in Table 4.6, approximately 23% of Na_2S was converted to H_2S. One may conclude that it is unlikely to produce elemental sulfur without the release of significant amount of H_2S under the most favourable conditions studied.

4.4 Effects of Bubble Size and Depth of Liquid Column on Na_2S Conversion to H_2S

In a heterogenous system, interfacial area usually plays an important role. In a bubble column, the total interfacial area strongly depends on the bubble size. The total mass flux through a given interface depends on the residence time of bubble in the solution, in addition to all other kinetic parameters.

4.4.1 Effects of Bubble Size on Na_2S Conversion to H_2S

To study the effects of bubble size, three types of bubble distributors were used, namely, fine, coarse and single-orifice. The diameter of bubbles produced by the fine distributor ranged from 0.5 to 1.5 mm, while diameters of bubbles produced by the coarse distributor ranged from 2 to 4 mm. The size of bubbles delivered by the single-orifice distributor (5mm I.D.) ranged from about 5 to 15 mm in the equivalent diameter with the change of volumetric feeding gas flow rate. Therefore, the specific gas-liquid interfacial area decreased by a factor of 10 and 100 when the fine distributor was replaced by the coarse one and by the single-orifice distributor, respectively.

One series of experiments were conducted at 59°C in the SFBR containing 400ml sodium sulfide solution at 0.017M with the use of both fine and coarse distributors. The gaseous mixture containing 10% sulfur dioxide was fed into the reactor at a rate of 190ml/min. The pattern of pH value change for both fine and coarse bubble distributors was essentially identical (Fig.4.17). During the second stage, the hydrogen sulfide content in the exit gases and the total hydrogen sulfide generated for both cases were very similar (Fig.4.18). Regarding SO_2 content in exit gases, similar results were observed, i.e. SO_2 content in the exit gas were below the detectable limit (100ppm) in the first and second stages. It would be reasonable to suggest that a shift of range of bubble size from 0.5-1.5mm to 2-4mm (the corresponding interfacial area decreased by a factor of 10) did not result in noticeable changes in this kinetic system under the conditions studied.

In another series of experiments, which was originally designed to study the

effects of CO_2 in the feeding gas on Na_2S conversion to H_2S (refer to Section 4.6.2), the coarse bubble distributor and the single-orifice distributor were used. A significant increase in the peak value of H_2S content in the exit gas was observed when the single-orifice distributor was replaced by the coarse one, for which the increase in the specific interfacial area is thought to be responsible. The details of these experiments will be given in Section 4.5.2.

4.4.2 Effects of Liquid Column Depth on Na_2S Conversion to H_2S

The effect of the depth of the liquid column in the reactor was studied by changing the volume of solution in the reactor at three different temperatures. The single-orifice distributor was used in this series of experiments to limit the specific interface area. Since the same bubble distributor was used for each experiment, different solution volumes corresponded to different travel distances of bubbles in the solution and hence, different residence times of bubbles in the solution.

The experiments were conducted isothermally at three different temperatures, namely, 40, 59 and 79°C. The experiments at 40 and 60°C were conducted with three different volumes of solution, 120, 165 and 220 ml. The distances from the edge of the downward orifice to the surface of the liquid, i.e. the depth of the liquid column through which bubbles travel, were 15, 40 and 60 mm, respectively. At 80°C, experiments were carried out with an additional volume of solution (100ml, a travel distance of 8 mm). In all cases, the flow rate of the 9.99%SO_2 feed gas was kept at 190ml/min and the initial Na_2S concentration of the solution was 0.017M.

The total amounts of hydrogen sulfide generated (M(H,S)) under the stated conditions were determined and are reported as molar ratios of hydrogen sulfide generated to sodium sulfide added ($M(H_2S)/M(Na_2S)$ in Table 4.7.

Table 4.7 Conversion Ratios of Sodium Sulfide to Hydrogen Sulfide for Different Depths of Liquid Column at Different Temperature

Depth of Liquid Column / Temperature	8 mm	15 mm	40 mm	60 mm	Average
40 ℃		0.36	0.37	0.35	0.36
59 ℃		0.38	0.38	0.40	0.39
79 ℃	0.52	0.50	0.50	0.54	0.52

There is no clear evidence that the conversion ratio of sodium sulfide to hydrogen sulfide increases with the increase of the bubble travel distance, although a higher concentration of hydrogen sulfide in the exit gas was observed. The temperature dependence of the average molar ratio was very similar to that listed in Table 4.1.

The hydrogen sulfide contents in the second stage at 40, 59 and 79°C were plotted and are shown in Figs.4.19, 4.20 and 4.21, respectively. These data indicate that both the hydrogen sulfide content in the exit gas as well as the total hydrogen sulfide generated increased with the increase in the bubble residence time at each of the three temperatures. Although the change in the hydrogen sulfide content was not large, it was clear that the H_2S content in the exit gases increased with the increase in the depth of the liquid phase. For each case studied, the sulfur dioxide content in the exit gases was below the detectable limit (100ppm) in the first or the second stages. Considering the

fact that the concentration of hydrogen sulfide in exit gas increased with the increased linear travel distance of bubbles (up to 60 mm), it may indicate that desorption of hydrogen sulfide is not fast enough to allow the gaseous phase to reach equilibrium with the liquid phase. The computed results using the mathematical model (Fig. 7.19) indicate that partial pressure of H_2S in exit gas does not depend on the total amount of Na_2S in the reactor, if the gaseous phase was in equilibrium with the liquid phase.

4.5 Estimation of G/L Interfacial Area and Bubble Residence Time

The gas-liquid interfacial area in a bubble reactor consists of two parts, the bubble/liquid interface and the surface of the pool. The interfacial area generated by bubbles depends on number of bubbles and the distribution of bubble size. Conversely, the surface of solution that is determined by the size of container may be considered to be constant. The size of bubbles formed at a single orifice may be estimated using the bubble-diameter correlation recommended by Kumar, Degaleesan, Ladda, and Hoelscher (1976) for air sparged into relatively inviscid liquids. To estimate the number of bubbles in the solution, the gas hold-up was measured. Moreover, the bubble residence time in solution (t_b) was determined as a function of gas hold-up volume (V_b) and the frequency of bubble production (F_b).

4.5.1 Determination of Bubble Diameter

Among three types of bubble distributors used, namely, fine, coarse and single orifice, the single-orifice distributor is capable of forming "single-size" bubbles.

Therefore, the bubble diameter was calculated for the single-orifice distributor (5mm I.D), only.

4.5.1.1 Reynolds Number (Re) and The Regime of Bubble Production

Size of bubble formed at a single orifice depends on the volumetric rate of gas which controls the regime of bubble production. The regime of bubble production is a function of the Reynolds number (Re), which is defined as follows:

$$Re = \frac{V_o D \rho_g}{\mu_g} \qquad (4\text{-}1)$$

where, V_o is gas velocity through orifice (m/sec); D is orifice diameter (m); ρ_g and μ_g are gas density (kg/m^3) and viscosity (kg/m sec), respectively. For the case where D=5x10^{-3}m, ρ_g=1.05kg/m^3, μ_g=10^{-5}kg/(m.sec), the Reynolds numbers for different volumetric rates of gas were calculated and are given in Table 4.8.

There are three regimes of bubble production depending on the Reynolds number, namely, the single bubble regime ($N_{Re} < 200$), the intermediate regime ($200 < N_{Re} < 2100$) and the jet regime ($N_{Re} > 2100$) (Kumar et.al 1976). Consequently, the bubble column used in the present study was operated under the conditions that covers from the single bubble regime to the intermediate regime.

In the single bubble regime and the intermediate regime, bubble size is determined primarily by the orifice diameter (D), the gas-liquid interfacial tension (σ) and the densities of the liquid (ρ_l) and gas (ρ_g). Bubble size in the single bubble regime is independent of gas rate. Conversely, in the intermediate regime, as the gas flow through

a submerged orifice increases, the frequency of bubble formation increases at a slower rate than the gas rate. Consequently, bubble size increases as the gas flow rate is increased.

4.5.1.2 Bubble Diameter for Different Volumetric Flow Rates of Gas

The bubble-diameter correlation recommended by Kumar et.al (1976) for air at near-atmospheric pressure sparged into relatively inviscid liquids [$\mu \leq 100$ Mpa·s (Cp)] was used to estimate the diameter of bubbles. The correlation fits experimental data well as shown in Fig.4.22. In the correlation, a dimensionless parameter, A, is presented as a function of the Reynolds number (Re). A is defined as follows:

$$A = \frac{D_b}{\left[\frac{\sigma D^2}{(\rho_l - \rho_g) g}\right]^{\frac{1}{4}}} \qquad (4\text{-}2)$$

where, D_b and D are the bubble diameter and orifice diameter, respectively. According to this equation, increased interfacial tension (σ) tends to increase bubble size. When the surface tension of water at 50°C (68mN/m or 68dynes/cm) was used, the estimated bubble size may be greater than the reality, since aqueous solution of salts usually has a lower surface tension than pure water. Moreover, the density of solution was measured as 1.05×10^3 kg/m^3 and the density of gas was calculated to be 1.05 kg/m^3 at 25°C.

Based on the correlation shown in Fig.4.22, the bubble diameters for different volumetric rates of gas were calculated and are summarized in Table 4.8. The dependence of bubble diameters on the volumetric rate of gas is plotted in Fig.4.23.

Table 4.8 Reynolds Number and Bubble Diameters for Different Volumetric Rates of Gas

Volumetric Rate of Gas (ml/min)	Reynolds Number	A	Bubble Diameter (mm)
200	86	2.2	8
300	134	2.5	9
400	179	2.8	10
500	223	3.3	12
600	268	3.5	13
700	313	3.7	13
800	358	3.8	14

Note: A is defined by Eq.(4-2).

4.5.2 Measurement of Gas Hold-Up and Estimations of G/L Interfacial Area and Bubble Residence Time in Solution

The fraction of the volume in a gas/liquid two-phase mixture that is occupied by the gaseous phase is called "gas hold-up". In the present work, gas hold-up was measured for several cases with different volumetric flow rates of gas in a bubble column containing 350 ml of distilled water. The gas (N_2) was introduce by a single-orifice bubble distributor at 25°C. The absolute value of the volume occupied by bubbles was determined by the volume difference between the gas-liquid mixture and liquid phase only. The results are list in Table 4.9 in the form of bubble volume and dimensionless gas hold-up (ε). It should be pointed out that there was a large uncertainty in these measurements due to the fluctuation of the level of liquid surface.

Table 4.9 Dependence of Gas Hold-up on Volumetric Rate of Gas

Volumetric Rate of Gas (ml/min)	Volume Occupied by Gas (ml)	Gas Hold-up (ε)
300	8 ± 6	0.02 ± 0.017
430	16 ± 6	0.04 ± 0.016
560	24 ± 6	0.06 ± 0.016
700	31 ± 6	0.08 ± 0.016
820	39 ± 6	0.1 ± 0.015

Knowing the average diameter of bubbles and the hold-up volume of gas, the number of bubbles and total interfacial area could be calculated. Since the frequency of bubble production increases with an increased volumetric rate of gas, there was an increase in the number of bubbles in solution and in the interfacial area generated. Interfacial area per unit volume of solution, volumetric gas rates and computed bubble diameters are listed in Table 4.10. The interfacial area is found to be approximately proportional to the volumetric gas rate. A linear regression gives the following relation:

$$A_b = -31+0.64F_g \qquad (4\text{-}3)$$

where the correlation coefficient is 0.994; A_b is interfacial area per unit volume of solution in cm^2/l; F_g is volumetric gas rate in ml/min.

Residence time of bubbles in a liquid column (t_b) depends on the rise velocity of bubble and the depth of the expended solution. Although the terminal velocity of spherical bubbles may be calculated using an empirical equation (Datta 1950), a preferred

method is to determine t_b directly based on its definition. Residence time of bubbles in a liquid column is the time when a bubble stays in the liquid phase, which may be defined as follows:

$$t_b = \frac{N_b}{N} = \left(\frac{V_g}{V_b}\right)\left(\frac{V_b}{F}\right) = \frac{V_g}{F} \qquad (4\text{-}4)$$

where N_b is the number of bubbles in the liquid column; N is the frequency of bubble production, i.e. the number of bubbles produced per unit time; V_g is the measured gas hold-up volume; V_b is the volume of a bubble; and F is the volumetric gas rate. Therefore, the t_b is the ratio of V_g to F. This method is preferred for the following reasons: [1] it takes time for the bubble to reach the terminal velocity; [2] the bubble rises along an irregular path when its diameter is larger than 4.0 mm. The residence times for different flow rates given in Table 4.10 were obtained from Eq.(4-4).

Table 4.10 Dependence of Interfacial Area (A_b) and Residence Time of Bubble in Solution (t_b) on Volumetric Rate of Gas

Volumetric Rate of Gas (ml/min)	Diameter of Bubble (mm)	Interfacial Area (cm^2/l)	Residence Time (sec)
300	9	150	1.6
430	10	260	2.2
560	12	340	2.5
700	13	400	2.7
820	14	490	2.9

4.6 Experiments Under Conditions Relevant to INCO's Operation in Thompson, Manitoba

The experimental studies on the effect of oxygen and carbon dioxide in feeding gases and the minor impurities in solution are described.

4.6.1 Effects of Oxygen in Feeding Gas on Na_2S Conversion to H_2S

The flue gases of roasters used by INCO's Thompson division currently contain approximately 2% O_2. To examine the effects of oxygen on Na_2S conversion to H_2S, two experiments were conducted with and without oxygen in the feeding gas at a constant temperature of 80°C. Both types of feed gas, the binary (9.99% SO_2 and balance N_2) and the ternary (9.99% SO_2, 2% O_2 and balance N_2), were used at a flow rate of 190ml/min. The solution had a volume of 400ml and an initial Na_2S concentration of 0.017M. The experimental results indicate that the 2% oxygen in the feeding gas did not result in a significant change in the kinetic behaviour of the system. As shown in Fig.4.24, the hydrogen sulfide contents in the exit gases and the corresponding change in pH value were essentially identical in both cases.

4.6.2 Effect of Carbon Dioxide in Feeding Gas on Na_2S Conversion to H_2S

To study the effect of carbon dioxide in feeding gas on the conversion of Na_2S to H_2S, three experiments were conducted in the SFBR. The carbon dioxide contents in feeding gas were kept at 1.2% and 10% in $SO_2/CO_2/N_2$ mixtures. The lower level (1.2%) represents the CO_2 content maintained currently at INCO's Thompson division.

The higher level was selected in consideration of the potential application of the system to coal-burning power stations. For the feeding gas containing 1.2% carbon dioxide, two bubble distributors were used, namely, coarse and single-orifice. The solution had an initial Na_2S concentration of 1.5 M and a volume of 350ml. The temperature was maintained at 85°C. Other conditions specific to the three experiments are presented in Table 4.11.

Table 4.11 Experimental Conditions for The Study on The Effect of CO_2 in Feeding Gas on Na_2S Conversion to H_2S

Experiment	Composition of Feeding Gas (vol%)	Volumetric Flow Rate of Feeding Gas (ml/min)	Bubble Distributor Used
I	1.2%CO_2, 9.1%SO_2	650	single orifice
II	1.2%CO_2, 10.9%SO_2	650	coarse
III	10%CO_2, 9.4%SO_2	700	single orifice

The composition of the exit gas in Experiments I, II and III are given in Figs.4.25, 4.26 and 4.27, respectively. In the first stage, as shown in Figs.4.25 and 4.27, the CO_2 in feeding gas was partially absorbed while the SO_2 in the feeding gas was removed completely by the solution. At the beginning of the second stage, the CO_2 content in the exit gas increased to a level which was close to the CO_2 content in the feeding gas, and the generation of hydrogen sulfide began. The CO_2 content in the exit gas increased with the decrease of the content of hydrogen sulfide in the second stage. At the end of the second stage, the CO_2 contents in the exit gas for both cases reached peak values (4% and 22%),which was much higher than the CO_2 content in feeding gas (1.2% and 10%).

There was a period of approximately 60 to 70 minutes between the end of the second stage and the beginning of release of sulfur dioxide from the solution. During this period, the CO_2 content in exit gas was slightly greater than its level in the feeding gas, i.e. the sulfur dioxide in the feeding gas was absorbed completely by the solution without any further absorption of carbon dioxide. Without carbon dioxide in the feeding gas, sulfur dioxide is usually detected in the exit gas immediately after the end of the second stage.

Another difference between these cases, with and without carbon dioxide in feeding gas, was the characteristics of the first stage. An increase in CO_2 content in the feeding gas reduced the duration of the first stage. As the first stage became shorter, the amount of sulfur dioxide absorbed in the first stage decreased. Table 4.12 gives the amounts of carbon dioxide and sulfur dioxide absorbed in the first stage for each of the three experiments. The higher CO_2 content in the feeding gas can result in a smaller amount of SO_2 absorbed in the first stage. It may be concluded that carbon dioxide (a weaker acidic gas than SO_2) could partially replace sulfur dioxide in the first stage as the supplier of hydrogen ions.

Table 4.12 Amounts of Carbon Dioxide and Sulfur Dioxide Absorbed in The First Stage

Experiment	I (1.2%CO_2)	II (1.2%CO_2)	III (10.0% CO_2)
Amount of CO_2 absorbed (mol)	0.018	0.019	0.094
Amount of SO_2 absorbed (mol)	0.174	0.172	0.118

As shown in Fig.4.26, when the smaller bubbles were introduced into the solution by the coarse bubble distributor, no carbon dioxide was found in the exit gas in the first stage. It may be concluded that absorption of CO_2 by aqueous Na_2S solution in the first and second stages is a slower process than absorption of SO_2 in the same stages. Under conditions studied, absorption of CO_2 in the first stage was likely to have been limited by a kinetic step involving interfacial area.

Table 4.13 gives the peak values of hydrogen sulfide content in the exit gas and the conversion ratios of sodium sulfide to hydrogen sulfide for the three experiments. As shown in Table 4.13, when the single-orifice distributor in Experiment I was replaced by the coarse bubble distributor in Experiment II, the peak value of H_2S content in exit gas increased from 12.7% to 15.5%. This may have been caused by the increase of specific interfacial area, i.e. the transfer of aqueous hydrogen sulfide to gaseous phase is likely to be limited by a kinetic step involving interfacial area.

Table 4.13 The Peak Values of H_2S Content in Exit Gas and The Conversion Ratios of Sodium Sulfide to Hydrogen Sulfide at 85°C

Experiment	I (1.2%CO_2)	II (1.2%CO_2)	III (10.0%CO_2)
Peak Value of H_2S Content (%)	12.7	15.5	11.4
Conversion Ratio	0.75	0.78	0.77

The extent of Na_2S conversion to H_2S is not significantly different for these three experiments. In earlier experiments, the conversion ratio obtained at 90°C without carbon dioxide in feeding gas ([Na_2S]=1.9M) was 0.81. Considering the lower

temperature (85°C) and the lower initial Na_2S content (1.5 M) in this series of experiments, it is reasonable to conclude that the presence of carbon dioxide did not have a significant effect on the conversion of sodium sulfide to hydrogen sulfide under the conditions studied.

The pattern of the change in the pH value of solution as a function of reaction time was similar for all three experiments. Fig.4.28 shows the change of pH value of the solution in Experiment II. The three inflections in the pH value correspond to the start of H_2S generation, the peak value of carbon dioxide content in exit gas and the start of SO_2 release, respectively.

4.6.3 Effects of Minor Impurities (Fe, Cu, Ni and Co) in Solution on Na_2S Conversion to H_2S

For the purpose of comparison, two experiments were conducted with and without impurities at a constant temperature (90°C). The solution in the reactor had a volume of 200ml and an initial Na_2S concentration of 1.95 M. The flow rate of the gaseous mixture, containing 10% SO_2 and balance N_2, was 520 ml/min.

The impurities were added to the fresh sodium sulfide solution as sulfates before the bubbling of sulfur dioxide started. The amounts of Fe, Ni, Cu and Co introduced to the reactor would result in maximum concentrations of 300 ppm Fe, 100 ppm Ni, 3 ppm Cu and 2 ppm Co, if there were no precipitations of sulfide of these metals. According to Freier (1976), the solubilities of FeS, NiS, CuS and CoS in water are extremely low (1.24, 0.72, 0.055 and 0.67 ppm at 18°C, respectively). Hence, with the

high concentration of sulfide in solution, the concentration of soluble metal ions (Fe^{+2}, Ni^{+2}, Cu^{+2} and Co^{+2}) could have been very low.

The change of hydrogen sulfide content in the exit gas with reaction time (Fig.4.29) indicates that the release of hydrogen sulfide started several minutes earlier with a higher peak value of H_2S content (about 17%) in the presence of impurities. However, it appeared to decay faster.

Table 4.14 Effect of Impurities (Fe, Ni, Cu and Co) in Solution on Na_2S Conversion to H_2S

Impurities	$M(Na_2S)$ (mole)	$M(SO_2)$ (mole)	$M(H_2S)$ (mole)	$\frac{M(H_2S)}{M(SO_2)}$	$\frac{M(H_2S)}{M(Na_2S)}$
without	0.39	0.52	0.33	0.63	0.84
with	0.39	0.50	0.31	0.62	0.80

$M(Na_2S)$:Total amount of Na_2S added initially;
$M(SO_2)$: Total amount of SO_2 bubbled in the 1st and 2nd stages;
$M(H_2S)$: Total amount of H_2S generated in the 2nd stage.

According to the data in Table 4.14, the presence of impurities did not result in a larger total amount of hydrogen sulfide produced, despite of the higher peak value of H_2S content in the exit gas. However, the impurities appeared to be responsible for the small decline of the conversion ratio of sodium sulfide to hydrogen sulfide. There are several reports about the catalytic influences of trace metal ions (Fe^{2+}, Cu^{2+}, Ni^{2+} and Co^{2+}) on the oxidation of aqueous H_2S at low concentration ($\sim 10^{-4}$ M) (Chen 1970, Chen and Morris 1972, Millero 1991a and 1991b). Furthermore, it is conceivable that the actual initial soluble sulfide concentration was lower before bubbling but after the precipitation of impurities.

4.7 Estimation of Error Involved in The Determination of Conversion Ratio of Na_2S to H_2S

Conversion Ratio of Na_2S to H_2S is the key parameter to evaluate the performance of the AGU in McMaster-INCO process. In this section, errors involved in the determination of this ratio are to be estimated based on statistical principles. Usually, there are two types of errors inherent in making measurements, random errors and systematic errors. The former affects precision of measurements, while the later changes accuracy of measurements. Systematic errors are attributable to known conditions and can be evaluated and applied as corrections to measured quantities. Moreover, systematic errors due to instruments can be eliminated by calibration. Random errors are random in nature, which is the subject of this section.

4.7.1 Conversion Ratio Obtained Using Semiflow Batch Reactor (SFBR)

The conversion ratio of Na_2S to H_2S (R) in the SFBR is defined by the following relation:

$$R = \frac{M_{H_2S}}{M_{Na_2S}} = \frac{\int_0^t \frac{(1-Y_{SO_2})\, Y_{H_2S} Q_G}{(1-Y_{H_2S})}\, dt}{V_L\,[Na_2S]^{\circ}} \qquad (4\text{-}5)$$

where, Y_{H2S} is molar fraction of H_2S in H_2S-N_2 exit gas on a dry basis;

Y_{SO2} is molar fraction of SO_2 in SO_2-N_2 feed gas;

Q_G is measured flow rate of feed gas (mol/min);

V_L is volume of solution in reactor (l);

$[Na_2 S]^\circ$ is initial concentration of sodium sulfide in solution (mol/l).

4.7.2 Relative Errors of Measured Parameters

The error involved in the determination of R will be a function of errors involved in the measurements of these five values. According to the principle of propagation of errors (Barry 1966), the relative error E_R may be described as follows:

$$E_R = \sqrt{2E_{Y_{H2S}}^{\ 2}+E_{Y_{SO2}}^{\ 2}+E_{Q_G}^{\ 2}+E_{V_L}^{\ 2}+E_{[Na2S]}^{\ 2}} \qquad (4\text{-}6)$$

where, E_i is the relative error in measurements of parameter "i".

The absolute uncertainty of a measurement can be presented by standard deviation (σ_s). For a certainty of 95%, the two-sigma ($\pm 2\sigma_s$) error is used to describe the absolute error.

As shown in Chapter Three, the standard deviations for measurement of H_2S molar fraction (Y_{H2S}) in exit gas are 0.00028 and 0.00027 for 0.05 and 0.10 in H_2S-N_2 gaseous mixture. The relative errors are (2x0.00028)/0.05 = 1.1% and (2x0.00027)/0.1 = 0.54% for these two gaseous mixture. Similarly, the relative error for the measurement of SO_2 molar fraction (Y_{SO2}) is determined to be (2x0.00036)/0.1 = 0.72%.

The standard deviation in the measurement of initial sodium sulfide content ($[Na_2S]$) in solution was determined to be 0.035 M for a 1.67M solution. Therefore, the relative error is 2x0.037/1.67 = 4.4%.

The error in measurements of flow rate of gas (Q_G) depends on the graduation of

the measuring tube and the rising speed of liquid film in the tube. The maximum error is estimated to be 0.5 ml for a 50 ml tube, i.e a 1.0% relative error. The error in measurements of volume of solution (V_L) depends on the graduation of the graduated cylinder and is estimated 1/250 = 0.4%.

In summary, E_{YH2S} = 1.1%; E_{YSO2} = 0.72%; $E_{[Na2S]}$ = 4.4%; E_{QG} = 1.0% and E_{VL} = 0.40%. The relative error in the determination of conversion ratios of Na_2S to H_2S in SFBR is estimated to be 4.8%.

4.8 Summary

Experiments conducted in the SFBR show that the $Na_2S_{(aq)}$-SO_2-H_2S system exhibits a three-stage pattern. The key parameters controlling the conversion ratio of sodium sulfide to hydrogen sulfide are the following: [1] reaction temperature; [2] sulfur dioxide content in feeding gas; and [3] initial sodium sulfide content in the solution. Results of kinetic studies suggest that the transfer of aqueous hydrogen sulfide to the gaseous phase is most likely the rate limiting step under conditions studied if the process is not limited by the supply of sulfur dioxide to the system. Although some influences of impurities in the solution were observed under conditions studied, the effects of oxygen at low concentrations and CO_2 in the feeding gas appeared to be insignificant in terms of the removal of sulfur dioxide from the feeding gas by Na_2S solution and the generation of hydrogen sulfide from the acidified solution.

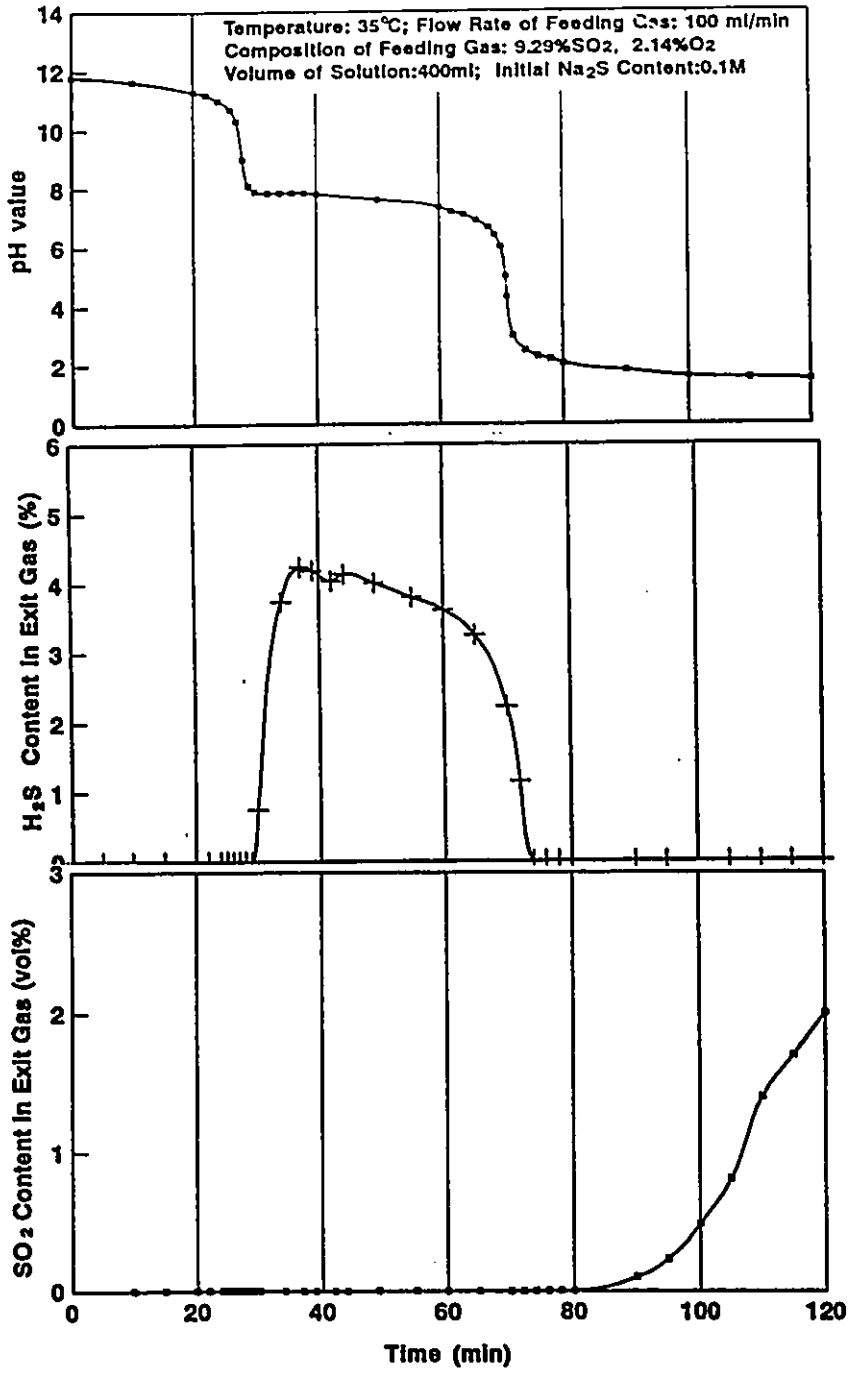

Fig.4.1: The typical result: a three-stage pattern

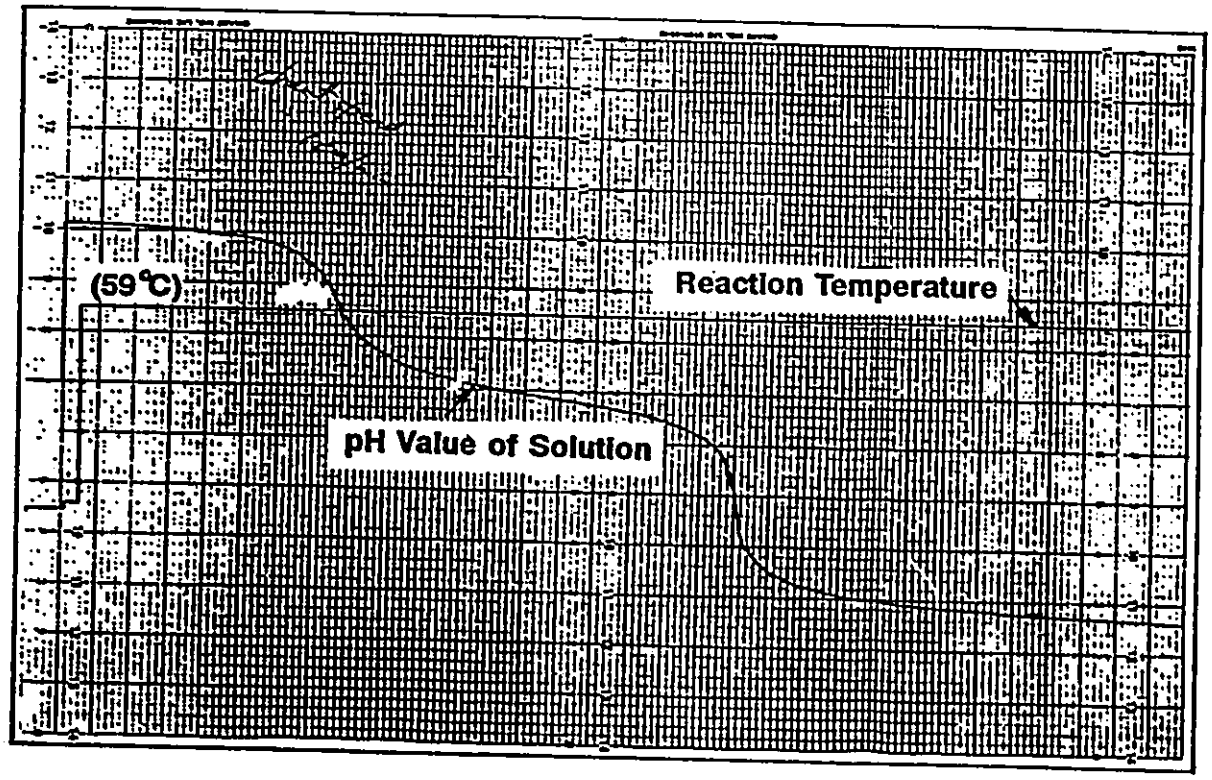

Fig.4.2: An example of the pH profile and reaction temperature recorded by a chart recorder

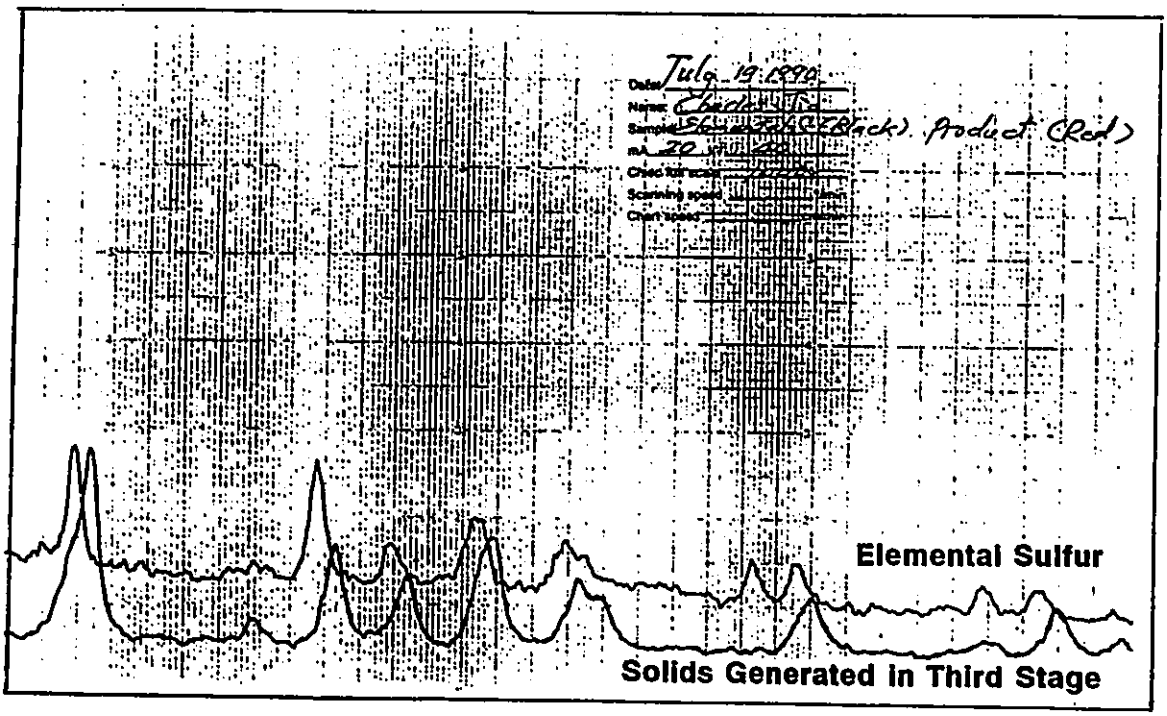

Fig.4.3: A comparison between the diffraction peaks of sample to be identified and elemental sulfur

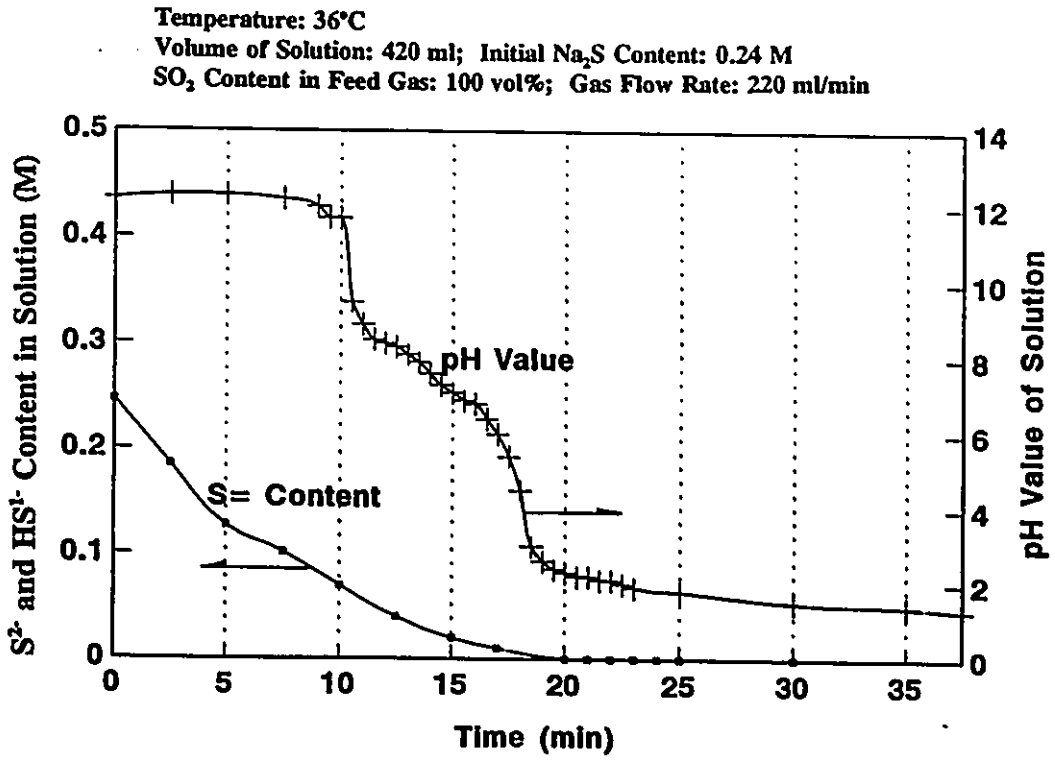

Fig.4.4: The content of sulfide in solution and pH value vs reaction time

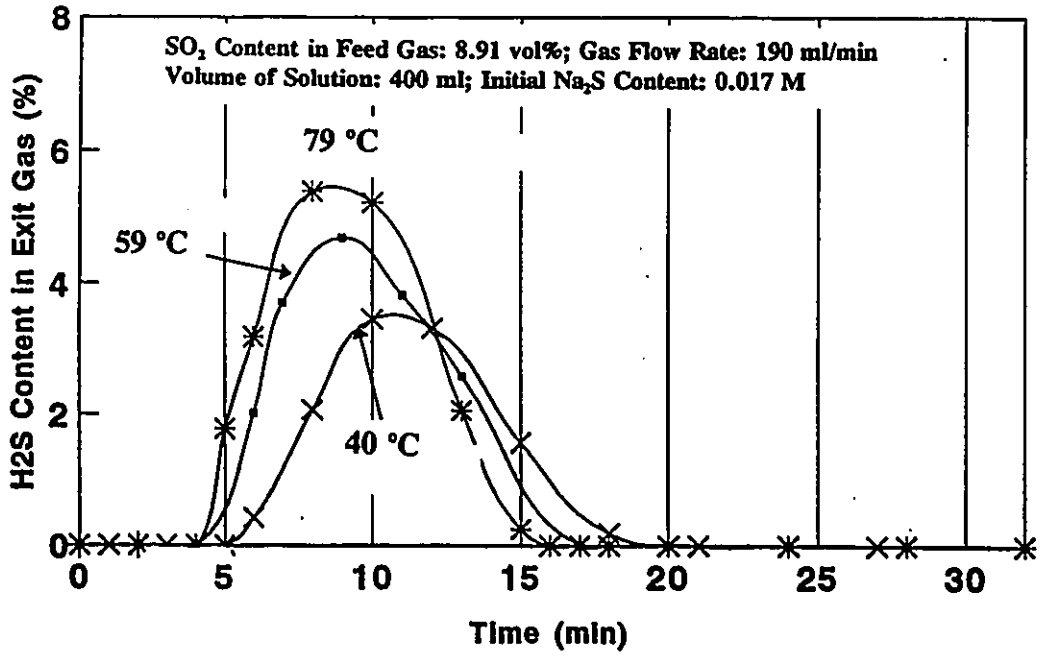

Fig.4.5: Temperature dependence of H_2S content in exit gases

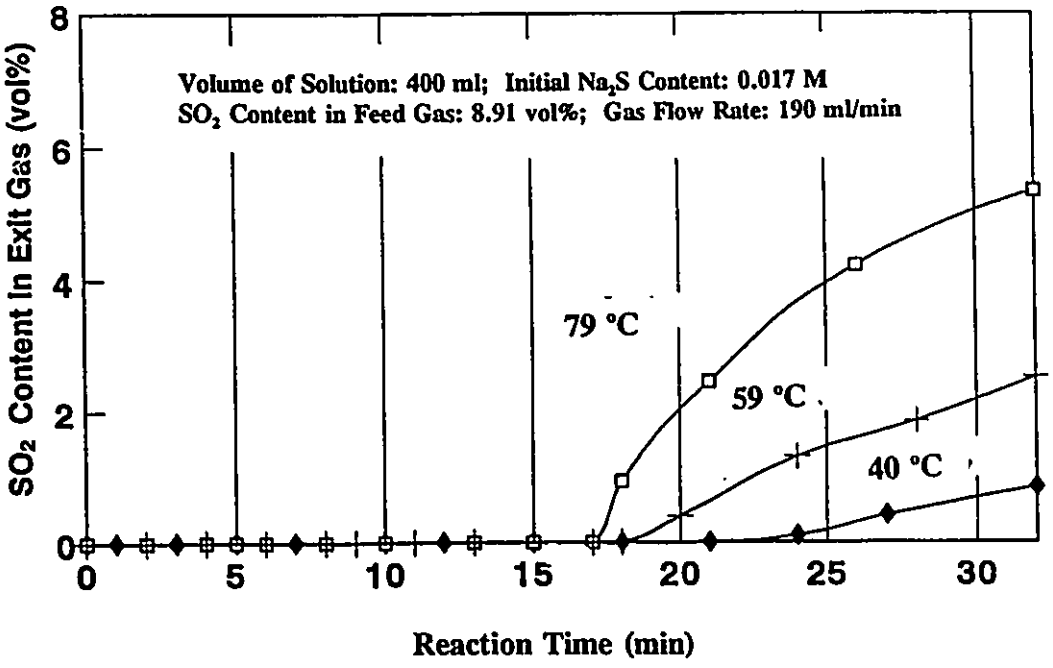

Fig.4.6: Temperature dependence of SO_2 content in exit gases

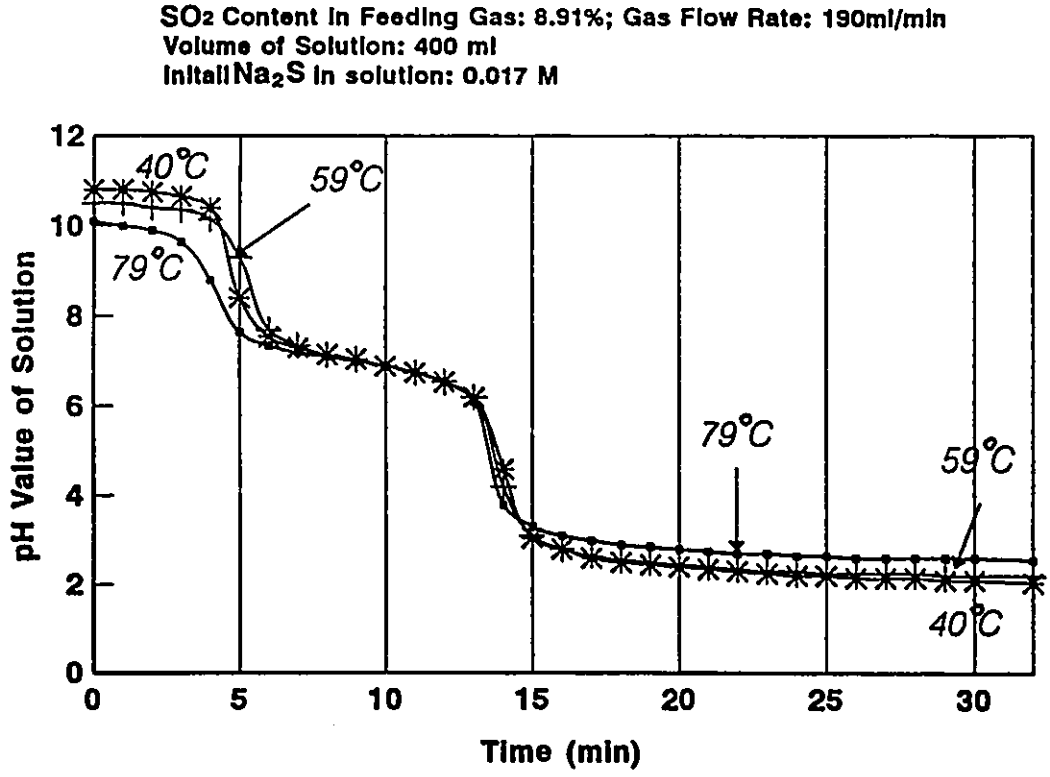

Fig.4.7: Temperature dependence of pH value of solution

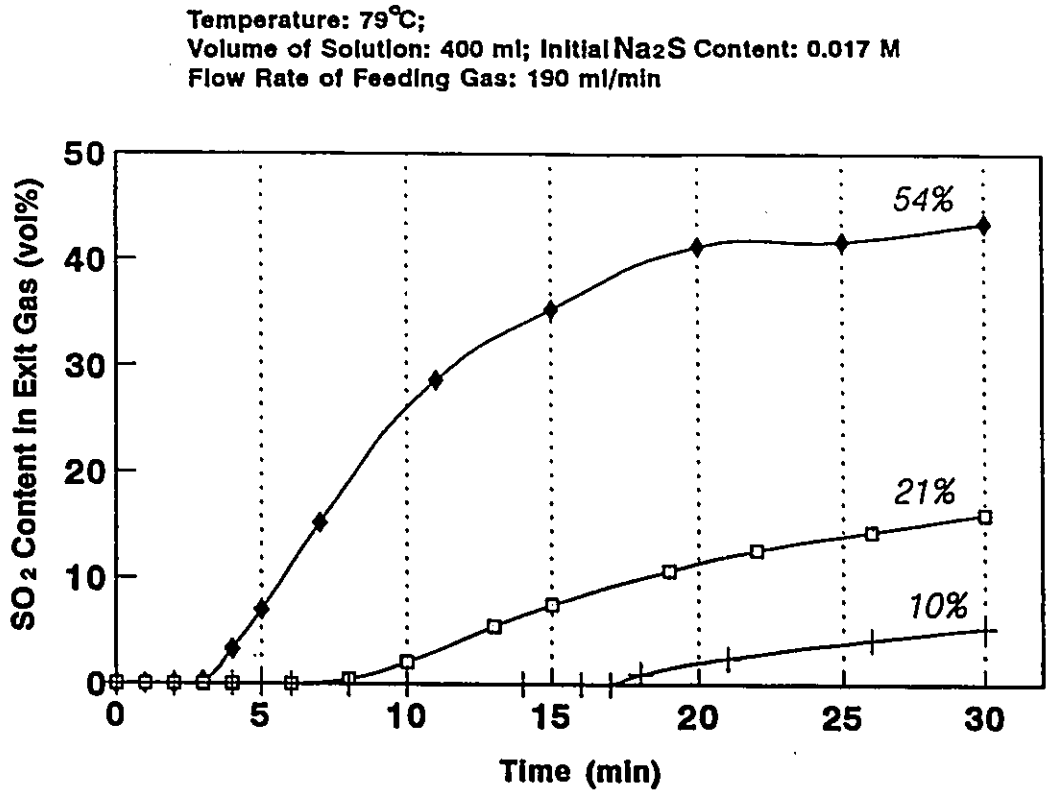

Fig.4.8: The dependence of SO_2 content in exit gases on SO_2 content in feed gases

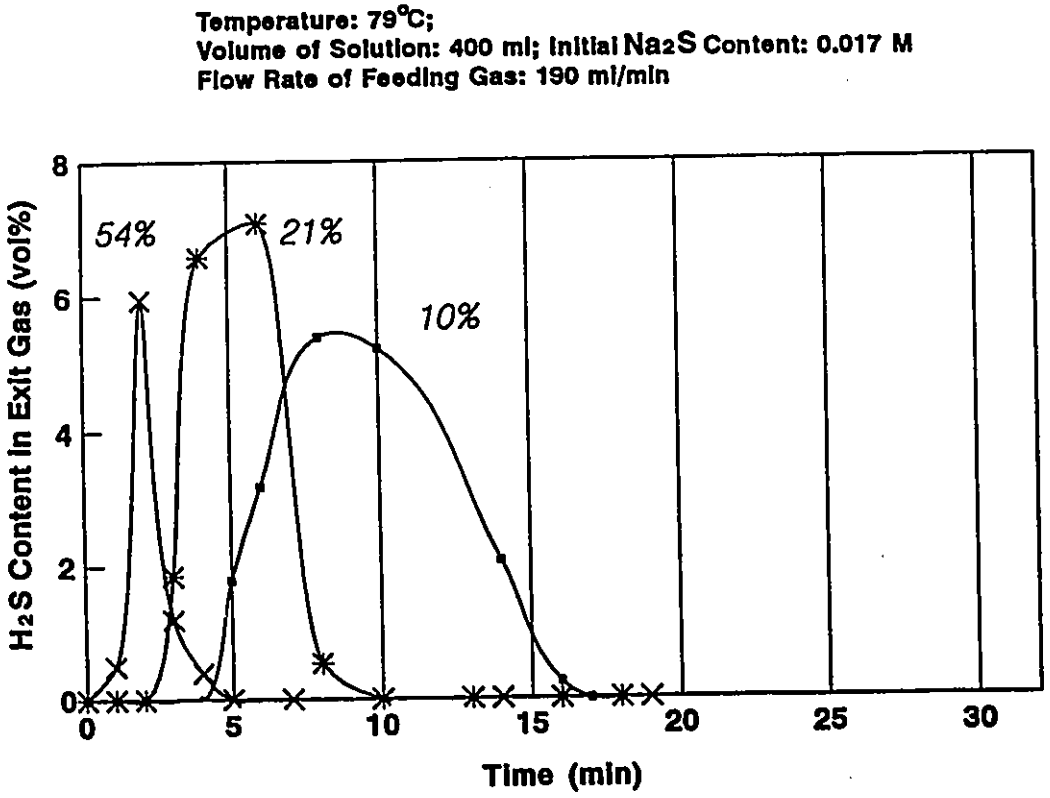

Fig.4.9: The dependence of H_2S content in exit gases on SO_2 content in feed gases

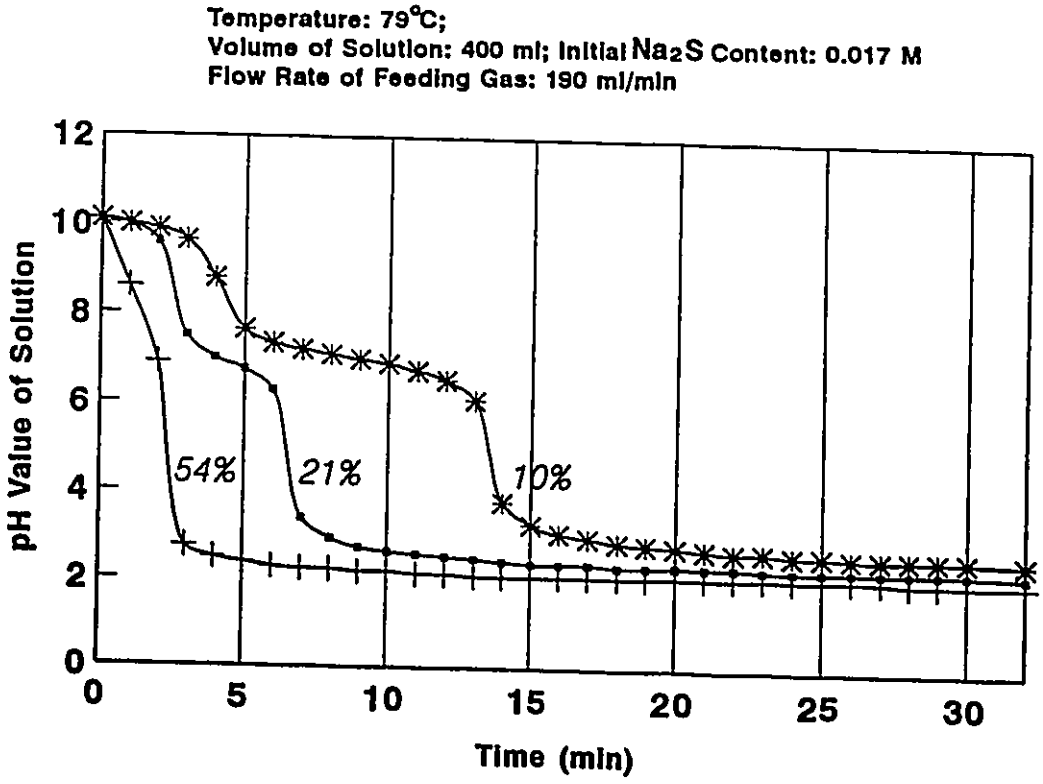

Fig.4.10: The dependence of pH value of solution on SO_2 content in feed gases

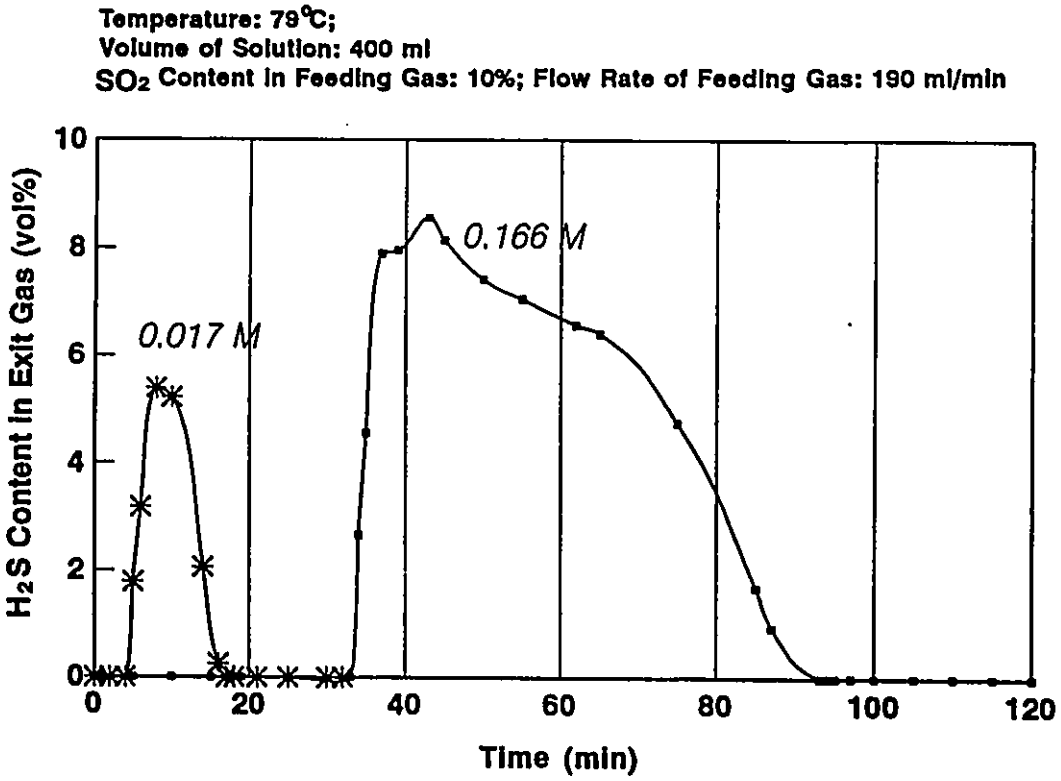

Fig.4.11: The dependence of H_2S content in exit gases on initial content of Na_2S in solution

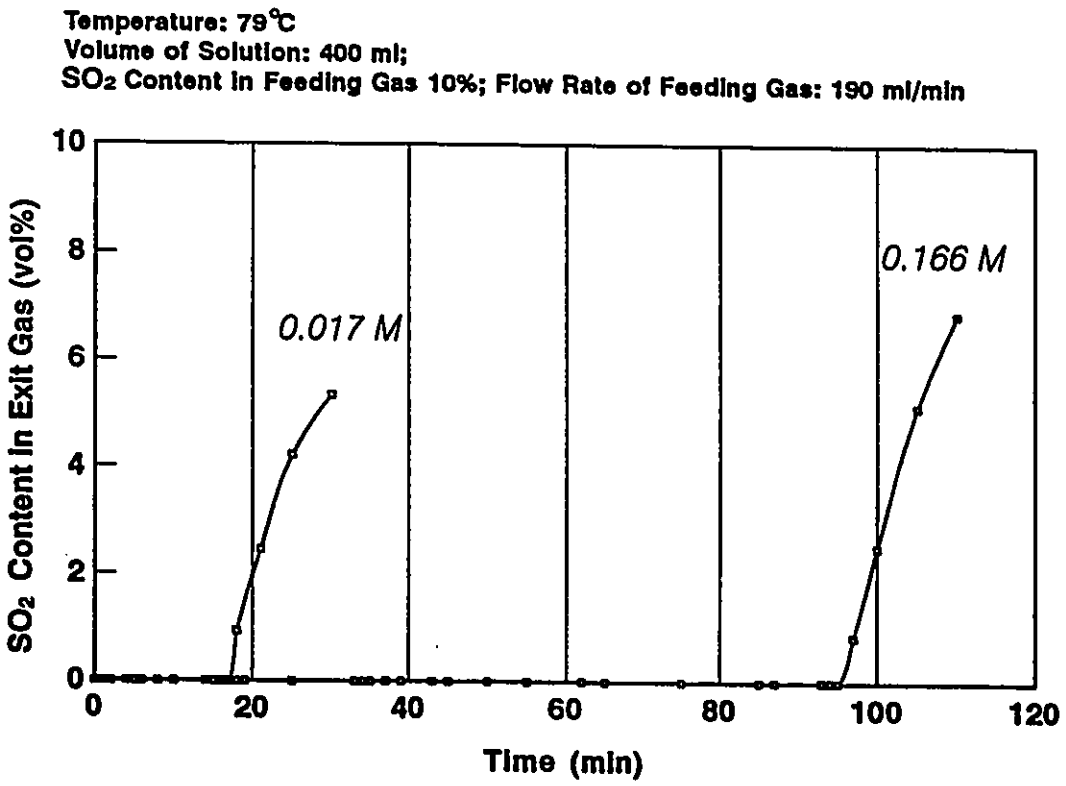

Fig.4.12: The dependence of SO_2 content in exit gases on initial content of Na_2S in solution

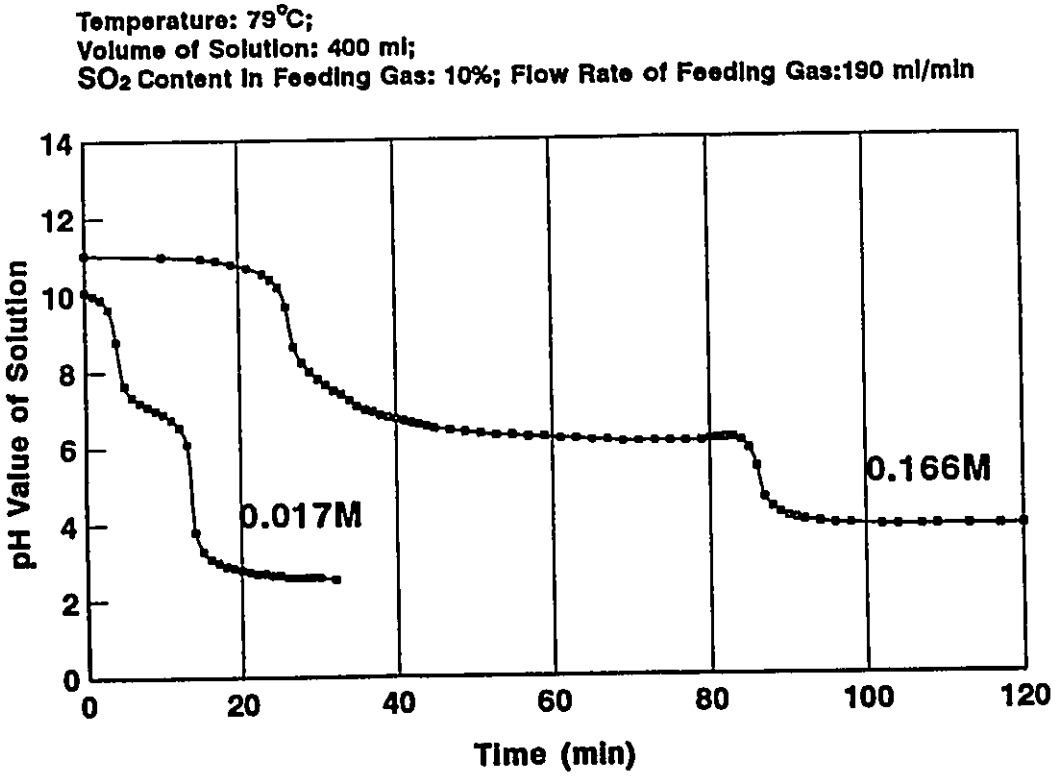

Fig.4.13: The dependence of pH value of solution on initial content of Na_2S in solution

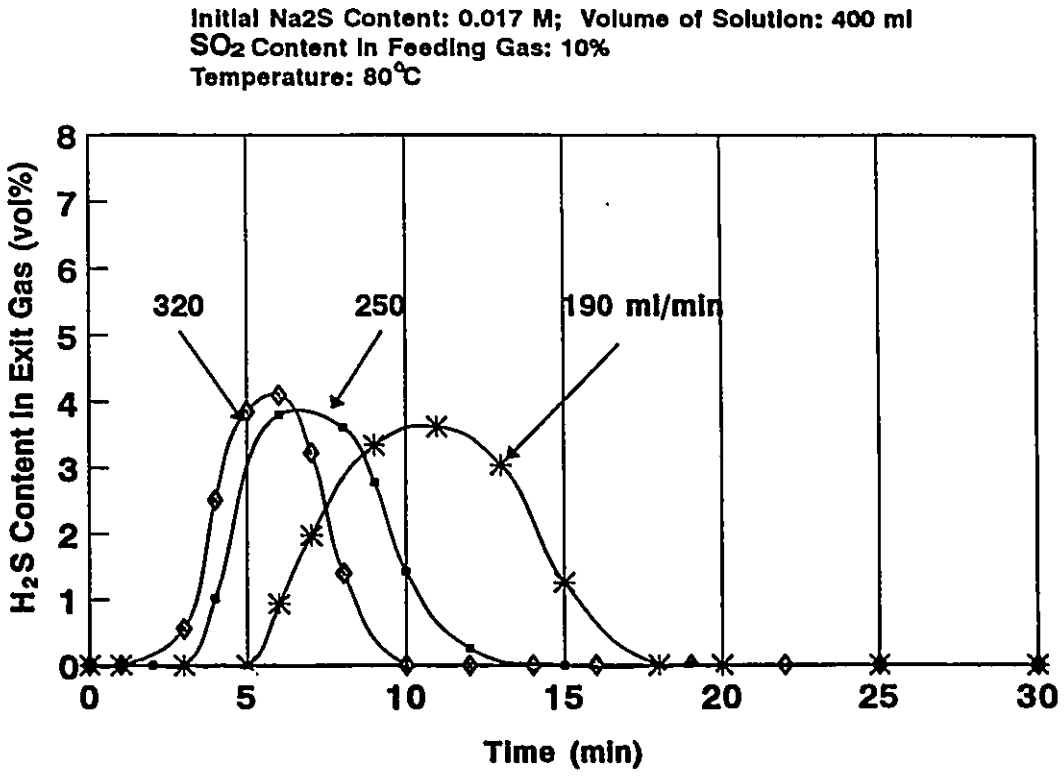

Fig.4.14: Effect of feed gas flow rate on H_2S content in exit gases

SO_2 Content in Feed Gas: 10 vol%; Gas Flow Rate: 340 ml/min
Volume of Solution: 350 ml; Initial Na_2S Content: 1.9 M

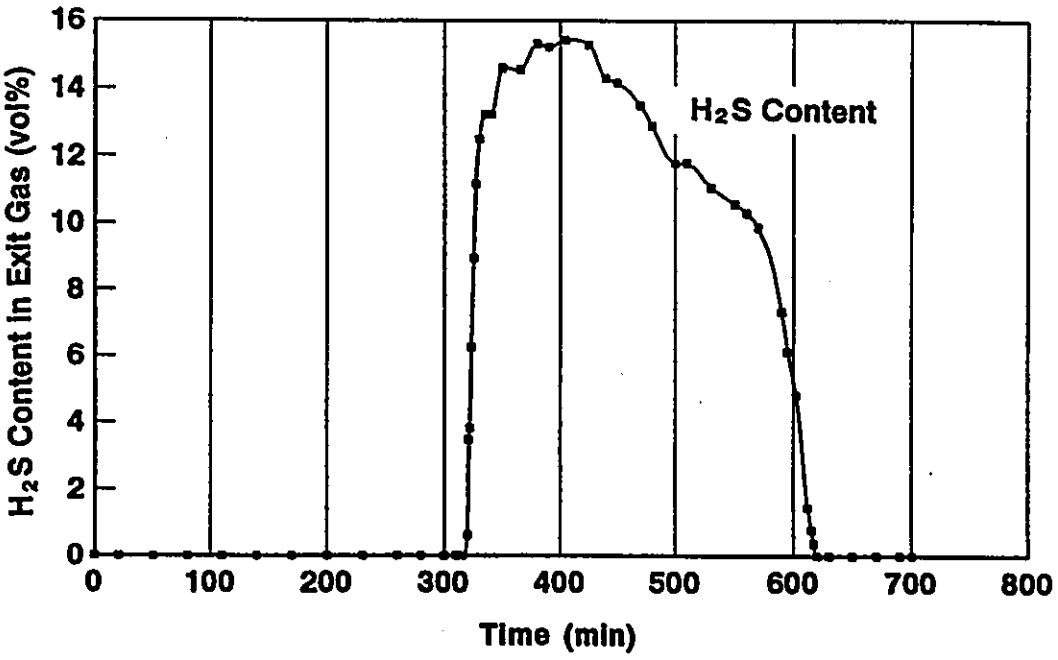

Fig.4.15: H_2S content in exit gases at 90 °C with 1.9 M Na_2S solution

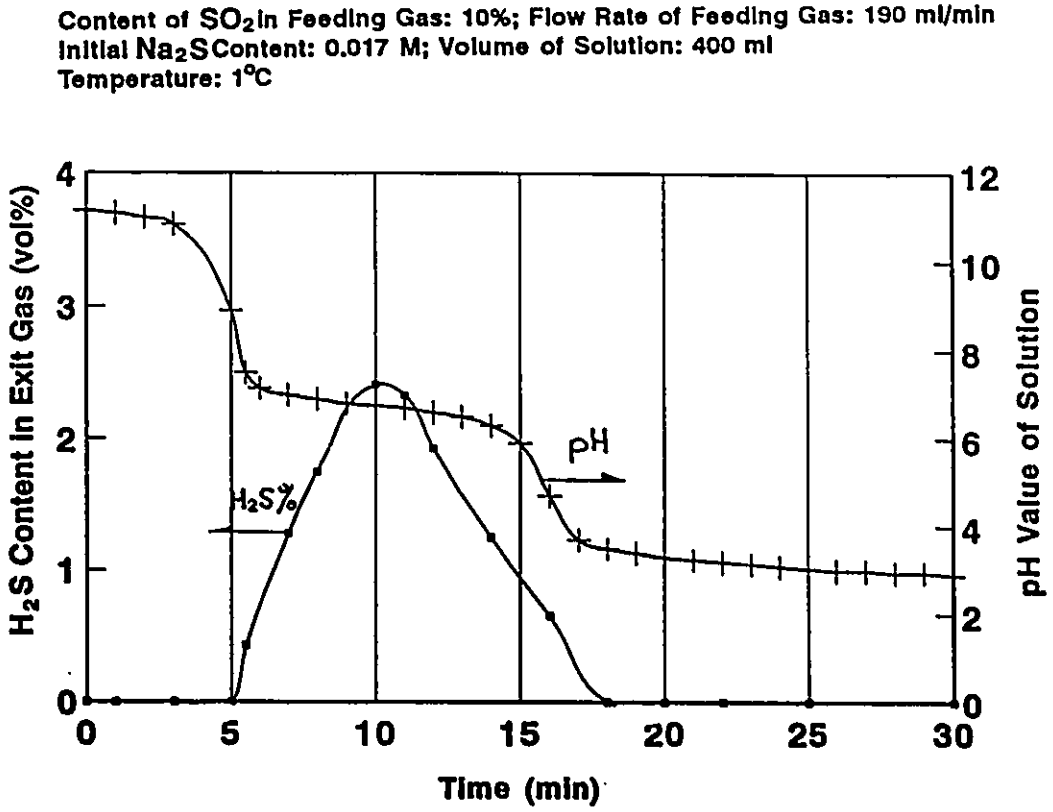

Fig.4.16: H_2S content in exit gases at 1 °C with 0.017 M Na_2S solution

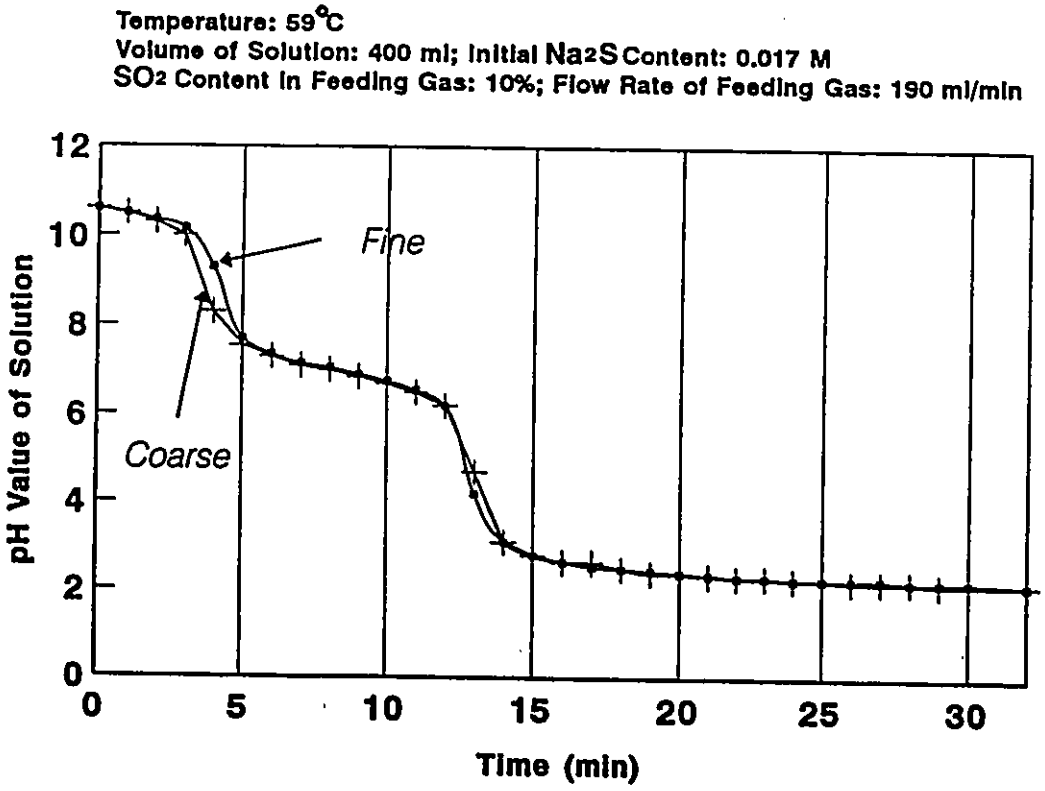

Fig.4.17: Effect of bubble size on pH value of solution

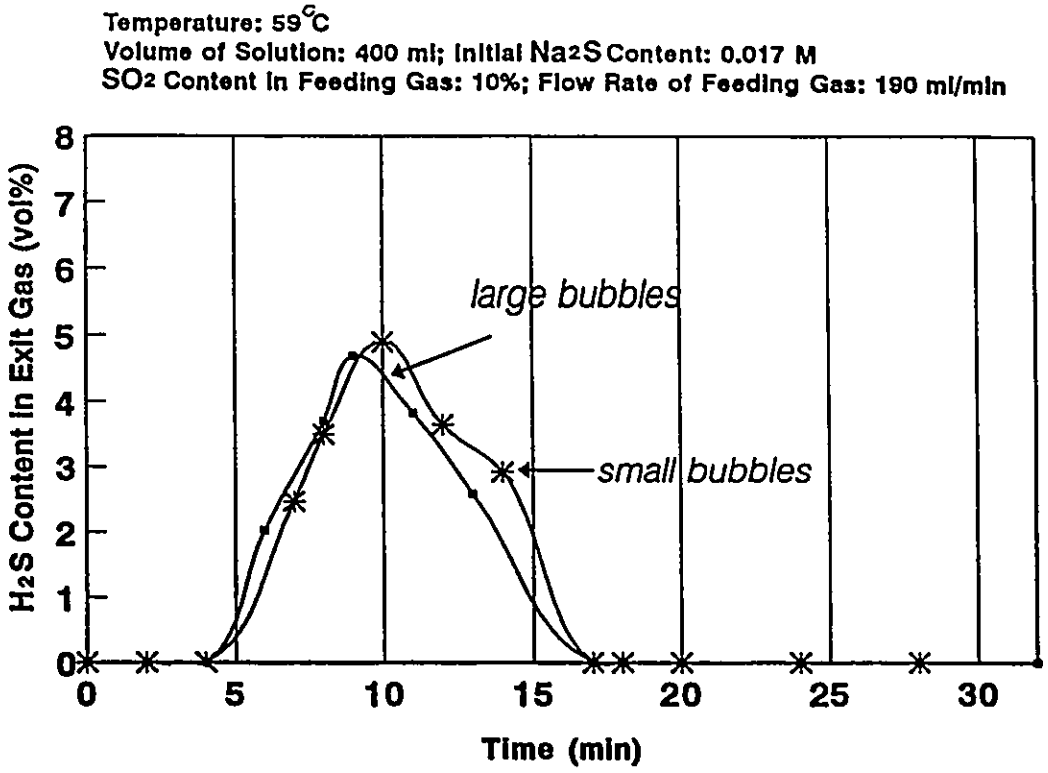

Fig.4.18: Effect of bubble size on H_2S content in exit gases

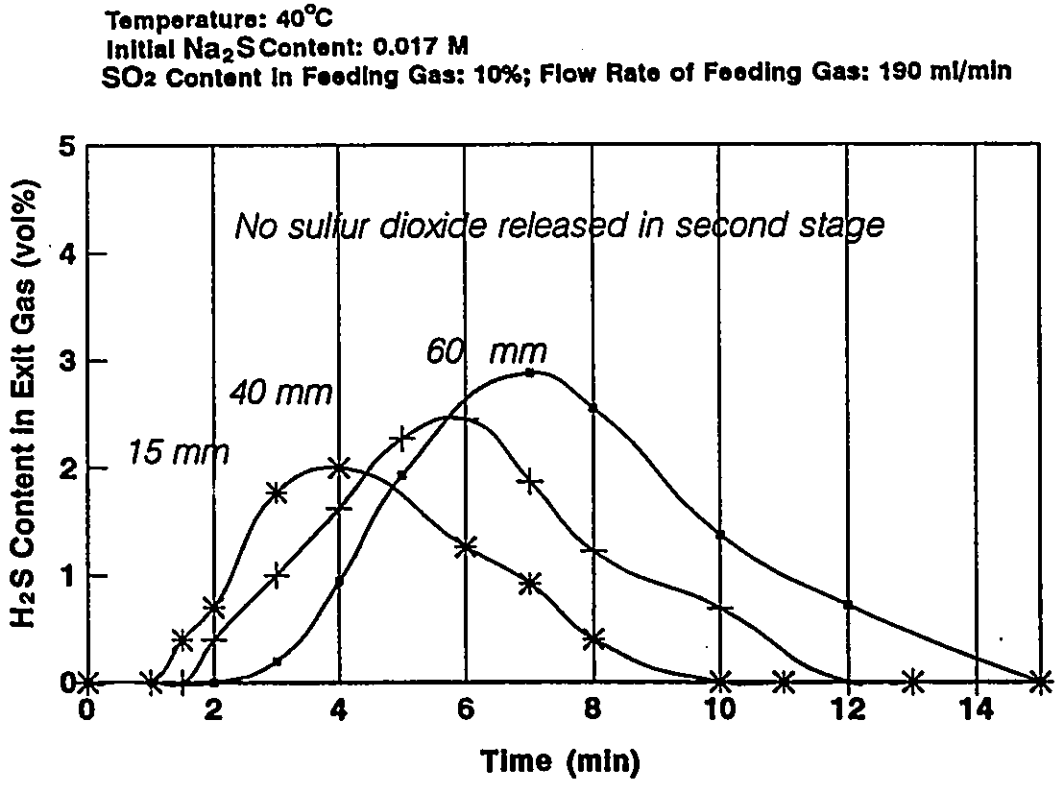

Fig.4.19: Effect of depth of liquid column on H_2S content in exit gases of second stage at 40 °C

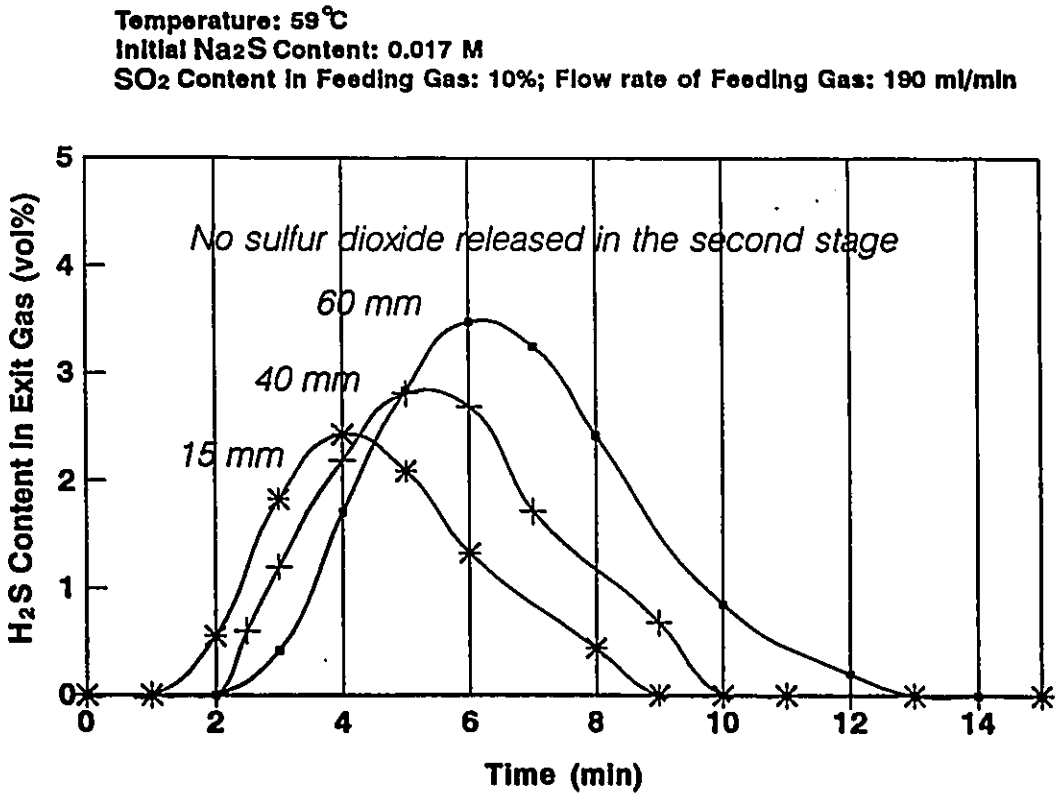

Fig.4.20: Effect of depth of liquid column on H_2S content in exit gases of second stage at 59 °C

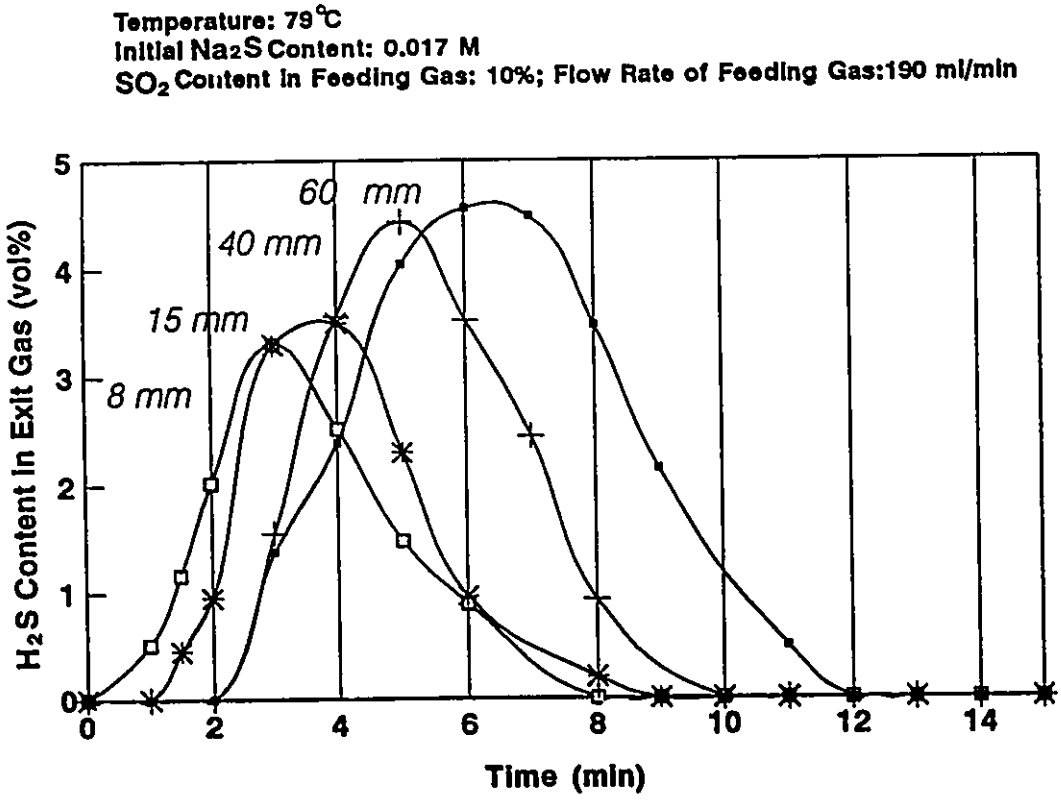

Fig.4.21: Effect of depth of liquid column on H_2S content in exit gases of second stage at 79 °C

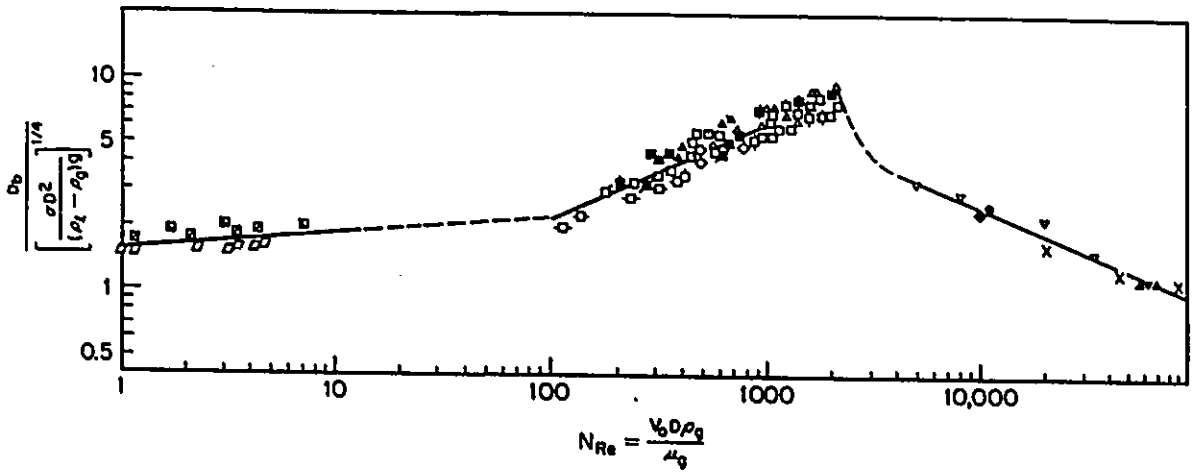

Fig.4.22: The bubble-diameter correlation for air at near-atmospheric pressure sparged into relatively inviscid liquids ($\mu \leq 100$ mPa.s) (after Kumar et.al 1976)

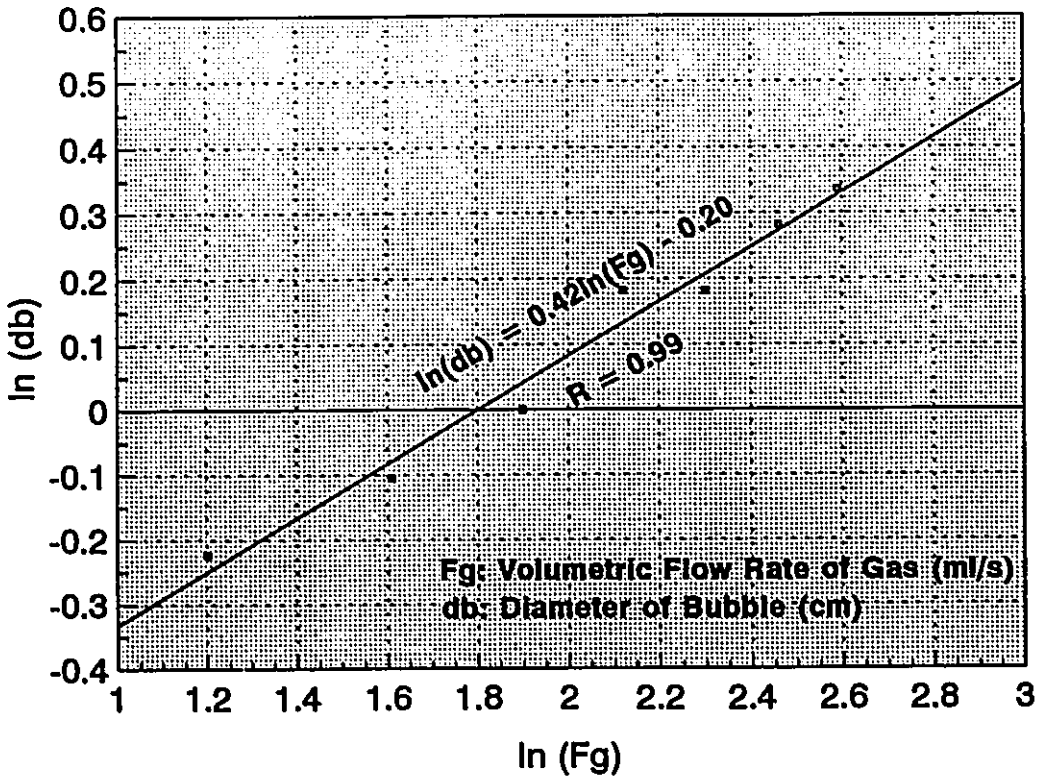

Fig.4.23: Dependence of bubble diameters on volumetric rate of gas

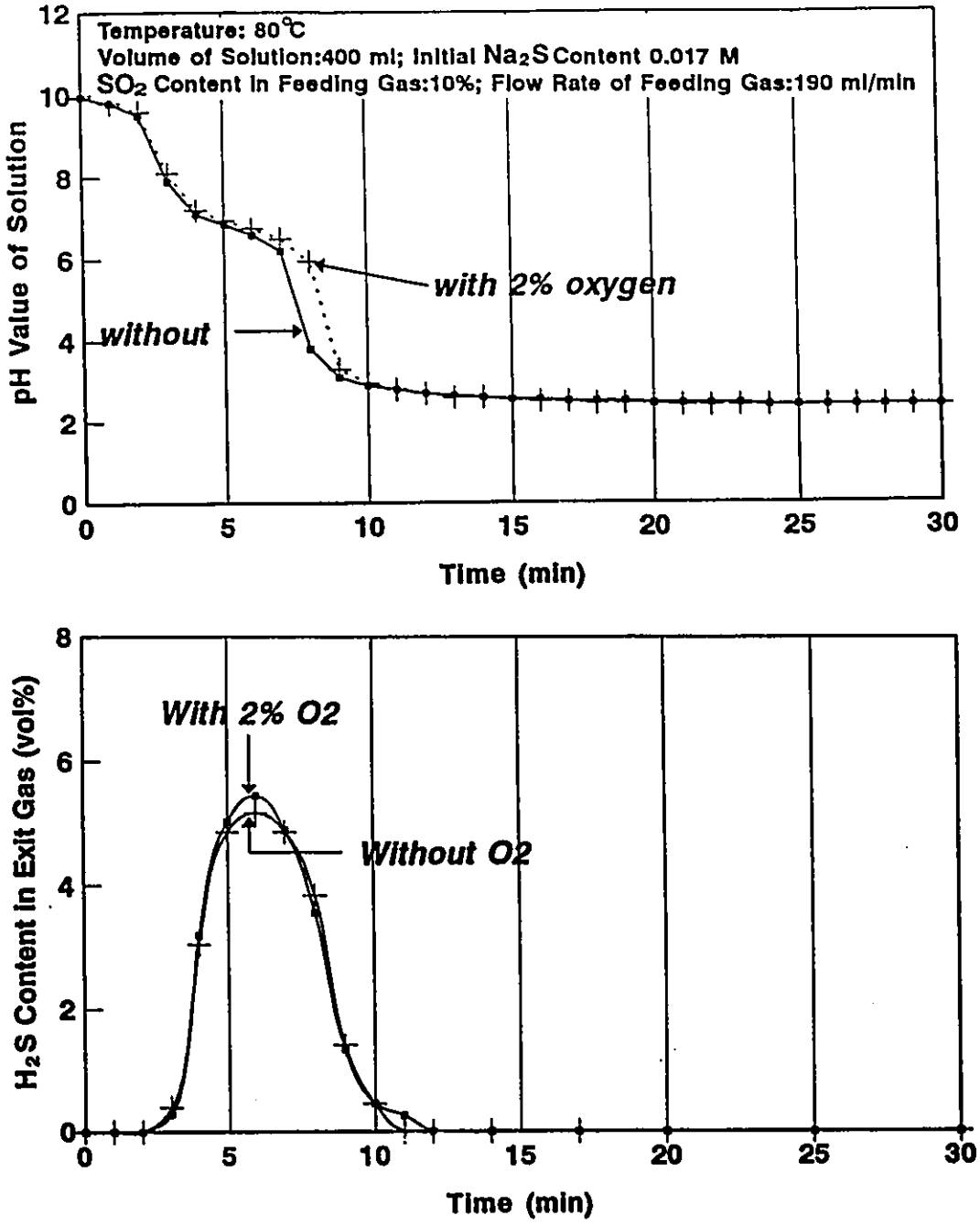

Fig.4.24: Effect of 2% oxygen in feed gas on H_2S content in exit gases and pH value of solution

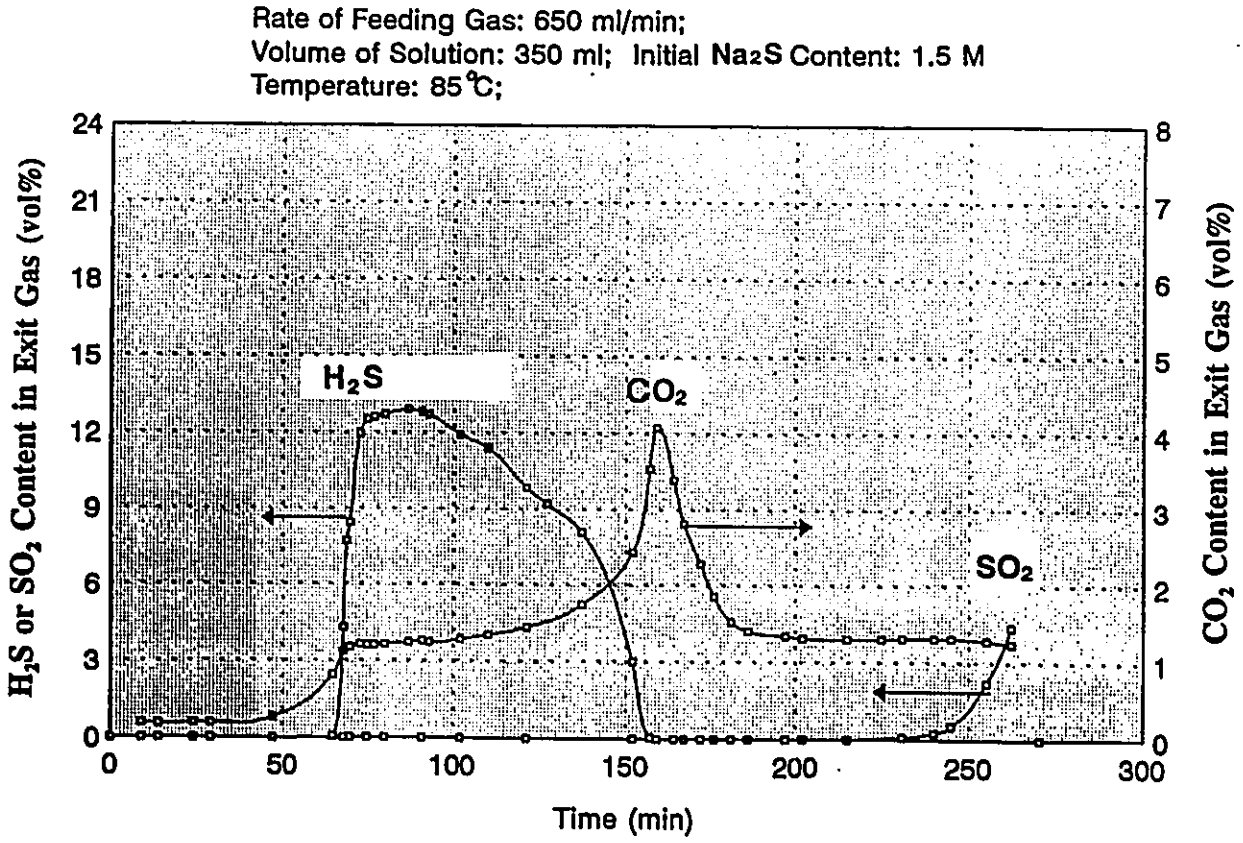

Fig.4.25: Composition of exit gases vs reaction time (1.2% carbon dioxide in feed gas, single-orifice bubble distributor used)

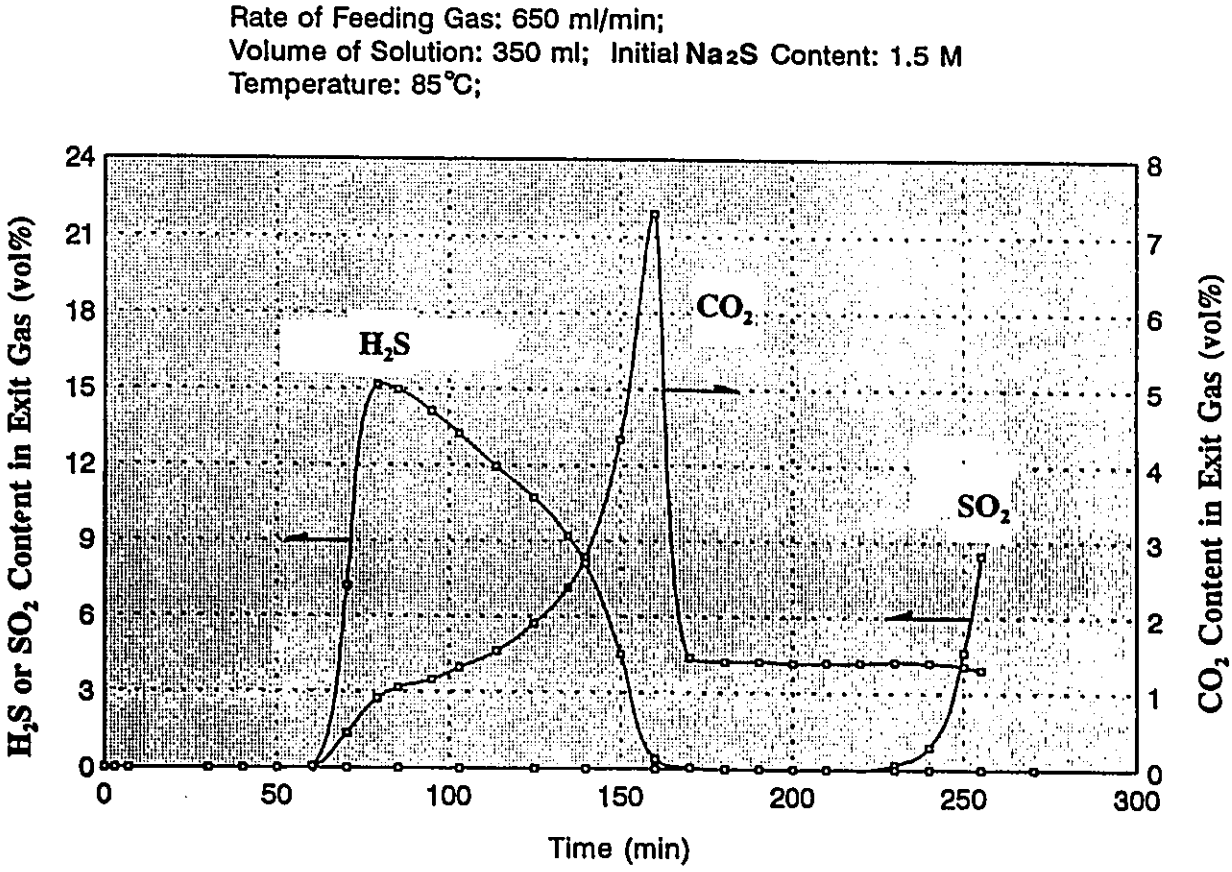

Fig.4.26: Composition of exit gases vs reaction time (1.2% carbon dioxide in feed gas, coarse bubble distributor used)

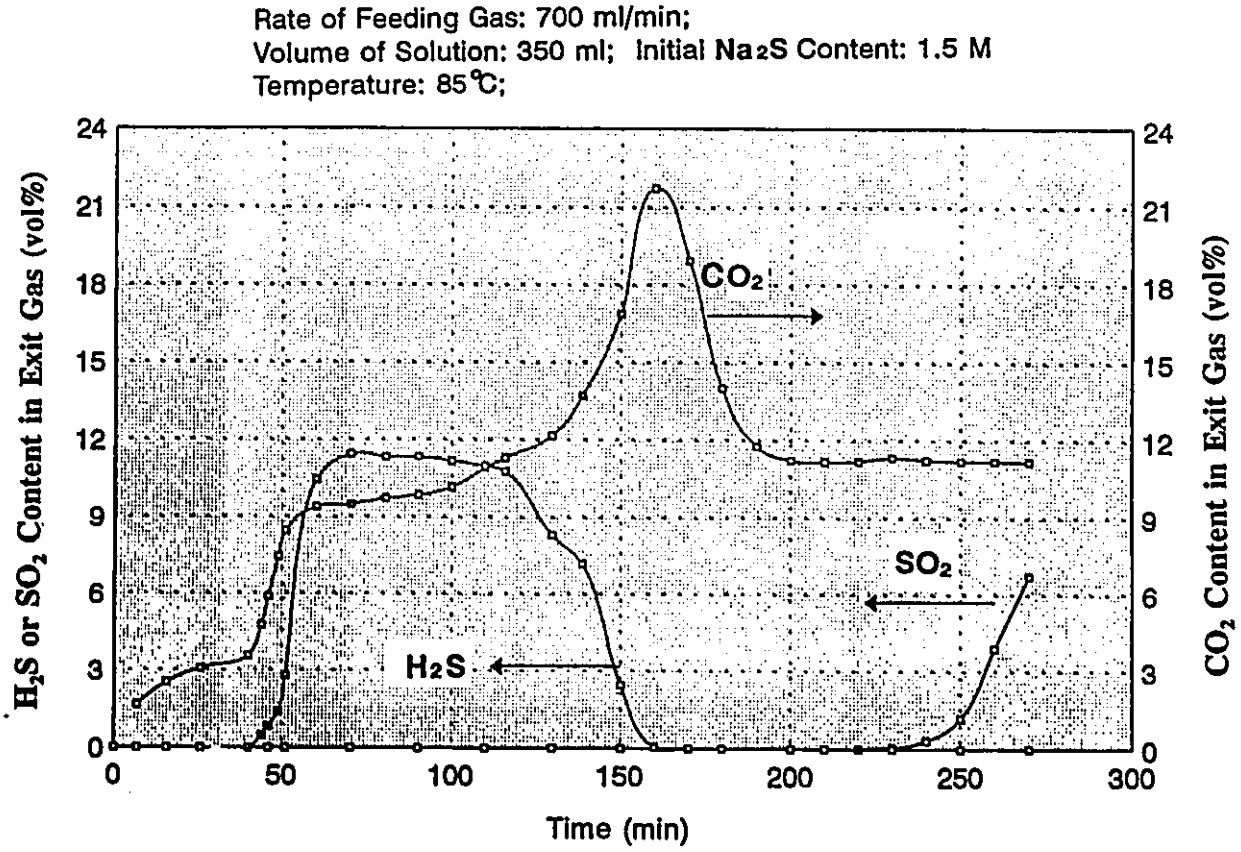

Fig.4.27: Composition of exit gases vs reaction time (10% carbon dioxide in feed gas, single-orifice bubble distributor used)

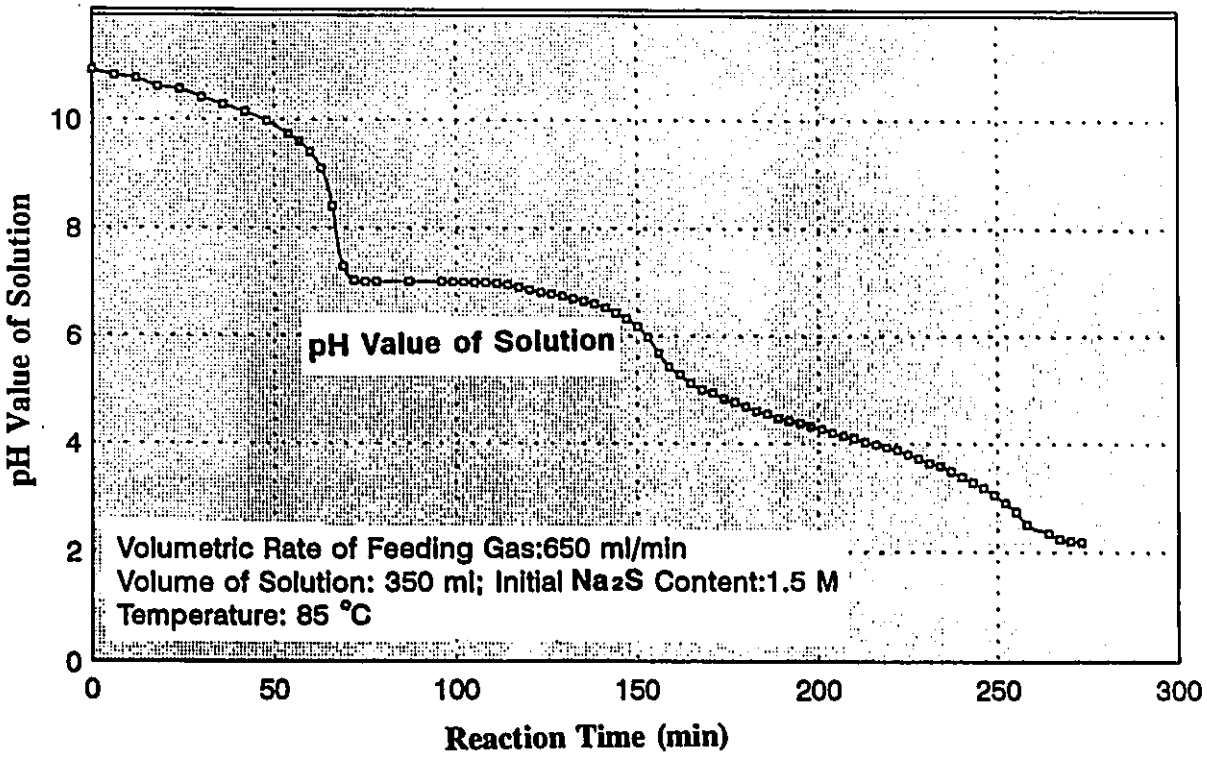

Fig.4.28: pH value of solution vs reaction time (1.2% carbon dioxide in feed gas, coarse bubble distributor used)

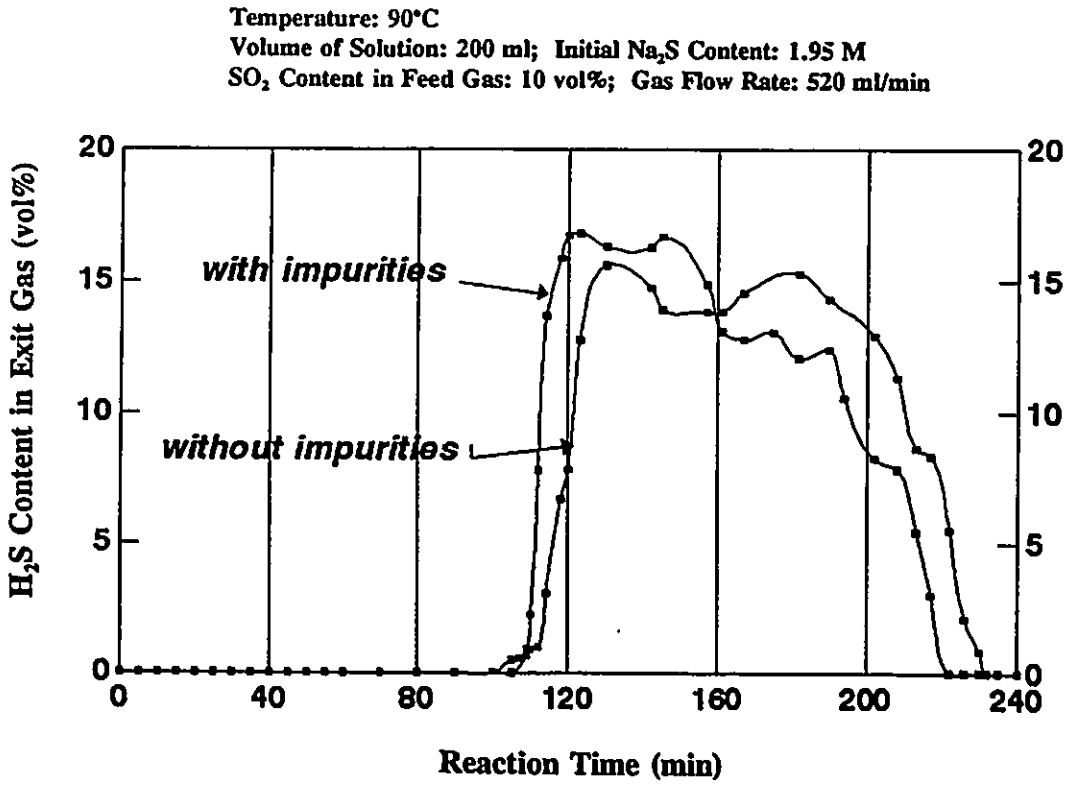

Fig.4.29: Effect of minor impurities (Fe, Cu, Ni and Co) on H_2S content in exit gases

CHAPTER FIVE

EXPERIMENTAL RESULTS OBTAINED USING A CONTINUOUS FLOW TANK REACTOR

In industry, virtually all absorption and desorption facilities, eg. packed towers and spray towers, are operated in a continuous mode for greater efficiency. A continuous flow tank reactor (CFTR), was used for these steady-state experiments so that data generated would be more relevant to the design and operation of a small pilot unit.

5.1 Establishment of A Steady State for Hydrogen Sulfide Generation

The CFTR is proposed to be operated under optimal conditions for H_2S generation, which were observed in the second stage of a SFBR experiment. Hydrogen sulfide is generated simultaneously with the absorption of sulfur dioxide. The experiments began with simultaneous feeding of fresh Na_2S solution and SO_2-containing gas under conditions corresponding to the later period of the second stage, when H_2S generation is limited by the concentration of sulfide in solution. After the fresh Na_2S solution and SO_2-containing gaseous mixture were fed into the reactor which was kept at a water bath at a desirable temperature at constant flow rates for a certain period of time, a steady state would be established. The steady state was marked by a constant composition of exit gas and a constant pH value of the solution.

It was observed that the period of time (5 to 30 minutes) before the CFTR

established its steady state depended primarily on the mass flow rate of Na_2S in solution. A higher mass flow rate of Na_2S in solution resulted in a shorter induction period. Furthermore, for a constant mass flow rate of SO_2 in feed gas, there existed an optimal mass flow rate of Na_2S in feed liquid at which the content of hydrogen sulfide in exit gas reached a maximum level, i.e. an optimal mass flux ratio of Na_2S to SO_2 was attained.

In the experiments conducted in the CFTR, the feeding rate of fresh Na_2S solution was monitored and held at the optimum value to ensure an appropriate H_2S content in exit gas. Several feeding rates were tested before the existence of an optimal value was confirmed. Fig.5.1 shows an example of the evolution of system towards a steady state. The increases in pH value and partial pressure of hydrogen sulfide after 110 minutes were the results of the increase of feeding rate of liquid.

5.2 Cases without Oxygen in The Feed Gas and Impurities in The Solution

Two SO_2/N_2 gaseous mixtures with different compositions were used, i.e. 7.0%SO_2 and 9.84 % SO_2. The fresh solution had a Na_2S content of 1.44 M for both cases. The volume of solution in the reactor was maintained at 300 ml. The temperature was maintained at 90°C. When the gas mixture containing 7.0% SO_2 was used, the flow rate of the feeding gas was held at 900 ml/min. The feeding rate of solution was 1.23 ml/min. For the gas mixture containing 9.84% SO_2, the flow rates of feeding gas and liquid were 540 ml/min and 1.00 ml/min, respectively. For a larger mass flow rate of SO_2 in feeding gas, a larger mass flow rate of sodium sulfide was required to maintain a high H_2S content in the exit gas.

For the cases with 7.0%SO_2 and 9.84%SO_2 in the feeding gas, the steady states were maintained for 90 and 60 minutes, respectively, as shown in Figs.5.2 and 5.3. The means and standard deviations of H_2S contents in exit gas are given in Table 5.1. Based on the average value of hydrogen sulfide content and the gas flow rate, the molar flow of hydrogen sulfide was calculated. Using the feeding rates of solution and gas, and their concentrations, the molar flows of Na_2S to SO_2 were determined. Mass flows established during the period of steady state are summarized in Table 5.2.

Table 5.1 A Summary of Chemical Analysis of Exit Gas

SO2 Content (%)	Period of Time observed (min)	Number of Samples	Mean of H_2S Content (%)	Standard Deviation (%)
7.00	90	17	4.28	0.07
9.84	60	14	5.84	0.05

Table 5.2 Molar Flows of Reactants and Product and Their Ratios

SO_2 Content in Feeding Gas (%)	$\dot{M}(Na_2S)$ (mol/min)	$\dot{M}(SO_2)$ (mol/min)	$\dot{M}(H_2S)$ (mol/min)	$\frac{\dot{M}(H_2S)}{\dot{M}(SO_2)}$	$\frac{\dot{M}(H_2S)}{\dot{M}(Na_2S)}$
7.00	1.77×10^{-3}	2.81×10^{-3}	1.67×10^{-3}	0.59	0.96
9.84	1.44×10^{-3}	2.37×10^{-3}	1.35×10^{-3}	0.57	0.94

As listed in Table 5.2, over 90% of sodium sulfide was converted to hydrogen sulfide at 90°C. It should be noted that the conversion ratio observed in the continuous flow tank reactor at 90 °C was about 10% higher than that in the semiflow batch reactor at the same temperature.

5.3 Case With 1.88% Oxygen in The Feeding Gas

To study the effect of oxygen on the Na_2S conversion to H_2S, the gas mixture containing 1.88% O_2, 9.47% SO_2 and balance N_2 was fed into the reactor at a rate of 600 ml/min. The aqueous Na_2S solution (1.44M) was fed into the reactor at a rate of 1.1 ml/min. The volume of solution in the reactor was maintained at 300 ml at a constant temperature of 90°C.

The H_2S content in the exit gas and the pH value of the solution were plotted against reaction time in Fig.5.4. The details of gas sampling and analysis in steady state are given in Table 5.3. The determined molar flows of reactants and molar flow ratios are listed in Table 5.4.

Table 5.3 A Summary of Chemical Analysis of Exit Gas

O_2 Content (%)	Period of Time observed (min)	Number of Samples	Mean of H_2S Content (%)	Standard Deviation (%)
1.88	60	9	5.52	0.06

Table 5.4 Molar Flows of Reactants and Product and Their Ratios

O_2 Content in Feeding Gas (%)	$\dot{M}(Na_2S)$ (mol/min)	$\dot{M}(SO_2)$ (mol/min)	$\dot{M}(H_2S)$ (mol/min)	$\frac{\dot{M}(H_2S)}{\dot{M}(SO_2)}$	$\frac{\dot{M}(H_2S)}{\dot{M}(Na_2S)}$
1.88	1.63×10^{-3}	2.54×10^{-3}	1.42×10^{-3}	0.56	0.87

Comparing data in Table 5.4 with that in Table 5.2, the presence of 1.88%O_2 in the feeding gas had lowered the conversion ratio of Na_2S to H_2S from 0.94 to 0.87. This may imply that oxygen in the feeding gas participated in the oxidation of sulfide in the system.

5.4 Cases With Oxygen in The Feeding Gas and Impurities in The System

Sodium sulfide solution of 1.44 M fed to the reactor at 1.1 ml/min was free of impurities. The reaction temperature was maintained at 90°C. The gas mixture containing 1.88 $\%O_2$ and 9.47 $\%SO_2$ was simultaneously fed into the reactor at a rate of 600 ml/min. The volume of solution in the reactor was about 300 ml.

Impurities were added to the reactor in the form of sulfates when the reactor was operated in the SFBR mode. The amounts of Fe, Ni, Cu and Co added to the reactor were determined by assuming all impurities would dissolve and form a solution of 300 ppm Fe, 100 ppm Ni, 5 ppm Cu and 4 ppm Co. According to Freier (1976), the solubilities of FeS, NiS, CuS and CoS in water are extremely low (1.24, 0.72, 0.055 and 0.67ppm at 18°C, respectively). Hence, the concentration of ions of these metals dissolved in the solution were expected to be extremely low due to the high concentration of soluble sulfide ion in the solution initially. However, some of the metal sulfide might have dissolved in the solution as metal ions when the content of soluble sulfide dropped with the generation of hydrogen sulfide.

The steady state was maintained for 30 minutes at 90°C, before the temperature was increased to 93°C. Approximately 5 minutes later, a new steady state was reached at 93 °C, which was maintained for another 20 minutes. As shown in Figs.5.5 and 5.6, the H_2S contents in the exit gas and the pH values of the solution were plotted against reaction time. The details of gas sampling and analysis in steady state are summarized in Table 5.5. The molar flows and the flow ratios of the reactants to the products are determined and are listed in Table 5.6.

Table 5.5 A Summary of Chemical Analysis of Exit Gas

Temperature (°C)	Period of Time observed (min)	Number of Samples	Mean of H_2S Content (%)	Standard Deviation (%)
90	30	6	5.31	0.08
93	20	3	5.82	0.02

Table 5.6 Molar Flows of Reactants and Product and their Ratios

Temperature (°C)	$\dot{M}(Na_2S)$ (mol/min)	$\dot{M}(SO_2)$ (mol/min)	$\dot{M}(H_2S)$ (mol/min)	$\frac{\dot{M}(H_2S)}{\dot{M}(SO_2)}$	$\frac{\dot{M}(H_2S)}{\dot{M}(Na_2S)}$
90	1.58×10^{-3}	2.54×10^{-3}	1.36×10^{-3}	0.54	0.86
93	1.58×10^{-3}	2.54×10^{-3}	1.49×10^{-3}	0.59	0.94

Comparing data in Table 5.6 with that in Table 5.4, it can be seen that the conversion ratio of sodium sulfide dropped slightly from 0.87 to 0.86 while the molar flow ratio of H_2S to SO_2 decreased from 0.56 to 0.54. These differences may not be significant as the impurities added initially seem not to play a significant role under the conditions studied. Conversely, the strong temperature dependence was observed in the CFTR.

5.5 The Effect of Liquid Residence Time in The Reactor on Na_2S Conversion to H_2S

The effect of liquid residence time was studied by varying the amount of liquid in the reactor but keeping the liquid feeding rate constant. For comparison, two experiments were carried out in the CFTR at 90°C. The volume of solution in the reactor for the tests were 200 and 350 ml, respectively. A 1.5 M aqueous Na_2S solution was fed into the reactor at a rate of 1.1 ml/min. The flow rate of the feed gas (10%

SO_2) was 610 ml/min. Values of mean residence time of liquid were calculated to be 182 and 318 minutes, respectively. To eliminate the possible effects of bubble travel time, which depends on the length of the immersed portion of the bubble distributor, a shorter distributor was used for the experiment with a larger amount of solution in the reactor. The experimental results are summarized in Table 5.7 and 5.8.

Table 5.7 A Summary of Chemical Analysis of Exit Gas

Mean Residence Time of Liquid	Period of Time Observed (min)	Number of Samples	Mean of H_2S Content (%)	Standard Deviation (%)
182 (min)	25	5	5.73	0.13
318 (min)	20	4	5.58	0.22

Table 5.8 Molar Flows of Reactants and Product and Their Ratios

Mean Residence Time of Liquid	$\dot{M}(Na_2S)$ (mol/min)	$\dot{M}(SO_2)$ (mol/min)	$\dot{M}(H_2S)$ (mol/min)	$\frac{\dot{M}(H_2S)}{\dot{M}(SO_2)}$	$\frac{\dot{M}(H_2S)}{\dot{M}(Na_2S)}$
182 (min)	1.65×10^{-3}	2.72×10^{-3}	1.49×10^{-3}	0.55	0.90
318 (min)	1.65×10^{-3}	2.72×10^{-3}	1.45×10^{-3}	0.53	0.88

Data listed above do not suggest that residence time of solution in the reactor could have any significant influence on the kinetics of the system under conditions studied.

5.6 Estimation of Errors Involved in the Determination of Conversion Ratio of Na_2S to H_2S

In this section, errors involved in the determination of this ratio are to be

estimated based on statistical principles.

5.6.1 Conversion Ratio Obtained Using Continuous Flow Tank Reactor (CFTR)

The conversion ratio of Na_2S to H_2S (R) in the CFTR is defined by the following relation:

$$R = \frac{\dot{M}_{H_2S}}{\dot{M}_{Na_2S}} = \frac{\dfrac{(1-Y_{SO_2})\,Y_{H_2S}Q_G}{(1-Y_{H_2S})}}{G_L\,[Na_2S]^{\circ}} \qquad (5\text{-}1)$$

where, Y_{H2S} is molar fraction of H_2S in H_2S-N_2 exit gas on a dry basis;

Y_{SO2} is molar fraction of SO_2 in SO_2-N_2 feed gas;

Q_G is measured flow rate of feed gas (mol/min);

Q_L is measured flow rate of feed liquid (l/min);

$[Na_2S]^{\circ}$ is initial concentration of sodium sulfide in solution (mol/l).

5.6.2 Relative Errors of Measured Parameters

The error in the determination of R will be a function of errors involved in the measurements of these five values. According to the principle of propagation of errors, the relative error E_R may be described as follows:

$$E_R = \sqrt{2E_{Y_{H2S}}^{\,2}+E_{Y_{SO2}}^{\,2}+E_{Q_G}^{\,2}+E_{Q_L}^{\,2}+E_{[Na2S]}^{\,2}} \qquad (5\text{-}2)$$

where, E_i is the relative error in measurements of parameter "i".

For a certainty of 95%, the two-sigma ($\pm 2\sigma_s$) error is used to describe the absolute error. As described in Section 4.7.2, the relative standard deviations for measurements of Y_{H2S}, Y_{SO2}, $[Na_2S]$, Q_G and Q_L are estimated to be $E_{YH2S} = 1.1\%$; $E_{YSO2} = 0.72\%$; $E_{[Na2S]} = 4.4\%$; $E_{QG} = 1.0\%$ and $E_{GL} = 1.0\%$, respectively. Based on Eq.5.2, the relative error in the determination of conversion ratios of Na_2S to H_2S in CFTR is estimated to be 4.9%.

5.7 Summary

In principle, the kinetic behavior observed using a continuous flow tank reactor (CFTR) was the same as that observed using a semiflow batch reactor (SFBR). The conversion ratio of sodium sulfide to hydrogen sulfide obtained by using a CFTR was higher than that obtained by using a SFBR operated under similar conditions. Impurities (Fe, Ni, Cu and Co) added initially in the CFTR did not result in any significant changes in Na_2S conversion to H_2S. However, the oxygen in feed gas lowers the conversion ratio of Na_2S to H_2S in the CFTR by a few percent.

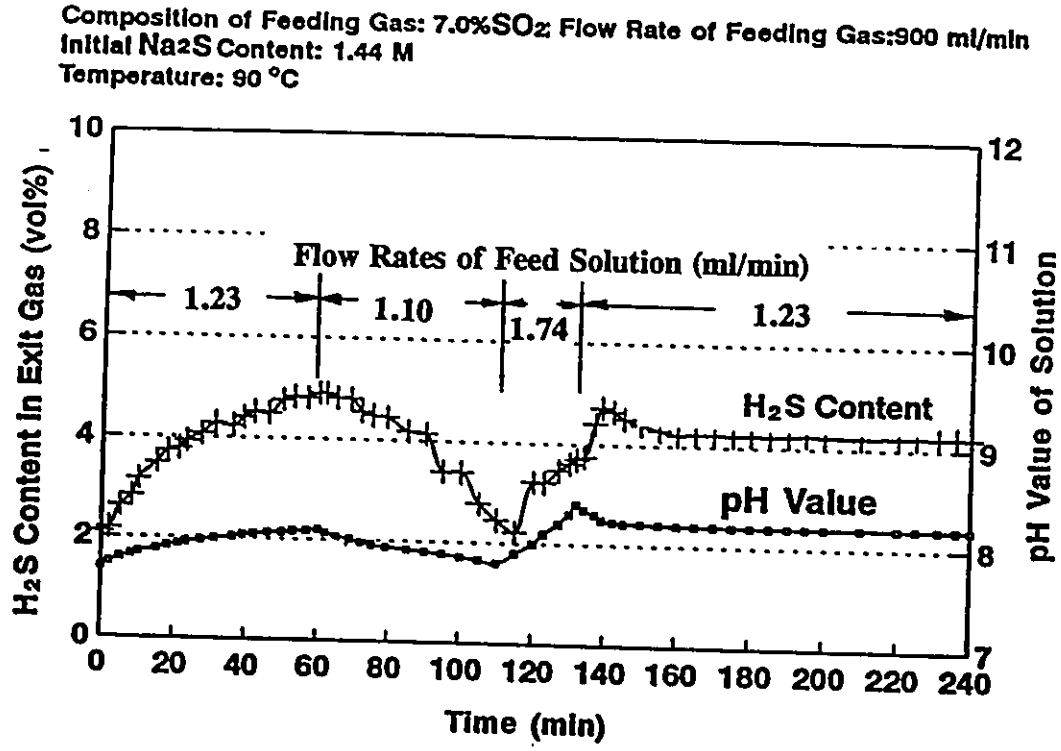

Fig.5.1: An example of the system's approaching to a steady state

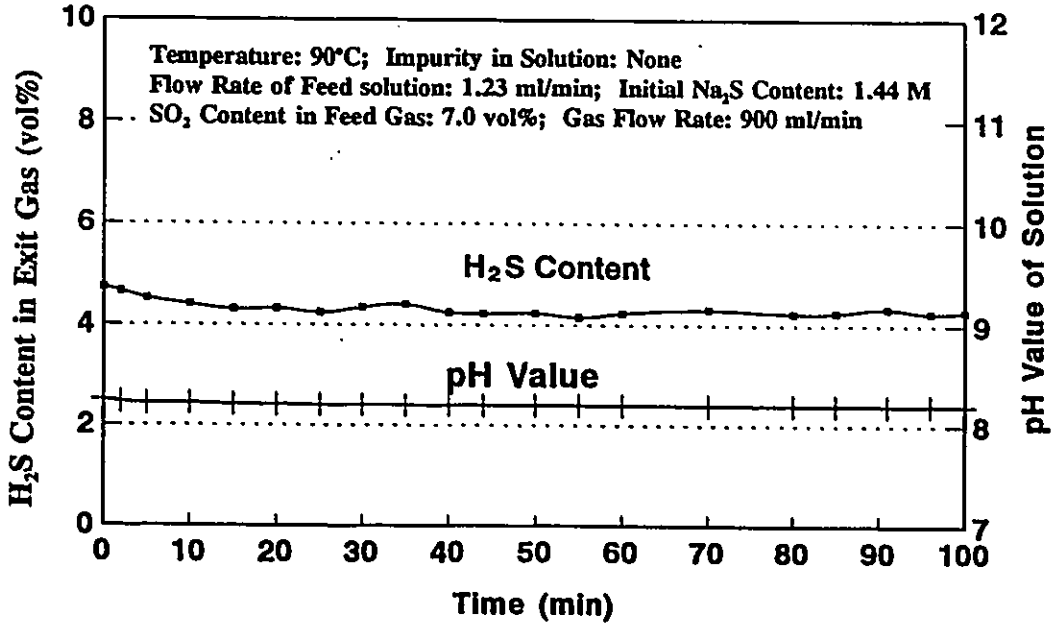

Fig.5.2: H_2S content in exit gases and pH value of solution under the steady state conditions

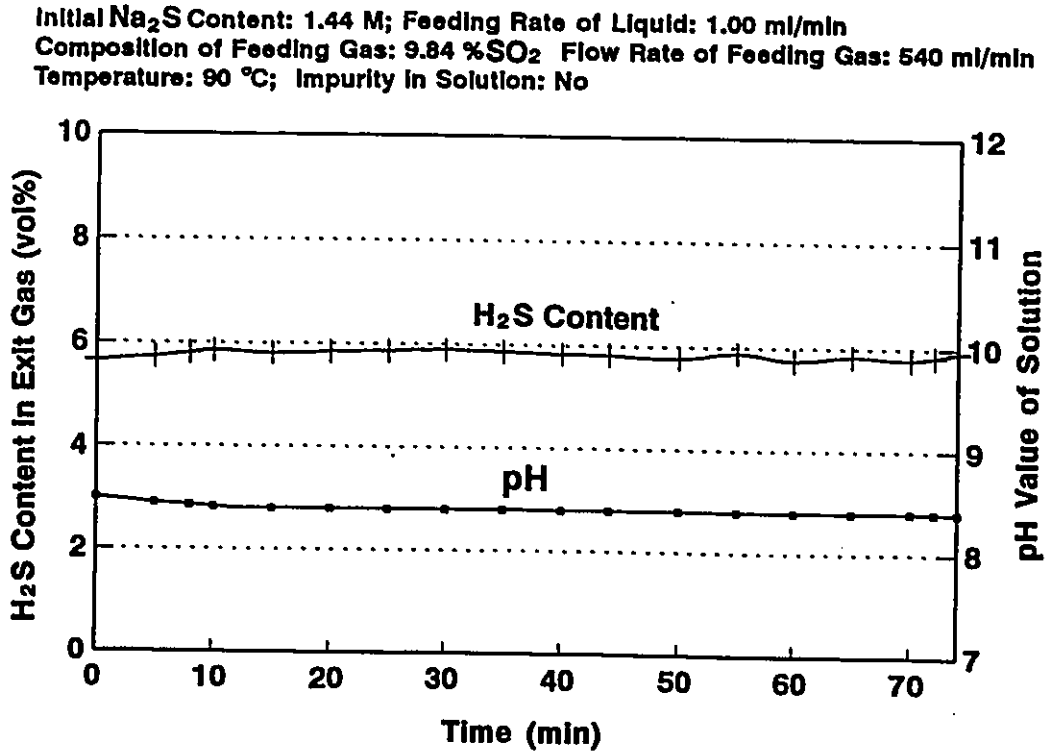

Fig.5.3: H_2S content in exit gases and pH value of solution under the steady state conditions

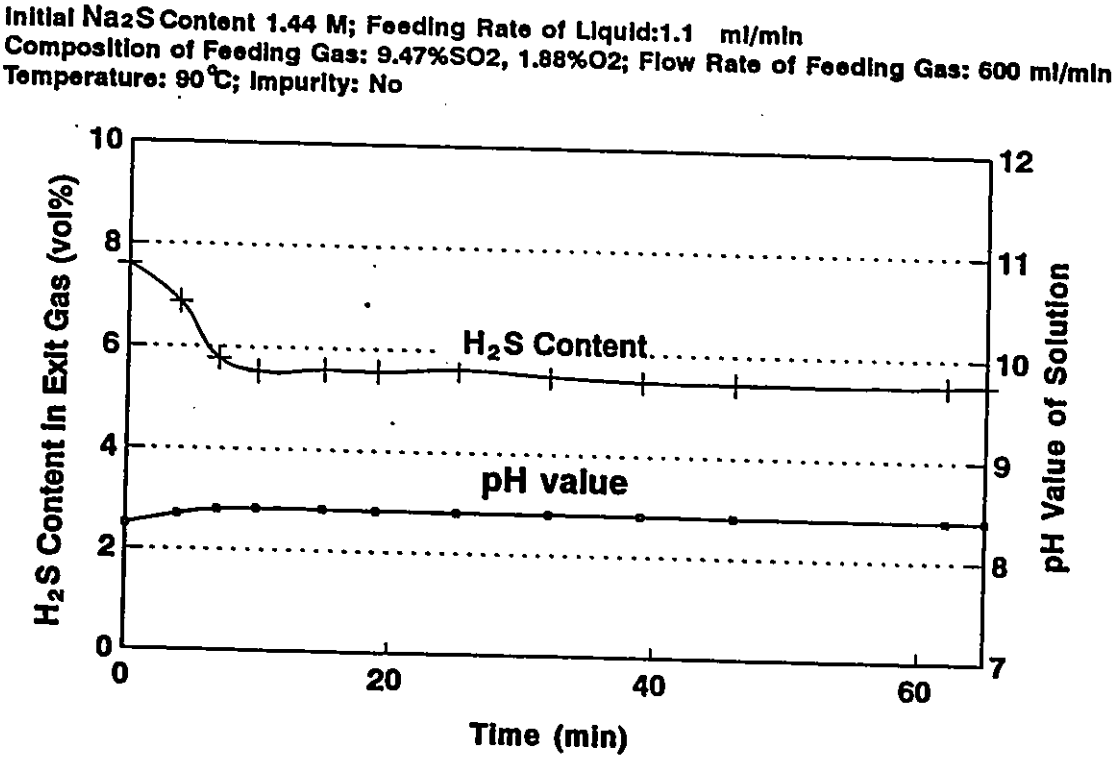

Fig.5.4: H_2S content in exit gases and pH value of solution under the steady state conditions

Initial Na_2SContent: 1.44 M; Feeding Rate of Liquid:1.10 ml/min
Composition of Feeding Gas: 9.47%SO_2;1.88%O2; Flow Rate of Feeding Gas: 600 ml/min
Temperature: 90℃; Impurities in Solution: Yes

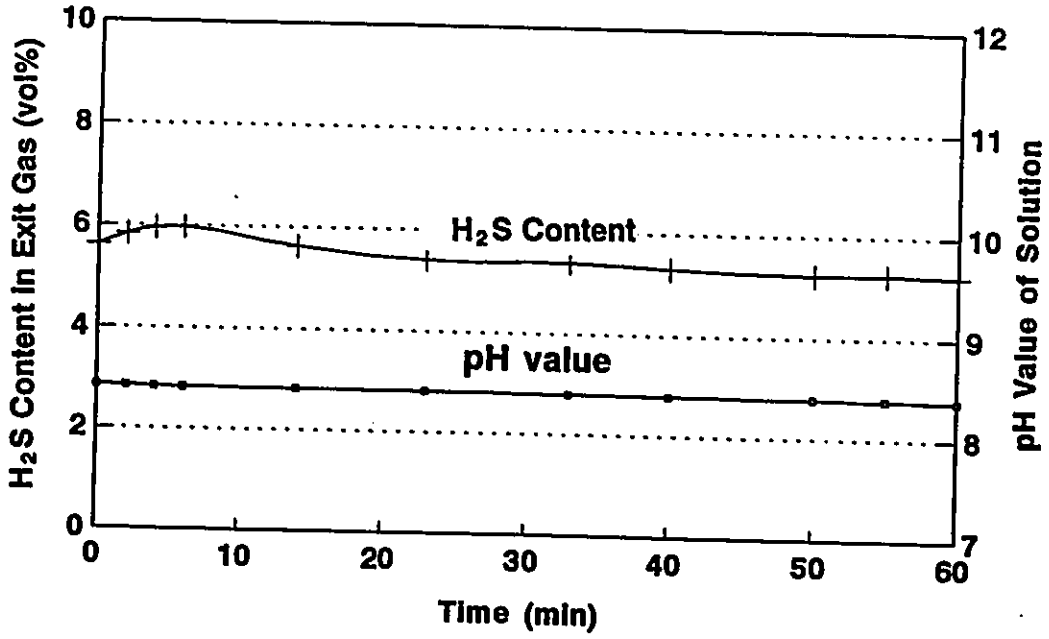

Fig.5.5: H_2S content in exit gases and pH value of solution under the steady state conditions

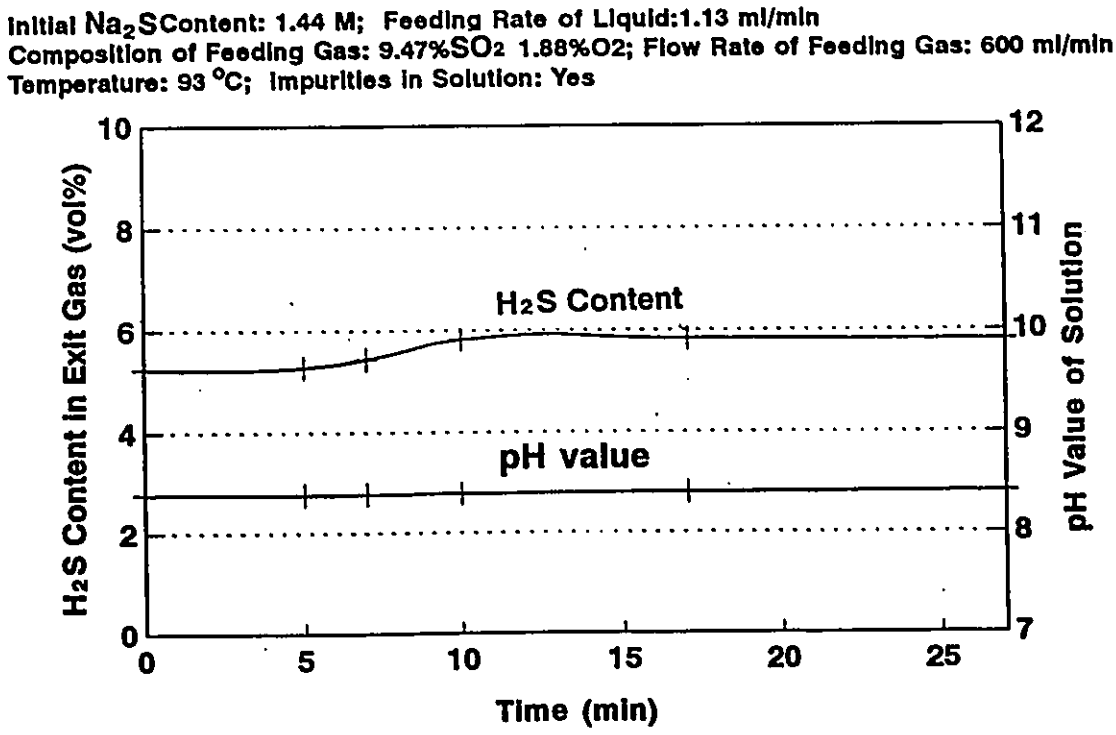

Fig.5.6: H_2S content in exit gases and pH value of solution under the steady state conditions

CHAPTER SIX:

THERMODYNAMICS OF CHEMICAL REACTIONS

In this chapter, standard enthalpy change and standard free energy change of the chemical reactions between $SO_{2(g)}$ and aqueous Na_2S solution are calculated at various temperatures (25, 50, 75 and 100°C). In addition, equilibrium constants of relevant chemical reactions in this system are also presented.

6.1 Thermodynamic Properties of Ions in Aqueous Solution

An understanding of the thermodynamic properties of ions in aqueous solution was required to study the behaviour of the SO_2-Na_2S-H_2S system. Although several reports provide extensive data at 25°C, no comprehensive studies regarding the thermodynamic properties of ions in aqueous solution at elevated temperatures has yet to be carried out. Barner and Scheuerman (1978) developed the high-temperature properties of ions and complexes from 25 °C data (US National Bureau of Standards 1968, 1969, 1971 and 1973; Latimer 1952; and Himmelblau 1959) by using the entropy correspondence principle developed by Criss and Cobble (1964a, 1964b).

The fundamental thermodynamic equation that relates the Gibbs free energy of a chemical reaction at temperature T to that at a reference temperature T_r is given by the following equation (Criss and Cobble 1964):

$$\Delta G_T^o = \Delta G_{T_r}{}^o - \Delta S_{T_r}{}^o \Delta T + \int_{T_r}^{T} \Delta Cp\,{}^o dT - T\int_{T_r}^{T} \Delta Cp\,{}^o d(lnT) \quad (6\text{-}1)$$

where $\Delta G°$ = the Gibbs free energy for the reaction.

$\Delta S°$ = the entropy change for the reaction

$\Delta Cp°$ = the change in heat capacity for the reaction (products minus reactants, including appropriate stoichiometric coefficients).

$\Delta T = T - T_r$.

The subscripts T and T_r designate the temperature and reference temperature, respectively. Since $\Delta G°$ and $\Delta S°$ for ions are often available at a reference temperature (usually 25°C), the problem can be solved by estimating the heat capacity of ions.

The partial molar entropy of an ion is related to its partial molar heat capacity by the following equation:

$$\bar{S}_T^o - \bar{S}_{Tr}{}^o = \int_{Tr}^{T} C_p^o dlnT \quad (6\text{-}2)$$

Denoting the average value of the heat capacity of the ion as $C_p°$ between temperature T and Tr it is now assumed that:

$$\bar{S}_T^o - \bar{S}_{Tr}^o = \bar{C}_p^o \int_{Tr}^{T} dlnT \quad (6\text{-}3)$$

which may then be rearranged as follows:

$$\bar{C}p^{o}_{T/Tr} = \frac{(\bar{S}^{o}_{T} - \bar{S}^{o}_{Tr})}{\ln(T/Tr)} \qquad (6\text{-}4)$$

Clearly, values of $S_T°$ and $S_{Tr}°$ must be known to evaluate the average heat capacity of an ion using Eq. 6.4. $S_{Tr}°$ is defined as the entropy of the ion in its standard state at 25°C and is usually known. S_Tx^E^Es generally unknown but can be estimated from the entropy correspondence principle (Criss and Cobble 1964).

The entropy correspondence principle forms a framework for relating the entropy of individual ions at different temperatures to the entropy at a reference temperature (taken to be 25 °C), according to the following linear relation:

$$\bar{S}^{o}_{T} = a(T) + b(T)\,\bar{S}^{o}_{298} \qquad (6\text{-}5)$$

where the coefficients a and b are function of temperature and ion type as defined by Criss and Cobble (1964a, 1964b). Criss and Cobble have shown that Eq.6.5 is satisfied if the entropies of ions are expressed on an "absolute" scale rather than on a conventional scale, i.e absolute scale in Kelvin. The conversion of scales for any ion is accomplished using the following relationship:

$$\bar{S}^{o}_{298}(absolute) = \bar{S}^{o}_{298}(conventional) - 5.0z \qquad (6\text{-}6)$$

where z is the ionic charge.

Once the entropy of an ion has been predicted, the average value of the heat capacity of the ion $Cp^{\circ}_{T/Tr}$ can be calculated. From this, the temperature dependence of the Gibbs free energy and the heat of formation of the ion can be predicted. Moreover, the heat of formation of an ion at temperature T is calculated from the following relationship:

$$\Delta H_T^o = \Delta G_T^o + T\Delta S_T^o \qquad (6\text{-}7)$$

The standard reference state for each element is chosen to be the state that is thermodynamically stable at the given temperature and 1 atm. pressure. For a gas, the standard state is defined by a hypothetical ideal gas at the given temperature and a fugacity of 1 atm. The standard state for a solute in aqueous solution is defined by a hypothetical ideal solution at a molality of 1.0.

6.2 Absorption of Sulfur Dioxide and Desorption of Hydrogen Sulfide

The term "absorption" refers to the transfer of a soluble component in a gaseous mixture into a liquid absorbent, while the term "desorption" is defined as the transfer of gas, dissolved in a liquid, into a gaseous phase. The absorption of sulfur dioxide into an aqueous solution is described by the following interfacial reaction:

$$SO_{2(g)} + H_2O_{(l)} \rightleftarrows H_2SO_{3(aq)} \qquad (6\text{-}8)$$

Based on the data given by Barner and Scheuerman (1978), standard enthalpy change, standard free energy change and equilibrium constant of this reaction are calculated and listed in Table 6.1. at four different temperatures.

Table 6.1-Thermodynamic Properties of Reaction 6-8

Temperature (°C)	25	50	75	100
$\Delta H°$ (kJ)	-26.0	-22.2	-15.9	-5.9
$\Delta G°$ (kj)	-0.4	1.3	3.3	3.3
$K_{6\text{-}8}$	1.2	0.62	0.32	0.35

As shown in Table 6.1, the absorption of sulfur dioxide is an exothermic reaction which results in a negative temperature dependence of equilibrium constant, $K_{6\text{-}8}$. For example, at 50°C, $K_{6\text{-}8} = a_{H2SO3(aq)} / (a_{H2O} P_{SO2}) = 0.62$, assuming the activity of $H_2SO_{3(aq)}$ at interface is 1.0 molarity and $a_{H2O} = 1.0$, the equilibrium value of P_{SO2} would be 1.6 atm at gas/liquid interface; for same liquid properties at 25°C, P_{SO2} would be 0.83 atm.

The desorption of hydrogen sulfide occurs when the dissolved hydrogen sulfide into liquid phase is transferred into the gaseous phase. This process is represented by the following interfacial reaction:

$$H_2S_{(aq)} \rightleftarrows H_2S_{(g)} \qquad (6\text{-}9)$$

Standard enthalpy change, standard free energy change and equilibrium constant of this reaction at four different temperatures are calculated and listed in Table 6.2.

Table 6.2-Thermodynamic Properties of Reaction 6-9

Temperature (°C)	25	50	75	100
$\Delta H°$ (kj)	19.3	21.4	21.8	21.8
$\Delta G°$ (kj)	-5.86	-7.96	-10.05	-12.56
K_{6-9}	10.7	19.4	32.3	57.4

The desorption of hydrogen sulfide is an endothermic reaction, and from K_{6-9}, this reaction is favoured at a higher reaction temperature. The saturated value of $H_2S_{(aq)}$ in molarity under 1 atm H_2S at 50 and 100 °C are 0.052 and 0.017, respectively.

6.3 Dissociation of Sulfurous Acid

The dissociation of sulfurous acid generates bisulfite, sulfite and H^+ ions, as indicated by the following two reactions:

$$H_2SO_{3(aq)} \rightleftharpoons HSO^-_{3(aq)} + H^+_{(aq)} \qquad (6\text{-}10)$$

$$HSO^-_{3(aq)} \rightleftharpoons SO^{2-}_{3(aq)} + H^+_{(aq)} \qquad (6\text{-}11)$$

Standard enthalpy change, standard free energy change and equilibrium constants of the two reactions at four different temperatures are calculated and listed in Tables 6.3 and 6.4, respectively.

Table 6.3-Thermodynamic Properties of Reaction 6-10

Temperature (°C)	25	50	75	100
$\Delta H°$ (kj)	-17.6	-21.4	-25.1	-31.0
$\Delta G°$ (kj)	10.1	12.6	15.1	18.4
K_{6-10}	1.7×10^{-2}	9.2×10^{-3}	5.4×10^{-3}	2.6×10^{-3}

Table 6.4-Thermodynamic Properties of Reaction 6-11

Temperature (°C)	25	50	75	100
$\Delta H°$ (kj)	-9.2	-20.1	-33.1	-46.1
$\Delta G°$ (kj)	41.0	46.1	52.3	58.2
$K_{6\text{-}11}$	6.5×10^{-8}	3.5×10^{-8}	1.4×10^{-8}	7.0×10^{-9}

As shown by the preceding tables, both reactions are exothermic and from $K_{6\text{-}10}$ and $K_{6\text{-}11}$ dissociation of sulfurous acid decreases with an increase in temperature.

6.4 Formation of Aqueous Hydrogen Sulfide

Hydrogen ions supplied by the dissociation of sulfurous acid may react with soluble sulfide ions (which enter the system as sodium sulfide) to form bisulfide and aqueous hydrogen sulfide. These two reactions are written as follows:

$$S^{2-}_{(aq)} + H^{+}_{(aq)} \rightleftarrows HS^{-}_{(aq)} \qquad \textbf{(6-12)}$$

$$HS^{-}_{(aq)} + H^{+}_{(aq)} \rightleftarrows H_2S_{(aq)} \qquad \textbf{(6-13)}$$

Standard enthalpy change, standard free energy change and equilibrium constant of these two reactions at four different temperatures are calculated and listed in Tables 6.5 and 6.6, respectively.

Table 6.5-Thermodynamic Properties of Reaction 6-12

Temperature (°C)	25	50	75	100
$\Delta H°$ (kj)	-51.1	-53.2	-56.9	-60.7
$\Delta G°$ (kJ)	-73.7	-75.8	-77.5	-78.3
$K_{6\text{-}12}$	8.3×10^{12}	1.8×10^{12}	4.3×10^{11}	9.2×10^{10}

Table 6.6-Thermodynamic Properties of Reaction 6-13

Temperature (°C)	25	50	75	100
$\Delta H°$ (kJ)	-22.2	-20.5	-17.2	-13.8
$\Delta G°$ (kJ)	-39.8	-41.5	-43.1	-45.2
$K_{6\text{-}13}$	9.5×10^6	5.1×10^6	2.9×10^6	2.1×10^6

Again, both reactions are exothermic and strongly favoured thermodynamically.

6.5 Oxidation of Sulfide (Formation of Elemental Sulfur)

Hydrogen sulfide can react with sulfur dioxide to form elemental sulfur and water according to the Claus reaction. In gaseous systems, the Claus reaction is slow and a catalyst has to be used at an elevated temperature (Paskall 1979). However, the reaction between aqueous hydrogen sulfide and aqueous sulfur dioxide (the wet Claus) is faster due to the catalytic role of water (Karchmer 1970, Brasted 1960). Specifically, the wet Claus reaction proceeds as follows:

$$2H_2S_{(aq)} + SO_{2_{(aq)}} \rightarrow 3/8S_{8(s)} + 2H_2O_{(l)} \qquad (6\text{-}14)$$

Standard enthalpy change, standard free energy change and equilibrium constant of the wet Claus reaction at four different temperatures are calculated and listed in Table 6.7.

Table 6.7-Thermodynamic Properties of The Wet Claus Reaction

Temperature (°C)	25	50	75	100
$\Delta H°$ (kJ)	-232.6	-227.8	-225.4	-222.2
$\Delta G°$ (kJ)	-97.3	-90.4	-85.0	-77.9
$K_{6\text{-}14}$	$1.1\text{x}10^{17}$	$4.2\text{x}10^{14}$	$5.7\text{x}10^{12}$	$8.1\text{x}10^{10}$

The wet Claus reaction is strongly exothermic and thermodynamically favoured. Its equilibrium constant is large but decreases significantly with an increase in temperature.

Another redox reaction may occur in the aqueous solution between bisulfide and bisulfite to form elemental sulfur and the hydroxide ion, according to the following reaction:

$$2HS^-_{(aq)} + HSO^-_{3(aq)} \rightarrow 3/8S_{8(s)} + 3OH^-_{(aq)} \qquad (6\text{-}15)$$

Standard enthalpy change, the standard free energy change and the equilibrium constant of this reaction at four different temperatures are calculated and listed in Table 6.8.

Table 6.8-Thermodynamic Properties of Reaction 6.15

Temperature (°C)	25	50	75	100
$\Delta H°$ (kJ)	-28.1	-31.4	-38.9	-48.2
$\Delta G°$ (kJ)	31.4	37.3	43.5	48.2
$K_{6\text{-}15}$	$3.1\text{x}10^{-6}$	$9.3\text{x}10^{-7}$	$3.0\text{x}10^{-7}$	$1.8\text{x}10^{-7}$

Reaction 6-15 is an exothermic reaction, as is the wet Claus reaction. However, its equilibrium constant is orders of magnitude smaller than that of the wet Claus reaction.

Furthermore, this reaction is unlikely to make a significant contribution to the oxidation of sulfide since both reactants share the same sign of electric charge, i.e. the reaction rate would be slow.

In an aqueous solution, the air oxidation of hydrogen sulfide is suggested as passing through an intermediate O_2SH^- (Brasted 1961), and the overall reaction is represented by the following equation:

$$2HS^- + O_2 \rightarrow 1/4S_{8(s)} + 2OH^- \qquad (6\text{-}16)$$

Standard enthalpy change, standard free energy change and equilibrium constant of this reaction at four different temperatures are calculated and listed in Table 6.9.

Table 6.9-Thermodynamic Properties of Reaction 6.16

Temperature (°C)	25	50	75	100
$\Delta H°$ (kJ)	-412.8	-417.0	-420.8	-426.7
$\Delta G°$ (kJ)	-358.8	-350.5	-344.6	-340.4
$K_{6\text{-}16}$	7.8×10^{62}	4.8×10^{56}	5.3×10^{51}	4.7×10^{47}

As indicated by Table 6.9, the air oxidation of bisulfide is strongly favoured thermodynamically. In addition, this reaction is enhanced by a lower reaction temperature and/or a lower pH value of solution.

6.6 Dissolution of Elemental Sulfur

Sulfide ions may react with elemental sulfur in basic solutions of the binary salts to

form polysulfide ($S_x^{=}$) according to the following reactions (Brasted 1961):

$$S^{2-}_{(aq)} + 1/8 S_{8(s)} \rightleftharpoons S^{2-}_{2(aq)} \quad \text{(6-17)}$$

$$S^{2-}_{2(aq)} + 1/8 S_{8(s)} \rightleftharpoons S^{2-}_{3(aq)} \quad \text{(6-18)}$$

$$S^{2-}_{3(aq)} + 1/8 S_{8(s)} \rightleftharpoons S^{2-}_{4(aq)} \quad \text{(6-19)}$$

$$S^{2-}_{4(aq)} + 1/8 S_{8(s)} \rightleftharpoons S^{2-}_{5(aq)} \quad \text{(6-20)}$$

Standard enthalpy changes, the standard free energy changes and the equilibrium constants of these reactions at four different temperatures are calculated and listed in Tables 6.10 to 6.13, respectively.

Table 6.10-Thermodynamic Properties of Reaction 6-17

Temperature (°C)	25	50	75	100
$\Delta H°$ (kJ)	-3.35	-3.77	-4.19	-5.44
$\Delta G°$ (kJ)	-6.28	-6.70	-7.12	-6.70
$K_{6\text{-}17}$	12.6	12.1	11.7	8.68

Table 6.11-Thermodynamic Properties of Reaction 6-18

Temperature (°C)	25	50	75	100
$\Delta H°$ (kJ)	-4.19	-5.02	-5.44	-6.28
$\Delta G°$ (kJ)	-5.44	-5.86	-5.86	-6.28
$K_{6\text{-}18}$	8.99	8.87	7.58	7.58

Table 6.12-Thermodynamic Properties of Reaction 6-19

Temperature (°C)	25	50	75	100
$\Delta H°$ (kJ)	-3.35	-3.77	-4.19	-5.02
$\Delta G°$ (kJ)	-4.19	-4.61	-4.61	-5.02
$K_{6\text{-}19}$	5.42	5.57	4.92	5.05

Table 6.13-Thermodynamic Properties of Reaction 6-20

Temperature (°C)	25	50	75	100
$\Delta H°$ (kJ)	-1.67	-2.51	-2.93	-4.19
$\Delta G°$ (kJ)	-3.35	-3.35	-3.77	-3.77
$K_{6\text{-}20}$	3.87	3.48	3.68	3.37

Many investigators (Schwarzenbach and Fisher 1960, Chen 1970, Peschanski and Valensi 1949) have reported that the polysulfuration index, x in $S_x^=$, is between 2 and 5 in an aqueous solution. Schwarzenbach (1960) showed that only $S_4^=$ and $S_5^=$ can be measured in aqueous polysulfide solution; $S_2^=$ and $S_3^=$ are either unstable or at such low concentrations that they cannot be detected. Chen (1970) proved that over the pH range from 6 to 14, $S_4^=$ and $S_5^=$ are the dominant polysulfide species present and comprise more than 90% of polysulfide species at a pH greater than 7.

Elemental sulfur disproportionates in a basic aqueous solution to form bisulfide and thiosulfate according to the following reaction (Tartar and Draves 1924; Farr and Ruhoff 1956):

$$\frac{1}{2}S_8 + 4OH^-_{(aq)} \rightleftharpoons S_2O^{2-}_{3(aq)} + 2HS^-_{(aq)} + H_2O \qquad (6\text{-}21)$$

Standard enthalpy change, standard free energy change and equilibrium constant of this reaction at four different temperatures are calculated and listed in Table 6.14.

Table 6.14-Thermodynamic Properties of Reaction 6-21

Temperature (°C)	25	50	75	100
$\Delta H°$ (kJ)	-59.9	-60.7	-58.2	-56.1
$\Delta G°$ (kJ)	-102	-106	-111	-114
$K_{6\text{-}21}$	$7.6\text{x}10^{17}$	$1.4\text{x}10^{17}$	$4.6\text{x}10^{16}$	$9.2\text{x}10^{15}$

This exothermic reaction is strongly favoured thermodynamically. Since aqueous sodium sulfide solution is basic, elemental sulfur formed in the first stage (defined in the present work, refer to Chapter Four) could dissolve according to Reaction 6.21.

Elemental sulfur reacts with sulfite to form thiosulfate in an alkali sulfite solution according to the following reaction (Karchmer 1970):

$$SO_{3(aq)}^{2-} + \frac{1}{8}S_8 \rightleftharpoons S_2O_{3(aq)}^{2-} \qquad \textbf{(6-22)}$$

Standard enthalpy change, standard free energy change and equilibrium constant of this reaction at four different temperatures are calculated and listed in Table 6.15.

Table 6.15-Thermodynamic Properties of Reaction 6-22

Temperature (°C)	25	50	75	100
$\Delta H°$ (kJ)	-23.0	-20.5	-17.6	-13.4
$\Delta G°$ (kJ)	-32.2	-33.1	-33.9	-35.6
$K_{6\text{-}22}$	$4.4\text{x}10^{5}$	$2.3\text{x}10^{5}$	$1.2\text{x}10^{5}$	$9.7\text{x}10^{4}$

This reaction is exothermic and is favored thermodynamically. This is the process usually used in commercial production of alkali thiosulfates (Karchmer 1970). In the present work (refer to Chapter Four), during the later period of the second stage. i.e. the concentration of sulfite in solution is high and sulfide concentration is low, elemental sulfur may dissolve according to this reaction.

6.7 The Overall Reaction without Oxidation of Sulfide

As observed in the present work (refer to Chapter Five), the oxidation of sulfide was suppressed by carrying out experiments at an elevated temperature. Without oxidation of sulfide, the reaction products of this system could be much simpler. It implies that sulfur dioxide gas is converted into aqueous sulfite and bisulfite while aqueous sulfide is converted into hydrogen sulfide gas. The overall reaction, without the oxidation of sulfide, may be represented in two different equations for two different products (bisulfite and sulfite):

$$Na_2S_{(aq)} + 2SO_{2(g)} + 2H_2O_{(l)} \rightarrow H_2S_{(g)} + 2NaHSO_{3(aq)} \quad (6\text{-}23)$$

$$Na_2S_{(aq)} + SO_{2(g)} + H_2O_{(l)} \rightarrow H_2S_{(g)} + Na_2SO_{3(aq)} \quad (6\text{-}24)$$

Standard enthalpy changes, standard free energy changes and equilibrium constants of these two reactions at four different temperatures are calculated and listed in Tables 6.16 and 6.17, respectively. Both reactions are strongly exothermic and strongly favoured thermodynamically.

Table 6.16-Thermodynamic Properties of Reaction 6-23

Temperature (°C)	25	50	75	100
$\Delta H°$ (kJ)	-141	-133	-134	-126
$\Delta G°$ (kJ)	-100	-97.6	-93.8	-92.5
$K_{6\text{-}23}$	$3.4\text{x}10^{17}$	$6.1\text{x}10^{15}$	$1.2\text{x}10^{14}$	$9.0\text{x}10^{12}$

Table 6.17-Thermodynamic Properties of Reaction 6-24

Temperature (°C)	25	50	75	100
$\Delta H°$ (kJ)	-107	-116	-126	-136
$\Delta G°$ (kJ)	-68.7	-65.3	-60.7	-56.1
$K_{6\text{-}24}$	$1.1\text{x}10^{12}$	$3.6\text{x}10^{10}$	$1.3\text{x}10^{9}$	$7.2\text{x}10^{7}$

In terms of the stoichiometry, the number of moles of sulfur dioxide required to react with one mole of aqueous sulfide depends on the equilibrium concentration ratio of bisulfite to sulfite, which is a function of the solution's pH value and temperature (based on Reaction 6-11). According to Reaction 6-23, if all sulfur dioxide absorbed is converted to bisulfite, one mole of aqueous sulfide requires two moles of sulfur dioxide. Conversely, if all sulfur dioxide absorbed is converted to sulfite (Reaction 6.24), one mole of aqueous sulfide requires only one mole of sulfur dioxide. In reality, both bisulfite and sulfite form in the aqueous solution. Consequently, the molar ratio of sulfur dioxide to aqueous sulfide would be between one and two. Moreover, since the formation of one mole hydrogen sulfide gas always requires at least one mole aqueous sulfide experimentally, one to two moles of sulfur dioxide would be needed to generate one mole of hydrogen sulfide gas. It should be pointed out that for a lower pH value of

solution Reaction (6-23) is more favored than Reaction (6-24).

6.8 The Overall Reaction With Oxidation of Sulfide

With oxidation of sulfide, thiosulfate will form and should be found in the spent solution, after all aqueous sulfide in solution is either converted to hydrogen sulfide or oxidized to elemental sulfur. Furthermore, if the amount of elemental sulfur formed is relatively large, the amount of sodium sulfite in the solution is insufficient to complete Reaction 6-22. Consequently, some elemental sulfur may remain in the spent solution. Hence, the overall stoichiometric relation with oxidation of sulfide may be described by the following equation:

$$Na_2S_{(aq)}+(z+v+w)SO_{2(g)}+(\frac{v}{2}+x)H_2O_{(l)} \rightarrow \qquad (6\text{-}25)$$

$$xH_2S_{(g)}+yS_{(s)}+zNa_2S_2O_{3(aq)}+vNaHSO_{3(aq)}+wNa_2SO_{3(aq)}$$

where $0 \leq x \leq 1$, $0 \leq y \leq 0.5$, $0 \leq z \leq 1$, $0 \leq v \leq 1$ and $0 \leq w \leq 1$.

In terms of these parameters, the index "x" may be considered as a measure of extent of sulfide oxidation, $x=0$ for complete oxidation and $x=1$ for no oxidation. The maximum amount of elemental sulfur that may form is 0.5 mole per mole sodium sulfide reacted, while the maximum amount of z for sodium thiosulfate is 1.0 mole. Since the maximum amount of elemental sulfur that may form through oxidation of one mole sulfide is 1.5 moles (according to wet Claus reaction), the sum of "y" and "z" should be

equal to or smaller than 1.5. Moreover, the sum of "z", "v" and "w" should be equal or smaller than 1.0 for one mole sodium sulfide reacted.

6.9 Summary

The basic and reductive sodium sulfide solution should react spontaneously with the acidic and oxidative sulfur dioxide gas under the conditions studied in the present work. The acid-base reactions contribute to the formation of hydrogen sulfide, while the redox reactions result in the formation of thiosulfate and/or elemental sulfur depending on the composition of solution. Under a lower pH, the formation of bisulfite is more favored than sulfite. It is interesting to note that all reactions discussed in this chapter are exothermic except the desorption of hydrogen sulfide.

CHAPTER SEVEN

MATHEMATICAL MODELS

In the following chapter, two mathematical models are described, namely, the continuous flow tank reactor model and the semiflow batch reactor model. These models were built based on the relations of chemical equilibrium, and mass and charge balance, which would be applicable when chemical reactions and mass transfer in the system are relatively fast.

7.1 The Continuous Flow Tank Reactor Model

This model was developed to extend the range of conditions studied experimentally for a better view and understanding of the phenomena observed in the system in a steady state operation. Furthermore, a valid mathematical model may be helpful to quantify some process parameters, therefore, to establish relations among process variables, such as, the flow rates and the compositions of incoming and outgoing streams, temperature etc.

7.1.1 Assumptions and Their Validity

The following assumptions were used to define the model which was built based on data presented in Chapter Five as well as theoretical considerations: [1] no redox reaction occurs in the continuous flow tank reactor; [2] the solution is well mixed so that

mass transfer in the liquid phase is not considered to be a rate-controlling step; [3] chemical reactions in the liquid phase are so fast that all aqueous species in the liquid phase are in thermodynamic equilibrium (thermal and chemical); [4] the absorption of SO_2 from the feeding gas by the liquid phase is complete; [5] the exit gas is in thermodynamic equilibrium with the liquid phase; and [6] equilibrium constants expressed in concentration for reactions in solution are independent of ionic strength (i.e. the solution is ideal). Reasons for these assumptions, and corresponding errors introduced are given below:

Assumption 1:

Experimental results (Chapter Five) indicated that the conversion ratio of sodium sulfide to hydrogen sulfide ranged from 0.86 to 0.96 without forming elemental sulfur. Considering the amount of unreacted sulfide in the outgoing liquid, the fraction of sulfide consumed by redox reactions should be less than 14%, even less than 4% depending on experimental conditions. These values (14% to 4%) are upper limit of the error introduced by assumption 1.

Assumption 2:

Assumption 2 was based on a series of experiments (refer to Section 4.2.4) in which the effect of feeding gas flow rate was studied. No notable difference in terms of hydrogen sulfide generation was observed when the flow rate was varied from 190 to 320 ml/min. In the present system where the movement of feed gas is the only source of power for mixing, mixing will be intensified with the increase of flow rate. This implies that this system is well mixed under the condition studied since the lowest flow

rate used in the steady state experiments was 540 ml/min.

Assumption 3:

Without considering the redox reactions, Assumption 3 was based on the following seven key chemical reactions which occur in this system:

$$SO_{2_{(g)}} + H_2O_{(l)} \rightleftharpoons H_2SO_{3_{(aq)}} \quad (7\text{-}1)$$

$$H_2SO_{3_{(aq)}} \rightleftharpoons H^+_{(aq)} + HSO_3^-{}_{(aq)} \quad (7\text{-}2)$$

$$HSO_3^-{}_{(aq)} \rightleftharpoons H^+_{(aq)} + SO_3^{2-}{}_{(aq)} \quad (7\text{-}3)$$

$$S^{2-}_{(aq)} + H^+_{(aq)} \rightleftharpoons HS^-_{(aq)} \quad (7\text{-}4)$$

$$HS^-_{(aq)} + H^+_{(aq)} \rightleftharpoons H_2S_{(aq)} \quad (7\text{-}5)$$

$$OH^-_{(aq)} + H^+_{(aq)} \rightleftharpoons H_2O_{(l)} \quad (7\text{-}6)$$

$$H_2S_{(aq)} \rightleftharpoons H_2S_{(g)} \quad (7\text{-}7)$$

The kinetics of reaction (1) were studied extensively by several authors (Eigen, Kustin and Maas 1961; Chang and Rochelle 1985; Hunger, Lapicque and Storck 1990) who suggested that this reaction occurs very fast. Experimental results regarding the effect of bubble size (Section 4.4.1), and the fact that the exit gas produced under the modelled conditions was found to be free of SO_2 confirms these conclusions. Reactions (7-2) to (7-6) react very rapidly since each involves only the transfer of a single proton.

Assumption 4:

Thermodynamic calculation indicates that the equilibrium constants of reaction (7-1) at 75 and 100 °C are of the order of magnitude of 10^{13} and 10^{11}, respectively. It is thus reasonable to assume that the dissolution of SO_2 in the solution is complete under the conditions specified in this model.

Assumption 5:

Assumption 5 implies that the transformation of hydrogen sulfide from the aqueous to the gaseous phase, Reaction (7-7), is not the rate-controlling step. Experimental results by varying bubble size from about 1 mm to 5 mm (Section 4.4.1) show that the change in liquid/gas interfacial area did not show noticeable impact on overall kinetics in the present work. However, when a gas distributor equipped with a single orifice of 5 mm in diameter was used to create much larger bubbles (8mm to 12 mm in diameter), a small but distinct increase in hydrogen sulfide content in exit gas was observed as bubble travel distance increased (refer to Section 4.4.2). Consequently, Reaction (7-7) appears to be taking part in the rate controlling step for larger bubbles (smaller specific interfacial area). Hence, assumption 5 may be accepted with caution.

Assumption 6:

In this model, the Debye-Hückel limiting law will not be used, since the ionic strength of the solution ,to which the model will apply, is much higher than 1 molar. By using the Debye-Hückel limiting law, theoretical prediction of activity coefficients is fairly accurate at ionic strengths below 0.1 molar. If only ions of charge ± 1 are involved, activity coefficients can be estimated to within 3% on the basis of the ionic strength. At higher ionic strengths, however, the activity coefficients of different ions vary widely, and experimental values of mean activity coefficients must be used. According to Butler (1964), results obtained using this approximation are generally not in error by more than a factor of two if all equilibria have been taken into account. Above 1 molar, Butler concluded that it is equally accurate and much easier to assume that the concentration equilibrium constants are independent of ionic strength.

7.1.2 Variables and Constraints

The variables in the system include flow rates and compositions of gaseous and liquid streams (in-coming and out-going) to and from the CFTR, and reaction temperature. These variables are summarized in Table 7.1.

Basically, the properties of in-coming streams are known and can be varied, which are named as the control parameters. The control parameters are $[Na+]^i$, $[H+]^i$, $[OH-]^i$, $[S=]^i$, $[HS-]^i$, $[SO_3^=]^i$, $[HSO_3^-]^i$, $[H_2SO_3]^i$,FLL^i, Y^i_{so2}, FLG^i and T. Conversely, the properties of out-going streams (the product parameters) are unknown and depend on the control parameters. The product parameters include $[Na+]^o$, $[H+]^o$, $[OH-]^o$, $[S=]^o$,

[HS-]°, [SO_3=]°,[HSO_3-]°, [H_2SO_3]° , FLL°, FLG° and $Y°_{H2S}$. The total number of the product parameters, which are unknown, is 11.

The constraints of the system include the equilibrium relations of five chemical reactions, the conservation of five chemical species (S^{4+}, $S^{=}$, N_2, Na^+ and H^+) and the conservation of electric charge in the solution. Consequently, the total number of constraints are 11. Hence, the system is mathematically solvable.

Table 7.1 A Summary of The Variables in CFTR Model

Variables	Description	Units
[Na+]^i, [Na+]°	Sodium Ion Content	mol/l (M)
[H+]^i , [H+]°	Hydrogen Ion Contents	mol/l (M)
[OH-]^i, [OH-]°	Hydroxide Ion Contents	mol/l (M)
[S=]^i, [S=]°,	Sulfide Ion Contents	mol/l (M)
[HS-]^i , [HS-]°	Bisulfide Ion Contents	mol/l (M)
[$SO_3^=$]^i, [SO_3=]°	Sulfite Ion Contents	mol/l (M)
[HSO_3^-]^i, [HSO_3-]°	Bisulfite Ion Contents	mol/l (M)
[H_2SO_3]^i , [H_2SO_3]°	Sulfurous Acid Contents	mol/l (M)
FLL^i, FLL°	Flow Rates of Liquid	l/min
FLG^i, FLG°	Flow Rates of Gas	mol/min
Y^i_{SO2} , $Y^=_{SO2}$	Molar Fraction of SO_2	
$Y°_{H2S}$	Molar Fraction of H_2S	
T	Reaction Temperature	K

Note: The superscripts "i" and "o" stand for the in-coming and out-going streams, respectively. The flow rate of outgoing gas (FLG°) is in mol/min, dry basis. The total pressure of the system is fixed at 1.0 atm.

7.1.3 Equilibrium Constants of Chemical Reactions

The equilibrium constants of Reactions (7-2), (7-3), (7-4), (7-5)/(7-7) and (7-6) are defined as follows:

$$K_2 = \frac{[H^+]^o\ [HSO_3^-]^o}{[H_2SO_3]^o} \tag{7-8}$$

$$K_3 = \frac{[H^+]^o[SO_3^{2-}]^o}{[HSO_3^-]^o} \tag{7-9}$$

$$K_4 = \frac{[HS^-]^o}{[S^-]^o\ [H^+]^o} \tag{7-10}$$

$$K_{5/7} = \frac{P_{H_2S}}{[HS^-]^o\ [H^+]^o} \tag{7-11}$$

$$K_6 = \frac{[H_2O]^o}{[OH^-]^o\ [H^+]^o} \tag{7-12}$$

The relations between their standard free energy change (in kcal) and temperature (in Kelvin) are listed below.

$$\Delta G_2^o = -6.077 + 0.028T \tag{7-13}$$

$$\Delta G_3^o = -7.784 + 0.058T \quad (7\text{-}14)$$

$$\Delta G_4^o = -14.257 - 0.012T \quad (7\text{-}15)$$

$$\Delta G_{5/7}^o = 1.153 - 0.04T \quad (7\text{-}16)$$

$$\Delta G_6^o = -11.219 - 0.026T \quad (7\text{-}17)$$

Regression equations (7-13) to (7-17) were calculated using the method of least squares with the data provided by Barner and Scheuerman (1978) in "Handbook of Thermodynamic Data for Compounds and Aqueous Species". For all five equations, the correlation coefficients are greater than 0.995.

7.1.4 Conservation of Chemical Species

Since it was assumed that no redox reactions occur in this system, the valence state of each species in this system may remain unchanged. The five chemical species concerned are S^{4+}, S^{2-}, N_2, Na^+ and H^+.

Sulfur with a Valency of +4

The sulfur with a valency of +4 enters the system as sulfur dioxide in the feeding gases and leaves the system as sulfite and bisulfite in the exit liquid according to the following equation:

$$\dot{M}_{S^{4+}}^i = \dot{M}_{S^{4+}}^o \quad (7\text{-}18)$$

where the $\dot{M}_{S4+}^{i}$, $\dot{M}_{S4+}^{o}$ are the molar fluxes of species S^{4+} , in moles per minute, in the in-coming and out-going streams, respectively. They are defined as follows:

$$\dot{M}_{S^{4+}}^{i} = Y_{SO_2} \cdot FLG^{i} + ([SO_3^{2-}]^{i} + [HSO_3^{-}]^{i} + [H_2SO_3]^{i}) FLL^{i} \qquad (7\text{-}19)$$

and

$$\dot{M}_{S^{4+}}^{o} = ([SO_3^{2-}]^{o} + [HSO_3^{-}]^{o} + [H_2SO_3]^{o}) FLL^{o} \qquad (7\text{-}20)$$

Sulfur with a Valency of -2

The sulfur with a valency of -2 enters the system as sodium sulfide in feeding liquid and leaves the system as hydrogen sulfide according to the following reaction:

$$\dot{M}_{S^{2-}}^{i} = \dot{M}_{S^{2-}}^{o} \qquad (7\text{-}21)$$

where the $\dot{M}_{S2-}^{i}$, $\dot{M}_{S2-}^{o}$ are the molar fluxes of species S^{2-} in the in-coming and out-going streams, respectively. They are defined as follows:

$$\dot{M}_{S^{2-}}^{i} = ([S^{2-}]^{i} + [HS^{-}]^{i}) FLL^{i} \qquad (7\text{-}22)$$

and

$$\dot{M}_{S^{2-}}^{o} = ([S^{2-}]^{o} + [HS^{-}]^{o}) FLL^{o} + Y_{H_2S}^{o} \cdot FLG^{o} \qquad (7\text{-}23)$$

Nitrogen Gas

Nitrogen is inert in this system. Specifically, nitrogen enters this system in the feeding gas and leaves this system in the exit gas. The amount of nitrogen remains

unaffected by the process and is described by the following equation:

$$\dot{M}_{N_2}^{i} = \dot{M}_{N_2}^{o} \tag{7-24}$$

where the $\dot{M}_{N2}{}^{i}$, $\dot{M}_{N2}{}^{o}$ are the molar fluxes of N_2 in the in-coming and out-going streams, respectively. They are defined for binary gas mixtures as follows:

$$\dot{M}_{N_2}^{i} = (1 - Y_{SO_2}^{i}) \cdot FLG^{i} \tag{7-25}$$

and

$$\dot{M}_{N_2}^{o} = (1 - Y_{H_2S}^{o}) \cdot FLG^{o} \tag{7-26}$$

Sodium Ions

Sodium ions enter this system with the feeding liquid and leave this system with the exit liquid according to the following equation:

$$\dot{M}_{Na^+}^{i} = \dot{M}_{Na^+}^{o} \tag{7-27}$$

where the $\dot{M}_{Na+}{}^{i}$, $\dot{M}_{Na+}{}^{o}$ are the molar fluxes of Na^+ in the in-coming and out-going streams, respectively. They are defined as follows:

$$\dot{M}_{Na^+}^{i} = [Na^+]^{i} FLL^{i} \tag{7-28}$$

and

$$\dot{M}^{o}_{Na^+} = [Na^+]^o FLL^o \tag{7-29}$$

Hydrogen

Hydrogen enters the system as water and other hydrogen-containing species (e.g. H^+, HS^- and HSO_3^-) in incoming liquid. It leaves the system as water and other hydrogen-containing species in outgoing liquid and as H_2S in the dried outgoing gas. The mass balance of hydrogen may be described by the following equation:

$$\dot{M}^{i}_{H} = \dot{M}^{o}_{H} \tag{7-30}$$

where the $\dot{M}_H^i$, $\dot{M}_H^o$ are the molar fluxes of H^+ in the in-coming and out-going streams, respectively. They are defined as follows:

$$\dot{M}^{i}_{H} = (2[H_2O]^i + [H^+]^i + [OH^-]^i +$$

$$+[HS^-]^i + [HSO_3^-]^i + 2[H_2SO_3]^i) \cdot FLL^i \tag{7-31}$$

and

$$\dot{M}^{o}_{H} = (2[H_2O]^o + [H^+]^o + [OH^-]^o + [HS^-]^o + [HSO_3^-]^o +$$

$$+ 2[H_2SO_3]^o) \cdot FLL^o + 2Y^o_{H_2S} \cdot FLG^o \tag{7-32}$$

It should be pointed out that the model is built in term of composition of dry gases. In the present experiments, the gas compositions of both incoming and outgoing streams were also measured when they were dry, after the removal of water vapour in the outgoing gas. Inside the reactor gas was wet, partial pressures of both SO_2 and H_2S were lower than that in dry basis. The effect of water vapour, as an inner gas, are different for different stages. In first and third stages, in which no hydrogen sulfide generates, the lowered Y_{SO2} in wet gas may result in a lower concentration of hydrogen ions in solution. On the other hand, in the second stage, SO_2 and H_2S participate in reactions through gas/liquid equilibria, and both are affected by the dilution of the same extent.

7.1.5 Electric Neutrality of Aqueous Solution

Ions with positive charges are sodium and hydrogen ions in this system, while ions with negative charges are sulfide, bi-sulfide, sulfite, bi-sulfite and hydroxide ions. These ions maintain a charge balance according to the following equation:

$$M_{\oplus}^{o} = M_{\ominus}^{o} \tag{7-33}$$

where the M_+^o, M_-^o are the molar concentrations of positive and negative-charged ions in the out-going stream, respectively. They are defined as follows:

$$M_{\oplus}^{o} = [Na^+]^o + [H^+]^o \tag{7-34}$$

and

$$M_{\ominus}^{o} = 2[S^{2-}]^{o} + [HS^{-}]^{o} + 2[SO_3^{2-}]^{o} + [HSO_3^{-}]^{o} + [OH^{-}]^{o} \quad (7\text{-}35)$$

7.1.6 Computation Method and Computation Strategy

This is a nonlinear problem presented by Equations (7-8), (7-9), (7-10), (7-11), (7-12), (7-18), (7-21), (7-24), (7-27), (7-30) and (7-33). To solve this set of equations, MATLAB, a software package, was used (refer to "PC-MATLAB User's Guide" and "Matrix Computation" by G.H.Golub et.al, 1983). In MATLAB, there is a function named "fsolve" designed to solve non-linear problem. The "fsolve" function is based on the Newtonian iteration method. The program used in the present study is given in Appendix I.

Since the problem has a strong nonlinearity, the solution is expected to be very sensitive to the initial values selected. Unfortunately, no general rule can be followed to search for a set of appropriate initial values. An estimation based on the nature of the solution was used as a start point for the searching process in the present work. When an iteration was used, the previous solution was used as the initial values for the next iterative run of computation. In addition to initial values, an appropriate step length is essential to obtain accurate and physically meaningful results. Moreover, special attention should be paid to the scaling of the variables due to the wide range of values.

7.1.7 Results of Computation

Computations have been carried out to study the dependence of [1] the chemical composition of the exit liquid; [2] the pH value of the exit liquid; and [3] the H_2S partial pressure of the exit gas on the variation of [a] the flow rate of the feeding liquid (FLL^i); [b] the flow rate of the feeding gas (FLG^i); [c] the initial Na_2S concentration in the feeding liquid ($[S^=]^i + [HS^-]^i$); [d] the partial pressure of SO_2 in the feeding gas (P_{SO2}); and [e] the reaction temperature (T). Since most of these parameters are related to the SO_2/Na_2S molar flux ratio in incoming streams, the results of computations have been presented as a function of the following ratio:

$$R_{\dot{M}} = \frac{\dot{M}^i_{S^{4+}}}{\dot{M}^i_{S^{2-}}} \qquad \textbf{(7-36)}$$

where the $\dot{M}_{S4+}{}^i$, $\dot{M}_{S=}{}^i$ are the molar fluxes of species SO_2 (S^{4+}) and Na_2S ($S^=$ and HS^-) in the incoming streams, respectively.

Effects of Sulfide ($S^=$ and HS^-) Content in Feeding Liquid on Properties of Out-Going Streams

In this series of computations, the initial sulfide concentration in the feeding liquid is varied from 0.75 M to 1.75 M at a constant temperature (90°C). The rates of feeding gas and liquid (FLG^i and FLL^i) are chosen to be 2.678×10^{-2} mol/min and 2.0×10^{-3} l/min, respectively. The partial pressure of SO_2 in the feeding gas is 0.1 atm/atm. The dependency of P_{H2S} and the pH value of outgoing solution on initial sulfide concentration of feeding liquid are given in Fig.7.1, while Figures 7.2 and 7.3 show relationships between composition of outgoing liquid and initial sulfide content of incoming liquid.

The computed results indicate that there is an optimum molar flux ratio of sulfur dioxide to sodium sulfide at which the equilibrium P_{H2S} reaches its maximum (Fig.7.1). As expected, the pH of the spent solution increases with the increase of initial concentration of sodium sulfide in the feeding liquid. As shown in Fig.7.2, the contents of both sulfide and bisulfide in the exit liquid decrease as the sulfide content decreases in the feeding liquid. The concentration of bi-sulfide in the exit liquid is approximately one hundred times greater than the sulfide concentration, i.e. the un-reacted sulfide exists in the exit liquid mostly in the form of bi-sulfide. However, the concentrations of sulfite and bi-sulfite in the exit liquid are of approximately same order of magnitude. As the sulfide content decreases in the feeding liquid the content of sulfite decreases, while the content of bi-sulfite increases in the spent solution. The concentration of sulfurous acid increases sharply when the content of sodium sulfide in feeding liquid decreases, although its absolute value is still not high (below 10^{-4}M).

Effects of Volumetric Flow Rate of Feeding Liquid on Properties of Out-Going Streams

The volumetric flow rate of the feeding liquid varies from 1.0 to 2.5 ml/min at a constant temperature of 90 °C. The sulfide concentration is kept at 1.5 M, while the molar flow rate of the feeding gas (P_{SO2} = 0.1atm) is chosen to be 2.7×10^{-2} mol/min.

The computed dependency of P_{H2S} and pH value of solution on the volumetric flow rate of feeding liquid are given in Fig.7.4, while the dependence of the exit liquid composition are shown in Fig.7.5 and Fig.7.6. As observed in experiments, the computed results confirm that there is an optimum value of flow rate of the feeding liquid at which the equilibrium P_{H2S} reaches its maximum value (Fig.7.4). The pH of the exit

liquid decreases from about 9 to 7 when the volumetric rate of feeding liquid decreases from about 2.5 to 1.0 ml/min. The contents of both sulfide and bi-sulfide in exit liquid decrease as the liquid volumetric rate decreases (Fig.7.5). The content of bi-sulfide is approximately one hundred times greater than that of sulfide in the exit liquid. As shown in Fig.7.6, the sulfite appears to behave differently from bi-sulfite. While the content of sulfite increases initially and then decreases, the content of bi-sulfite increases as the volumetric flow rate of the feeding liquid is decreased. Moreover, the concentration of sulfurous acid increases by several orders of magnitude from 10^{-7} to 10^{-4} M.

In view of the fact that Figs.7.1 to 7.3 are very similar to Fig.7.4 to 7.6 in terms of the effect of SO_2/Na_2S molar flow ratio, this dimensionless ratio defined by equation (7-36) has played an important role in the determination of the behavior of this system.

Effects of Reaction Temperature and SO_2 Partial Pressure in Feeding Gas on Properties of Out-Going Streams

In this series of computations, the SO_2 partial pressure of feed gas at a constant rate of 2.678×10^{-2} mol/min was varied at three reaction temperatures. The feed liquid has a sulfide content of 1.5 M and a feeding rate of 2 ml/min. The temperatures studied are in the range in which elemental sulfur formation can be suppressed, namely, 80, 90 and 100 °C. The computed results are shown in Fig.7.7 to Fig.7.13.

As shown in Fig.7.7, the temperature dependence of the equilibrium P_{H2S} appears to be weak. Moreover, the temperature effect changes from positive to negative as the SO_2 content in the feeding gas is increased. As expected, the equilibrium P_{H2S} increases with an increase of P_{SO2} in the feeding gas. However, the relationship between P_{H2S} in the exit

gas and P_{SO2} in the feeding gas is not linear over the whole range in Fig.7.7.

As shown in Fig.7.8, the pH of the exit liquid decreases with the increase of SO_2 content in feed gas; at higher temperature the effect of P_{SO2} on pH value is weaker. Fig.7.9 shows that the sulfide content in the exit liquid drops sharply when the SO_2 content in the feeding gases increases. Consequently, with a higher reaction temperature it may lead to a higher sulfide content in the exit liquid especially when the SO_2 content in the feeding gases is low. The bisulfide content in the exit liquid drops and its temperature effect changes from negative to positive with the increase of P_{SO2} in feeding gases as shown in Fig.7.10. The sulfite concentration increases first and then decreases with a negative temperature dependence when P_{SO2} is increased as indicated by Fig.7.11. However, the concentration of bi-sulfite increases with a small, positive temperature effect as shown in Fig.7.12. As expected, the amount of sulfurous acid in the exit liquid increases with the increase of P_{SO2} in feeding gases. The negative effect of temperature on the sulfurous acid content is small as shown by Fig.7.13.

7.1.8 Comparison between The Observed P_{H2S} and The Computed P_{H2S}

Five experiments have been conducted using CFTR under different conditions (refer to Chapter Five for details of experiments). For all five experiments, the initial sulfide concentration of feeding liquid was 1.44 M . A comparison between observed and measured pH values of solution is given in Table 7.2. Observed partial pressures of H_2S and conversion ratio of Na_2S to H_2S with corresponding computed values are listed in Tables 7.3 and 7.4. The observed values and computed values agree very well.

Table 7.2 Comparison between Observed and Computed pH Values of Solution

Experiments:	A	B	C	D	E
pH Value Observed	8.2	8.4	8.4	8.4	8.4
pH Value Computed	7.6	7.5	7.7	7.6	7.6

Table 7.3 Comparison between Observed and Computed Partial Pressure of H_2S

Conditions of Feeding Gas & Liquid, Temperature	Measured P_{H2S} (atm)	Computed P_{H2S} (atm)	Relative Difference
A: no O_2, no impurity, 7.00% SO_2, 90 °C	0.043	0.045	4.4%
B: no O_2, no impurity, 9.84% SO_2, 90 °C	0.058	0.062	6.4%
C: 1.88% O_2, no impurity, 9.47% SO_2, 90 °C	0.055	0.060	8%
D: 1.88% O_2, with impurities, 9.47% SO_2, 90 °C	0.053	0.060	12%
E: 1.88% O_2, with impurities, 9.47% SO_2, 93 °C	0.058	0.060	3.3%

Table 7.4 Comparison between Observed and Computed Molar Flow Ratios

Conditions of Feeding Gas & Liquid, Temperature	$\dot{M}(H_2S)/\dot{M}(Na_2S)$ observed	$\dot{M}(H_2S)/\dot{M}(Na_2S)$ computed
A: no O_2, no impurity, 7.00% SO_2, 90 °C	0.96	0.99
B: no O_2, no impurity, 9.84% SO_2, 90 °C	0.94	0.99
C: 1.88% O_2, no impurity, 9.47% SO_2, 90 °C	0.87	0.99
D: 1.88% O_2, with impurities, 9.47% SO_2, 90 °C	0.86	0.99
E: 1.88% O_2, with impurities, 9.47% SO_2, 93 °C	0.94	0.99

In these tables, $M(H_2S)$ and $M(Na_2S)$ are the molar flows of H_2S in dry exit gas and Na_2S in feed solution, respectively.

7.2 The Semi-Flow Batch Reactor Model

Experimental studies carried out using a semiflow batch reactor have shown that the solution pH and the exit gas composition as functions of reaction time varied in three distinct stages with a continuous feeding of SO_2. However, the following questions still remain: [1]. What determines the observed three-stage pattern in reactions? and [2] What are quantitative relations among process variables? The semiflow batch reactor model was created to investigate the mechanism of reactions in this system and to answer these questions.

7.2.1 Assumptions and Their Validity

The six assumptions which define this model are the same as those used in the CFTR model in Section 7.1. They are based on experimental results obtained in the present work as well as theoretical considerations. Due to the introduction of the assumption that absorption of SO_2 from feed gas by liquid phase is complete (Assumption 4 in Section 7.1), the model is only valid for the first and second stages. Since the arguments about the validity of the assumptions are basically the same as those in Section 7.1, they will not be discussed again.

7.2.2 Variables and Constraints

The variables in the system include the compositions and volume of the solution the properties of the gaseous streams, and reaction temperature. These variables are summarized in Table 7.5. Among these variables, the volume of solution and concentration of sodium sulfide initially placed in the reactor, the flow rate and SO_2 partial pressure in feed gas and reaction temperature are known. Consequently, the total number of unknowns is nine.

Table 7.5 A Summary of The Variables in The SFBR Model

Variables	Description	Units
[Na+]	Sodium Ion Content	mol/l (M)
[H+]	Hydrogen Ion Content	mol/l (M)
[OH-]	Hydroxide Ion Content	mol/l (M)
[S=]	Sulfide Ion Content	mol/l (M)
[HS-]	Bisulfide Ion Content	mol/l (M)
$[SO_3^=]$	Sulfite Ion Content	mol/l (M)
$[HSO_3^-]$	Bisulfite Ion Content	mol/l (M)
$[H_2SO_3]$	Sulfurous Acid Content	mol/l (M)
VOL	Volume of Liquid	litre
FLG^i, FLG^o	Flow Rates of Gas	mol/min
Y^i_{SO2}	Molar Fraction of SO_2	
Y^o_{H2S}	Molar Fraction of H_2S	
T	Reaction Temperature	K

Note: The superscripts "i" and "o" stand for the In-coming and Out-going streams, respectively. FLG^o is the mass flow rate of outgoing gas, dry basis. The total pressure of the system is fixed at 1.0 atm.

The constraints selected for the system include the equilibrium constants for five chemical reactions, the conservation of three chemical species (S^{4+}, $S^{=}$, and N_2) and the conservation of electric charge in the solution. Consequently, the total number of constraints or equations are also nine. Since the chemical reactions concerned in this model are the same as those in the CFTR model, only conservation equations of S^{4+} and S^{2-}, which are in the form of integration, are given in this section.

Sulfur with a Valency of +4

The sulfur with a valency of +4 enters the system as sulfur dioxide in the feeding gas and remains in the system as sulfite, bisulfite and sulfurous acid. Its mass balance at time t after the commencement of reaction is described as follows:

$$M^{i}_{S^{4+}} = M^{sol}_{S^{4+}} \tag{7-37}$$

where the $M_{S4+}{}^{i}$ and $M_{S4+}{}^{sol}$ are the total amount of S^{4+} fed by the feeding gas and the amount of S^{4+} in the solution, respectively. They are defined as follows:

$$M^{i}_{S^{4+}} = \int_0^t Y^{i}_{SO2} \times FLG^{i} \times dt \tag{7-38}$$

and

$$M^{sol}_{S^{4+}} = ([SO_3^{2-}]+[HSO_3^{-}]+[H_2SO_3])VOL \tag{7-39}$$

Sulfur with a Valency of -2

The sulfur with a valency of -2 in this system is originally from sodium sulfide in the solution and leaves the system as hydrogen sulfide. Its mass balance is described as follows:

$$M_{S^{2-}}^{i} = M_{S^{2-}}^{sol} + M_{s^{2-}}^{H_2S} \tag{7-40}$$

where the $M_{S=}^{i}$, $M_{S=}^{sol}$ and $M_{S=}^{H2S}$ are the amount of sulfide added initially to the reactor as Na_2S, the amount of sulfide left in the solution and the total amount of sulfide leaving the solution as H_2S up to the time t, respectively. They are defined as follows:

$$M_{S^{2-}}^{i} = ([S^{2-}]^{i}+[HS^{-}]^{i})VOL \tag{7-41}$$

$$M_{S^{2-}}^{sol} = ([S^{2-}]+[HS^{-}])VOL \tag{7-42}$$

and

$$M_{S^{-}}^{H_2S} = \int_0^t Y_{H_2S} \times FLG^{o} \times dt \tag{7-43}$$

7.2.3 Solver and Computation Strategy

This set of nine non-linear equations including two integral equations were solved using the MATLAB software mentioned previously in Section 7.1.6. Due to the strong nonlinearity involved, initial values should be selected with caution. To maintain the

accuracy of computed results, when the integration equations are being solved, the step length should not be large (below 1/200 of total reaction time in the present work). In addition, the previous solution should be used as initial values for the next run of computation. Moreover, special attention should be paid to the scaling of the variables due to the wide range of variable values.

7.2.4 Results of Computation

In Fig.7.14, computed and measured results at 90 °C of P_{H2S} in outgoing gas and pH value of solution as functions of reaction time are compared. In terms of the pattern of changes in P_{H2S} and pH value with reaction time, the agreement is reasonably good. The agreement indicates that the buffer effect observed in the first and second stages is due to the reactions 7-4 and 7-5, respectively. The drops of pH at the end of first and second stages are resulted from the exhaustion of sulfide and bisulfide in solution, respectively. In the first stage, the observed pH is higher than the computed one. The higher observed pH appears to be due to the consumption of sulfur dioxide by redox reactions. As a result of redox reactions, less sulfur dioxide acts as a supplier of proton. As shown in Fig.4.17, there is a time delay in terms of the start of hydrogen sulfide generation. The difference in the hydrogen sulfide partial pressure is believed to be mainly caused by the oxidation of sulfide.

The changes of the solution composition with reaction time are given in Figs.7.15 and 7.16. As shown in Fig.7.15, the initial concentration of sulfide is approximately five times higher than that of bisulfide. In the first stage, the absorption of SO_2 by the

solution would result in decrease of concentration of sulfide and increase of concentration of bisulfide in solution. Once the system has entered the second stage, the bisulfide concentration decreases with the release of H_2S as the absorption of SO_2 continues. At the end of second stage, all sulfides added as sodium sulfide initially are converted into hydrogen sulfide and no sulfide or bisulfide ions remain in the solution. The S^{+4}-containing ions in the solution accumulate as the absorption of sulfur dioxide continues. The S^{+4}-containing ions exist as sulfite, bisulfite and sulfurous acid with their relative amounts determined by thermodynamic relations. As shown in Fig. 7.16, in the first stage, sulfur dioxide is absorbed and forms mainly sulfite. In the second stage, the absorbed sulfur dioxide exists in the solution in the forms of sulfite and bisulfite. At the end of the second stage, the concentrations of sulfite and bisulfite are comparable. Although the concentration of sulfurous acid increases with the absorption of sulfur dioxide, its strength is still several order of magnitudes smaller than that of sulfite and bisulfite.

Temperature Dependence of Na_2S Conversion to H_2S with SO_2 Absorption

In this series of computations, the only parameter varied was temperature. As indicated by Fig. 7.17, an increased temperature may not enhance the generation of hydrogen sulfide thermodynamically. As shown in Fig.7.18, the pH of solution in the first stage is lower at a higher temperature, which agrees with the observations (see Fig.4.7).

Effects of Volume of Solution on Na_2S Conversion to H_2S with SO_2 Absorption

As shown in Figs.7.19 and 7.20, varying the volume of solution does not lead to any change in the peak value of P_{H2S}. As expected, the pH of solution remains the same, as well. The only difference is that the period of time to complete the reactions is longer with a larger volume of solution.

Effects of Initial Na_2S Concentration on Na_2S Conversion to H_2S with SO_2 Absorption

The dependencies of P_{H2S} and pH value of solution on initial Na_2S concentration are given in Figs.7.21 and 7.22. The peak value of P_{H2S} increases from approximately 0.14 to 0.16 atm when the initial concentration of sodium sulfide increases from 0.5 to 1.5 M, respectively. As observed in experiments (see Fig.4.13), the initial pH of solution is higher with the increase of concentration of sodium sulfide.

7.3 Summary

With the help of these computed results, the range of conditions studied experimentally has been extended for a better view and understanding of phenomena observed in the system. The complexity of these mathematical models has been greatly reduced by recognizing that proton transfer reactions and SO_2 absorption are relatively fast in comparison with the rate of supply of SO_2 to the system. The computed results using the CFTR model indicate that the dimensionless parameter, the molar flow ratio of sulfur dioxide in feed gas to sodium sulfide in feed liquid ($\dot{M}_{SO2}/\dot{M}_{Na2S}$), has played an important role in determination of behaviour in terms of hydrogen sulfide generation.

The computed results using the CFTR model (Figs.7.1, 7.4 and 7.11) confirm the observation that there is an optimum molar flow ratio of sulfur dioxide to sodium sulfide at which the P_{H2S} reaches its maximum. The computed patterns of dependencies of P_{H2S} in exit gases and pH of solution on reaction time using the SFBR model agree with that observed in experiments (Fig.7.14). In the experiment conducted in the SFBR, hydrogen sulfide started to generate later than that expected by the mathematical model. The redox reactions which consume sulfur dioxide appeared to be responsible for the time delay.

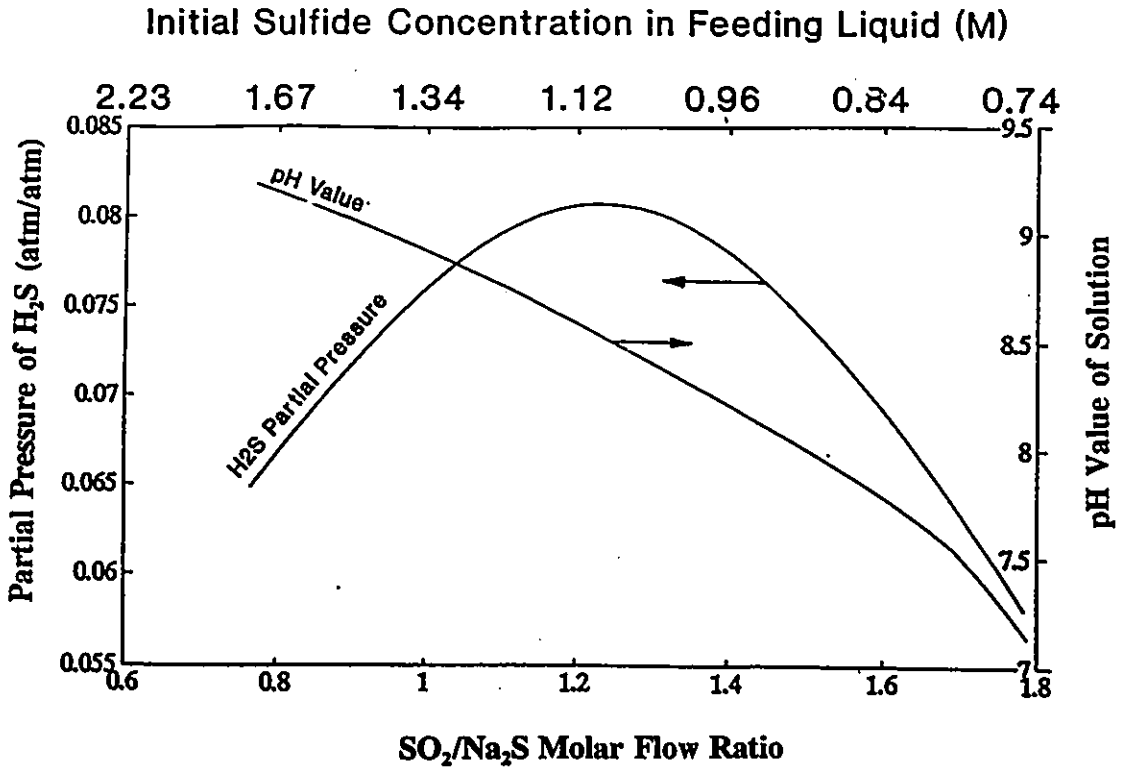

Fig.7.1: Dependence of equilibrium partial pressure of H_2S in exit gases and pH value of exit solution on sulfide concentration in feed solution

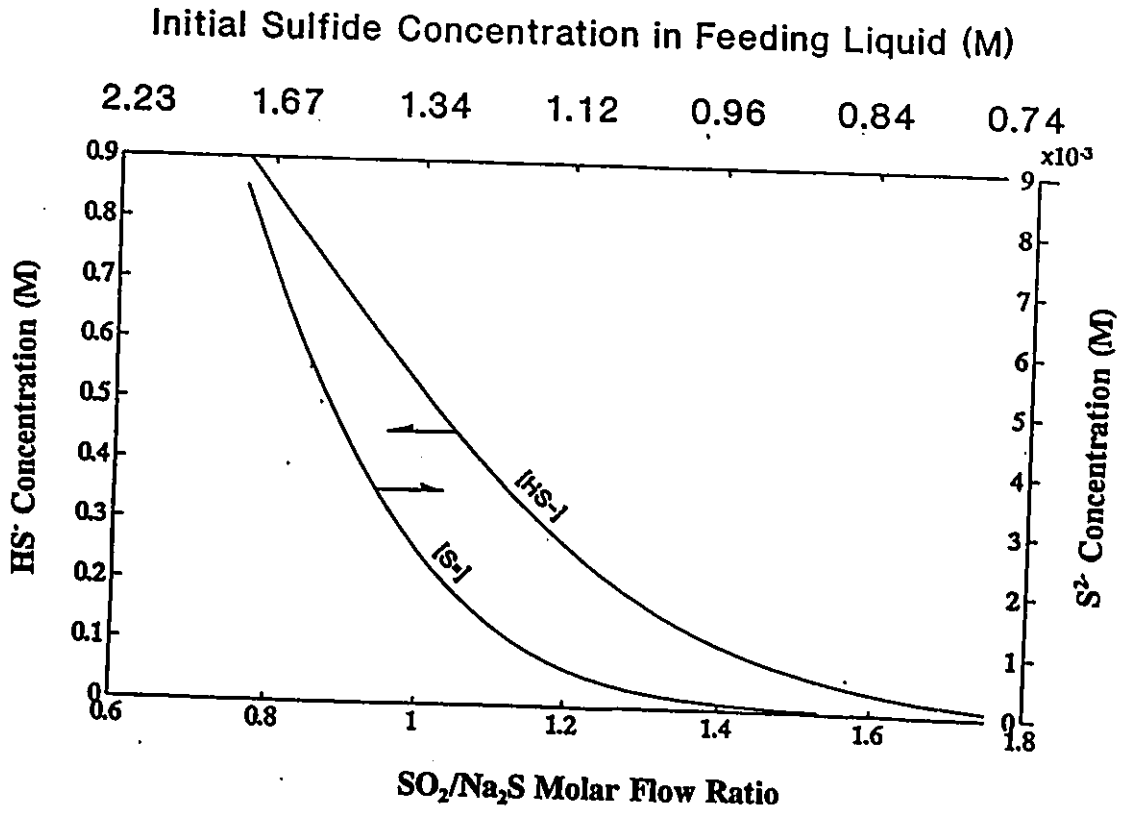

Fig.7.2: Dependence of sulfide and bisulfide contents in exit solution on sulfide concentration in feed solution

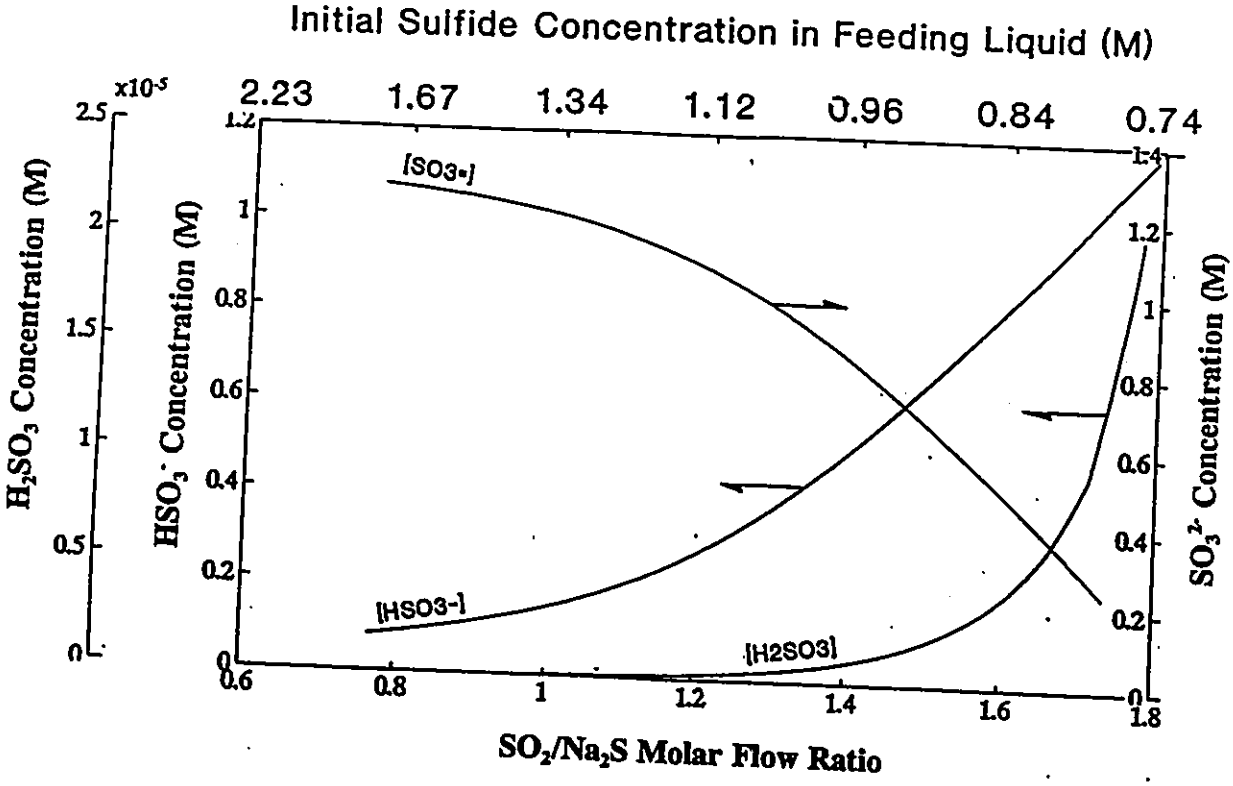

Fig.7.3: Dependence of sulfite, bisulfite and sulfurous acid contents in exit solution on sulfide concentration in feed solution

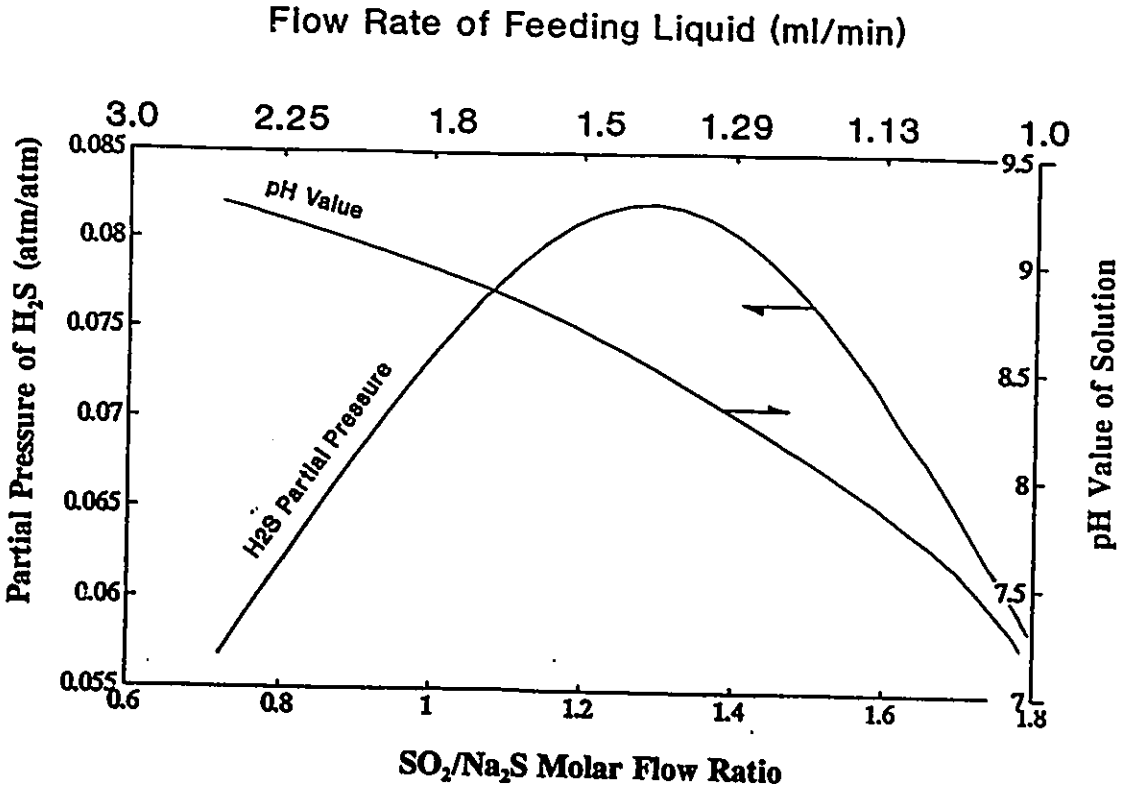

Fig.7.4: Dependence of equilibrium partial pressure of H_2S in exit gases and pH value of exit solution on volumetric flow rate of feed solution

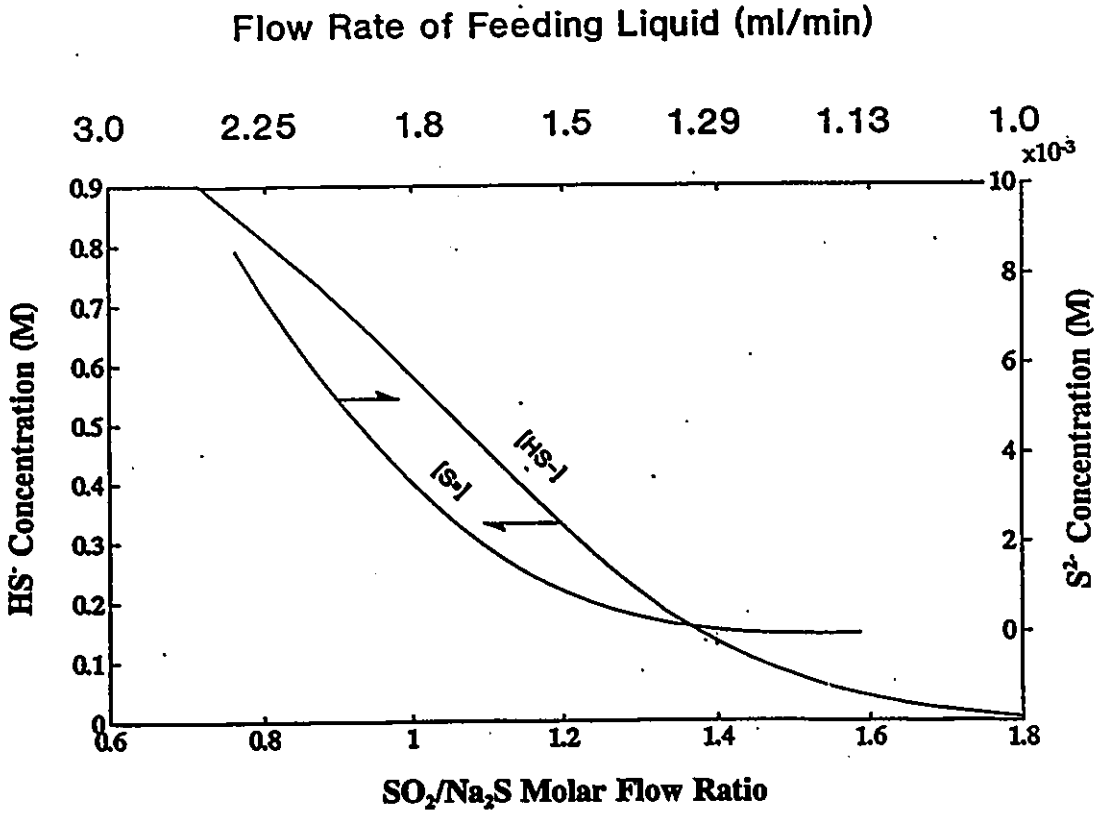

Fig.7.5: Dependence of sulfide and bisulfide contents in exit solution on volumetric flow rate of feed solution

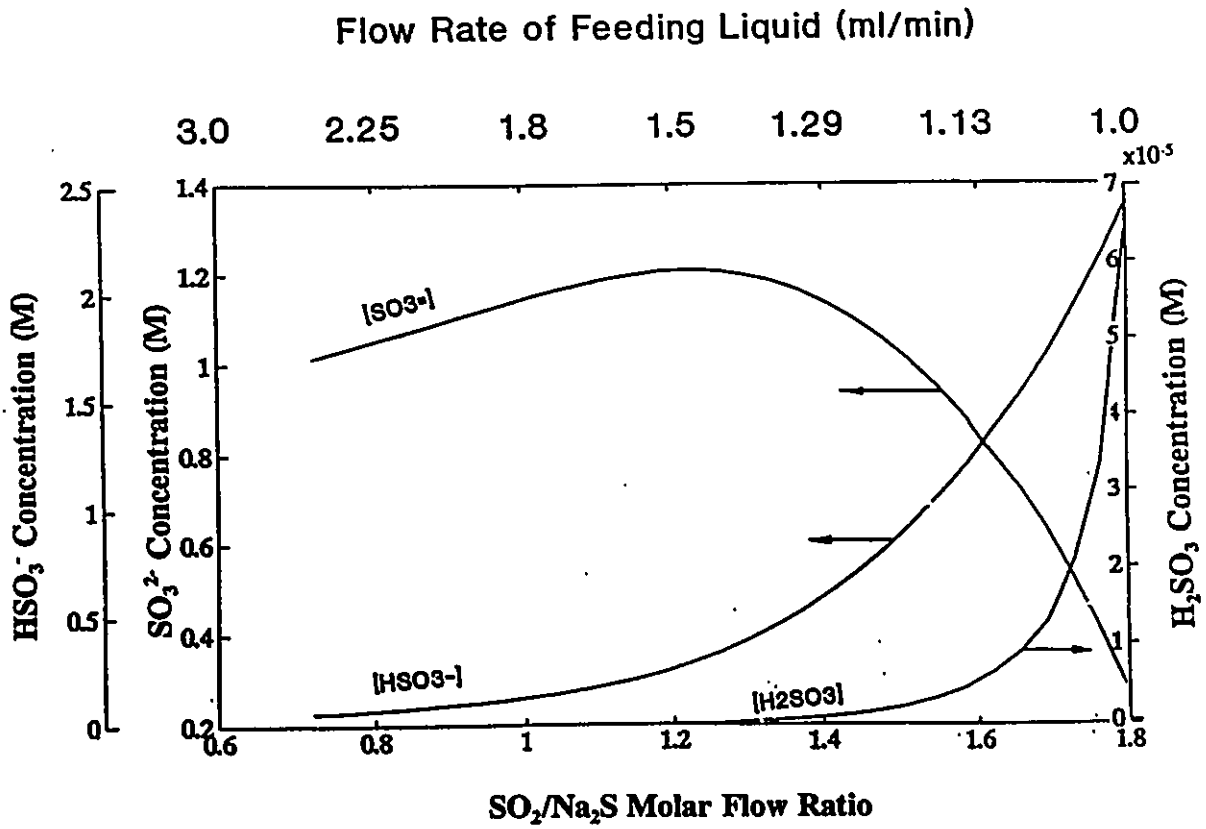

Fig.7.6: Dependence of sulfite, bisulfite and sulfurous acid contents in exit solution on volumetric flow rate of feed solution

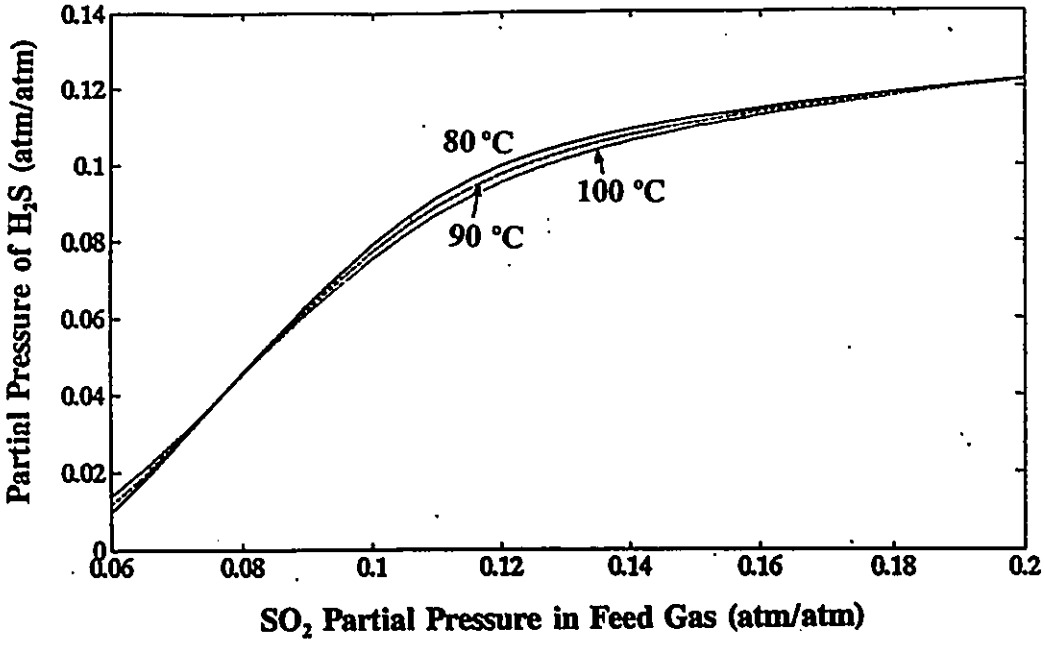

Fig.7.7: Dependence of equilibrium partial pressure of H_2S in exit gases on SO_2 partial pressure in feed gases at three reaction temperatures

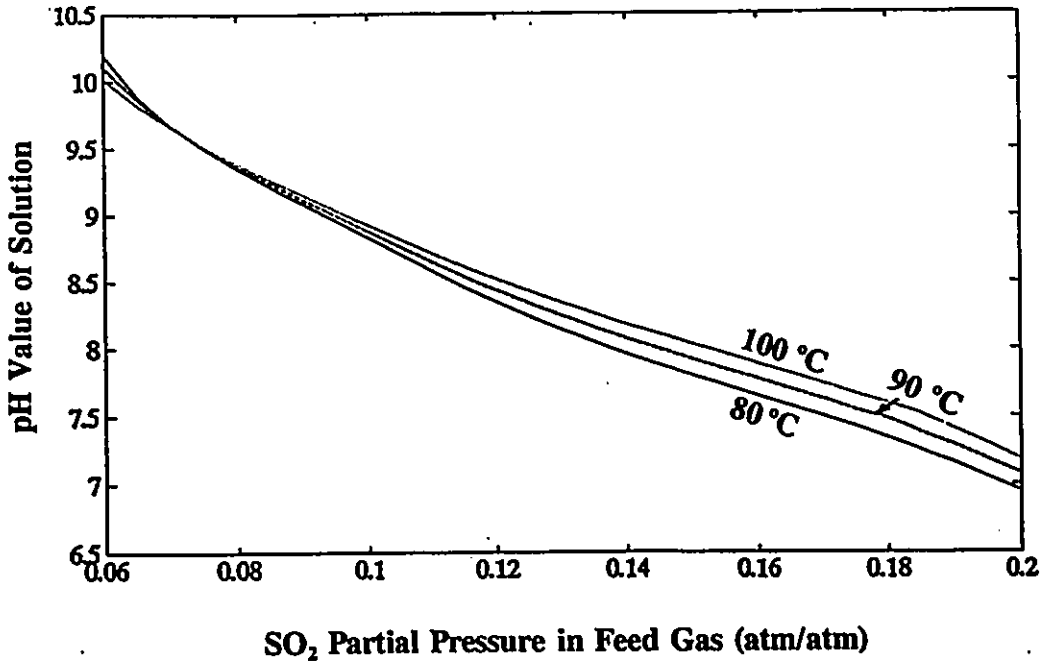

Fig.7.8: Dependence of pH value of exit solution on SO_2 partial pressure in feed gases at three reaction temperatures

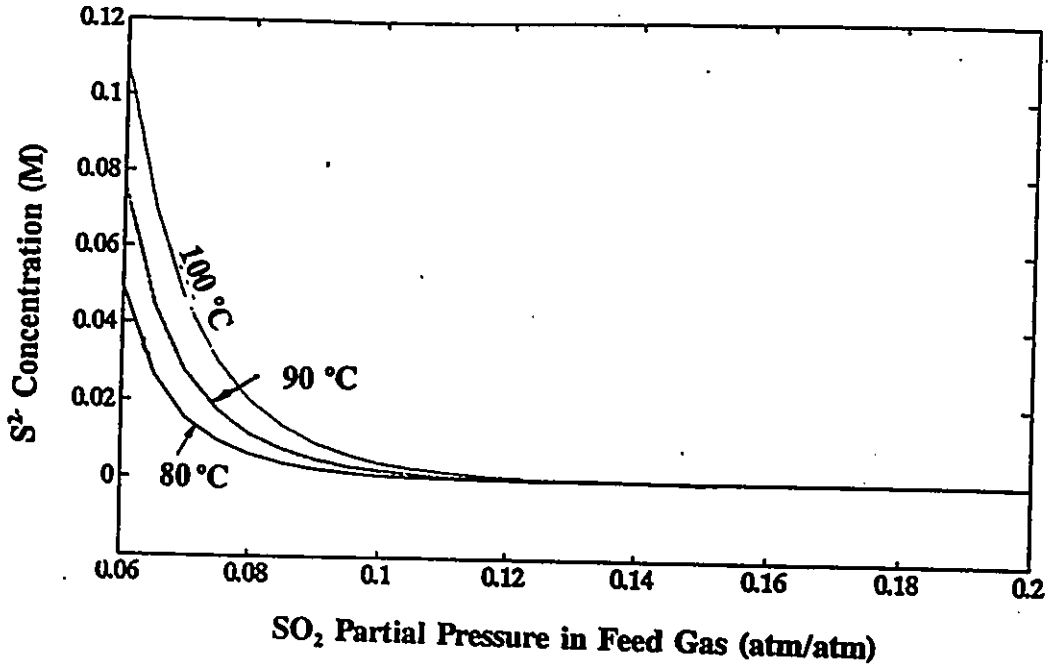

Fig.7.9: Dependence of sulfide content in exit solution on SO_2 partial pressure in feed gases at three reaction temperatures

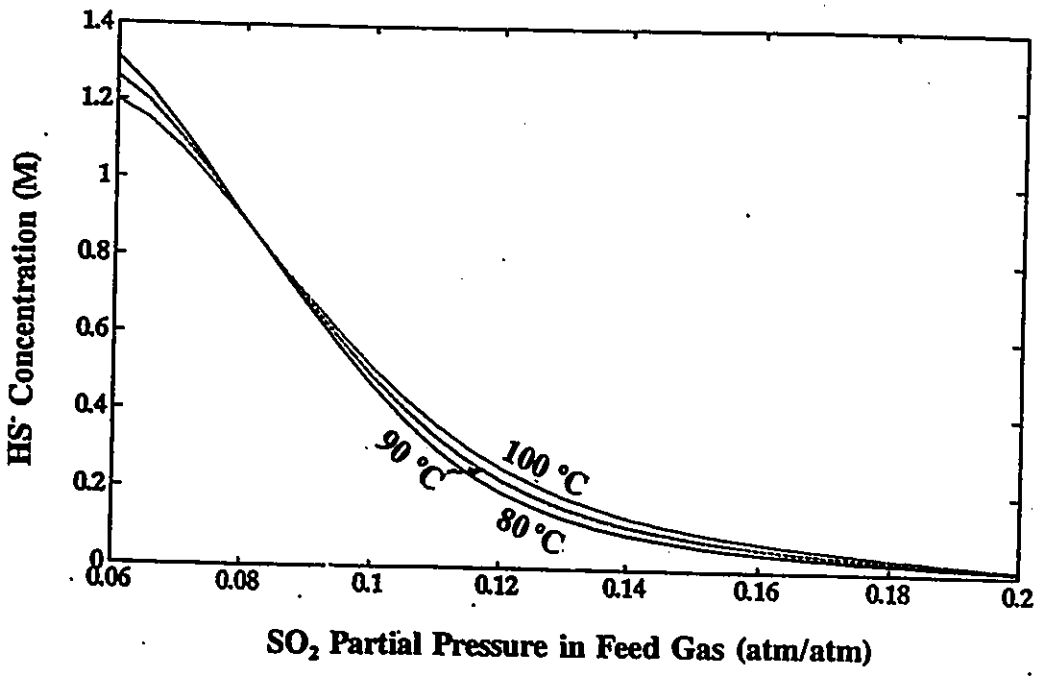

Fig.7.10: Dependence of bisulfide content in exit solution on SO_2 partial pressure in feed gases at three reaction temperatures

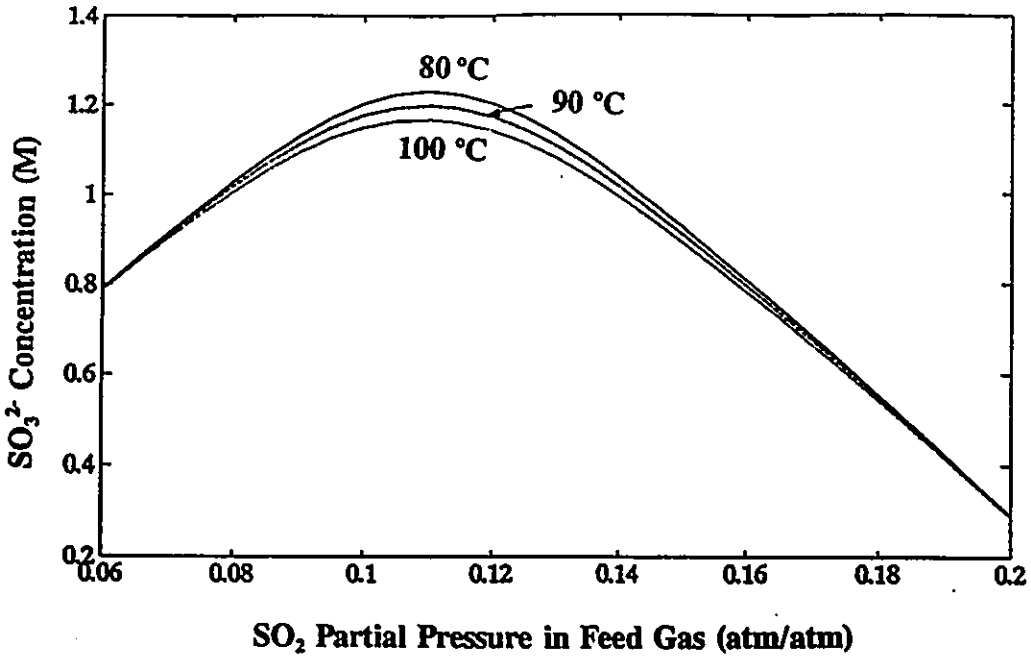

Fig.7.11: Dependence of sulfite content in exit solution on SO_2 partial pressure in feed gases at three reaction temperatures

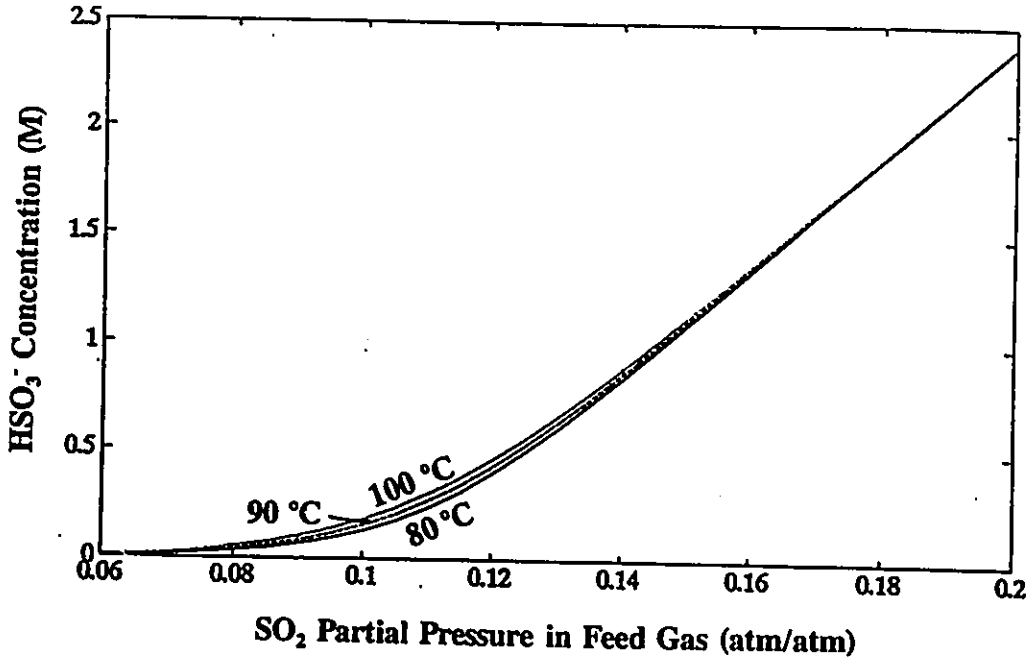

Fig.7.12: Dependence of bisulfite content in exit solution on SO_2 partial pressure in feed gases at three reaction temperatures

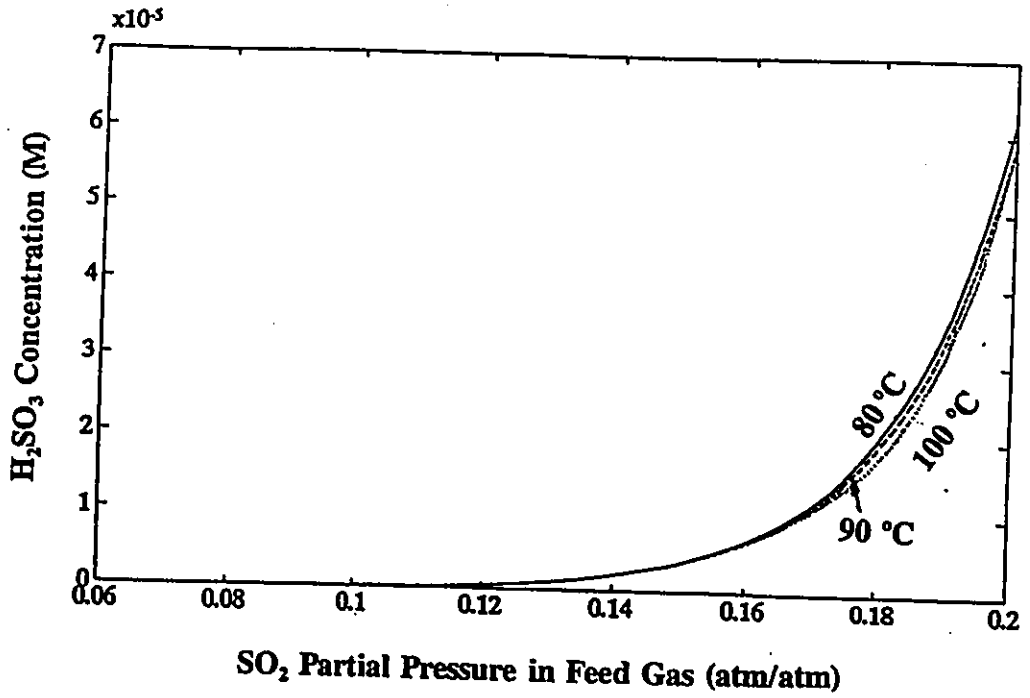

Fig.7.13: Dependence of sulfurous acid content in exit solution on SO_2 partial pressure in feed gases at three reaction temperatures

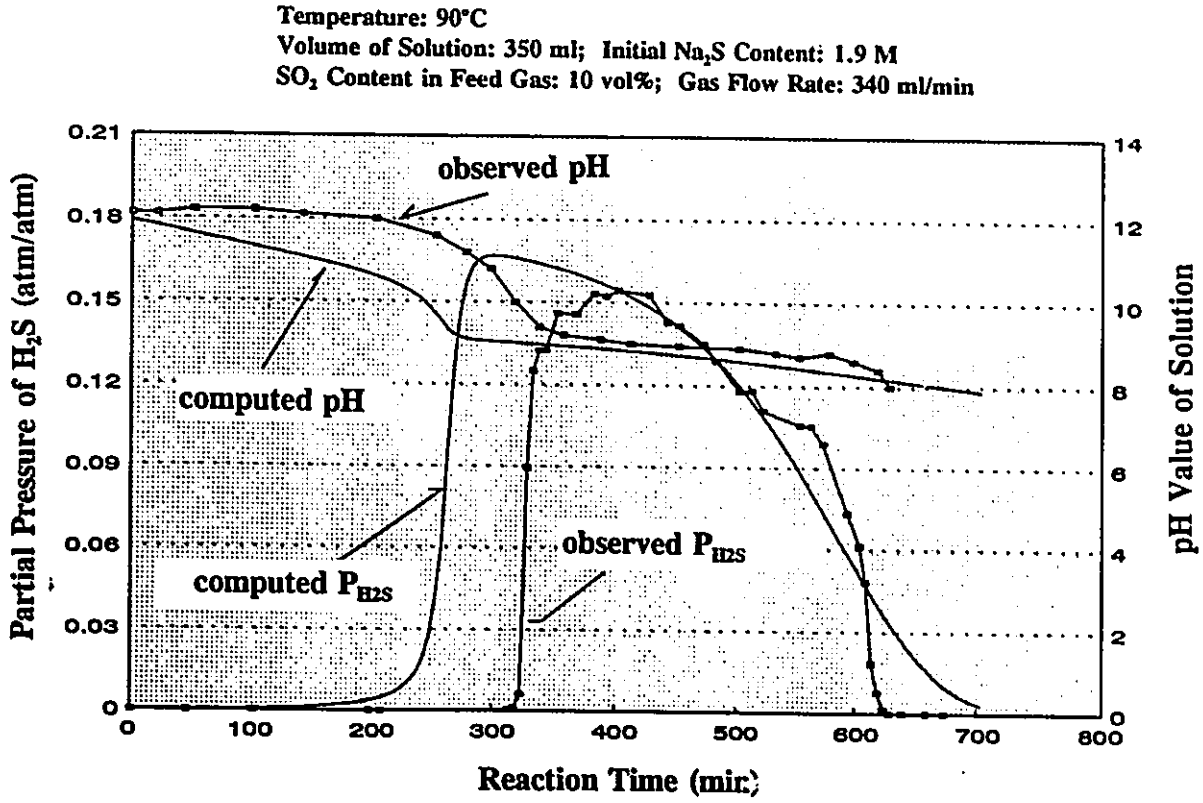

Fig.7.14: A comparison between computed P_{H2S} and observed P_{H2S} in exit gases, computed pH value of solution and observed pH value of solution

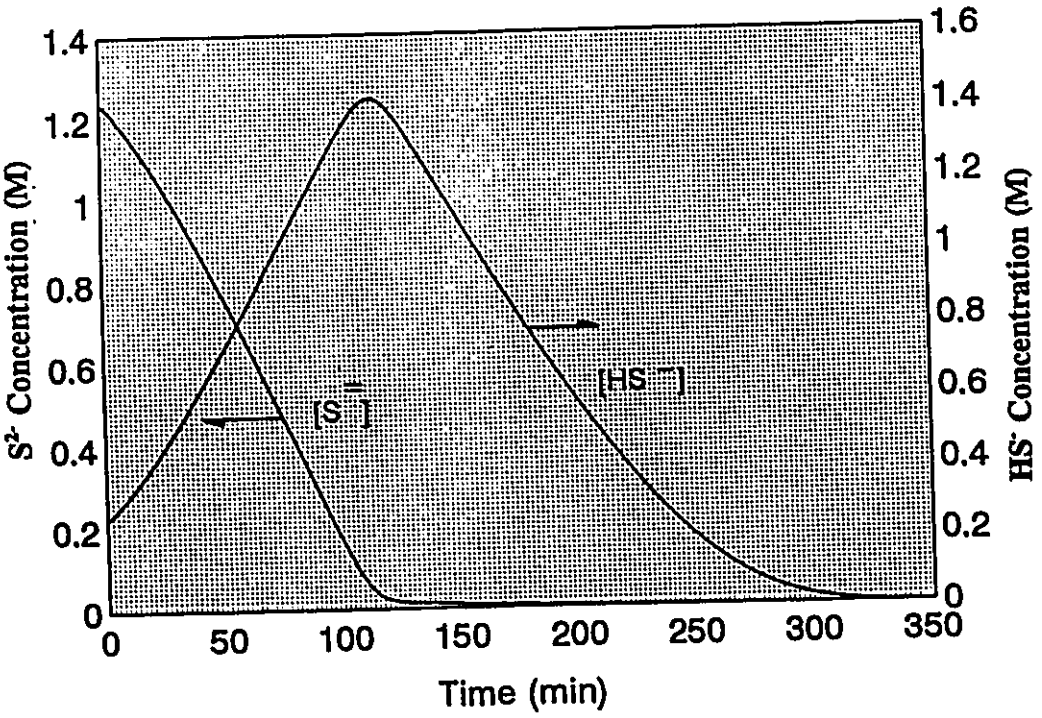

Fig.7.15: Computed changes in sulfide and bisulfide contents in solution with reaction time

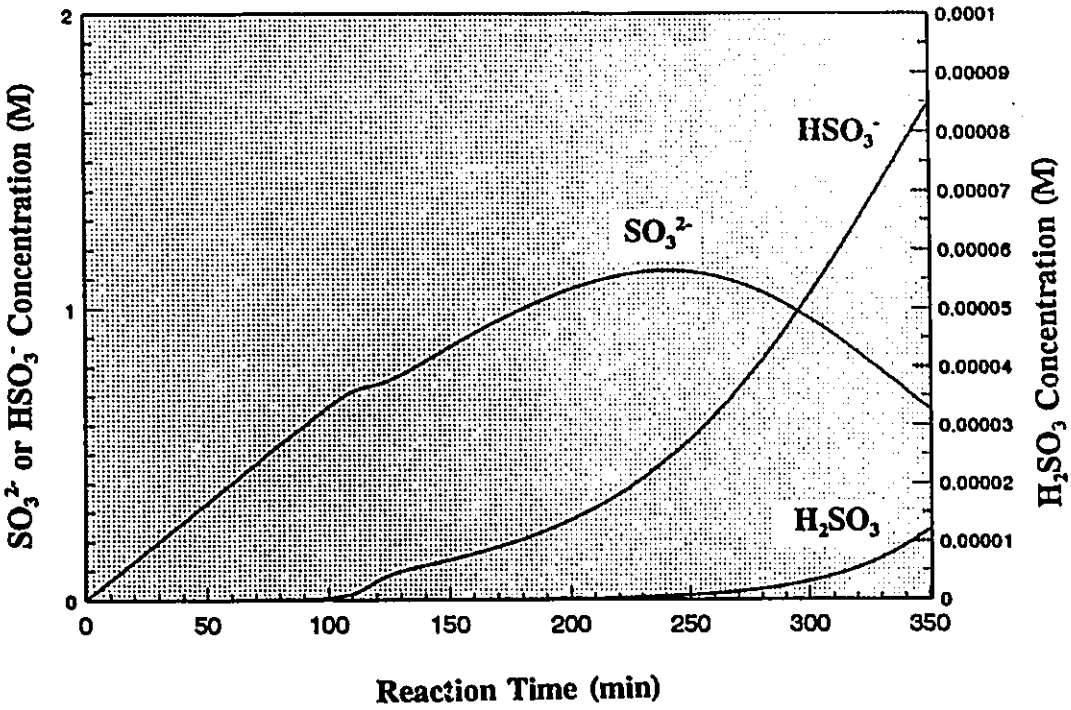

Fig.7.16: Computed changes in sulfite, bisulfite and sulfurous acid contents in solution with reaction time

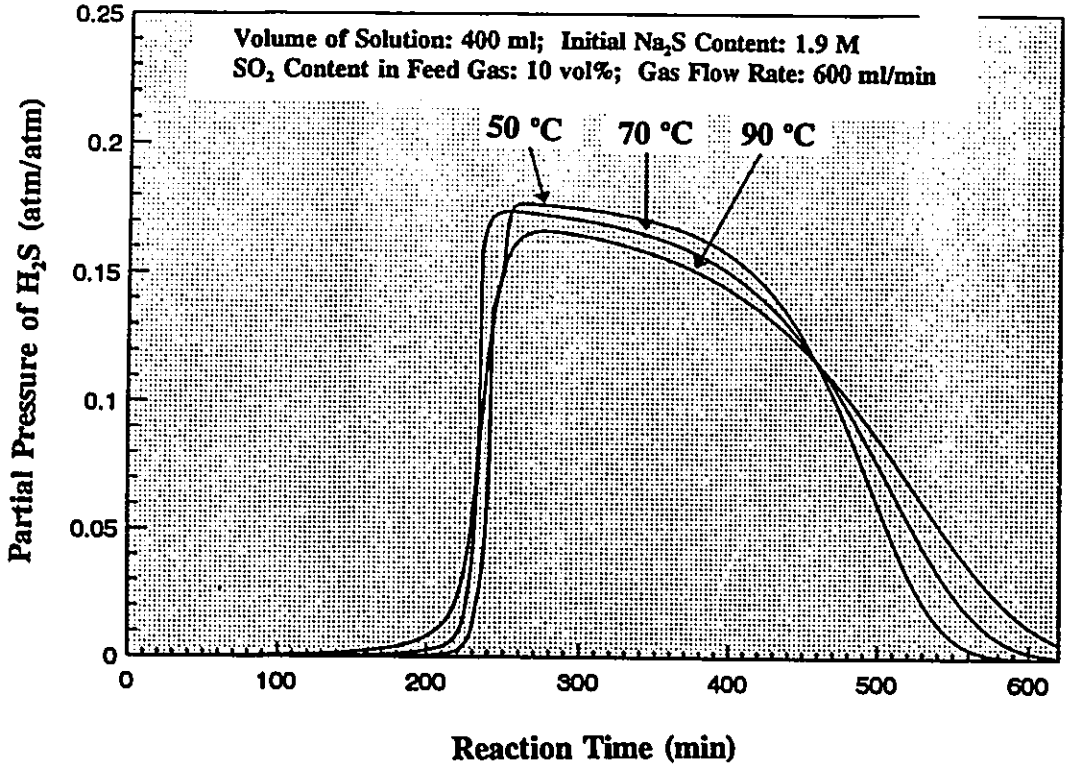

Fig.7.17: Temperature dependence of computed equilibrium partial pressure of H_2S

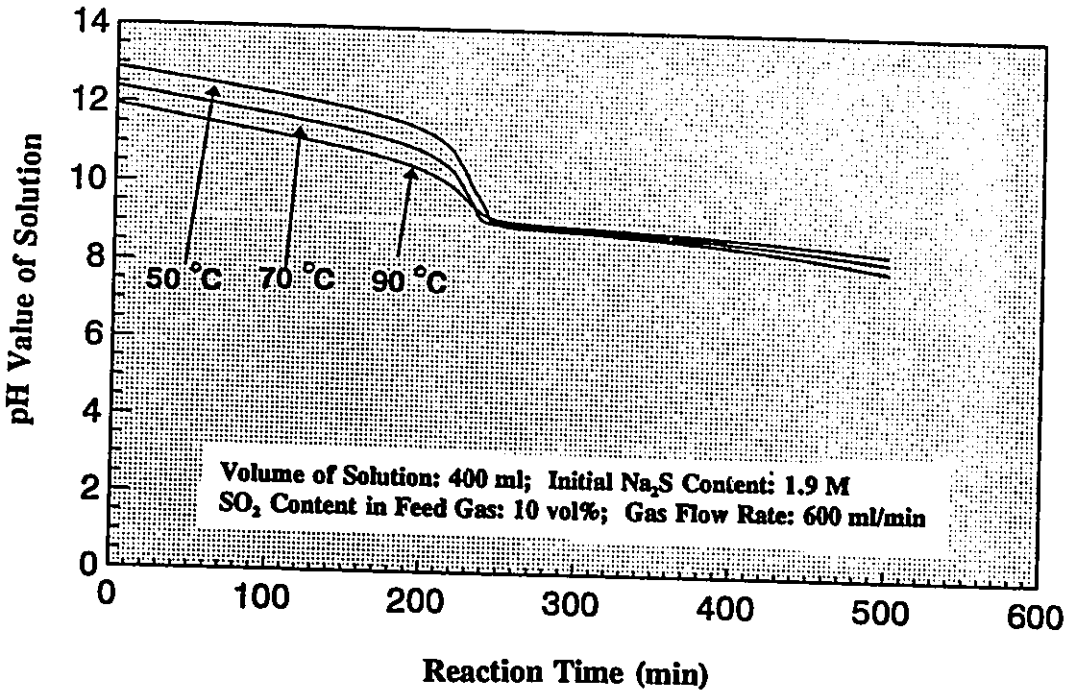

Fig.7.18: Temperature dependence of computed pH value of solution

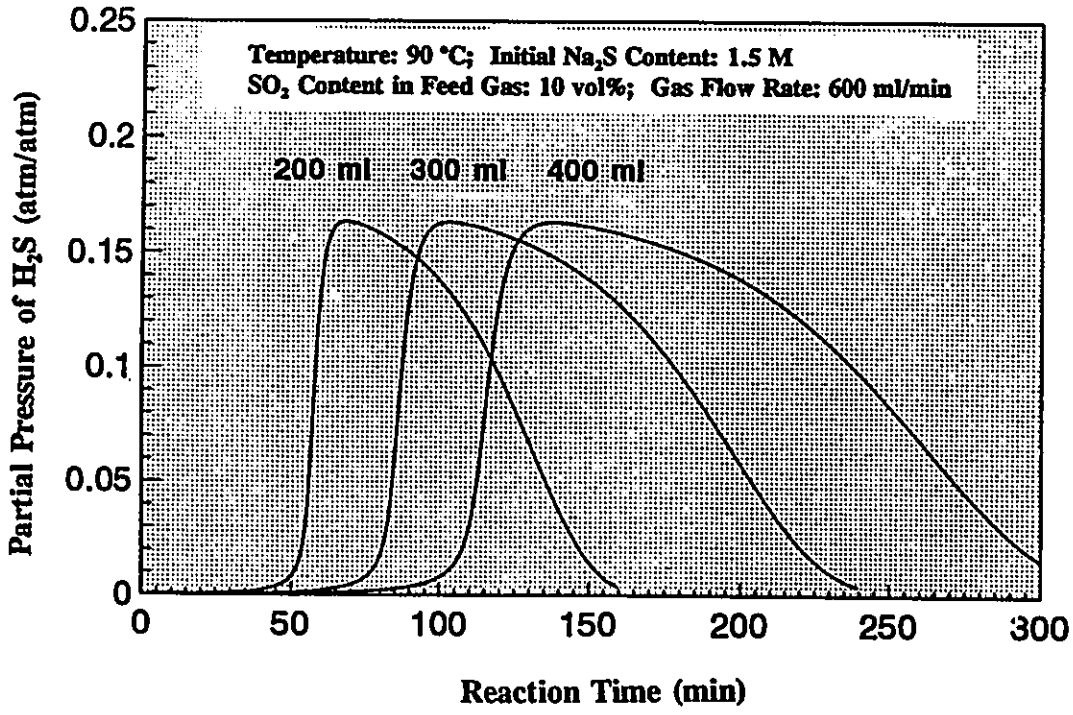

Fig.7.19: Effect of volume of solution in reactor on computed equilibrium partial pressure of H_2S in exit gases

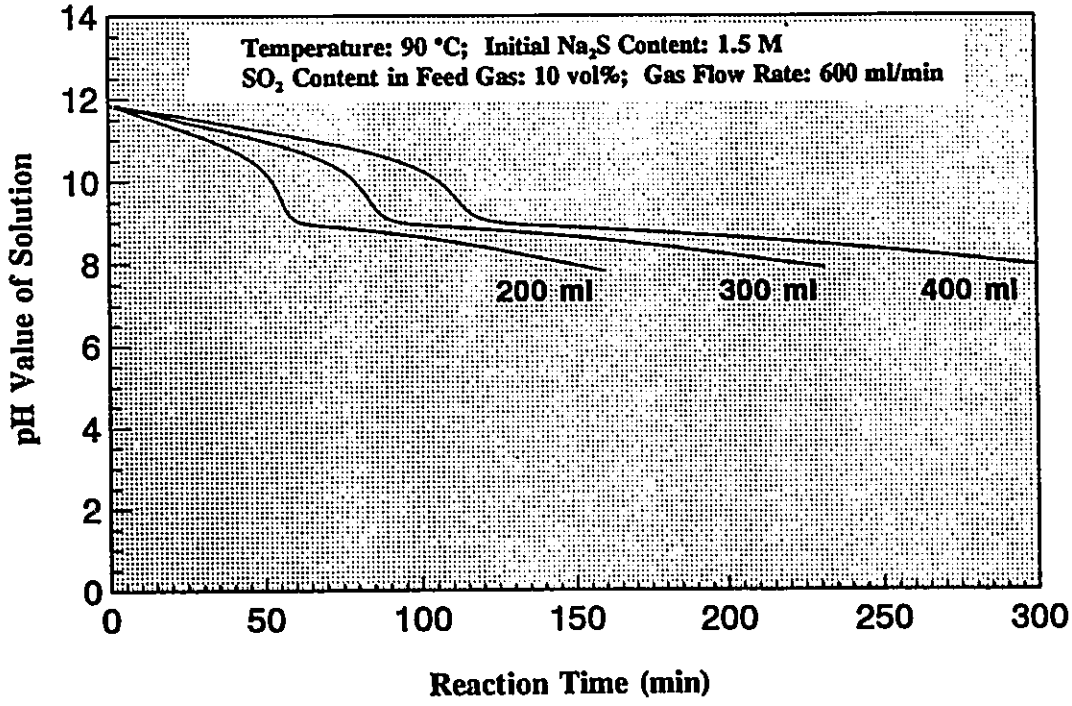

Fig.7.20: Effect of volume of solution in reactor on computed pH value of solution

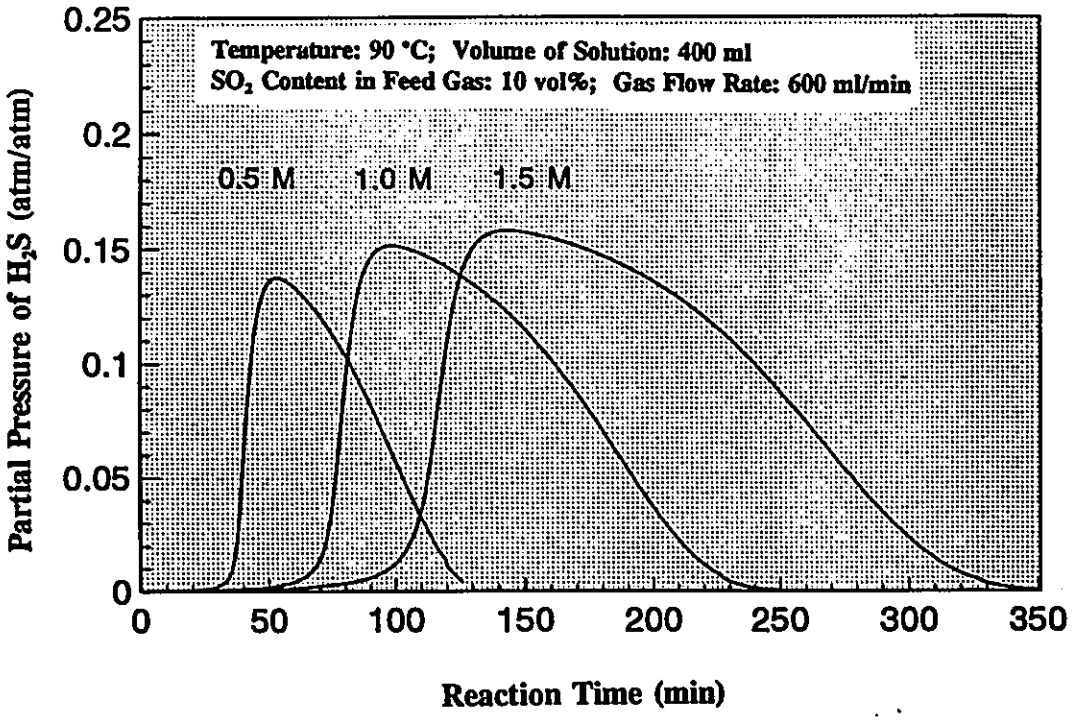

Fig.7.21: Effect of initial Na_2S content in solution on computed equilibrium partial pressure of H_2S in exit gases

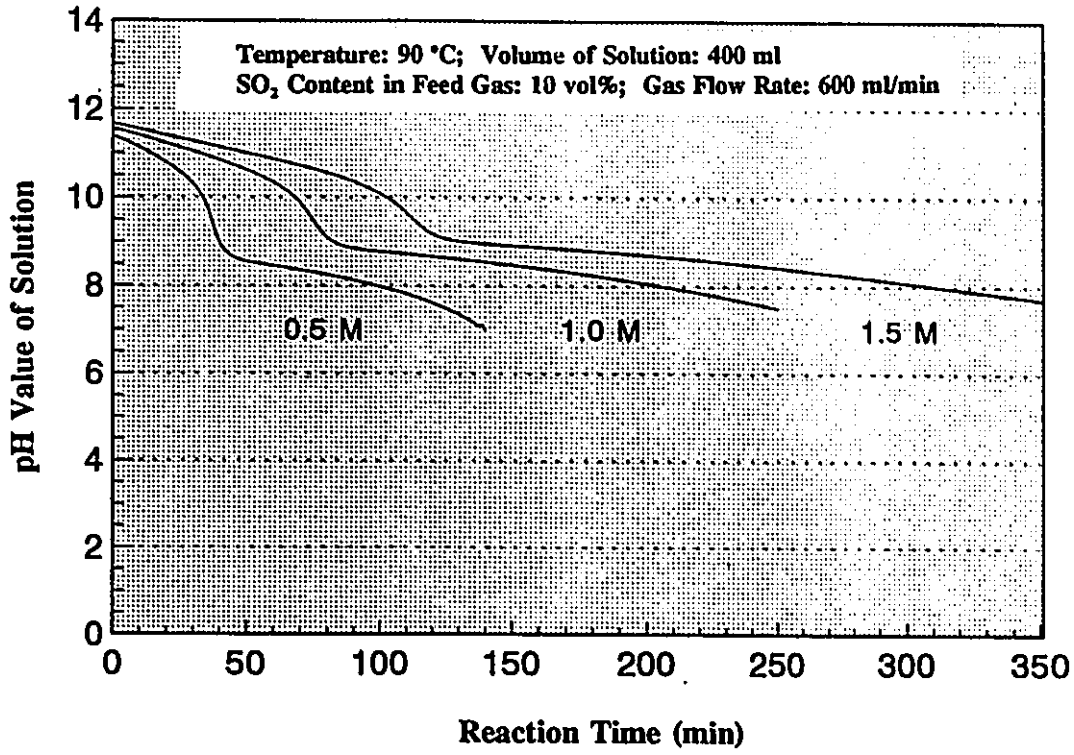

Fig.7.22: Effect of initial Na_2S content in solution on computed pH value of solution

CHAPTER EIGHT

DISCUSSIONS AND THE UP-DATED MCMASTER-INCO PROCESS

The heterogeneous system being studied involves interfacial reactions and reactions in the aqueous solution (including acid-base reactions and redox reactions). Since acid-base reactions in the liquid phase are very fast, the discussion on kinetics in this chapter will focus on interfacial reactions, namely SO_2 absorption and H_2S desorption (Sections 8.1 and 8.2). Section 8.3 is devoted to the overall reaction, i.e. simultaneous SO_2 absorption and H_2S generation with the acidified aqueous solution of Na_2S. Finally, based on the present study, the proposed McMaster-Inco process is modified for better control and higher efficiency (Section 8.4).

8.1 The Absorption of Sulfur Dioxide

This section will start with a comparison of rate of SO_2 absorption in aqueous Na_2S solution and distilled water. Then, the ability of SO_2 absorption with the use of a packed tower will be discussed.

To study the effect of Na_2S in solution on the transfer of SO_2 from gaseous to liquid phase, the SO_2 /N_2 gaseous mixture at a rate of 700 std liters/min was allowed to contact quiescent surface (2.8×10^{-3} m^2) of the aqueous solution of Na_2S (1.5 M) and distilled water at 70 and 90 °C, respectively. The concentrations of SO_2 of incoming gas

was measured before the start of the experiment. The dry outgoing gas was sampled every one minute and was analyzed with a GC. Knowing the difference of SO_2 mass flux between incoming and outgoing streams, amount SO_2 absorbed by the liquid may be determined. The results are listed in Table 8.1.

Table 8.1 Overall Rates of Mass Transfer of SO_2 from 11% SO_2 -N_2 Gaseous Mixture to Aqueous Na_2S Solution of 1.5 M and Distilled Water at 70 and 90°C

Temperature (°C)	Na_2S Solution	Distilled Water
70	1.02 mol/m^2 min	0.13 mol/m^2 min
90	0.98 mol/m^2 min	0.07 mol/m^2 min

The beneficial effect of Na_2S in solution on the kinetics of SO_2 absorption is clear and significant. With sodium sulfide in the solution, the mass flux of SO_2 is about one order of magnitude higher than that with distilled water. The increase of the overall rate of SO_2 absorption may be due to the higher basicity of solution.

For distilled water, a negative temperature effect on SO_2 absorption was observed because it is an exothermic process. At higher temperature, solubility of SO_2 in water is lower. It is interesting to note that the temperature effect on SO_2 absorption in aqueous Na_2S solution was smaller than that observed for distilled water.

On an industrial scale, it is undesirable to operate a bubble column with high flow rates of gas because of the cost of gas compression. Consequently, a packed tower is considered to be more appropriate. As an example, consider a packed tower of 1 m^2 cross section and 10 m high, fed typically at a superficial gas velocity of 1 m/s (a total

mass flow of 0.044 kmol gas/s). If the feed gas contains 10% SO_2, as most cases in the present work, the feed rate of SO_2 per unit volume of packed column is (0.044x10%)/10 = 0.00044 kmol SO_2 per m^3 per sec (or 0.44 mol/m^3s or 26.4 mol/m^3min). The specific contact area in a packed tower with 3 cm packing is about 100 m^2 per m^3 packed volume. In order to remove all sulfur dioxide from the feed gas, the rate of SO_2 absorption has to be larger than (26.4 mol/m^3min)/100m^2/m^3 = 0.3 mol/m^2 min. This required rate of SO_2 absorption is lower than that observed at 90 °C with quiescent 1.5 M Na_2S solution (0.98 mol/m^2 mol). Therefore, it suggests that the aqueous Na_2S solution (1.5 M) in the assumed packed column may be more than adequate for SO_2 absorption under conditions specified above.

8.2 The Desorption of Hydrogen Sulfide

When the 10% SO_2-N_2 gaseous mixture was contacted with the flat and quiescent surface of aqueous Na_2S solution (1.5 M), as described in Section 8.1, the rate of hydrogen sulfide generation was measured to be 0.12 mol/m^2min in the outgoing gas, although pH value of bulk solution (around pH11) represents an early period of first stage. It demonstrated that the interfacial concentration was different from the bulk of the solution. The rate of hydrogen sulfide desorption observed by chemical analysis of exit gas at 70 and 90 ° C were determined to be 0.09 and 0.12 mol/m^2min (5.4×10^{-3} and 7.2×10^{-3} kmol/m^2h). Unlike absorption of sulfur dioxide, desorption of hydrogen sulfide is an endothermic process. Hence, the observed positive effect of temperature on H_2S desorption was expected. Since desorption of hydrogen sulfide is the only endothermic

step involved in the conversion of Na_2S to H_2S, the observed positive temperature effect on the overall reaction (Section 4.2.1 Table 4.1) may suggest that the contribution of desorption of H_2S to the resistance for the overall process would be significant.

Hydrogen sulfide is anticipated to form in the area near the interface in which the absorbed sulfur dioxide made H^+ available for reaction. It has been shown, both experimentally and theoretically (via the SFBR model), that the partial pressure of hydrogen sulfide in exit gas depends on the concentration of protons in solution, i.e. on the pH value. When absorbed sulfur dioxide acidifies the solution near interface, the pH value of the solution near the interface may be low enough for hydrogen sulfide to form. A higher rate of H_2S generation is expected if the bulk solution is in the second stage. If the bulk solution is in the first stage (high pH), part of the hydrogen sulfide formed in the area near the interface may diffuse towards the bulk solution. As indicated by both the experimental observations and the mathematical modelling, the equilibrium partial pressure of H_2S in first stage is low due to the high pH (10^{-5} atm for the early period of first stage at 90°C).

The observed rate of desorption of H_2S from a quiescent solution is expected to be an underestimation of that in a bubble reactor in the second stage for stronger turbulence in both phases. Based on the estimated interfacial area, the maximum rate of H_2S generation observed using the SFBR can be determined. According to Eq.4.3, interfacial area provided by 10 mm bubbles in 350 ml solution with a gas rate of 650 ml/min was estimated to be 135 cm^2 (1.35×10^{-2} m^2). Considering the area of liquid surface (20 cm^2), the total area of the interface was 1.55×10^{-2} m^2. A typical content of

10% H_2S in an exit gas of 650 ml/min represents a desorption rate of H_2S of 0.2 mol/m^{2}min, compared to 0.12 mol/m^{2}min at 90°C for the quiescent solution in first stage.

8.3 Conversion Ratio of Sodium Sulfide to Hydrogen Sulfide

In the semi-flow batch reactor (SFBR), the conversion ratio is defined as the total number of moles of hydrogen sulfide generated in the second stage over the moles of sodium sulfide added initially in the reactor. In the continuous flow tank reactor (CFTR), it is defined as the molar flux of hydrogen sulfide in exit gas over the molar flux of sodium sulfide in the feeding solution. For the intended purpose of the present work, a perfect process will have a ratio of 1.0. If the ratio is below 1.0 and there is no sulfide left in the solution, it implies that a certain amount of sulfide that fails to form H_2S has been oxidized.

8.3.1 Temperature Dependence of Na_2S Conversion to H_2S

The conversion ratio was found experimentally to be very sensitive to the change of reaction temperature. With the increase of temperature, the conversion ratios observed in both the SFBR and CFTR increased significantly (refer Tables 4.1, 4.5 and 5.6). The reasons are thought to be the following: [1] the desorption of hydrogen sulfide, which is more likely than any other steps to be a rate-limiting step, is endothermic; [2] the wet Claus reaction, which converts sulfide to elemental sulfur, is strongly exothermic and could be better suppressed; and [3] at a higher temperature, the content of water vapour in exit gas is higher, which may lead to a lower partial pressure

of hydrogen sulfide, and hence a larger driving force for hydrogen sulfide desorption.

8.3.2 Effects of Conditions of Feed Streams on Na_2S Conversion to H_2S

In experiments conducted in SFBR, the conversion ratio decreased from 0.52 to 0.12 when the content of sulfur dioxide increased from 10% to 54% (refer Table 4.2). Dissolved sulfur dioxide is the oxidant in wet Claus reaction. It is not surprising if a higher concentration of sulfur dioxide in solution results in a high rate of wet Claus reaction, i.e. increased amount of elemental sulfur formed at the expense of H_2S.

When the initial content of sodium sulfide increased from 0.017 to 0.166 M, the conversion ratio increased slightly from 0.52 to 0.56 (Table 4.3). Since the aqueous solution of sodium sulfide is basic, a higher concentration of sodium sulfide will result in a higher pH of solution, in which acid-base reactions may become stronger than the competing redox reactions.

8.4 The Current Flow Sheet of the Proposed McMaster-Inco Process

Referring to Fig.8.1, in the proposed McMaster-Inco process, sulfur dioxide-containing gas is fed into the absorption/generation unit (AGU). In the AGU sulfur dioxide is absorbed in the sulfide solution and converted into hydrogen sulfide gas. At a higher temperature for the suppression of formation of elemental sulfur, such as 90 °C, the efficiency of the conversion of sodium sulfide to hydrogen sulfide is higher. Data obtained in the present work suggest that the pH range of 7.0 to 9.5 favours Na_2S

conversion to H_2S.

To make elemental sulfur in a Claus plant, part of the sulfur dioxide required may be supplied from the decomposition of bisulfite in spent solution. Spent bisulfite/sulfite liquor is readily regenerated. To regenerate the bisulfite/sulfite liquor, the liquor is first exposed to a heat source such as steam to evaporate excess water. Upon heating, bisulfite decomposes to SO_2 gas which is fed to the Claus plant leaving the sulfite for reduction. To reduce the sulfite, the sulfite is mixed with coke or carbon which is partially burned to provide gaseous reductant and heat in a reductive burning reactor (RBR). Air or oxygen enriched air may be used in RBR. The molten sulfide may be tapped from RBR. The Na_2S solution to be used in AGU may be prepared by dissolving solidified salt in water and followed by filtration to remove ashes from coal or coke.

As shown in Fig.8.2, the two-tower AGU may be substituted for the single tower design shown in Fig.8.1. The main purpose for using two-tower design is to increase the strength of hydrogen sulfide in the exit gas and to decrease the amount of N_2 in the gas to be processed in the Claus plant. In the two-tower design, the first tower is operated under the conditions of the first stage (pH 10.0 to 12.5) to absorb sulfur dioxide gas and remaining N_2 to be discharged. The second tower is AGU and operated under the conditions of the second stage (pH 7.0 to 9.5) to have simultaneous absorption of SO_2 and generation of H_2S. The fresh sulfide solution is fed into the first tower. The spent solution from the first tower is fed into the second tower instead of using the fresh sulfide solution. By having a portion of untreated flue gas entering directly into the first tower, part of the nitrogen associated in this portion of the flue gas will bypass the Claus

plant. The total volumetric flow of gases to the Claus plant will be decreased, hence reducing capital and operating costs of elemental sulfur production.

As illustrated in Fig.8.3, a third tower may be employed to absorb more SO_2 and to reject more N_2 by converting remaining sulfite to bisulfite. In the subsequent treatment similar to Wellman-Load process (Leckner, Pearson and Wood 1982), the generation of high grade SO_2 may be carried out. This tower should be operated at conditions of the transition period between the second and third stages (pH 3 to 6). The operating temperature may be much lower than that in the second tower. Experimentation has indicated that absorption of sulfur dioxide may be enhanced by decreasing temperature. The exit gas from the third tower may contain small amounts of hydrogen sulfide and/or sulfur dioxide. The removal of small amounts of H_2S and SO_2 may be accomplished by feeding it to the first tower which is operated under the first-stage conditions.

In summary, the proposed McMaster-Inco process is capable of desulfurizing SO_2-containing flue gas and to generate H_2S for elemental sulfur production in a Claus plant, as shown in Fig. 8.1. INCO and McMaster have filed for patent application for this process. In comparison with what has been proposed in the literature, the ESI process as shown in Fig. 1.1, the McMaster-INCO process has fewer steps and is likely more economical. The simplification in McMaster-INCO process is mainly due to: (a) SO_2 is a stronger acidic gas in comparison with CO_2; and (b) processing steps related to CO_2 and carbonate in ESI design may be eliminated.

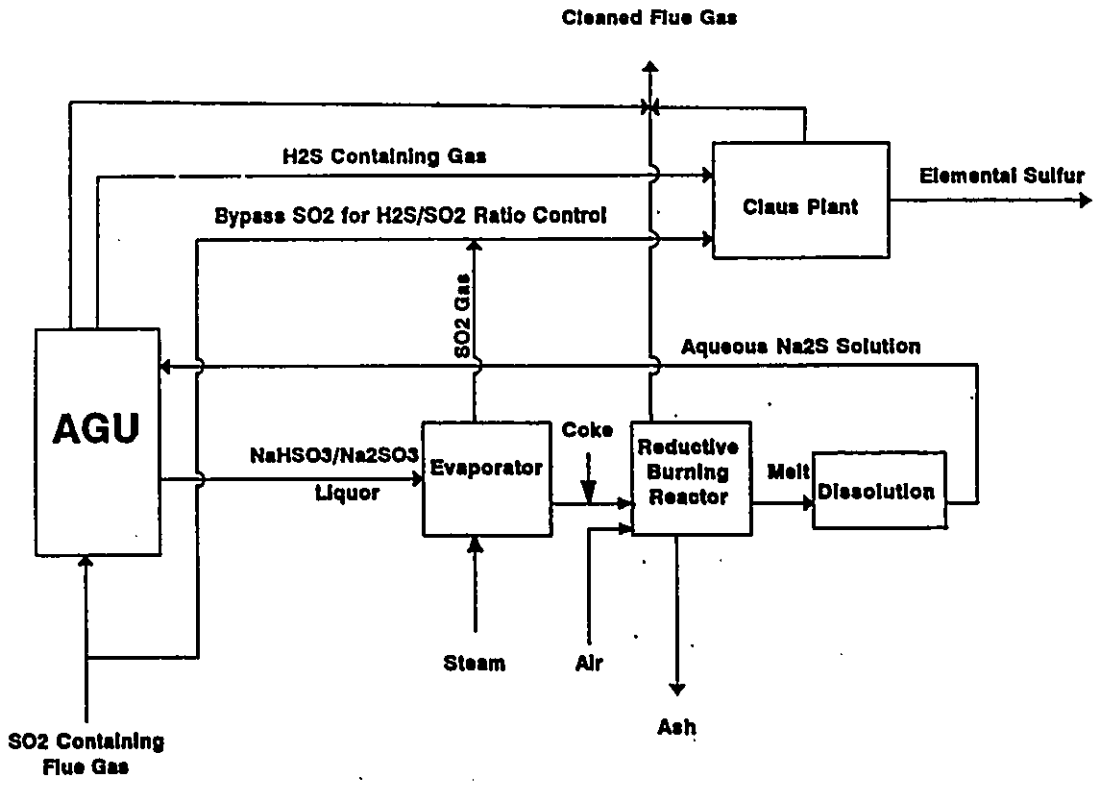

Fig.8.1 The current flow sheet of the proposed McMaster-INCO process (AGU: absorption/generation unit)

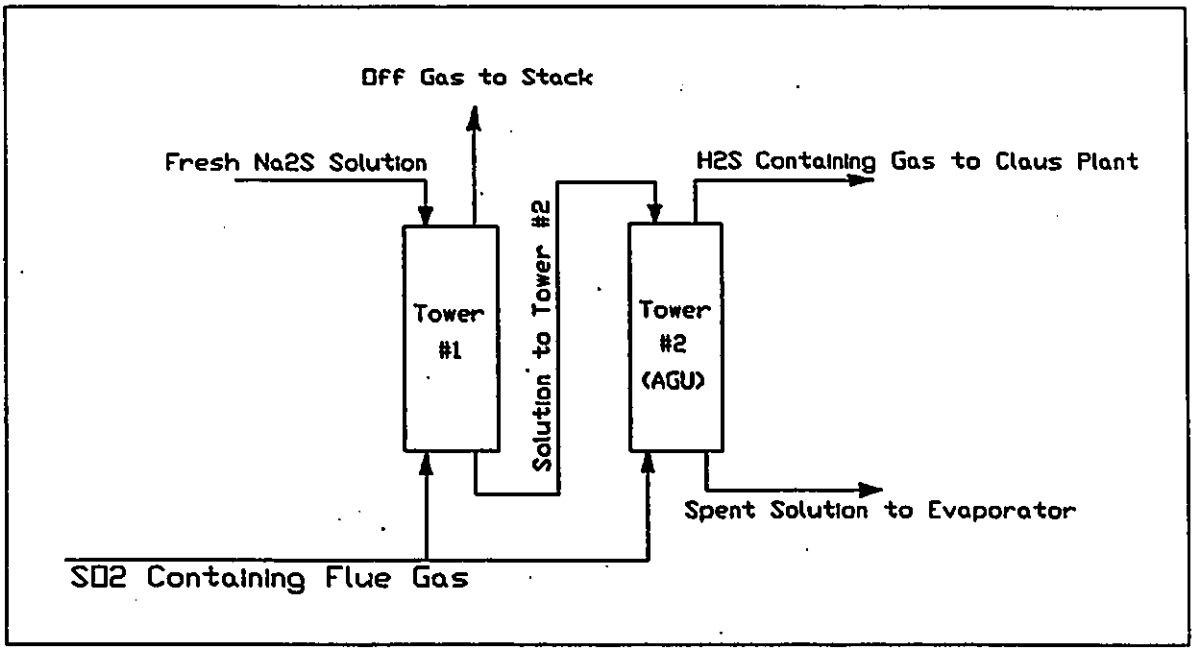

Fig.8.2 A flow sheet of the proposed two-tower AGU system in McMaster-INCO process

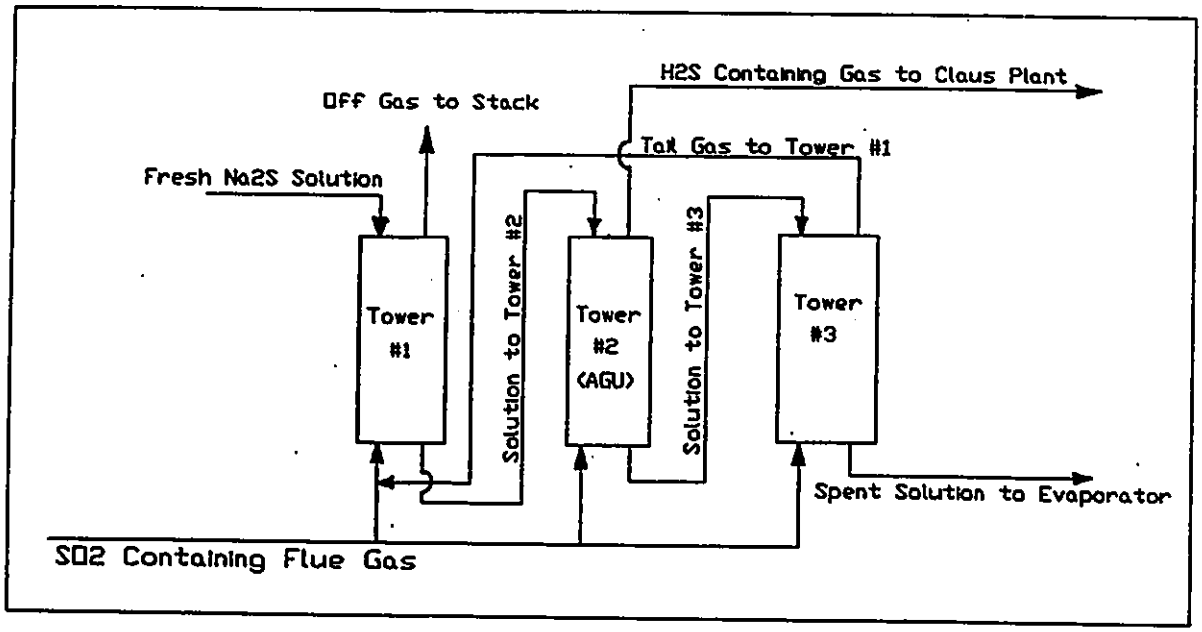

Fig.8.3 A flow sheet of proposed three-tower AGU system in McMaster-INCO process

CHAPTER NINE

CONCLUSIONS AND FUTURE WORK

For the purpose of converting SO_2 in the flue gas to H_2S, and then to elemental sulfur, thermodynamics and kinetics of $Na_2S_{(aq)}$-SO_2-H_2S reacting system have been studied, both experimentally and theoretically. Based on experimental and computed results obtained in the present work the following conclusions may be reached.

[1] Aqueous solution of sodium sulfide may be used to absorb sulfur dioxide and to generate hydrogen sulfide simultaneously according to acid-base reactions.

[2] At higher temperatures, higher Na_2S concentration and low SO_2 partial pressure, the generation of hydrogen sulfide may be enhanced with further suppression of redox reactions. When 1.5 M sodium sulfide solution reacted with 10%SO_2 feed gas at 90 °C in the CFTR, the conversion ratio of Na_2S to H_2S was greater than 0.9.

[3] The $Na_2S_{(aq)}$-SO_2-H_2S reacting system demonstrated a three-stage pattern as a function of time in the SFBR. This pattern was reproduced for first and second stages by the mathematical model based on mass and charge balances and thermodynamic relations. The three-stage pattern is found to be determined by the acid-base reactions, and hence reflects the change in the acidity of solution.

[4] There is an optimum value of molar flow ratio of SO_2 in feed gas to Na_2S in feed liquid, at which the partial pressure of H_2S in exit gas reach a maximum. The optimal value of this ratio observed in CFTR was in a range of 1.6 to 1.7, while the mathematical model gave a range of 1.3 to 1.4.

[5] Absorption of sulfur dioxide has been significantly accelerated by the presence of sodium sulfide in the aqueous solution.

[6] The overall reaction and all steps involved, except desorption of hydrogen sulfide, are exothermic. The observed positive effect of increasing temperature on the overall reaction suggests that desorption of H_2S may contribute more resistance to the kinetics of overall reaction under conditions studied in the present work.

After reviewing the results of the present work, INCO Limited decided to support the research on McMaster-Inco process one step further. As the continuation of the present work, a technical feasibility study at bench scale has started. The objective of this study is to demonstrate in a mini packed tower (4" I.D.) that the AGU can be used to remove SO_2 in flue gas and generate H_2S for the purpose of elemental sulfur production. In addition to the establishment of technical feasibility, parameters required for the design of a commercial packed tower are to be determined.

REFERENCES

Akita, K. and Yoshida, F. (1973), Ind. Eng. Chem. Process Des. Dev. Vol.12, p76.

Alyea, H.N. and Backstrom, H.L.J. (1929), JACS, Vol.51, p90.

Arntson, R.H., Dickson, F.W. and Tunell, G. (1958), Science, Vol.128, p716.

Astarita, G. (1966), Mass Transfer with Chemical Reactions, Elsevier, Amsterdam.

Averbukh, T.D. (1969), Int.Chem. Eng., No.9, p317.

Azbel, D. (1981) Two-Phase in Chemical Engineering, Chap.7, Cambridge Univ. Press, New York.

Backstrom, H.L.J. (1927), JACS, Vol.49, p1460.

Backstrom, H.L.J. (1929), JCS (London), p601.

Baird, M.H.I. and Davidson, J.F. (1962), Chem. Eng. Sci., Vol.17, p87-93.

Barner, H.E. and Scheuerman, R.V. (1978), Handbook of Thermochemical Data for Compounds and Aqueous Species, John Wiley and Sons, N.Y.

Barry, B.A. (1966), Engineering Measurements, John Wiley and Son, New York.

Bartlett, P.D., Cox, E.F. and Divis, R.E. (1961), JACS, Vol.83, p103.

Bartlett, P.D., Lohaus, G. and Weis, C.D. (1958), JACS, Vol.80, p5064-5069.

Bell, M.C., Blanco, J.A., Davies, H. and Garritsen, P. (1990), CIM Bulletin, Vol.83, No.933, p47-50.

Bertozzi, E.R., Divis, F.O. and Fettes, E.M. (1956), J. Polymer Sci., Vol.19, p17.

Bertozzi, E.R. (1957) US Patent No.2,796,325, (June 18,1957)

Birk, D., Heidemann R.A., Svrcek, W.Y. and Behie, L.A. (1991), Canadian Journal of Chemical Eng. Vol.69, August, p944-952.

Von Bogdandy, L, Rutsch, W. and Stranski, I.N. (1959), Chem. Ing. Techn., Vol.31, p580-582.

Bottoms, R.R. (1931), Ind.Eng.Chem., No.23, p501.

Bowman, C.W. (1960), Ph.D. Thesis, University of Toronto.

Brasted, R.C. (1961), Comprehensive Inorganic Chemistry, Vol.VIII, van Nostrand, Princeton, N.J.

Braulick, W.J., Fair, J.R. and Lerner, B.J. (1965) AIChEJ, No.7 p73.

Brignell, A.S. (1974) Chem. Eng. Sci. Vol.29 p135-147.

Brimacombe, J.K. (1991), Proc. of International Symp. on Injection in Process Metallurgy, edited by Lehnes, T. et.al., p11-23.

Brydges, T.G. and Wilson, R.B. (1991) Proceedings of the Royal Society of Edinburgh, 97B, p1-16.

Butler, J.N. (1964) Ionic Equilibrium: A Mathematical Approach, Addison-Wesley Pub. Company, Reading, Massachusetts.

Calderbank, P.H. (1958), Trans. Instn. Chem. Engrs., Vol.36, p443.

Calderbank, P.H. and Lochiel, A.C. (1964), Chem. Eng. Sci., Vol.19, p485-503.

Calderbank, P.H. (1967), Mixing: Theory and Practice, edited by Uhl, V.W. and Gray, I.B., Vol.II, Chap.1, Academic Press, New York.

Calderbank, P.H., Johnson, D.S.L. and London, J. (1970), Chem. Eng. Sci., Vol.25, p235-256.

Calvert, J.G. and McQuigg, R. D. (1973) J.Chem. Kinet. Symposium No.1, Suppl. to Vol.7, p113-154.

Calvert, J.G. and Stockwell, W.R. (1983), ES&T, Vol.17, p428A.

Chang, C.S. and Rochelle, G.T. (1985), Ind. Eng. Chem. Fundam., Vol.24 p7-11.

Chen, K.Y. (1970), Ph.D. Thesis, Harvard University.

Chen, K.Y. and Morris, J.C. (1972), ES&T, Vol.6, p529-537.

Chivers, T., Hyne, J.B. and Lau, C. (1980), Int. J. Hydrogen Energy, No.5, p499-506.

Chivers, T. and Lau, C. (1987a), Int. J. Hydrogen Energy, No.12, p235-243.

Chivers, T. and Lau, C. (1987b), Int. J. Hydrogen Energy, No.12, p561-569.

Clift, R., Grace, J.R. and Weber, M.E. (1978) Bubbles, Drops and Particles, Chap.8 Academic Press, New York.

Coppock, P.D. and Meiklejohn, G. (1951), Trans. Instn. Chem. Engrs., Vol.29, p75.

Coppus, J.H.C. and Rietema, K. (1980) Trans. Inst. Chem. Engrs., Vol.59, p54-63.

Cotton, F.A. and Wilkinson, G. (1967), Advanced Inorganic Chemistry, Chapter 21, Interscience, N.Y.

Crank, J. (1957), The Mathematics of Diffusion, Clarenden Press, Oxford.

Criss, C.M. and Cobble, J.W. (1964a), JACS, Vol.86, p5385.

Criss, C.M. and Cobble, J.W. (1964b), JACS, Vol.86, p5390.

Danckwerts, P.V. (1951), Trans. Farad. Soc., Vol.47, p1014-1023.

Datta, J. (1952) J. Indian Chem. Soc., Vol.29, p101; through Chem. Abstracts, Vol.46, 9004f.

Datta, R.L., Napier, P.H. and Newitt, D.W. (1950), Trans. Instn. Chem. Engrs., Vol.28, p14.

Davidson, J.F. and Schüler, B.O.G., (1960), Trans. Instn. Chem. Engrs., Vol.38, p335-342.

Davies, R.M. and Taylor, G.I., (1950), Proc. R. Soc. London, Vol.A200, p375-390.

Davis, R.E. (1958) JACS, Vol.80, p3565.

Diendoerfer, F. and Humphrey, A. (1961), Ind. Eng. Chem. Vol.53, p755.

Donohue, J (1974), The Structure of Elements, John Wiley and Sons, N.Y.

Ehret, W.F. (1946), Smith's College Chemistry, 6th ed. Appleton-Century, N.Y. p312-314.

Eigen, M., Kustin, K., and Maas, G.Z. (1961), Phys. Chem., Vol.30, p130.

Elliott, T.C. and Schwieger, R.G. (1984), The Acid Rain Sourcebook, McGraw-Hill, Inc., N.Y..

Fair, J.R. (1967a), Chem. Eng. Vol.74, p67.

Fair, J.R. (1967b), Chem. Eng. Vol.74, p207.

Fair, J.R., Lambright, A.J. and Anderson, J.W. (1962), IEC Process Design and Development, No.1, p33.

Farr, H.V. and Ruhoff, J.R. (1952), US. Patent 2,586,459 (Feb.19,1952); Chem. Abstracts, Vol.46, 5276i.

Freier, R.K. (1966), Aqueous Solutions: data for inorganic and organic compounds, W.de Gruyter, Berlin, N.Y.

Gal-or, B. and Hoelscher, H.E. (1966), AIChEJ, Vol.12, p499.

Geohring, Appel and Helbing (1947), Z.Anorg.Chem. Vol.254, p185.

George, D.R., Crocker, L. and Rosenbaum, J.B. (1970), Min. Engr. Vol.22, No.1, p75.

Gilliland, E.R. and Sherwood, T.K. (1934), Ind. Eng. Chem. Vol.26, p516.

Godfrey, P (1993) ES&T, Vol.27, No.7, p1247.

Golding, R.M. (1960), J. Chem. Soc. p3711-3716.

Goodgame, T.H. (1954), Chem. Eng. Sci., No.3, p37.

Gordon, G.E. (1987), Chemistry of Acid Rain, Johnson, R.W. and Gordon, G.E. (editors), American Chemical Society, Washington D.C., p2-9.

Gordon, K.F. and Sherwood, T.K. (1954), Chem. Eng. Progr. Symp. Ser. Vol.50, No.10 p15.

Gorham, E.(1957), Limnilogy and Oceanography, No.2, p12.

Gorham, E. and Gordon, A.G. (1960), Canadian Journal of Botany, Vol.38, p477.

Gorham, E. and Gordon, A.G. (1961), Canadian Journal of Botany, Vol.41, p371.

Grace, J.R. (1973) Trans. Instn. Chem. Engrs., Vol.51, p116-120.

Gunn, J.M. and Keller, W. (1990) Nature, No.345, p431-433.

Guyer, R.L. and Pfister, X. (1946), Helv. Chim. Act., Vol.29, p1400-1412.

Haberman, W.L. and Morton, R.K. (1956), Trans. Amer. Soc. Civil Engrs., Vol.121, p227-252.

Hamielec, A.E. and Johnson, A.I. (1962), Can. J. Chem. Eng., Vol,40, p41.

Hammerton, D. (1953), Ph.D. Thesis, Birmingham University.

Hansen, C. (1933), Ber. Chem. Ges. Vol.66, p819.

Hatta, S. (1928), Tohoku Imperial U. Tech. Rept., Vol.8, p1.

Hatta, S. (1932), Tohoku Imperial U. Tech. Rept., Vol.10, p119.

Hauhs, M. and Wright, R.E. (1989), Acid Deposition Reversibility of Soil and Water Acidification- A Review, Commission of the European Communities, Air Pollution Research Report II.

Heath, P. (1954), Analyst, No.7, p787-799.

Himmelblau, D.H. (1959), J Phy. Chem. Vol.63, p1803.

Hunger, T., Lapicque, F. and Storck, A. (1990), J. Chem. Eng. Data, Vol.35, p453-463.

Huntley, D.R. (1990a), Surface Science, No.240, p13-23.

Huntley, D.R. (1990b), Surface Science, No.240, p24-36.

Irons, G.A. and Guthrie, R.I.L.(1978), Metal. Trans. B., Vol.9B, p101-110.

Jackson, R. (1964), The Chem. Engrs., Vol.42, p107.

Jia, C.Q. and Lu, W-K. (1992), Proceedings of the International Symposium on Waste Processing and Recycling in Mining and Metallurgical Industries. Edmonton, Canada, p215-228.

Johnson, A.I., Hamielec, A.E. and Houghton, W.T. (1967), AIChEJ, Vol.13, p379.

Karchmer, J.H. (1970), The Analytical Chemistry of Sulfur and Its compounds, Part I, Wiley Interscience, N.Y.

Kato, N. and Akimoto, H. (1992) Atmos. Environ., Vol.26A, No.16, p2997-3017.

King, C.J. (1964), AIChEJ, Vol.10, p670.

Kirk, R.E. and Othmer, D.F. (eds.) (1954), Encyclopedia of Chemical Technology, Vol.13, Interscience Encyclopedia, N.Y. p390-398.

Kohl, A.L. and Riesenfeld, F.C. (1985), Gas Purification, 4th ed., Gulf Pub. Company, Texas.

Kolthoff, I.M. and Elving, P.J. (1961), Treatise on Analytical chemistry, Part II, Vol.7, p17, Interscience, N.Y.

Kolthoff, I.M., Sandell, E.B., Meehan, E.J., Bruckenstein, S. (1969), Quantitative Chemical Analysis, The Macmillan Company, London.

Van Krevelen, D.W. and Hoftijzer, P.J. (1950), Chem. Eng. Prog., Vol.46, p29.

Kumar, A., Degaleesan, T.E., Ladda, G.S. and Hoelscher, H.E. (1976), Can. J. Chem. Eng., Vol.54, p503.

Landolt, C.A., Dutton, A., Edwards, J.D. and McDonald, R.N. (1992), JOM, sept., p50-55.

Latimer, W.M. (1964), Oxidation Potentials, Prentice-Hill Inc. N.Y.

Leckner, P., Pearson, R.O. and Wood, R.T. (1982), CEP, Feb., p65-70.

Leibson, I., Holcomb, E.G., Cacoso, A.G. and Jacmic, J.J. (1956), AIChEJ, No.2, p297.

Leonard, J.H. and Houghton, G. (1963), Chem. Eng. Sci., Vol.18, p133-142.

Levich, V.G. (1962) Physicochemical Hydrodynamics, Prentice-Hall, Englewood Cliffs, N.J.

Levy, M.A. (1992) Environment, May, p16.

Lewis, J.B. (1954), Chem. Eng. Sci., No.3, p248-260.

Lewis, J.B. (1953), Trans. Inst. Chem. Eng. (London), Vol.31 p323-325.

Lewis, J.B. and Pratt, C.R. (1953 b), Nature, Vol.171, p1155.

Lewis, W.K. and Whitman, W.G. (1924), Ind. Eng. Chem. Vol.16, p1215-1220.

Li, P.S., West, F.B., Vance, W.H. and Moulton, R.W. (1965), AIChEJ, Vol.11, p581.

Lochiel, A.C. and Calderbank, P.H. (1964), Chem. Eng. Sci., Vol.19, p471.

Lu, W-K. and Hamielec, A.E. (1973), Chemical Metallurgy of Iron and Steel, published by The Iron and Steel Institute, London, p110-111.

Lu, W-K. (1989), A Research Proposal, Submitted to Canada Center for Mineral and Energy Technology, Energy, Mine and Resources Canada.

Matuszek, J.E., Wales, D.L. and Gunn, J.M. (1992) Can. J. Fish. Aquat. Sci., Vol.49, (Suppl.1) p87-94.

McManamey, W.J. (1961), Chem. Eng. Sci., Vol.15, p251.

Mehta, V.D. and Sharma, M.M. (1966) Chem. Eng. Sci., Vol.21, p361.

Millero, F.J. (1991a), Deep-Sea Research, Vol.38, Suppl.2, pS1139-S1150.

Millero, F.J. (1991b), Estuarine, Coastal and Shelf Science, Vol.33, p521-527.

Molburg, J.C. (1993), Air & Waste, Vol.43, Feb., p180-186.

Ng, S.H. (1990), Master of Science Thesis, McMaster University.

Nickens, H.V. and Yannitell, D.W. (1987) Int. J. Multiphase Flow, Vol.13, No.1, p57-69.

Oden, S. (1967), Stockholm Newspaper, Dagens Nyheter, October 24,1967.

Olander, D.R. (1964), Chem. Eng. Sci., Vol.19, p67.

Orell, A. and Westwater, J.W. (1962), AIChEJ. Vol.8, p350.

Orr, R. and Burnett, T.C. (1990), Proposal for Pilot Plant Demonstration of Sulfur Dioxide Abatement Technology, A Report Submitted by Inco Limited, Manitoba Division to Western Economic Diversification of Canada.

Paschanski, D. and Valensi, G. (1949), J. Chim, Phys., Vol.49, p602-619.

Paskall, H.G. (1979), Capability of the Modified-Claus Process, A Final Report to the Dept. of Energy and Natural Resources of Province of Alberta.

Pearce, F. (1993) New Scientist, Vol.137, No.1864, p4-4.

Perry, R.H. and Green, D.W. (1984), Perry's Chemical Engineers' Handbook, 6th Edition, McGraw-Hill Inc., N.Y.

Pollard, F.H. and Jones, D.J. (1959), The Chem. Soc. London Special Publication, No.12.

Price, C.C. and Oal,S. (1962), Sulfur Bonding, Ronald Press, N.Y.

Pryor, W.A., (1960), JACS, Vol.82, p4794-4797.

Pryor, W.A., (1962), Mechanism of Sulfur Reactions, McGraw Hill, N.Y.

Rasmussen, H.E., Hansford, R.C. and Sachanen, A.N. (1946), Ind.Eng. Chem., Vol.38, p376.

Remy, H. (1956), Treatise on Inorganic Chemistry, Vol.I, Elsevier, N.Y.

Rice, F.O. and Sparrow, C. (1955), JACS, Vol.75, p848.

Rinker, R.G., Lynn, S., Mason, D.M. and Corcoran, W.H. (1965), Ind.Eng.Chem.Fundamentals, Vol.4, p282.

Rosenbaum, J.B., George, D.R. and Crocker, L. (1971), The Citrate Process for Removing SO_2 and Recovering Sulfur From Waste Gases, presented at AIME Environmental Quality Conference, Washington, D.C., June 7-9, 1971.

Rosenbaum, J.B., McKinney, W.A., Beard, H.R., Crocker, L and Nissen, W.I. (1973), Bureau of Mines, Report of Investigation, No.7774.

Schaftlein, R.W. and Russell, T.W.F. (1968), Ind. Eng. Chem., Vol.16, p1215-1220.

Scharzenbach, G. and Fisher, A. (1960), Helv.Chem.Acta., No.196, p1365.

Schulek, E. and Koros, E. (1952), Chem. Abstracts, Vol.46, 1380f.

Schulek, E. and Koros, E. (1953), Chem. Abstracts, Vol.47, 10390e.

Schwartz, S.E. (1986), Aerosols: Research Risk Assessment and Control Strategies, Lee,S.D. et.ai. Ed., Lewis Chelsea, M.I., p349-375.

Sherwood, T.K., Pigford, R.L. and Wilke, C.R. (1975) Mass Tansfer, McGraw Hill, New York.

Shulman, H.L. and Molstad, M.C. (1950), Ind. Eng. Chem. Vol.42, p1058.

Sideman, S., Hortacsu, O. and Fulton, J.W. (1966), Ind. Eng. Chem., Vol.58, No.7, p33.

Slack, A.V. and Hollinden, G.A. (1975), Sulfur Dioxide Removal from Waste Gases, Noyes Data Corp., N.J.

Stamm, H. (1941), Z. Anorg. Chem., Vol.247, p277.

Stuke, B. (1952), Naturwiss., Vol.39, p325-326.

Tartar, H.V. and Draves, C.Z. (1952), JACS, Vol.46, p574.

Thorne, P.C.L. and Roberts, E.R. (1949), Inorganic Chemistry, 5th ed. Interscience, N.Y.

Toland, W.G. (1955), US Patent No.2.722,473 (Nov.1,1955).

Treadwell, F.P. and Hall, T.H. (1956), Analytical Chemistry, Qualitative Analysis, 9th ed. Vol.5, Wiley, N.Y.

U.S. National Bureau of Standards (1968, 1969, 1971 and 1973), Selected value of Chemical thermodynamic Properties, Technical Notes, 270-3 (1968), 270-4 (1969), 270-5 (1971), 270-6 (1971) and 270-7 (1973).

Vesilind, P.A. and Peirce, J.J. (1988), Environmental Engineering, 2nd ed., Butterworths, Boston.

Vigide, F.G. and Hermida, L.A. (1959), Inf. Quim. Anal., No.13, p61-67; through Analy. Abstr., No.7, p1236, (1960).

Vivian, J.E. and King, C.J. (1964), AIChEJ, No.10, p221.

Weber, M.E. (1975) Chem. Eng. Sci., Vol.30, p1507-1510.

Wilson, W.E. Jr. and Levy, A. (1970), J. Air Pollut. Control Assoc. Vol.20, p385.

Weitz, E. and Spohn, K. (1956), Chem.Ber., Vol.89, p2332.

Whitman, W.G. (1923), Chem. Met. Eng., Vol.29, p146.

Widmer, M. and Schwarzenbach, G. (1964), Helv. Chem. Acta. Vol.47, p206.

Winterhalder, K. (1988), Trigger Factors Initiating Natural revegetation Progresses on Barren Acid, Metal-Toxic Soils Near Sudbury Ontario Smelter, the 1988 Mine Drainage and Surface Mine Reclamation Conference, Pittsburgh P.A.

Yau, A.Y. (1966), M.Eng. Thesis, McMaster University.

Yau, A.Y., Hamielec, A.E. and Johnson, A.I. (1969), Co-current Gas-Liquid Flow, Scott, D.S. and Rhodes, E. T. Ed., Plenum Press, N.Y.

Yoshida, F. and Akita, K. (1965) AIChEJ. No.11, p9.

Zdonik, S.B. (1942), M.S. Thesis, MIT.

Zhao, Y.F. and Irons, G.A. (1990), Metal. Trans. B., Vol.21B, Dec., p997-1003.

APPENDIX A

A SAMPLE OF PROGRAMS USED FOR SOLVING MATHEMATICAL MODELS

SFBR Model

```
function q = brmn(p)

s2 = p(1);
s1 = p(2);
s0 = p(3);
a2 = p(4);
a1 = p(5);
a0 = p(6);

q = zeros(6,1);

q(1) = s1*a1 - K1*a0*K3*s2;
q(2) = s1*a2 - K2*a1*K3*s2;
q(3) = s1*s1 - s0/K4*K3*s2;
q(4) = Na + s1/(K3*s2) - K3*s2/(K5*s1) - s1 - 2*s2 -a1 - 2*a2;
q(5) = (Na/2 - s1 - s2)*VOL - MHS;
q(6) = Tt*PSO2*FLG1 - (a0 + a1 + a2)*VOL;

format long e;
global K1 K2 K3 K4 K5 Na PSO2 FLG1 VOL MHS Tt;

T=363;

G1 = -6.077333+0.028*T;
G2 = -7.784+0.058*T;
G3 = -14.257333-0.012*T;
G4 = 1.15333-0.04*T;
G5 = -11.21887-0.026*T;

K1 = exp(-1000*G1/(1.987*T));
K2 = exp(-1000*G2/(1.987*T));
```

```
K3 = exp(-1000*G3/(1.987*T));
K4 = exp(-1000*G4/(1.987*T));
K5 = exp(-1000*G5/(1.987*T));

Na = 3.0;
PSO2 = 0.1;
FLG1 = 2.679e-02;
VOL = 0.4;
MHS = 0;

C = [0 0 0 0 0 0 ]';
A = 0;
B = 0;

Tt=1;

X1 = fsolve('brmn', [2 1e-1 1e-6 2e-6 2e-8 7e-10]')

for Tt = 1:1:90
   X1 = fsolve('brmn',X1);
   MHS = MHS + (1-PSO2)*FLG1*X1(3)/(1-X1(3))*1;
   pH = -log10(X1(2)/X1(1)/K3);
   C = [C,X1];
   B = [B,pH]
end

for Tt = 300.5:0.1:301;
   X1 = fsolve ('brmn',X1);
   MHS = MHS + (1-PSO2)*FLG1*X1(3)/(1-X1(3))*0.1;
   pH = -log10(X1(2)/X1(1)/K3);
   C = [C,X1];
   B = [B,pH]
end

save pH1 B /ascii
save COMP1 C /ascii
```

CFTR Model

```
function q = ssmn(p)

s2 = p(1);
```

```
s1 = p(2);
s0 = p(3);
a2 = p(4);
a1 = p(5);
a0 = p(6);
h = p(7);
oh = p(8);
waterout = p(9);
FLL2 = p(10);

q = zeros(10,1);

q(1) = h*a1 - K1*a0;
q(2) = 1.0e4*h*a2 - 1.0e4*K2*a1;
q(3) = 1.0e5*h*s2 - 1.0e5*s1/K3;
q(4) = 1.0e4*h*s1 - 1.0e4*s0/K4;
q(5) = 1.0e6*h*oh - 1.0e6*1/K5;
q(6) = Na + h - oh - s1 - 2*s2 -a1 - 2*a2;
q(7) = 1/2*Na*FLL1 - s0*(1-PSO2)*FLG1/(1-s0) - (s1 + s2)*FLL2;
q(8) = PSO2*FLG1 - (a0 + a1 + a2)*FLL2;
q(9) = 104*FLL1-2*s0*(1-PSO2)*FLG1/(1-s0)-(s1+a1+2*a0+waterout)*FLL2;
q(10) = FLL1*waterout-FLL2*100;


format long e;
global K1 K2 K3 K4 K5 Na PSO2 FLG1 FLL1 FLL2;

T=363;

G1 = -6.077333+0.028*T;
G2 = -7.784+0.058*T;
G3 = -14.257333-0.012*T;
G4 = 1.15333-0.04*T;
G5 = -11.21887-0.026*T;

K1 = exp(-1000*G1/(1.987*T));
K2 = exp(-1000*G2/(1.987*T));
K3 = exp(-1000*G3/(1.987*T));
K4 = exp(-1000*G4/(1.987*T));
K5 = exp(-1000*G5/(1.987*T));

Na = 3.0;
PSO2 = 0.1;
FLG1 = 2.68e-02;
```

```
FLL1 = 2.0e-03;

C = [0 0 0 0 0 0 0 0 0 0]';
B = 0;
X1 = fsolve('ssmn', [2e-6 1e-2 1e-1 2e-1 2e-0 7e-5 7e-8 7e-6 90 1e-03]')

for FLG1=2.68e-2:0.5e-3:3.68e-2
   X1 = fsolve('ssmn',X1)
   pH = -log10(X1(7));
   B = [B,pH];
   C = [C,X1];
end

save COMP C /ascii
save PH B /ascii
```